Développement de nouveaux systèmes photoamorceurs pour la polymérisation radicalaire et cationique dans des conditions douces

Mahmoud Rahal

THESE EN CODIRECTION

Pour obtenir le titre de

DOCTEUR DE L'UNIVERSITE DE HAUTE-ALSACE

ET

L'UNIVERSITE LIBANAISE

Présentée et soutenue publiquement par

MAHMOUD RAHAL

Le 12 Mai 2022

Développement de nouveaux photoamorceurs pour la polymérisation radicalaire et cationique dans des conditions douces.

Jury :

Dr. Sami Lakhdar	CNRS/Université de Toulouse	Rapporteur
Dr. Erwan Nicol	Université Le Mans	Rapporteur
Pr. Souad AMMAR	Université Paris Diderot	Examinatrice
Pr. Tayssir Hamieh	Université Libanaise	Codirecteur de thèse
Pr. Joumana Toufaily	Université Libanaise	Codirecteur de thèse
Pr. Jacques Lalevée	Université de Haute-Alsace	Directeur de thèse

Dédicace

À tous ceux que me sont chers,

À mes très chers parents ***Akram*** *et* ***Amal****, pour votre cœur qui m'a tant donné, pour vos yeux qui furent parfois mouillés, pour vous qui m'avez tant aimé, ma gratitude et ma reconnaissance que j'éprouve pour vous. Que Dieu me permette de vous rendre au moins une partie de tout ce qui je vous dois.*

À ma fiancée si précieuse ***Nadine****, aucun remerciement et dédicace ne sauraient pour t'exprimer mon amour et mon attachement à toi. Je te remercie de ne m'avoir jamais décu, tu es la joie de ma vie. Je remercie mon Dieu qui a croisé nos chemins.*

À mes chers frères : ***Bilal****,* ***Mohammad****,* ***Ali*** *et* ***Houssein****, et ma chère sœur* ***layla****, vous êtes le support de ma vie.*

Remerciements

Les travaux de thèse ont été effectués à l'Institut de Science de Matériaux de Mulhouse (IS2M), sous la direction du ***Prof. Jacques Lalevée.***

Tout d'abord, je tiens à exprimer mes vifs remerciements et ma sincère gratitude à mon directeur de thèse : **Professeur Jacques LALEVEE** responsable de l'équipe CRM au laboratoire IS2M qui m'a guidé avec soin et m'a donné l'opportunité de me lancer dans cette grande aventure. Un très grand Merci à lui pour ses encouragements, ses conseils précieux et son enthousiasme. J'ai eu la chance de travailler avec une personne ayant pas seulement des qualités scientifiques, mais aussi des qualités humaines. Merci Jacques, merci pour ta patience, pour toutes nos discussions pendant toute la période de thèse.

Je remercie également mes codirecteurs de thèse **Prof. Tayssir Hamieh** et **Prof. Joumana Toufaily** qui m'ont guidé et soutenu tout au long de ce travail. Merci pour leur confiance, leurs disponibilités et leurs précieux conseils.

Un grand merci au Dr**. Fabrice Morlet-Savary** pour ses aides, ses conseils ainsi que sa disponibilité.

Mes sincères remerciements s'adressent à l'association de spécialisation et d'orientation scientifique **(ASOS**), qui a financé mes trois années de thèse, ainsi que la Fondation Pierre et Jeanne Spiegel qui m'a aidé les derniers mois de ma thèse.

Ce travail n'aurait pu être mené à bien sans la présence de notre collaborateur **Dr. Frédéric Dumur** qui a fait la synthèse de la majorité des produits utilisés dans ce travail. Un grand merci pour toi **Frédéric**.

Je tiens à remercier également **Dr. Sami Lakhdar**, **Dr. Erwan Nicol**, et **Pr. Souad Ammar** qui m'ont fait l'honneur de participer au jury de cette thèse.

Mes remerciements s'adressent aussi à tous les doctorants, post-doctorants, ingénieurs, stagiaire et membres de l'IS2M : **Sylvie, Philippe, Aissam, Gautier, Eric, Cyrille, Chaima, Tuba, Mariem, Elodie, Marie, valentine, Aurore, Valentin, Loïc, Alexis, Romain, Méline, Noëlle, Alexandre, Estelle, Asma…**

Je remercie spécialement : **Ahmad, Haifaa, Fatima et Hanine** pour leur soutien, je n'oublierai jamais les agréables moments qu'on a passés ensemble.

Je remercie particulièrement mes cousins : **Hassan** et **Mohammad** pour leur soutien, leurs aides et leurs conseils. Ce travail n'aurait pu être mené à bien sans vous.

Mes vifs remerciements vont également à mon oncle **Nehme** et sa famille **(Angela, Amir et la petite Yara)** ainsi que mon oncle **Mohammad** et sa famille **(Faouziya et Doha)**.

Nadine Mahmoud, ma belle fiancée et avec qui j'ai passé des jolis moments depuis qu'elle est arrivée en France, je la remercie pour son soutien, pour ses encouragements. Tu m'encourages quand je baisse les bras et tu me consoles quand je subis un échec. Les mots sont peu de choses pour te dire merci pour tout cela. Tu es la source qui illumine ma vie !

Mon modèle dans la vie, mon père **Akram**, ma force et ma foi dans cette vie, ma mère **Amal,** c'est à vous deux que j'adresse mes derniers remerciements. Merci pour avoir fait de moi ce que je suis aujourd'hui, merci d'être les meilleurs parents qu'un homme puisse avoir. Je n'oublierai jamais vos sacrifices pour que je puisse continuer en Doctorat.

Bilal, Mohammad, Ali et Houssein, mes frères, ma sœur **layla**, vous êtes mon support !!

Table des matières

Introduction générale

Les polymères sont les unités de base de la préparation de nombreux matériaux. Ils sont presque utilisés dans tous les secteurs de notre vie moderne tels que le transport, l'énergie, la santé, les nanotechnologies, l'emballage… Ainsi, ces matériaux représentent le centre d'intérêt de nombreuses industries et sont au centre de recherches académiques avec leur grande compatibilité, leurs propriétés mécaniques et pour leur grande facilité d'accès.

Par ailleurs, le développement de nouvelles voies de synthèses de matériaux polymères à faible coût, respectueux de l'environnement, écologiques et moins énergivores reste plus que jamais au cœur des préoccupations académiques et industrielles et l'objet de nombreuses nouvelles stratégies de recherche.

En effet, des sources lumineuses à la fois peu coûteuses, efficaces et à faible consommation d'énergie ont été récemment développées pour induire des réactions photochimiques. La photopolymérisation déjà présente dans de nombreux domaines de notre vie quotidienne tel que : les cosmétiques **[1]**, les revêtements **[2]**, les emballages **[3]**, la dentisterie **[4]** etc. **(Schéma 1)**, est un processus photochimique très utilisé aux niveaux académique et industriel **[5-9]**.

Schéma 1. Quelques exemples de domaines d'applications des photopolymères.

Ce procédé de synthèse, quasi instantanée et menant à des polymères réticulés ou linéaires, consiste en une transformation chimique d'un monomère (résine) liquide ou visqueux en un matériau solide (ou un film) sous l'effet de la lumière. Cette transformation exige la présence, dans la résine organique, d'une molécule photosensible appelée photoamorceur **[10]** puisque le monomère seul ne peut pas de lui même amorcer une polymérisation. Suite à une activation lumineuse, le photoamoceur se trouve excité et sera ainsi capable de générer des espèces réactives (radicaux, cations, anions…) responsables de la réaction de polymérisation **(Schéma 2).** La nature des espèces réactives ainsi formées contrôle la nature du monomère choisi et donc la nature du polymère formé ; par exemple, des monomères acryliques ou vinyliques seront utilisés dans le cas de la photopolymérisation radicalaire alors que les monomères époxydes seront préférentiellement utilisés dans le cas de réactions cationiques. Donc c'est un procédé divisé en trois étapes : photoamorçage (considéré comme l'étape clé de la photopolymérisation), propagation et terminaison. Un photoamoceur (PA) peut soit se dissocier suite à une activation lumineuse selon un mécanisme unimoléculaire, on parlera donc d'un PA de Type I, soit par l'intervention d'une autre molécule on parlera donc d'un PA de Type II.

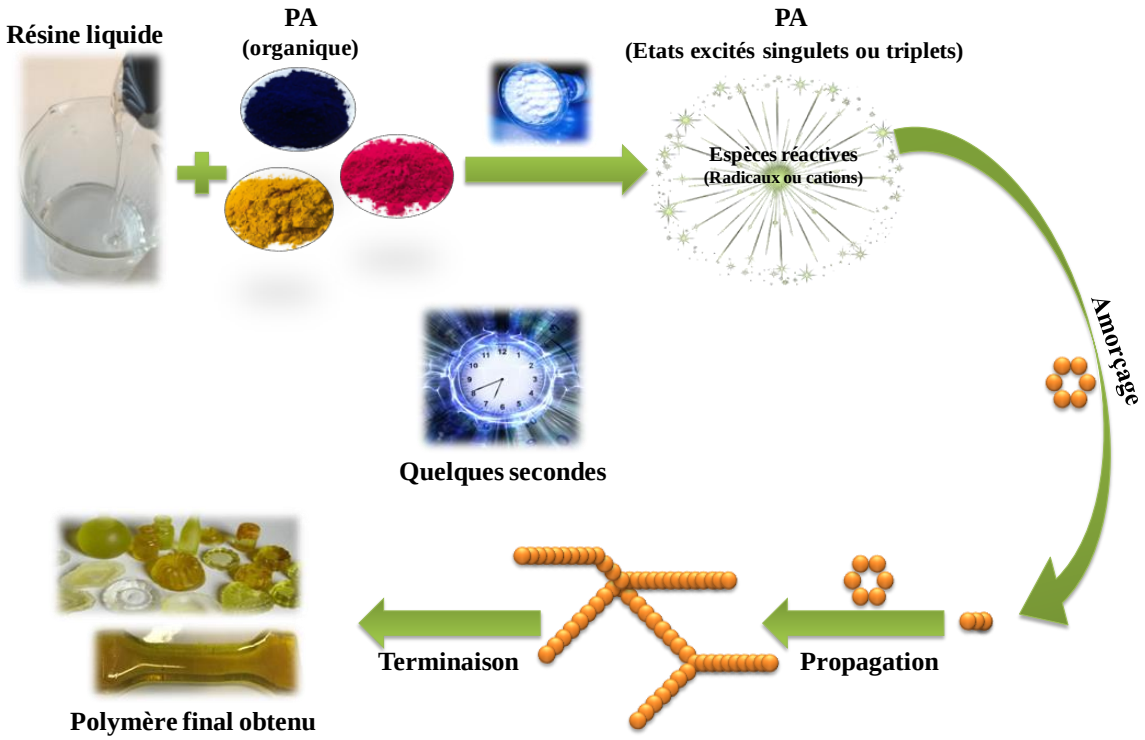

Schéma 2. Principe d'une photopolymérisation.

Généralement, le processus de polymérisation est amorcé thermiquement **[11]**. Ce procédé de synthèse présente tout de même plusieurs inconvénients: son caractère énergivore, l'emploi de solvant, réaction assez lente ainsi qu'un mauvais contrôle spatio-temporel. Cependant, les réactions de polymérisation photoinduite sont considérées comme une alternative verte à celles activées thermiquement avec leur faible consommation d'énergie, leur aspect écologique (moins de Composés Organiques Volatils **(COV)** sont émis, réaction à température ambiante), leur rapidité ainsi qu'un bon contrôle spatio-temporel observé (impression 3D) **[12-15] (Schéma 3).**

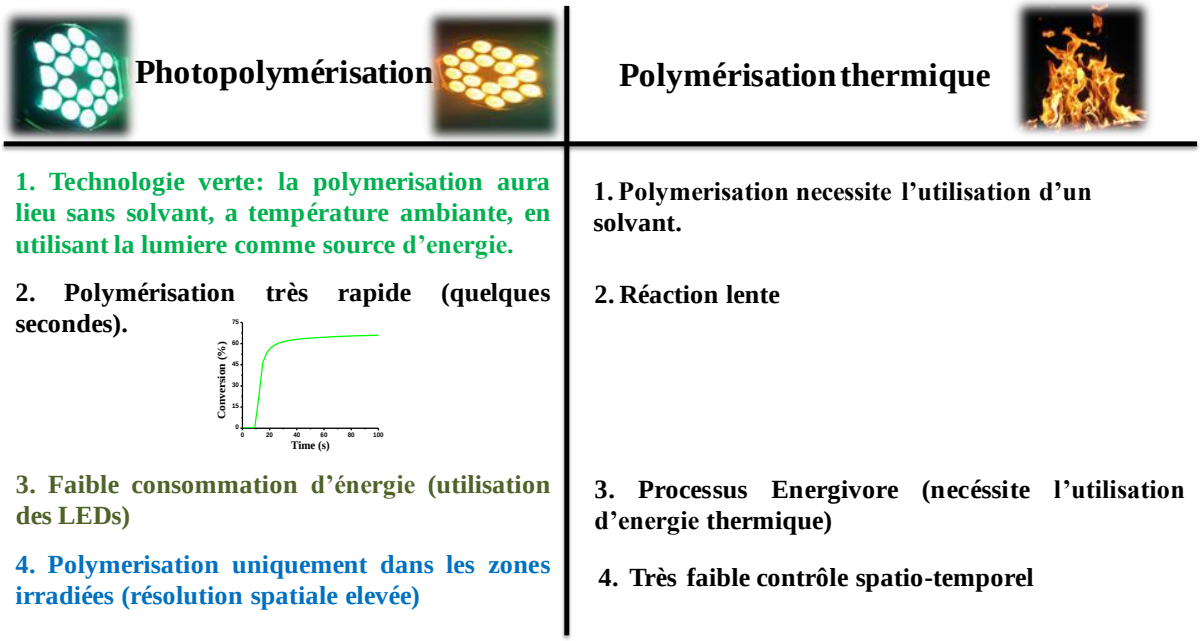

Schéma 3. Les avantages de la photopolymérisation par rapport à la polymérisation thermique.

La stéréolithographie ou l'impression 3D par photopolymérisation est une technologie de fabrication additive qui permet l'élaboration des objets 3D dans des conditions douces en ajoutant des couches successives les unes sur les autres jusqu'à ce que la pièce soit terminée **[16]**. Sous l'effet de la lumière UV émise par le laser, la résine durcit uniquement dans les zones irradiées. Les objets obtenus présentent, donc, une résolution spatiale élevée et un aspect lisse. Afin de remédier aux inconvénients liés à l'utilisation de la lumière UV, des imprimantes 3D à projecteur LED ont été élaborées depuis 2014, ce type d'imprimante permet une projection complète d'une couche en une seule fois, ce qui réduit les coûts énergétiques liés à l'utilisation de la lumière UV. Actuellement, de nombreux domaines sont

intéressés par l'utilisation de l'impression 3D : la médecine, l'architecture, l'aéronautique **[17-20]** et bien d'autres domaines.

Au cours des dernières décennies et jusqu'à aujourd'hui, la production de matériaux composites représente un marché très dynamique, puisqu'elle est estimée à 90,6 milliards de dollars en 2019, le marché mondial devrait atteindre plus de 131,6 milliards en 2024 (avec un taux de croissance annuel moyen de 7,7 %) **[21]**. Cette production très importante repose sur les propriétés mécaniques très intéressantes de ces nouveaux matériaux (plus légers, chimiquement inertes, avec une résistance thermique et mécanique améliorée…). Récemment, les processus de photopolymérisation ont été fortement incorporés dans la fabrication de photocomposites par les industries souhaitant élaborer de nouveaux matériaux ayant de bonnes propriétés mécaniques et chimiques avec moins de consommation d'énergie. Leurs propriétés très intéressantes font de ces matériaux l'un des meilleurs utilisés dans différents domaines tels que : les applications électriques **[22]**, les automobiles **[23]**, les infrastructures **[24]**, les applications médicales **[25]**, l'aéronautique **[26]**, les technologies militaires **[27]** et les matériaux anticorrosion…

En fait, l'efficacité d'une réaction de photopolymérisation dépend de plusieurs facteurs dont la majorité est liée au choix du photoamorceur **(PA)** qui est l'élément clé de la polymérisation. Ainsi le PA doit répondre aux critères suivants:

- Il doit présenter de bonnes propriétés d'absorption bien adaptées à la zone d'émission de la source lumineuse utilisée pour pouvoir former les espèces réactives.
- Il doit fournir un rendement quantique, en espèces actives, le plus élevé possible.
- Il doit être totalement soluble dans le monomère choisi.
- Une courte durée de vie de leur état excité est favorable surtout dans le cas de PA Type I, cependant une longue durée de vie est souhaitable dans le cas de PA de Type II.
- Les radicaux générés doivent être faiblement sensibles à l'oxygène pour la polymérisation radicalaire.

Limitations

Introduction générale

La synthèse de photopolymères au niveau industriel se produit par voie radicalaire ou ionique. La génération des radicaux ou des ions se fait uniquement par absorption du système photoamorceur d'une énergie lumineuse convenable. En effet, la majorité des photoamorceurs commerciaux absorbent la lumière Ultra-violette, ainsi les photopolymères synthétisés industriellement sont accompagnés par une consommation d'énergie qui reste forte liée à la haute intensité de la lumière UV. Ceci exige l'utilisation des dispositifs d'irradiation émettant dans l'UV (lampes UV à vapeur de mercure) qui présentent plusieurs inconvénients : ils nécessitent un certain temps de chauffage, le rayonnement est nocif pour la santé humaine, le prix élevé, faible durée de vie des bulbes, ainsi qu'une faible pénétration de la lumière en profondeur dans les échantillons épais est souvent observée (limite l'accès aux matériaux composites).

Par ailleurs, le développement de nouvelles sources d'irradiation depuis plusieurs années telles que les Diodes Electroluminescentes (LED) a augmenté l'engouement des industries pour la polymérisation photoinduite avec leur longue durée de vie, leur prix raisonnable, la faible consommation d'énergie, leur spectre d'émission relativement étroit, la portabilité, la sûreté pour l'opérateur (possibilité d'émission dans le visible) **(Schéma 4).**

 **Lampe UV**	 **Diodes Electroluminescentes**
1. **Source d'irradiation dangereuse (UV): i)** Cancer de peau, **ii)** Impact environnemental	1. **Source d'irradiation Sûres :** Rayonnement visible ou proche UV.
2. **Source d'irradiation énergivore :** nécessite un chauffage avant utilisation	2. **Faible consommation d'énergie**
3. **Faible durée de vie**	3. **Longue durée de vie**
4. **Dispositifs volumineux**	4. **Forme compacte**
5. **Forte génération de la chaleur au cours d'utilisation**	5. **Faible libération de la chaleur :** Adaptées aux applications sensible à la chaleur

Schéma 4. Comparaison entre les dispositifs d'irradiations à base des LEDs et celle à base des lampes UV (e.g. lampe à vapeur de Hg).

Cependant, la longueur d'onde plus décalée de ces nouveaux dispositifs est associée à des photons moins énergétiques, ce qui rend plus difficile la génération des espèces réactives en utilisant les systèmes PA conventionnels.

La transition entre les dispositifs d'irradiation UV et leurs alternatives (LED) réside principalement par le choix du système PA qui représente la clé de voute puisqu'il est responsable de la génération des espèces réactives, il contrôle la vitesse de polymérisation ainsi que des propriétés finales du polymère obtenu. Le développement de nouveaux systèmes photoamorceurs à haute performance, absorbant dans le visible, capables d'amorcer en faible quantité la réaction ainsi que d'être régénérés au cours de la réaction de polymérisation peut remédier au problème de la perte d'énergie liée à la transition UV-visible. Ce type de PA nous mène à la fin à l'utilisation d'un cycle catalytique, le PA est alors nommé "Catalyseur photoredox" **[28-30] (Schéma 5).**

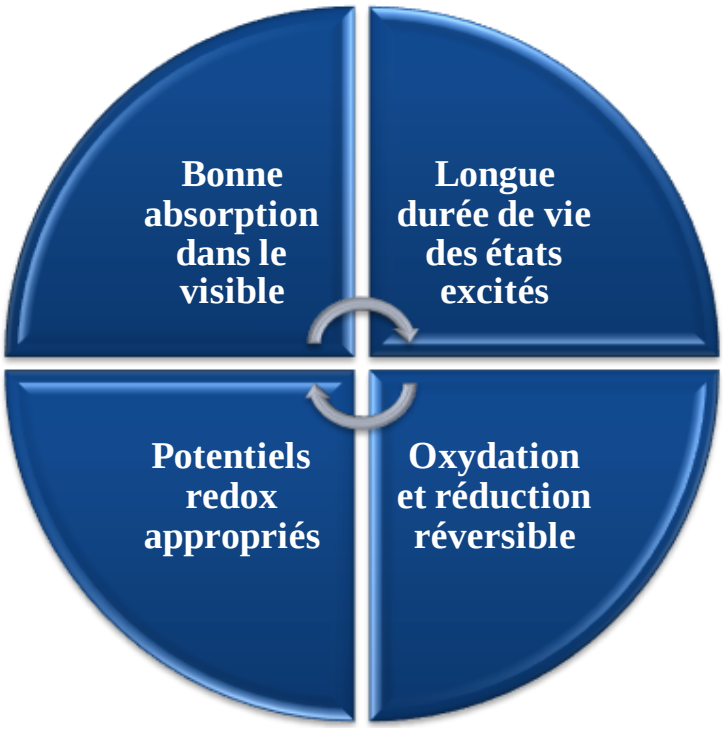

Schéma 5. Caractéristique d'un catalyseur photoredox.

L'objectif de ce travail de thèse est lié au développement de nouveaux systèmes photoamorceurs haute performance, efficaces et plus respectueux de l'environnement pour l'amorçage de la polymérisation radicalaire et cationique sous lumière visible. Les principales thématiques de mon travail de thèse sont basées essentiellement sur :

- ❖ Le développement de nouveaux PA type II à base de colorants organiques absorbant fortement dans le visible.
- ❖ Le développement de nouveaux PA photoredox.
- ❖ La recherche de nouveaux PA hydrosolubles pour la synthèse des hydrogels.
- ❖ L'utilisation des Diodes Electroluminescentes (LED) comme source d'irradiations sûres qui se caractérisent par une longue durée de vie et une faible consommation d'énergie.
- ❖ Comme applications : **i)** la synthèse de photocomposites par imprégnation des fibres de verre par résine organique, et **ii)** l'impression 3D.

Le présent manuscrit s'articulera autour de quatre grandes parties principales dont le contenu est résumé ci-dessous et représenté dans le **Schéma 6.**

- ➢ **La première partie** contient un état de l'art divisé en trois chapitres abordant :
  - La Photopolymérisation Radicalaire **(FRP).**
  - La Photopolymérisation Cationique **(CP).**
  - Les systèmes hybrides **(RIP ou IPN).**

La deuxième et la troisième partie de la thèse sont consacrées à l'étude de différentes familles de colorants organiques (non métallique) à base de coumarines, cétocoumarines, Phénothiazine et d'autres chromophores. Ces composés, synthétisés par nos collaborateurs de l'université de Cergy et l'université d'Aix Marseille, ont été utilisés comme photoamorceurs pour la polymérisation radicalaire et cationique sous lumière visible. En effet, ces colorants ont montré des fortes capacités d'amorçage du processus de photopolymérisation.

- ➢ **La deuxième partie** est donc consacrée aux coumarines et céto-coumarines et sera divisée en deux chapitres :
  - **Chapitre I :** Ce chapitre comporte deux sections. Il couvrira deux familles de colorants organiques à base de coumarines qui sont dotées d'excellentes performances comme photoamorceurs de polymérisation radicalaire.

- **Chapitre II :** Ce chapitre est dédié à l'étude d'une série de composés de céto-coumarines pour la synthèse de photopolymères ainsi que pour la génération des matériaux par impression 3D.

➢ **La troisième partie** est divisée aussi en deux chapitres et sera consacrée à d'autres chromophores comme photoamorceurs :

- **Chapitre I :** Ce chapitre porte sur le développement de nouveaux systèmes photoredox basés sur les dérivés de Naphthalimide comme photoamorceurs Type II. L'un de ces colorants avait la capacité de produire des hydrogels par polymérisation dans l'eau. La synthèse de réseaux polymères interpénétrés (IPN) a été aussi examinée dans ce travail.

- **Chapitre II :** Le présent chapitre est dévolu à la polymérisation radicalaire et cationique en se basant sur l'utilisation de colorants organiques dérivés de phénothiazines. Certains composés ont été évalués comme catalyseur photoredox (PCs).

➢ **La quatrième partie** concerne les photoamorceurs à base de métaux en particulier les composés contenants des métaux de transition comme le cuivre. Deux composés organométalliques ont été évalués comme photoamorceurs à haute performance.

L'ensemble de ce travail de recherche et de développement de nouveaux systèmes photoamorceurs a fait appel à diverses techniques de caractérisation : **i)** la spectroscopie **UV-Visible** qui sert à déterminer les coefficients d'extinction molaire des colorants utilisés ainsi que d'étudier leur comportement suite à l'interaction avec les additifs par 'Photolyse', **ii)** la spectroscopie Infrarouge à transformée de Fourier en Temps Réel **(RT-FTIR)** qui vise à étudier la capacité d'amorçage de nos systèmes en suivant l'évolution de l'intensité du pic caractéristique du monomère utilisé, **iii)** la spectroscopie de fluorescence et la spectroscopie de fluorescence résolue en temps nous aident à évaluer les énergies des états excités, le rendement quantique en espèces réactives ainsi que la durée de vie des états excités, **iv)** la Voltammétrie Cyclique **(VC)** avec les techniques de fluorescence, permet de calculer les énergies libres des réactions de transfert d'électron (ΔG_{et}), **v)** la Résonance Paramagnétique Electronique **(RPE)** à partir de laquelle est possible de détecter et de déterminer la nature des espèces réactives libérées lors de la polymérisation,

vi) Les imprimantes 2D et 3D permettent la production de matériaux polymères en 2D et 3D.

La combinaison de toutes ces techniques de caractérisations fournit la méthodologie nécessaire pour comprendre le mécanisme réactionnel lors du processus de polymérisation et d'évaluer les utilisations potentielles des PA proposés.

PLAN DE LA THESE

Introduction générale

Partie I : Etude Bibliographique
- **Chapitre I :** Photopolymérisation Radicalaire **(FRP)**
- **Chapitre II :** Photopolymérisation Cationique **(CP)**
- **Chapitre III :** Réseaux Polymères Interpénétrés **(IPN ou RIP)**

Partie II : Colorants organiques comme PA
- **Chapitre I :** Dérivés de coumarine
- **Chapitre II :** Dérivés de Cétocoumarine

Partie III : Nouveaux PA à base de colorants pour la FRP et CP
- **Chapitre I :** Dérivés de Phénothiazine
- **Chapitre II :** Dérivés de Naphthalimide

Partie IV : PA organométalliques à base de complexes de cuivre
- Dérivés de Complexes de cuivre

Schéma 6. Plan de la thèse

Valorisation du travail

Ce travail de thèse fait l'objet de 7 publications dans des journaux internationaux et deux autres articles sont en préparation. Les résultats obtenus durant mes travaux de thèse ont été aussi présentés à des congrès internationaux (Virtual 6th European Symposium of Photopolymer Science **VESPS**, 2021) et nationaux (Colloque troisième Édition du **Young Scientists Day**, Mulhouse, 2021).

Liste des publications

[1] Rahal, M.; Abdallah, M.; Bui, TT.; Goubard, F.; Graff, B.; Dumur, F.; Toufaily, J.; Hamieh, T.; Lalevee, J. Design of new phenothiazine derivatives as visible light photoinitiators Polym.Chem., **2020**, 11, 3349.

[2] Rahal, M.; Mokbel, H.; Graff, B.; Toufaily, J.; Hamieh, T.; Dumur, F.; Lalevee, J. Mono vs. Difunctional Coumarins as Photoinitiators in Photocomposite Synthesis and 3D printing. Catalyst, **2020**, 10, 1202.

[3] Rahal, M.; Mokbel, H.; Graff, B.; Pertici, V.; Gigmes D.; Toufaily, J.; Hamieh, T.; Dumur, F.; Lalevee, J. Naphthalimide-Baed Dyes as Photoinitiators under Visible Light Irradiation and their applications: Photocomposites synthesis, 3D printing and polymerization in Water. ChemPhotoChem, **2021**, 5, 1.

[4] Rahal, M.; Graff, B.; Toufaily, J.; Hamieh, T.; Noirbent, G.; Gigmes, D.; Dumur, F.; Lalevee, J. Molecules 3-Carboxylic Acid and Formyl-Derived Coumarins as Photoinitiators in Photo-oxidaton or Photo-reduction Processes for Photopolymerization upon Visible Light: Photocomposite Synthesis and 3D printing Applications. Molecules, **2021**, 26, 1753.

[5] Rahal, M.; Graff, B.; Toufaily, J.; Hamieh, T.; Dumur, F.; Lalevee, J. Design of keto-coumarin based photoinitiator for Free Radical Photopolymerization: Towards 3D printing and photocomposites applications. Eur. Polym. J., **2021**, 154, 110559.

[6] Hammoud, F.; Rahal, M.; Egly, J.; Morlet-Savary, F.; Hijazi, A.; Bellemin-Laponnaz, S.; Mauro, M.; Lalevee, J. Cubane Cu4I4(phosphine)4 complexes as new co-initiators for free radical photopolymerization: towards aromatic amine-free systems. Polym. Chem., **2021,** 12, 2848.

[7] Rahal, M.; Graff, B.; Toufaily, J.; Hamieh, T.; Ibrahim-Ouali, M.; Dumur, F.; Lalevee, J. Naphthyl-naphthalimides as high performance visible light photoinitiators for 3D printing and photocomposites synthesis. Catalysts, **2021**, 11, 1269.

Références

[1] Morgan, S.E.; Havelka, K.O.; Lochhead, R.Y. Cosmetic Nanotechnology : Polymers and Colloids in Cosmetics. Eds. ACS symposium series 961, **2007.**

[2] Thèse Heydel, C. Elaboration d'un matériau barrière à base de poly(chlorure de vinyle) en vue d'améliorer la résistance aux salissures de revêtements de sol réalisés par enduction. Université de Lyon 1, **1997.**

[3] Chomon, P. Emballages plastiques : polymères utilisés. Conceptions d'emballages, Techniques de l'ingénieur, Paris, **2008**.

[4] Leprince, J.; Leloup, G.; Vreven, J.; Weiss, P.; Raskin, A. Polymères et résines composites. EMC Odontologie, Elsevier Masson, **2011.**

[5] Bouzrati-Zerelli, M.; Maier, M.; Fik, C.P.; Dietlin, C.; Morlet-Savary, F.; Fouassier, J.P.; Klee, J.E.; Lalevée, J. A low migration phosphine to overcome the oxygen inhibition in new high performance photoinitiating systems for photocurable dental type resins. Polym.Int. **2016**, 66, 504.

[6] Smela, E.; Zuccarello, G.; Kariis, H.; Liedberg, B. Thiol-Modified Pyrrole Monomers: 1. Synthesis, Characterization, and Polymerization of 1-(2-Thioethyl)pyrrole and 3-(2-Thioethyl)pyrrole. Langmuir. **1998**, 14, 2970.

[7] Zhu, Y.; Rabindranath, A.R; Beyerlein, T.; Tieke, B. Highly Luminescent 1,4-Diketo-3,6-diphenylpyrrolo[3,4-c]pyrrole-(DPP-) Based Conjugated Polymers Prepared Upon Suzuki Coupling. Macromolecules. **2007**, 40, 6981.

[8] Alamiry, M.A.H.; Harriman, A.; Haefele, A.; Ziessel, R. Photochemical Bleaching of an Elaborate Artificial Light-Harvesting Antenna. ChemPhysChem. **2015**, 16, 1867.

[9] Wu, P.T.; Kim, F.S.; Jenekhe, S.A. New Poly(arylene vinylene)s Based on Diketopyrrolopyrrole for Ambipolar Transistors. Chem.Mater., **2011**, 23, 4618.

[10] Fouassier, J.P.; Lalevée. J. Photoinitiators for polymer synthesis: Scope, Reactivity, and efficiency,Wiley-VCH Verlag GmbH & Co. KGaA, **2012**.

[11] Walling, C.; Briggs, E.R. The Thermal Polymerization of Methyl Methacrylate J.Am.Chem.Soc., **1946**, 68, 1141.

[12] Zhang, J.; Xiao, P. 3D Printing of Photopolymers. Polym.Chem. **2018**, 9 , 1530.

[13] Ambrosi, A.; Pumera, M. 3D-Printing Technologies for electrochemical applications. Chem.Soc.Rev. **2016**, 45, 2740.

[14] Ligon, S.C.; Liska, R.; Stampfl, J.; Gurr, M.; Mülhaupt, R. Polymers for 3D Printing and Customized Additive Manufacturing. Chem. Rev. **2017**, 117, 10212.

[15] Pandey, R. Photopolymers in 3D Printing Applications. 2014.

[16] Jariwala, A.S.; Ding, F.; Boddapati, A.; Breedveld, V.; Grover, M.A.; Henderson, C.L.; Rosen, D.W. Modeling effects of oxygen inhibition in mask-based stereolithography. Rapid Prototyping Journal. **2011,** 17, 168.

[17] Tumbleston, J.R.; Shirvanyants, D.; Ermoshkin, N.; Janusziewicz, R.; Johnson, A.R.; Kelly, D.; Chen, K.; Pinschmidt, R.; Rolland, J.P.; Ermoshkin, A.; Samulski, E.T.; DeSimone, J.M. Additive manufacturing. Continuous liquid interface production of 3D objects. Science. **2015**, 347, 1349.

[18] Chiappone, A.; Fantino, E.; Roppolo, I.; Lorusso, M.; Manfredi, D.; Fino, P.; Pirri, C.F.; Calignano, F. 3D Printed PEG-Based Hybrid Nanocomposites Obtained by Sol-Gel Technique. ACS Appl.Mater.Interfaces. **2016**, 8, 5627.

[19] Credi, C.; Fiorese, A.; Tironi, M.; Bernasconi, R.; Magagnin, L.; Levi, M.; Turri, S. 3D Printing of Cantilever-Type Microstructures by Stereolithography of Ferromagnetic Photopolymers ACS Appl. Mater. Interfaces. **2016**, 8, 26332.

[20] Mao, Y.; Yu, K.; Isakov, M.S.; Wu, J.; Dunn, M.L.; Qi, H.J. Sequential Self-Folding Structures by 3D Printed Digital Shape Memory Polymers. Sci. Rep., **2015**, 5, 13616.

[21] Composites Market Global Forecast to 2024, MarketsandMarkets, **2019**.

[22] Ramasubramaniam, R.; Chen, J.; Liu, H. Homogeneous Carbon Nanotube/Polymer Composites for Electrical Applications. Appl.Phys.Lett. **2003**, 83, 2928.

[23] Holbery, J.; Houston, D. Natural-Fiber-Reinforced Polymer Composites in Automotive Applications. JOM. **2006**, 58, 80.

[24] Barbero, E.; Gangarao, H.V.S. Structural Applications of Composites in Infrastructure. SAMPE Journal. **1991**, 27, 9.

[25] Shahinpoor, M.; Kim, K.J. Ionic Polymer-metal Composites : IV. Industrial and Medical Applications. Smart Mater.Struct. **2004**, 14, 197.

[26] Soutis, C. Fibre Reinforced Composites in Aircraft Construction. Prog. Aerosp.Sci. **2005**, 41, 143.

[27] Bhatnagar, A.; Lang, D. Military and Law Enforcement Applications of Lightweight Ballistic Materials. In Lightweight Ballistic Composites; Elsevier, **2006**, 364.

[28] Zeitler, K. Photoredox Catalysis with Visible Light. Angew. Chem.Int.Ed. **2009**, 48, 9785.

[29] Narayanam, J.M.R.; Tucker, J.W.; Stephenson, C.R.J. Electron-Transfer Photoredox Catalysis: Development of a Tin-Free Reductive Dehalogenation Reaction. J.Am.Chem.Soc. **2009**, 131, 8756.

[30] Rueping, M.; Zhu, S.; Koenigs, R.M. Visible-light photoredox catalyzed oxidative Strecker reaction. Chem.Commun. **2011**, 47, 12709.

Partie I : ETUDE BIBLIOGRAPHIQUE

Partie I : ETUDE BIBILIOGRAPHIQUE

Rappels bibliographiques

La polymérisation est un procédé de synthèse chimique souvent irréversible permettant l'élaboration d'un matériau de haut poids moléculaire **(Polymères)** à partir des molécules de faibles masses molaires **(Monomères)**. Ce processus nécessite la formation d'un centre actif qui permettra la fixation de monomères qui peut se faire selon deux mécanismes distincts : **par étapes, en chaîne**. Cette dernière consiste en une addition successive de plusieurs molécules de monomère, ainsi des chaînes polymères avec de grandes masses molaires peuvent être obtenues même pour des faibles taux de conversion. Par contre, la polymérisation par étapes est un procédé produisant des chaînes polymères d'importantes masses molaires pour des taux de conversion élevées uniquement, ce processus résulte d'une réaction chimique entre deux monomères de différentes fonctionnalités.

Ce présent travail se concentrera uniquement sur la synthèse des polymères en chaînes où le centre actif responsable de l'amorçage et la propagation contrôle la nature de la polymérisation qui peut être : Radicalaire, cationique ou anionique. Ce manuscrit portera sur les deux premiers types de polymérisation puisque la polymérisation par voie anionique est encore rarement décrite au niveau industriel.

En fait, la synthèse des matériaux polymères se produit suivant deux procédés : Thermique et photochimique. Ce dernier est au cœur de ces travaux de thèse vue leur avantage intéressant par rapport au processus thermique. L'enjeu principal de ce travail est donc la recherche de nouveaux systèmes photoamorceurs absorbant dans le visible pour la polymérisation radicalaire et cationique. En effet, le processus de polymérisation photoinduite repose sur l'excitation d'une molécule photosensible capable de générer des espèces réactives pour l'amorçage de la polymérisation.

Différents processus photochimiques/physiques résultent de l'interaction lumière-PA, de ce fait, la compréhension de la réactivité des systèmes PA sera fournie en expliquant ces processus.

1. Propriétés d'un Photoamorceur (PA)

1.1 Spectre d'absorption du PA : Activation du PA

Les propriétés d'absorption d'une molécule dépendent fortement de sa structure chimique, et notamment des groupements chromophores qu'elle contient **[1,2]**. Ainsi, la nature de ces groupes contrôle la localisation de spectre d'absorption du PA (UV, Visible ou Infrarouge) sur le spectre électromagnétique. L'absorbance ou la densité optique (D.O) dans une gamme de longueur d'onde reflète les propriétés d'absorption de la molécule photosensible qui sont décrites par la loi de Beer-Lambert : D.O = ε.l.C, où **ε** est le coefficient d'extinction molaire **($M^{-1}.cm^{-1}$), l** correspond à la longueur du chemin optique **(cm)** et **C** représente la concentration de la solution contenant le PA **($mol.L^{-1}$).**

En effet, l'absorbance est reliée directement à la transmittance suivant l'équation : $A= -\log_{10}(T)$, autrement dit, si le coefficient d'extinction molaire est trop élevé l'absorbance aura ainsi une valeur importante induisant une forte diminution de la transmittance du rayon incident. Ceci entraine un faible taux de conversion en profondeur des échantillons épais connu sous le nom **'Effet de filtre interne',** la polymérisation aura lieu uniquement en surface **[3]**. Ce phénomène observé est un problème répandu dans la synthèse de photopolymères, ce qui explique le recours à la polymérisation couche par couche **[4]**.

Pour une bonne génération des espèces réactives, un bon chevauchement entre le spectre d'émission des dispositifs d'irradiations et le spectre d'absorbance de la molécule photosensible (ou PA) est fortement demandé.

1.2. Photoamorceur : Clé de voute de la polymérisation

Chaque molécule est décrite par des orbitales moléculaires ayant différents niveaux électroniques obtenues par combinaison linéaire d'orbitales atomiques **(CLOA)**. Lorsqu'une molécule (PA) absorbe une fraction de lumière du rayonnement électromagnétique, le PA passe de l'état fondamental (S_0) à l'état excité (S_1, S_2….). Un électron du PA passe de l'orbitale moléculaire la plus haute occupée **(HOMO)** vers l'orbitale moléculaire la plus basse vacante **(LUMO).** La différence entre ces deux niveaux d'énergie correspond à l'énergie gap, plus l'écart entre ces deux orbitales est faibles (E_{gap} faible), moins d'énergie est nécessaire pour que la transition électronique ait lieu, ainsi la transition sera plus décalée dans le visible ($\mathbf{E = h.c/\lambda = h.\nu}$ où **h** est la constante de Planck, ν la fréquence de l'onde électromagnétique,

c correspond à la célérité de la lumière et λ représente la longueur d'onde de la lumière absorbée). Le PA sera ensuite capable de générer des espèces réactives pour la polymérisation.

2. Réactivité de l'état excité

Après avoir passé vers son état excité (Singulet S_1 ou Triplet T_1), le photoamorceur peut subir de nombreux processus photophysiques/chimiques qui sont détaillés à l'aide du diagramme de Perrin-Jablonski **(Schéma 1)**. Tout d'abord, les niveaux d'énergie électroniques correspondent à une molécule et les transitions sont rapportées dans le **Schéma 1.** Différents types de transition sont observés :

i) Transition non-radiative qui n'émet pas de photons, et se produit soit par **relaxation vibrationnelle** (v=i → v=0 dans un même état électronique; i : numéro d'un état vibrationnel) soit par **conversion interne** (transition de S_1 vers S_0 sans émission) ou **conversion intersystème** (passage de l'électron de **S_1 → T_1 →S_0** sans émission). L'excès d'énergie est libéré par dissipation thermique.

ii) Transition radiative qui implique l'émission de photons. Ce type de transition est à l'origine des phénomènes de **fluorescence (S_1 vers S_0)** et de **phosphorescence (S_1 →T_1 → S_0)**.

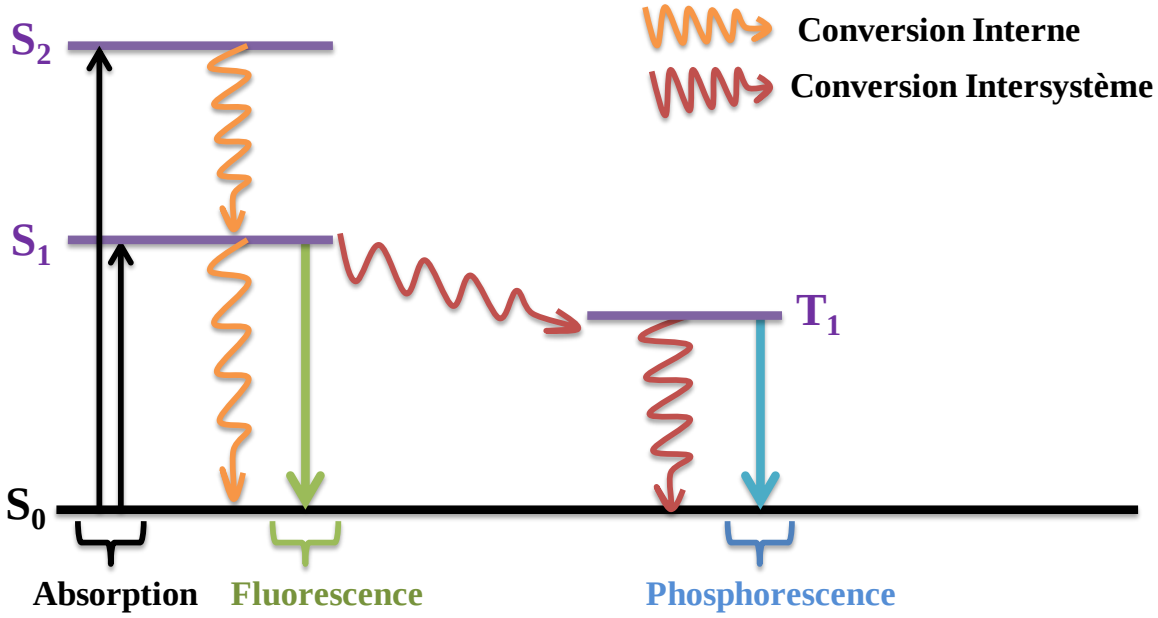

Schéma 1. Diagramme de Perrin-Jablonski

Alors que ces différents phénomènes photophysiques ont lieu sans aucune modification chimique de la molécule photosensible, d'autres phénomènes peuvent aussi se produire au niveau des états excités S_1 et T_1, qui sont responsables de la génération des espèces réactives capables d'amorcer le processus de polymérisation **[5]**. En fait, le rendement quantique en espèces réactives est un paramètre très important caractérisant l'efficacité d'un système photoamorceurs et ainsi le processus de polymérisation. Ce paramètre peut être calculé suite à l'ajout d'un additif sur la molécule photosensible, ce phénomène physico-chimique ainsi observé est appelé 'Quenching' ou désactivation de l'état excité résultant de l'interaction entre le PA et le quencher. L'interaction peut être suivie en mesurant la variation de l'intensité de fluorescence ou de phosphorescence du PA. Cette réaction de désactivation obéit à la loi de Stern-Volmer: $\mathbf{1/\tau_s = 1/\tau_s^0 + k_q . [Q]}$ ([Q] représente la concentration du quencher).

3. Type de photoamorceurs

Le mécanisme ainsi que le type de processus de polymérisation dépendent fortement de la nature des espèces réactives générées au cours de l'amorçage, et la nature des monomères à polymériser (acrylate, méthacrylate, époxyde…). De ce fait, il existe trois types de polymérisation en chaîne : Radicalaire, cationique et anionique. La photopolymérisation radicalaire et cationique sera au cœur de nos travaux de recherche puisque la polymérisation anionique est faiblement décrite au niveau industriel. Ces deux types de polymérisation possèdent différentes caractéristiques qui affectent fortement les propriétés finales du polymère obtenu **(Tableau 1) :**

Tableau 1 : Différences entre le processus de polymérisation radicalaire et cationique.

Caractéristiques	***Type de polymérisation et photoamorceur***	
	Radicalaire (FRP)	***Cationique (CP)***
Choix en amorceurs	Important	Limité
Nature des centres actifs	Radicaux	Cations, acides

Vitesse de la réaction	Très rapide	Lente à modérée
Sensibilité	à l'oxygène: très sensible à l'humidité: non sensible	à l'oxygène: non sensible à l'humidité: très sensible
Propriétés finales du polymère	Retrait important	Faible retrait

Dans le premier et deuxième chapitre de cette partie, la photopolymérisation radicalaire (FRP) et cationique (CP) seront détaillées. Le troisième chapitre est dévolu à la polymérisation hybride d'un mélange de deux monomères différents (Acrylate et époxydes) pour la formation de Réseaux Polymères Interpénétrés (RIP ou IPN).

Références

[1] Wayne, R.P. Principles and applications of photochemistry. Oxford science and publications, Oxford, **1988**.

[2] Turro, N.J. Modern Molecular Photochemistry. Benjamin, New York, **1978** and **1990**.

[3] Thèse Henry, I. Synthèse et polymérisation de polyuréthanes acrylates à base de polybutadiène hydroxytéléchélique morphologie et propriétés. INSA Lyon, **1998**.

[4] Garra, P.; Dumur, F.; Morlet-Savary, F.; Dietlin, C.; Fouassier, J.P.; Lalevée, J. A New Highly Efficient Amine-Free and Peroxide-Free Redox System for Free Radical Polymerization under Air with Possible Light Activation, Macromolecules, **2016**, 49, 6296.

[5] Fouassier J.P.; Lalevée J. Photoinitiatorsfor Polymer Synthesis: Scope, Reactivity and Efficiency. Wiley-VCH Verlag GmbH & Co. KGaA. **2012**.

Chapitre I : la Photopolymérisation Radicalaire (FRP)

1. Introduction

Les processus de polymérisation photoinduite sont toujours en évolution rapide et touchent de plus en plus les industries souhaitant l'élaboration de matériaux écologiques et à faible coût, surtout avec les évolutions technologiques développées telles que les dispositifs d'irradiation à base de LEDs. Parmi ces processus, le procédé de photopolymérisation radicalaire demeure le plus répandu par rapport aux autres types de photopolymérisation (Cationique, anionique…) **[1-3]**, puisqu'il offre l'accès à un grand nombre de polymères avec des propriétés très variées.

Ce processus met en jeu des espèces réactives radicalaires générées par un photoamorceur suite à une excitation lumineuse. Ces radicaux formés peuvent réagir facilement avec les doubles liaisons des fonctions (méth)acrylates pour amorcer la photopolymérisation radicalaire qui est considérée comme procédé très efficace pour la synthèse des matériaux polymères hautement réticulés (réseau 3D) par polymérisation de monomères multifonctionnels **(>2)**. Par ailleurs, de nombreux avantages et bénéfices font de ce type de polymérisation le plus utilisé : (1) la rapidité du processus, (2) l'insensibilité a l'humidité, (3) les propriétés de polymères obtenus (résistance chimique et thermique, rigidité), (4) large choix de monomère **[4].** De ce fait, les photopolymères obtenus par voie radicalaire entrent dans diverses applications industrielles : les revêtements, les encres, la dentisterie, l'impression 3D, les composites…

Comme déjà évoqué, notre travail est dévolu à l'étude de nouveaux systèmes photoamorceurs, il est donc centré sur l'étape d'amorçage. Ainsi, il est nécessaire de classifier les photoamorceurs mais il est aussi indispensable de mentionner les monomères photopolymérisables pour chaque type de polymérisation.

2. Les résines photopolymérisables

De nos jours, les résines radicalaires à base de (méth)acrylates dominent le marché malgré l'existence d'une large gamme de monomère telle que : les vinyles, les esters, les styrènes, les uréthanes. Le choix de monomères (structure et fonctionnalité) dans le processus de polymérisation contrôle les propriétés chimiques et mécaniques finales des polymères obtenus, de sorte que des matériaux élastomériques seront obtenus avec des chaînes

aliphatiques, des polymères durs seront produits avec des chaînes aromatiques. En effet, des polymères souples sont souvent obtenus pour des monomères monofonctionnels, d'autres rigides et dures (fortement réticulés) sont produits avec des monomères multifonctionnels. En fait, la dureté, l'élasticité ainsi que la résistance à l'abrasion **[4]** font des (méth)acrylates la famille la plus utilisée dans différentes applications (vernis, bois…). Les monomères les plus couramment incorporés dans les formulations photosensibles sont représentés dans le **Tableau 1.**

Tableau 1: Quelques exemples de monomères radicalaires.

Monomère	Fonctionnalité	Nom
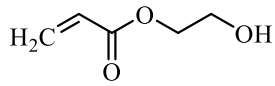	1	*2-Hydroxyéthyl acrylate* ***(HEA)***
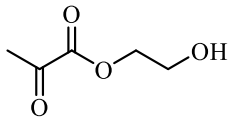	1	*2-Hydroxyéthyl méthacrylate* ***(HEMA)***
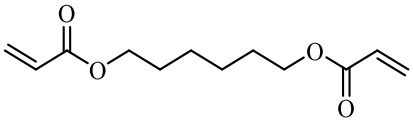	2	*Hexanedioldiacrylate* ***(HDDA)***
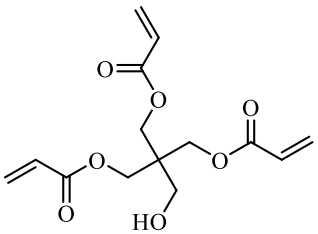	3	*Pentaérythritoltriacrylate* ***(PETIA)***
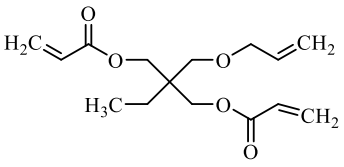	3	*Triméthylolpropane triacrylate* ***(TMPTA)***
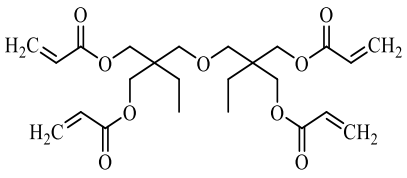	4	Di(triméthylolpropane)tetraacrylate **(TA)**

Durant ces trois années de thèse, nous nous sommes intéressés à l'utilisation des monomères acryliques multifonctionnels, qui ont la capacité de générer des réseaux polymères hautement réticulés, tels que : **(1)** Triméthylolpropane triacrylate **TMPTA (trifonctionnel)**, **(2)** Di (trimethylolpropane) tetraacrylate **TA (tetrafonctionnel).** D'autre part, un mélange de trois monomères méthacryliques (**Mix-MA)** a été utilisé **:** Uréthane diméthacrylate (**UDMA)**, butanediol diméthacrylate **(BDDMA)** et l'hydroxypropyl méthacrylate (**HPMA**). Par ailleurs, le polyéthylèneglycol diacrylate **(PEGDA)** a été également utilisé comme monomère acrylique pour la polymérisation dans l'eau et la formation d'hydrogel **(Schéma 1).**

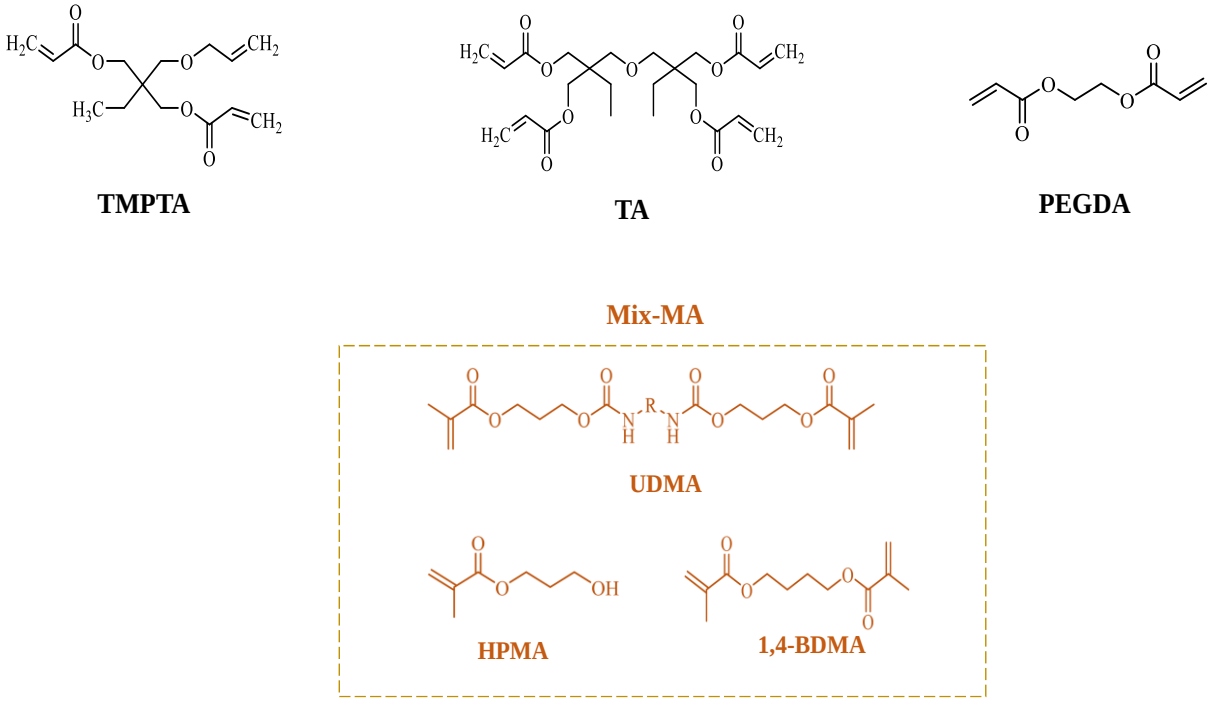

Schéma 1. Monomères (méth)acryliques utilisés dans ce travail.

3. Mécanismes réactionnels

La photopolymérisation radicalaire est un procédé de synthèse où une résine liquide se solidifie en un matériau sous l'effet de la lumière par l'intervention des espèces radicalaires actives. Ce processus suit le même mécanisme qu'une polymérisation thermique traditionnelle, avec une différence notable au niveau de l'étape d'amorçage où les radicaux sont produits par voie photochimique. Ainsi la polymérisation radicalaire photoinduite est divisée principalement en trois étapes: l'amorçage, la propagation et la terminaison.

La forte réactivité des radicaux générés vis-à-vis de l'oxygène de l'air représente un frein majeur à ce type de polymérisation. Ce problème ainsi que les solutions proposées pour en remédier seront traités dans les parties qui suivent.

3.1. Photoamorçage

Cette étape est divisée en deux processus qui seront à l'origine de l'amorçage de la polymérisation :

- ***Génération des radicaux primaires par décomposition du PA***

La compatibilité entre le spectre d'émission des dispositifs d'irradiation et le spectre d'absorption du photoamorceur impliqué dans la réaction représente un paramètre très important dans la génération des radicaux. Une fois excité (S_1 ou T_1), le PA peut subir soit une coupure homolytique d'une liaison chimique **(PA Type I)**, soit un transfert d'électron et/ou arrachement d'hydrogène **(PA Type II)** en présence d'une autre molécule (additif ou un co-amorceur). Par ailleurs, un photosensibilisateur **(PS)** sera incorporé dans la résine photosensible dans le cas où le PA n'absorbe pas la lumière incidente, ainsi le PS absorbe l'énergie lumineuse et la transfert vers le PA qui va lui-même générer les radicaux primaires **($R^{\bullet}$).**

$PA \rightarrow PA^{*} \rightarrow R^{\bullet}$ **(Type I)**

$PA \rightarrow PA^{*}$ **+ coamorceur** $\rightarrow R^{\bullet}$ **(Type II)**

- ***L'amorçage : addition des radicaux primaires sur les insaturations***

Les radicaux primaires produits réagissent efficacement avec les fonctions réactives du monomère utilisé, le macroradical **($RM^{\bullet}$)** ainsi formé aura la capacité de propager le processus de polymérisation en chaîne par additions successives d'autres unités monomères.

3.2. Propagation

Cette étape est définie comme étant l'addition successive des unités monomères sur le premier macroradical formé jusqu'à la formation d'un macroradical **($RM_n^{\bullet}$).** Ces réactions sont très rapides et conservent le même nombre de radicaux générés. Les réactions de propagations sont très rapides, mais une diminution de la vitesse de polymérisation est observée à la fin de la réaction avec la consommation du monomère ainsi que l'augmentation de la viscosité du milieu réactionnel.

3.3. Terminaison

Dans cette étape, le centre actif de polymérisation est complètement consommé ce qui entraine un arrêt de croissance des chaînes polymères actives. Cette réaction se fait essentiellement par voie **bimoléculaire** (Recombinaison ou dismutation).

i) Recombinaison

Ce processus se produit par une recombinaison entre deux macroradicaux en croissance aboutissant à la formation d'une liaison covalente simple. Ce mode augmente la longueur des chaînes polymères obtenues. Moins les chaînes en croissance sont substituées (faible encombrement stérique), plus la probabilité pour une terminaison par recombinaison est élevée.

$$RM_m^{\bullet} + RM_n^{\bullet} \rightarrow RM_{(n+m)}$$

ii) Dismutation

Ce mode de terminaison aura lieu par capture d'un hydrogène par le radical en croissance et formation d'une instauration en position terminale. Dans ce cas il n'y aura pas un doublement de la longueur de chaîne.

$$RM_m^{\bullet} + RM_n^{\bullet} \rightarrow RM_{n(-H)} + RM_{m\,(+H)}$$

Un autre mode de terminaison peut aussi entrainer la disparition du centre actif : la terminaison **Monomoléculaire.** Ce mode aura lieu lorsque le milieu réactionnel devient très visqueux, la diffusion du monomère vers les radicaux actifs ne sera alors plus possible. Ainsi les chaînes polymères en croissance se trouvent piégées dans la matrice polymère.

4. Les systèmes photoamorceurs conventionnels

Selon la réactivité de leur état excité, autrement dit selon le mécanisme de génération des espèces réactives, les PA sont principalement classés en deux grandes familles : **PA Type I** et **PA Type II [5].**

En fait, la majorité des photoamorceurs conventionnels sont hautement sensibles à la lumière UV. Par ailleurs, certaines cétones aromatiques, cétocoumarines et thioxanthones ont leur spectre d'absorption plus décalé dans le visible.

4.1. Photoamorceurs Type I

Ce sont des systèmes qui procèdent par coupure unimoléculaire suite à une absorption lumineuse. C'est une réaction photochimique très utile pour générer des radicaux libres susceptibles d'amorcer une réaction de photopolymérisation, car c'est un processus très efficace.

Les cétones aromatiques, notamment les dérivés d'acétophénone constituent la famille la plus fréquente des PA Type I. D'autres PA Type I efficaces existent déjà : les dérivés des éthers de benzoïne, les cétones halogénées, les esters sulfoniques de cétone, les dérivés de thiobenzoate, et les oximes-esters **[6-9]**. La coupure homolytique s'effectue généralement en α ou β de la cétone aromatique. Ce processus conduit à la formation de deux radicaux libres suite à une absorption lumineuse dans la zone UV du spectre électromagnétique, soit par :

- **Coupure de la liaison en position α par rapport au carbonyle**

Les dérivés des éthers de benzoïne constituent une famille hautement sensible à la lumière UV et amorcent efficacement la polymérisation radicalaire des acrylates. Le 2,2-Diméthoxy-2-phénylacétophénone **(DMPA)** est l'un de ces dérivés, il conduit à un durcissement rapide des résines (méth)acryliques). Une fois excité, ce composé subit une scission homolytique en α de carbonyle et aboutit à la formation de deux radicaux : le radical benzoyle et le radical acétal **[10]**. En effet, le premier est bien connu pour sa réactivité envers les acrylates, tandis que le deuxième est dépourvu d'une activité d'amorçage importante **(Schéma 2)**.

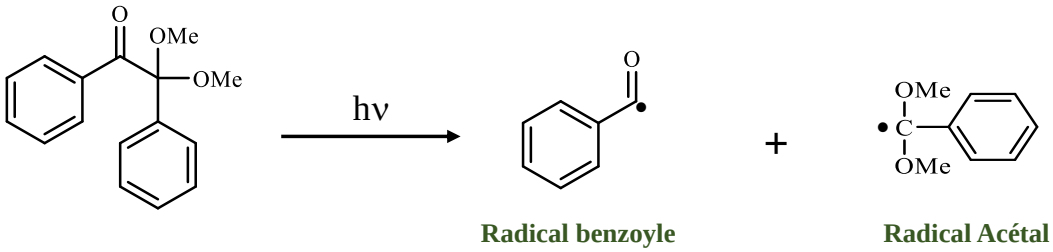

Schéma 2. Coupure en α du 2,2-Diméthoxy-2-phénylacétophénone.

L'avantage principal de la rupture en α est sa faible sensibilité au dioxygène de l'air puisque la durée de vie de l'état excité triplet du DMPA est très faible et par conséquent la désactivation triplet-triplet par l'O_2 est presque négligeable. Cependant, les radicaux primaires générés ainsi que les macroradicaux restent eux sensibles.

- **Coupure de la liaison en position β par rapport au carbonyle**

C'est le cas des cétones aromatiques halogénées qui peuvent facilement subir une rupture de la liaison en position β du carbonyle et génèrent des radicaux phénacyles et des radicaux halogènes **(Schéma 3).**

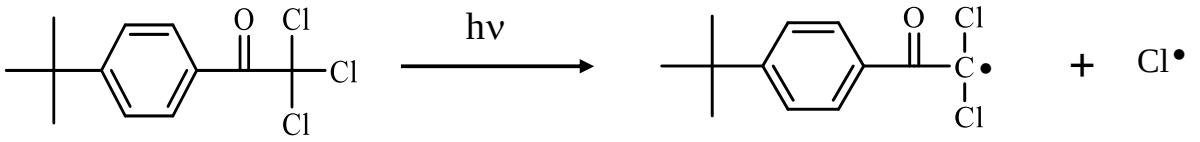

Schéma 3. Scission homolytique en β de la 2,2,2 - trichlorotertiobutylacétophenone

4.2. Photoamorceurs Type II

Certaines cétones aromatiques ne sont pas capables de subir une rupture unimoléculaire suite à une absorption lumineuse, et réagissent ainsi en deux étapes successives en présence d'une autre molécule (Co-amorceur) qui favorise la génération des radicaux libres. La thioxanthone (ITX), la benzophenone (BP), la camphorquinone (CQ) constituent les familles principales des photoamorceurs organiques Type II **[11-14].** La majorité de ces composés possèdent une gamme d'absorption qui se limite à la zone UV, cependant, la camphorquinone et l'anthraquinone absorbent fortement dans le visible **(Schéma 4).**

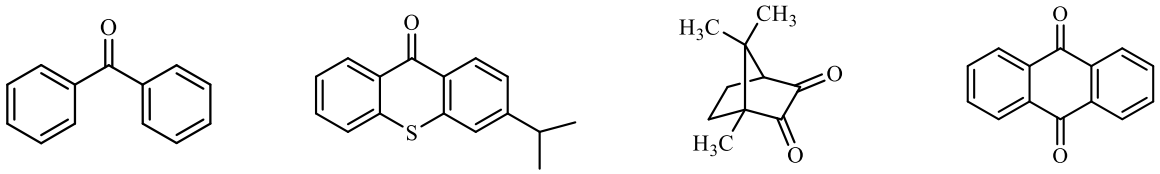

Benzophénone **(BP)** | 2-Isopropylthioxanthone **(ITX)** | Camphorquinone **(CQ)** | Anthraquinone (AQ)

Schéma 4. Exemples de Photoamorceurs de Type II

Selon l'interaction mise en jeu avec le co-amorceur, les photoamorceurs réagissant à partir de leur état excité (souvent triplet) suivant généralement deux mécanismes :

i) Un mécanisme d'arrachement d'hydrogène qui aura lieu en présence d'un donneur d'hydrogène tel que : les alcools, les éthers (ou thiols), les thioéthers.

ii) Un mécanisme par transfert d'électrons suivi de proton qui nécessite la présence d'un donneur d'électron portant un hydrogène labile : les amines (aromatiques et aliphatiques).

- **Mécanisme d'arrachement d'hydrogène**

Ce processus d'amorçage se fait en une seule étape : transfert d'hydrogène entre le photoamorceur et le donneur d'hydrogène menant à la formation de deux radicaux. Les dérivés de thioxanthone et de benzophénone excités dans leur états triplet réagissent efficacement avec un co-amorceur donneur d'hydrogène (alcools, éthers…) pour former un radical cétyle et un radical alkyle issu du co-amorceur **(Schéma 5).** Ce dernier est responsable de l'amorçage de la polymérisation radicalaire, tandis que le radical cétyle (fortement stabilisé par délocalisation électronique) est dépourvu d'une activité d'amorçage et sera consommé par réaction de terminaison avec les chaînes macromoléculaires en croissance **[13,15]**.

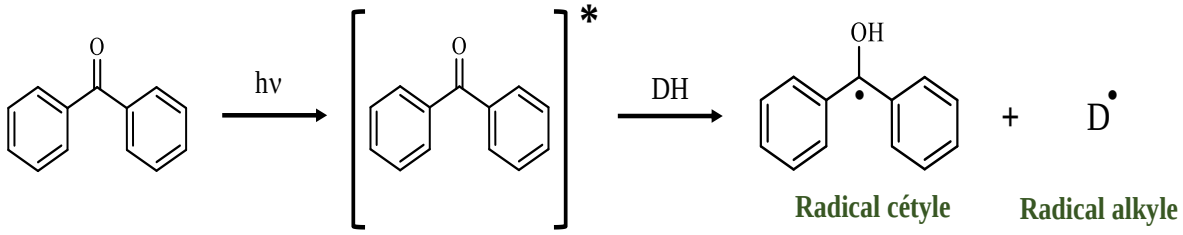

Schéma 5. Formation des radicaux par un processus d'arrachement d'hydrogène

- **Mécanisme de transfert d'électron suivi de proton**

Une fois excité par absorption d'une énergie lumineuse, le PA subit un transfert d'électron avec le co-amorceur qui est généralement une amine. Ce transfert d'électron est à l'origine d'un exciplexe qui se désactive par transfert de proton aboutissant ainsi à la formation de deux radicaux : Cétyle et Aminoalkyle **(Schéma 6)**. Le premier intervient dans la réaction de terminaison de la polymérisation radicalaire, tandis que le deuxième est considéré comme l'agent d'amorçage de la polymérisation.

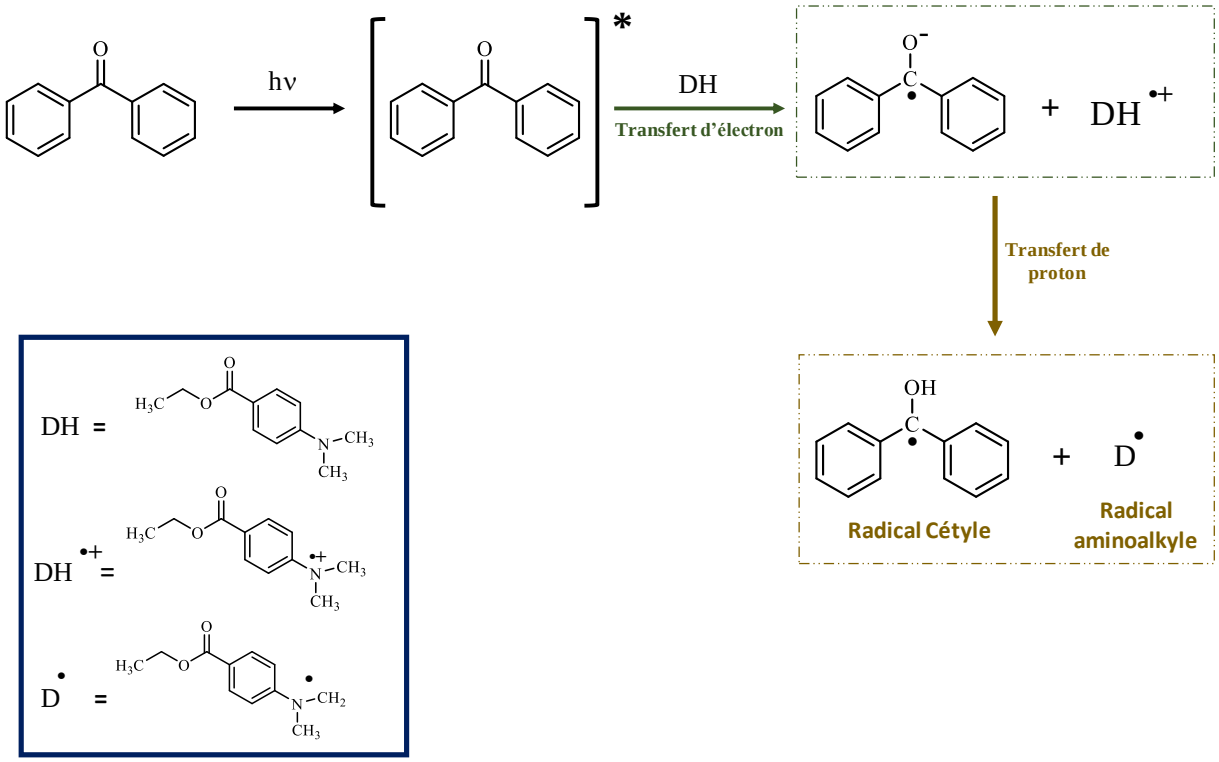

Schéma 6. Formation des radicaux à partir de la benzophénone (PA Type II) par un mécanisme de transfert d'électron suivi de proton.

Ce transfert d'électron entre le donneur et l'accepteur d'électrons obéit à l'équation de Rhem-Weller à partir de laquelle on peut calculer l'énergie libre **(ΔG)** pour la réaction :

$$\Delta G_{et} = E_{ox} - E_{red} - E^{*} + C \qquad \textbf{(Eq 1)}$$

Comme déjà évoqué, les co-amorceurs utilisés dans ce type de processus sont des amines secondaires ou tertiaires (aliphatiques ou aromatiques) qui réagissent fortement selon un mécanisme de transfert d'électron suivi de proton avec les PA Type II. Ils sont largement utilisés dans le domaine de photopolymérisation aux niveaux académique et industriel **[16].** La N-phénylglycine (dérivé d'acide aminé), l'éthyle 4-(diméthylamino) benzoate (EDB), la méthylediéthanol amine (MDEA), la diméthylaniline (DMA) sont les amines les plus utilisées comme co-amorceurs par transfert d'électron **(Schéma 7).**

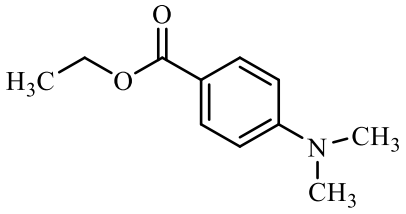

EDB

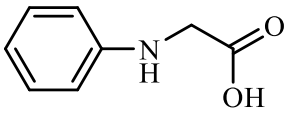

NPG

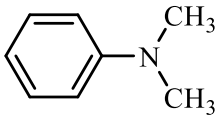

DMA

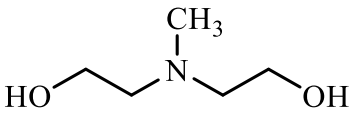

MDEA

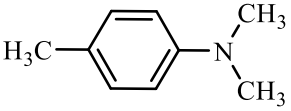

4-N,N,TMA

Schéma 7. Exemples de différentes amines comme co-amorceurs.

Comme exemple de ce type de photoamorceurs, on peut citer la camphorquinone, la benzophénone **(Schéma 4)** ou l'éosine Y **(Schéma 8).**

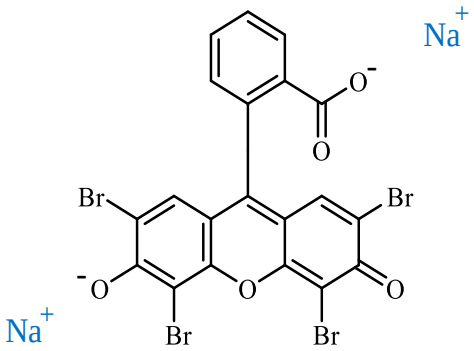

Eosine Y

Schéma 8. PA avec un mécanisme de transfert d'électron suivi de proton.

Les amines ainsi utilisées sont capables de réduire l'inhibition par l'oxygène observé, lors de la polymérisation radicalaire. Les radicaux aminoalkyles générés durant l'amorçage réagissent efficacement avec les molécules d'O_2 présentes dans le milieu réactionnel en évitant la destruction des sites actifs des chaînes de polymères en croissance.

5. Limitation de la Photopolymérisation Radicalaire (FRP)

Comme toute réaction chimique, le processus de photopolymérisation radicalaire est accompagné par de nombreux désavantages qui influencent les propriétés finales de matériaux synthétisés.

5.1. Inhibition par l'oxygène

Le processus de photopolymérisation radicalaire est fortement perturbé par la présence de l'oxygène de l'air dans le milieu réactionnel, de sorte que les radicaux amorceurs générés par le PA entrent en compétition avec la désactivation bimoléculaire par l'O_2 **(Schéma 9).** D'autres processus de désactivation peuvent être observés (désactivation par un Quencher, par le monomère…)

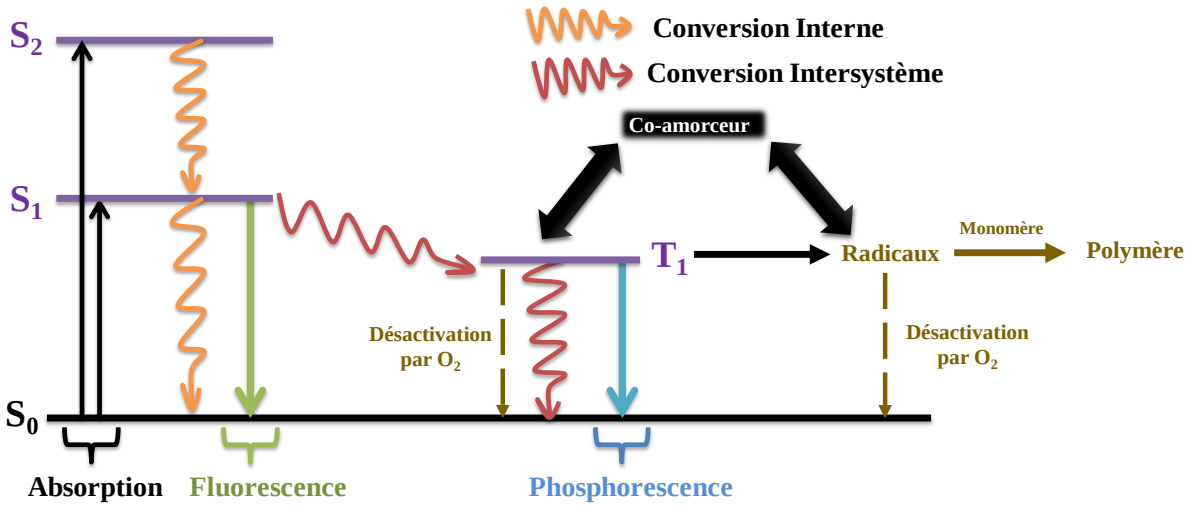

Schéma 9. Différentes voies de désactivation d'un PA excité.

La forte réactivité de l'oxygène vis-à-vis des radicaux ainsi que des états excités du PA est à l'origine de cet effet inhibiteur. En fait, l'oxygène est une molécule diatomique paramagnétique qui possède deux électrons non appariés, elle existe donc sous forme triplet à l'état fondamental **(multiplicité de spin = 3)**. Cette structure électronique, confère à l'oxygène un pouvoir désactivateur favorisant le croisement intersystème de l'état triplet à l'état singulet du PA. Il peut aussi réagir par un transfert d'énergie en provoquant la désactivation du PA excité vers l'état fondamental.

La présence de l'oxygène dans la formulation photosensible implique une période d'induction durant laquelle la consommation d'O_2 est nécessaire pour démarrer la

polymérisation, ce qui implique une perturbation de la cinétique de polymérisation. Physiquement, l'O_2 désactive les états excités singulets et triplets du PA, engendrant leur retour à l'état fondamental, ainsi le rendement quantique en radicaux est fortement affecté. D'autre part, la forte réactivité de l'O_2 contre les radicaux, désactive ces derniers ainsi que les chaînes de polymères en croissance aboutissant à la formation des radicaux péroxyles **($ROO^{\bullet}$ et $RM_nOO^{\bullet}$)** inactifs vis-à-vis des fonctions (méth)acrylates **[17-20]** ce qui provoque une baisse de la vitesse de polymérisation ainsi qu'un faible taux de conversion finale en fonctions réactives (voire même une réduction de la longueur de chaîne polymère). Par ailleurs, la forte présence de l'O_2 en surface, conduit également à des surfaces collantes (cas des revêtements). À noter que l'épaisseur de l'échantillon et la viscosité de la résine polymérisable jouent un rôle très important en diminuant ou augmentant le phénomène d'inhibition par l'oxygène. Par exemple une polymérisation plus performante est observée dans les échantillons épais et les résines visqueuses puisque le processus de réoxygénation est potentiellement lent **[21].**

Les différents effets néfastes de l'inhibition par l'oxygène (faible taux de conversion, surfaces collantes, l'apparition d'une période d'induction) ont été mis en évidence en utilisant la Spectroscopie Infrarouge à Transformée de Fourier en Temps Réel (RT-FTIR) **[22-24].**

Mais la question que se pose : **Comment peut-on remédier aux inconvénients liés à la présence de l'oxygène ?**

En fait, différentes stratégies ont été adoptées pour pallier cette inhibition, parmi lesquelles on cite :

- Augmenter l'intensité de la LED utilisée, ou utiliser des pourcentages élevés en PA afin d'augmenter la réactivité intrinsèque du système amorceur (le rendement quantique en espèces réactives augmente) **[25,26].**
- Le travail sous atmosphère inerte en purgeant la formulation photosensible avec un gaz inerte tel que : l'azote **[27],** le dioxyde de carbone **[28]** et l'argon. Mais à l'échelle industrielle ceci nécessite des installations encombrantes et coûteuses. Pour cela, de nouveaux systèmes PA Type I à base d'oximes-esters ont été développés. Ces composés libèrent des molécules CO_2 lors du processus de photopolymérisation, diminuant ainsi l'inhibition par l'oxygène **[29,30].**
- La manipulation dans des conditions laminées en utilisant des films de polypropylène comme barrière (la diffusion d'O_2 dans la formulation diminue) **[31].**

- L'incorporation dans la résine photosensible d'additifs tels que les amines **[32],** les thiols etc… qui seront capables de consommer l'oxygène présent dans la résine.
- L'ajout dans la formulation contenant le système PA, des composés phosphorés tels que les phosphates ou les phosphines (triphénylphosphine) **[33-35]** qui sont capables de piéger les radicaux péroxyles et les convertir en radicaux actifs **(Schéma 10)**. Les silanes, amines, boranes peuvent aussi jouer ce rôle **[36,37].**

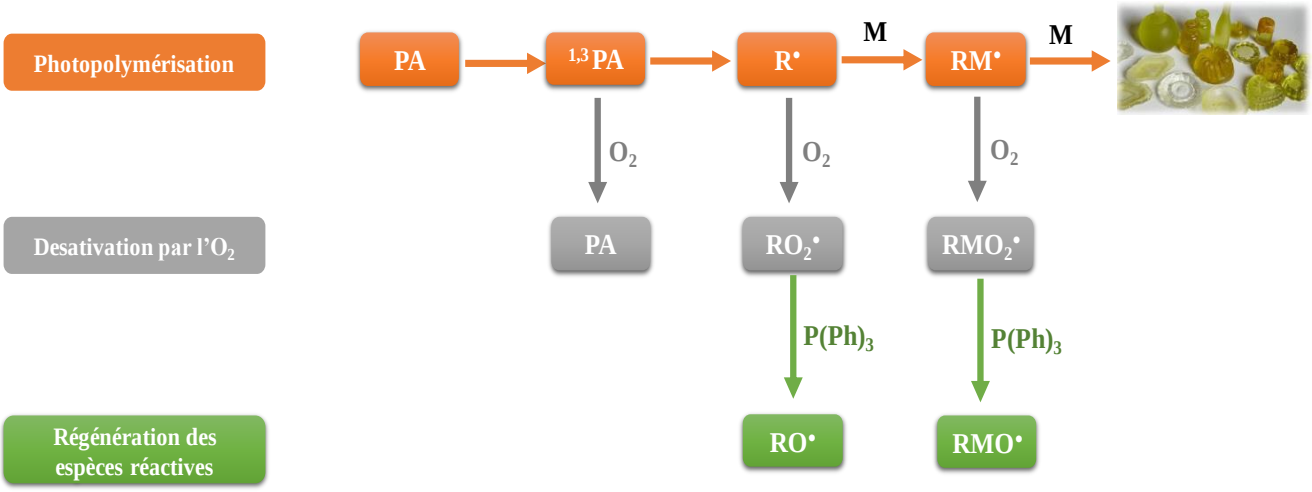

Schéma 10. Processus de Photopolymérisation Radicalaire, désactivation par l'O_2 et régénération de radicaux amorceurs.

5.2. Le retrait

Un deuxième inconvénient majeur de la polymérisation radicalaire est le phénomène de retrait qui peut varier entre 5 et 15% pour les acrylates multifonctionnels **[38].** Ce processus affecte fortement les propriétés finales du polymère obtenu. Par exemple sur le revêtement, les contraintes et défauts provoqués par le retrait peuvent être importants (fissuration, délaminage). Les objets obtenus par impression 3D peuvent également être modifiés, ce qui présente un grand inconvénient pour certaines applications (restauration dentaire…).

Généralement, ce phénomène est dû à une forte réticulation du système qui entraine une réduction de la distance intermoléculaire entre les unités de monomères. En fait, les unités de monomères, avant polymérisation, sont séparées les unes des autres par des liaisons Van der Waal's. Une fois l'irradiation lancée, la résine photopolymérisable durcit, les doubles liaisons portées par le monomère se convertissent en simples liaisons. Cette conversion aboutit à une diminution de la distance entre les motifs monomères polymérisés. C'est l'exemple de

l'éthylène, où la distance entre deux molécules vaut 3.4Å, tandis que deux atomes de carbone adjacents dans une chaîne polymère sont séparés d'une distance de 1.54Å **[39] (Schéma 11).**

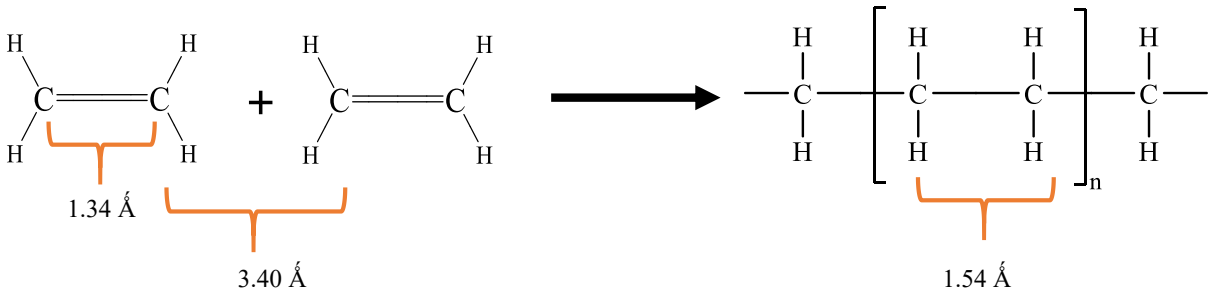

Schéma 11. Phénomène de retrait.

Le problème de 'Shrinkage' ou le retrait représente un grand défi dans les recherches actuelles, par ailleurs ce phénomène peut être résolu en diminuant la densité C=C par incorporation des charges dans la résine ou même en utilisant des structures optimisées de monomères **[40]**. Une autre solution réside par polymérisation hybride d'un mélange de deux monomères différents (acrylates et époxydes) aboutissant à la formation de Réseau Polymères Interpénétrés (RIP ou IPN), ce réseau est le résultat d'une polymérisation radicalaire et cationique qui induit moins de retrait que la polymérisation des acrylates seuls **[41].**

6. Photopolymérisation Radicalaire dans des conditions douces

De nos jours, les processus de durcissements photoinduits sont réalisables avec le développement de nouveaux dispositifs d'irradiation (Diodes Electroluminescentes LEDs) capable d'émettre de la lumière visible. Par ailleurs, le spectre d'absorption des photoamorceurs commerciaux est souvent limité à la zone UV qui nécessite l'utilisation de dispositifs émettant une lumière connue par sa nocivité, sa faible pénétration dans les échantillons épais, et de telles sources sont assez énergivores.

Pour cela, différentes stratégies ont été adoptées afin d'assurer la transition de l'irradiation UV vers le visible :

- L'incorporation dans la résine photosensible d'un photosensibilisateur capable d'absorber la lumière visible et la transmettre vers le système PA par un processus de transfert d'énergie.
- Décaler le spectre d'absorption d'un **photoamorceur UV** vers le **visible** en modifiant sa structure par l'ajout d'un groupe chromophore.

- Le développement de nouveaux systèmes photoamorceurs ayant de bonnes propriétés d'absorption dans le visible (colorants organiques)

6.1. Dérivés de Photoamorceurs UV

Comme déjà été mentionné dans la **partie 4,** les cétones aromatiques (Benzophénone, thioxanthone etc.) constituent une famille des PA de Type I et de Type II qui est largement utilisée dans les réactions de durcissement des acrylates. Vu leur incapacité à amorcer la polymérisation sous lumière visible, ces composés ont été modifiés par ajout des groupements chromophores pour qu'ils puissent absorber dans la zone visible.

Le truxène et le pyrène sont les groupements les plus utilisés pour modifier la photochimie de la benzophénone. Ainsi, les dérivés tels que : Benzophenone-di-1,3-dioxane **(BP-DDO) [42]** et 5-Benzoyl-13-Piperidino-2,1-([1,8]Naphthalenomethano)-1H-Benzoimidazole-16-One **(BPD5) [43],** ont montré de bonnes propriétés d'absorption dans le proche-UV et le visible ainsi que de bonnes performances en FRP.

D'autre part, des groupes alkyles et/ou halogénés ont été incorporés sur les thioxanthones pour décaler leur spectre d'absorption dans le visible **[44-48].**

6.2. Photoamorceurs pour la polymérisation dans le visible.

La limitation des photoamorceurs UV, implique la recherche et le développement de nouveaux systèmes PA sensibles à la lumière visible. Actuellement, la camphorquinone **(CQ)** et l'anthraquinone **(AQ)** représentent deux excellents exemples de photoamorceurs commerciaux de Type II ayant une forte capacité à absorber la lumière visible. En fait, de bonnes performances en FRP ont été obtenues en utilisant la **CQ** couplée avec des amines **[49,50],** ce système est principalement utilisé pour les applications dentaires. **L'AQ** et ses dérivés ont également montré une forte capacité d'amorçage de la polymérisation radicalaire **[51,52].** Cependant, la faible disponibilité en photoamorceurs visible exige la recherche et la synthèse de nouvelles molécules (colorants) ayant leurs spectres d'absorption plus décalés dans le visible pour l'élaboration de matériaux polymères en utilisant des dispositifs d'irradiation douce. Les dérivés de l'anthracène **[53]**, de pyrène **[54]** et beaucoup d'autres composés représentent des exemples de colorants développés dans notre laboratoire (Chalcone **[55]**, phénothiazine **[56]**, coumarine **[57]**, naphthalimide **[58]**) **(Schéma 12).**

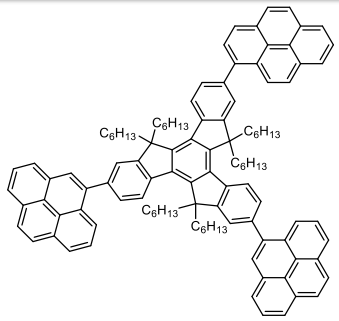

Pyrène

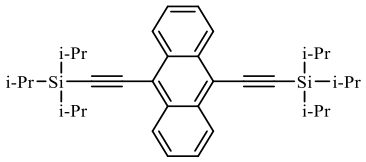

Anthracène

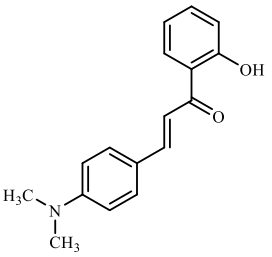

Chalcone

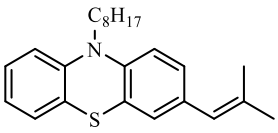

Phénothiazine

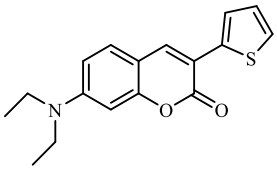

Coumarine

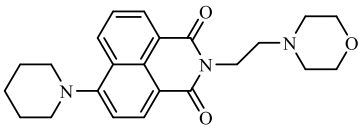

Naphthalimide

Schéma 12. Quelques exemples de colorants organiques utilisés comme PA.

De ce fait, le développement de nouveaux systèmes PA capable d'amorcer la polymérisation radicalaire sous irradiation visible reste toujours un défi majeur pour la synthèse des matériaux polymères moins énergivores. Pour cela, de nombreuses familles de colorants organiques à base de phénothiazine, de coumarine, de naphthalimide… ont été synthétisés et développés dans ce travail de thèse. Ces composés ont montré d'excellentes propriétés d'absorption dans le visible ainsi que de très bons profils de photopolymérisation des acrylates.

6.3. Amorceurs photoredox

Certains photoamorceurs développés durant ces trois années de thèse ont été évalués comme PA photoredox capable de produire des espèces réactives suivant un cycle catalytique de photo-oxydation ou photo-réduction. Ces composés sont très efficaces dans les réactions de polymérisations **[59-61]** et capables en faible quantité d'amorcer le processus de photopolymérisation.

Références

[1] Fouassier, J.P. Photoinitiation, photopolymerization, photocuring : Fundamentals and Applications. Munich : Hanser. **1995**.

[2] Pappas, S.P. UV Curing: Science and Technology. Technology Marketing Corporation, Pub. Division, **1978**, 2, 23.

[3] Crivello, J.V. Photoinitiators for Free Radical Cationic and Anionic Photopolymerization. John Wiley & Sons, Inc, NY and Sita Techn., London, **1998**.

[4] Reiser, A. Photoreactive polymers : The science and technology of resists. John Wiley and Sons, New York. **1989**.

[5] Stöver, H.D.H.; Li, K. In Polymeric Materials Encyclopedia. JC Salamone, Ed; CRC Press: New York, **1996**.

[6] Fouassier, J.P.; Lalevée, J. Photoinitiators for Polymer Synthesis: Scope, Reactivity and Efficiency. Wiley-VCH Verlag GmbH & Co. KGaA. **2012**.

[7] Lee, Z.H.; Hammoud, F.; Hijazi, A.; Graff, B.; Lalevee, J.; Chen Y.C. Synthesis and free radical photopolymerization of triphenylamine-based oxime ester photoinitiators. Polym. Chem. **2021,** 12, 1286.

[8] Liu, S.; Graff, B.; Xiao, P.; Dumur, F.; Lalevee, J. Nitro-Carbazole Based Oxime Esters as Dual Photo/Thermal Initiators for 3D Printing and Composite Preparation. Macromol. Rapid Comm. **2021**, 42, 2100207.

[9] Hammoud, F.; Lee, Z.H.; Graff, B.; Hijazi, A.; Lalevee, J.; Chen Y.C. Novel phenylamine-based oxime-ester photoinitiators for LED-induced free radical, cationic, and hybrid polymerization. J.Polym.Sci. **2021,** 59, 1711.

[10] Mucci, V.; Vallo, C. Efficiency of 2,2-Dimethoxy-2-phenylacetophenone for the Photopolymerization of Methacrylate Monomers in Thick Sections. Journal of Applied Polymer Science. **2012**, 123, 418.

[11] Fouassier, J.P.; Ruhlmann, D.; Graff, B.; Morlet-Savary, F.; Wieder, F. Excited state processes in polymerization photoinitiators. Prog. Org. Coat. **1995**, 25, 235.

[12] Eiselé, G.; Fouassier, J.P.; Reeb, R. Photocrosslinkable paints for crack-bridging applications and anti-soiling properties (renovation of building facades). Angew. Makromolek. Chem. **1999**, 264, 10.

[13] Block, H.; Ledwith, A.; Taylor, A.R. Polymerization of methyl methacrylate photosensitized by benzophenones. Polymer. **1971**, 12, 271-288.

[14] Anderson, D.G.; Davidson, R.S.; Elvery, J.J. Thioxanthones: their fate when used as photoinitiators. Polymer. **1996**, 37, 2477.

[15] Hutchison, J.; Lambert, M.C.; Ledwith, A. Rôle of semi-pinacol radicals in the benzophenone-photoinitiated polymerization of methyl methacrylate. Polymer. **1973**, 14, 250.

[16] Davidson, R.S. Radiation Curing in Polymer Science and Technology. Eds. Fouassier J.P. Rabek J. F. Elsevier, Barking. **1993**.

[17] Fouassier, J.P.; Lalevée. J. Photosensitive systems in Photoinitiators for Polymer Synthesis. Wiley-VCH Verlag GmbH & Co. KGaA, **2012**, 114.

[18] Dietliker, K.A. A compilation of photoinitiators : commercially available for UV today. SITA Technology Ltd.: London, UK, **2002**.

[19] Rabek, J.F. Mechanisms of Photophysical Processes and Photochemical Reactions in Polymers : Theory and Applications. Wiley : Chichester, **1987.**

[20] Lalevée, J.; Allonas, X.; Fouassier, J. P. New Access to the Peroxyl Radicals Reactivity? Chemical Physics Letters. **2007**, 445 (1), 62.

[21] Garra, P.; Morlet-Savary, F.; Dietlin, C.; Fouassier, J.P.; Lalevée. J. On-Demand visible light activated amine/benzoyl peroxide redox Initiating systems: A unique tool to overcome the shadow areas in photopolymerization processes. Macromolecules. **2016**, 49, 9371.

[22] Biswal, D.; Hilt, J.Z. Analysis of Oxygen Inhibition in Photopolymerizations of Hydrogel Micropatterns Using FTIR Imaging. Macromolecules. **2009**, 42, 973.

[23] O'Brien, A.K.; Bowman, C.N. Impact of oxygen on photopolymerization kinetics and polymer structure. Macromolecules, **2006**, 39, 2501.

[24] Feng, L.; Suh, B.I. Acrylic Resins Resisting Oxygen Inhibition During Free-Radical Photocuring. I. Formulation Attributes. J.Appl.Polym.Sci., **2009**, 112, 1565.

[25] Studer, K.; Decker, C.; Beck, E.; Schwalm, E. Overcoming oxygen inhibition in UV-curing of acrylate coatings by carbon dioxide inerting, Part I. Prog.Org.Coat. **2003**, 48, 92.

[26] Awokola, M.; Lenhard, W.; Loffler, H.; Flosbach, C.; Frese, P. UV crosslinking of acryloyl functional polymers in the presence of oxygen. Prog.Org.Coat. **2002**, 44, 211.

[27] Crivello, J.V.; Dietliker, K. Photoinitiators for Free Radical, Cationic and Anionic Photopolymerization, of the Surface Coatings Technology Series, Eds., G. Bradely, John Wiley & Sons, Inc, NY and Sita Techn., London, **1999**, 3.

[28] Schwalm, R. UV Coatings : Basics, Recent Developments and New Applications. Elsevier, Oxford. **2007.**

[29] Liu, S.; Graff, B.; Xiao, P.; Dumur, F.; Lalevee, J. Nitro-Carbazole Based Oxime Esters as Dual Photo/Thermal Initiators for 3D Printing and Composite Preparation. Macromol. Rapid Commun. **2021**, 42, 2100207.

[30] Chen, S.; Jin, M.; Malval, J.P.; Fu, J.; Morlet-Savary, F.; Pan, H.; Wan, D. Substituted stilbene-based oxime esters used as highly reactive wavelength-dependent photoinitiators for LED photopolymerization. Polym.Chem. **2019**, 10, 6609.

[31] Bolon, D.A.; Webb, K.K. Barrier Coats Versus Inert Atmospheres. The Elimination of Oxygen Inhibition in Free-Radical Polymerizations. J.Appl.Polym.Sci. **1978**, 22, 2543.

[32] Decker, C.; Jenkins, A.D. Kinetic approach of oxygen inhibition in ultraviolet- and laser-induced polymerizations. Macromolecules. **1985**, 18, 1241.

[33] Hageman, H.J. Photoinitiators for free radical polymerization. Prog.Org.Coat.,**1985**, 13, 123.

[34] Belon, C.; Allonas, X.; Croutxé-Barghorn, C.; Lalevée. J. Overcoming the Oxygen Inhibition in the Photopolymerization of Acrylates : A Study of the Beneficial Effect of Triphenylphosphine. J.Polym.Sci.,Part A: Polym.Chem. **2010**, 48, 5462.

[35] Baxter, J.E.; Davidson, R.S.; Hageman, H.J. Use of Acylphosphine Oxides and Acylphosphonates as Photoinitiators. Polymer. **1988**, 29, 1569.

[36] Ligon, S.C.; Husár, B.; Wutzel, H.; Holman, R.; Liska, R. Strategies to Reduce Oxygen Inhibition in Photoinduced Polymerization. Chem.Rev. **2014**, 114, 557.

[37] Aubry, B.; Subervie, D.; Lansalot, M.; Bourgeat-Lami, E.; Graff, G.; Morlet-Savary, F.; Dietlin, C.; Fouassier, J.P.; Lacôte, E.; Lalevée, J. A Second-Generation Chameleon N-Heterocyclic Carbene-Borane Co-initiator for the Visible-Light Oxygen-Resistant Photopolymerization of both Organic and Water-Compatible Resins. Macromolecules. **2018**, 51, 9730.

[38] Rudin, A.; Choi, P. Chapter 8 - Free-Radical Polymerization. In The Elements of PolymerScience & Engineering (Third Edition); Rudin, A., Choi, P., Eds.; Academic Press: Boston. **2013**, 341.

[39] Sadhir, R.K.; Luck, R.M. Expanding Monomers: Synthesis, characterization, and applications; CRC press. **1992**.

[40] Schneider, L.F.J.; Cavalcante, L.M.; Silikas, N. Shrinkage Stresses Generated during Resin-Composite Applications: A Review. J.Dent.Biomech. **2010**. 1, 131630.

[41] Harreld, J.H.; Esaki, A.; Stucky, G.D. Low-Shrinkage, High-Hardness, and Transparent Hybrid Coatings : Poly(Methyl Methacrylate) Cross-Linked with Silsesquioxane. Chem.Mater. **2003**, 15, 3481.

[42] Wang, K.; Jiang, S.; Liu, J.; Nie, J.; Yu, Q. Benzophenone-di-1,3-dioxane as a novel initiator for free radical photopolymerization. Prog.Org.Coat. **2011**, 72, 517.

[43] Xiao, P.; Dumur, F.; Graff, B.; Gigmes, D.; Fouassier, J.P.; Lalevée, J. Variations on the Benzophenone Skeleton: Novel High Performance Blue Light Sensitive Photoinitiating Systems. Macromolecules. **2013**, 46, 7661.

[44] Yilmaz, G.; Aydogan, B.; Temel, G.; Arsu, N.; Moszner, N.; Yagci, Y. Thioxanthone−Fluorenes as Visible Light Photoinitiators for Free Radical Polymerization. Macromolecules. **2010**, 43, 4520.

[45] Yilmaz, G.; Beyazit, S.; Yagci, Y. Visible Light Induced Free Radical Promoted Cationic Polymerization Using Thioxanthone Derivatives. Journal of Polymer Science Part A: Pol. Chem. **2011**, 49, 1591.

[46] Tunc, D.; Yagci, Y. Thioxanthone-Ethylcarbazole as a Soluble Visible Light Photoinitiator for Free Radical and Free Radical Promoted Cationic Polymerizations. Pol. Chem. **2011**, 2, 2557.

[47] Balta, D.K.; Temel, G.; Goksu, G.; Ocal, N.; Arsu, N. Thioxanthone–diphenyl Anthracene: Visible Light Photoinitiator. Macromolecules. **2011**, 45, 119.

[48] Tar, H.; Sevinc Esen, D.; Aydin, M.; Ley, C.; Arsu, N.; Allonas, X. Panchromatic Type II Photoinitiator for Free Radical Polymerization Based on Thioxanthone Derivative. Macromolecules. **2013**, 46, 3266.

[49] Ullrich, G.; Herzog, D.; Liska, R.; Burtscher, P.; Moszner, N. Photoinitiators with functional groups. VII. Covalently bonded camphorquinone–amines. J. Polym. Sci. Part A: Pol. Chem. **2004**, 42, 4948.

[50] Jakubiak, J.; Allonas, X.; Fouassier, J.P.; Sionkowska, A.; Andrzejewska, E.; Linden, L.Å.; Rabek, J.F. Camphorquinone-amines photoinitating systems for the initiation of free radical polymerization. Polymer. **2003**, 44, 5219.

[51] Tozuka, M.; Igarashi, T.; Sakurai, T. 1-(Arylmethyloxy)-9,10-anthraquinones: Photoinitiators for Radical and Cationic Polymerizations. Polymer Journal. **2009**, 41, 709.

[52] Pullen, G.K.; Allen, N.S.; Edge, M.; Weddell, I.; Swart, R.; Catalina, F.; Navaratnam S. Anthraquinone photoinitiators for free radical polymerisation: Structure dependence on photopolymerisation activity. Eur.Polym.J. **1996**, 32, 943.

[53] Tehfe, M.A.; Lalevée, J.; Morlet-Savary, F.; Graff, B.; Blanchard, N.; Fouassier, J.P. Organic Photocatalyst for Polymerization Reactions: 9,10-Bis[(triisopropylsilyl)ethynyl] anthracene. ACS Macro. Lett. **2012**, 1, 198.

[54] Tehfe, M.A.; Lalevée, J.; Telitel, S.; Contal, E.; Dumur, F.; Gigmes, D.; Bertin, D.; Nechab, M.; Graff, B.; Morlet-Savary, F.; Fouassier, J.P. Polyaromatic Structures as Organo-Photoinitiator Catalysts for Efficient Visible Light Induced Dual Radical/Cationic Photopolymerization and Interpenetrated Polymer Networks Synthesis. Macromolecules. **2012**, 45, 4454.

[55] Tehfe, M.A.; Dumur, F.; Xiao, P.; Delgove, M.; Graff, B.; Fouassier, J.P.; Gigmes, D.; Lalevée, J. Chalcone Derivatives as Highly Versatile Photoinitiators for Radical, Cationic, Thiol-ene and IPN Polymerization Reactions upon Exposure to Visible Light. Polym.Chem. **2014**, 5, 382.

[56] Abdallah, M.; Bui, T.T.; Goubard, F.; Theodosopoulou, D.; Dumur, F.; Hijazi, A.; Fouassier, J.P.; Lalevée, J. Phenothiazine Derivatives as Photoredox Catalysts for Cationic and Radical Photosensitive Resins for 3D Printing Technology and Photocomposites Synthesis. Polym.Chem. **2019**, 10, 6145.

[57] Abdallah, M.; Hijazi, A.; Graff, B.; Fouassier, J.P.; Rodeghiero, G.; Gualandi, A.; Dumur, F.; Cozzi, P.G.; Lalevée, J. Coumarin derivatives as versatile photoinitiators for 3D printing, polymerization in water and photocomposite synthesis. Polym.Chem. **2019**, 10, 872.

[58] Bonardi, A.H.; Zahouily, S.; Dietlin, C.; Graff, B.; Morlet-Savary, F.; Ibrahim-Ouali, M.; Gigmes, D.; Hoffmann, N.; Dumur, F.; Lalevée, J. New 1,8-Naphthalimide Derivatives as Photoinitiators for Free-Radical Polymerization Upon Visible Light. Catalysts. **2019**, 9, 637.

[59] Rahal, M.; Abdallah, M.; Bui, T.T.; Goubard, F.; Graff, B.; Dumur, F.; Toufaily, J.; Hamieh, T.; Lalevee, J. Design of new phenothiazine derivatives as visible light photoinitiators. Polym.Chem. **2020**, 11, 3349.

[60] Rahal, M.; Graff, B.; Toufaily, J.; Hamieh, T.; Noirbent, G.; Gigmes, D.; Dumur, F.; Lalevee, J. 3-Carboxylic Acid and Formyl-Derived Coumarins as Photoinitiators in Photo-Oxidation or Photo-Reduction Processes for Photopolymerization upon Visible Light: Photocomposite Synthesis and 3D Printing Applications. Molecules. **2021**, 26, 1753.

[61] Rahal, M.; Mokbel, H.; Graff, B.; Pertici, V.; Gigmes, D.; Toufaily, J.; Hamieh, T.; Dumur, F.; Lalevee, J. Naphthalimide-Baed Dyes as Photoinitiators under Visible Light

Irradiation and their applications: Photocomposites synthesis, 3D printing and polymerization in Water. ChemPhotoChem. **2021**, 5, 1.

Chapitre II : Photopolymérisation Cationique (CP)

1. Introduction

Bien que la littérature fait état d'un très grand nombre d'études sur les résines (méth)acrylates photopolymérisées par voie radicalaire, la photopolymérisation cationique (CP) est étudiée depuis plus de 40 ans et est aussi largement utilisée dans les domaines des revêtements, des encres, des adhésifs et des composites. La CP suit le même principe qu'une polymérisation radicalaire mais la différence réside par le choix du monomère et ainsi le choix du système PA. Ce procédé a connu de très grands développements ces dernières années **[1-4].**

Par ailleurs, ce processus se caractérise par l'insensibilité au dioxygène de l'air ce qui présente un avantage majeur (bonne polymérisation sous air) par rapport à la photopolymérisation radicalaire, puisque les espèces réactives mises en jeu lors de l'amorçage photochimique sont des cations, cations radicals ou de l'acide La résistance chimique et mécanique, l'adhésion, la stabilité aux UV et aux intempéries ainsi que le faible retrait **[5,6]** constituent des propriétés attrayantes des polymères générés par voie cationique. La réactivité du système cationique utilisé et les propriétés finales des polymères obtenus dépendent fortement de la structure du monomère choisi, ainsi que la nature du photoamorceur incorporé dans la formulation photosensible.

Contrairement aux processus radicalaires où les espèces réactives peuvent se recombiner au cours de la réaction, les centres actifs cationiques sont incapables de réagir entre eux et possèdent donc un caractère vivant, cette caractéristique permet la poursuite de la polymérisation cationique même après arrêt de l'irradiation en raison de la longue durée de vie des espèces réactives générées : ce phénomène est connu sous le nom **'Post-polymérisation ou Dark polymerization'.** De plus, des épaisseurs plus importantes peuvent être polymérisées grâce à la mobilité des espèces cationiques qui permet d'atteindre des zones inatteignables par le rayonnement incident **[7-10].** En effet, Ficek et al **[11]** ont montré que grâce à la post-polymérisation, il est possible de multiplier par un facteur 10 l'épaisseur polymérisée. Bien que ce soit un avantage majeur surtout dans le domaine de photocomposites, la post-polymérisation a un grand inconvénient parce qu'elle peut affecter la résolution spatiale dans les applications d'impression 3D.

Cependant, le processus de photopolymérisation cationique est fortement sensible à la présence d'impuretés, des espèces nucléophiles ou de l'eau **[12,13]** dans la résine photopolymérisable.

2. les résines photopolymérisables

Généralement, il existe deux grandes familles de résines époxydes :

2.1. Les résines époxydes glycidyléther

Parmi ces résines, le diglycidyl éther de bisphénol A (DGEBA) est le plus utilisé **(Schéma 1).** En fait, les propriétés finales des polymères issus de ce produit dépendent fortement de la valeur de n (nombre d'unités répétitives dans DGEBA). Les groupes aromatiques et hydroxyles du squelette améliorent la résistance thermique et offrent une bonne adhérence au polymère époxy.

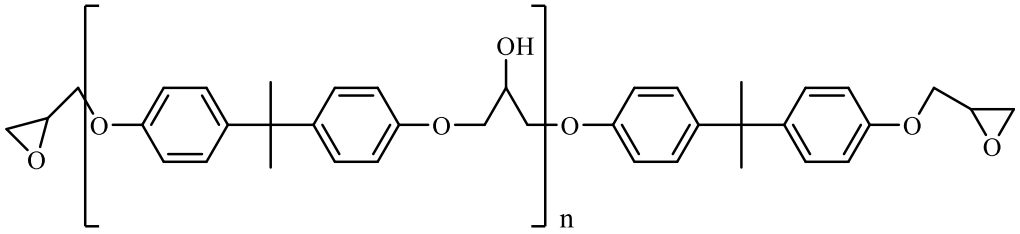

Schema 1. Structure du DGEBA

Il existe également des résines époxydes tétrafonctionnels tel que : le 4,4-tétradiglycidyl diaminophényle (TGDP) et le 4,4-tétradiglycidyl diaminodiphényl méthane (TGDDM) **(Schéma 2)**. Ces composés conduisent à des matériaux aux propriétés mécaniques, thermiques et résistance chimique très intéressantes. Ils sont particulièrement utilisés pour des applications de haute performance **[14,15]**.

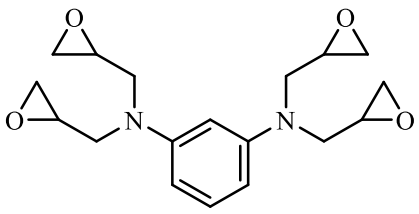

TGDP

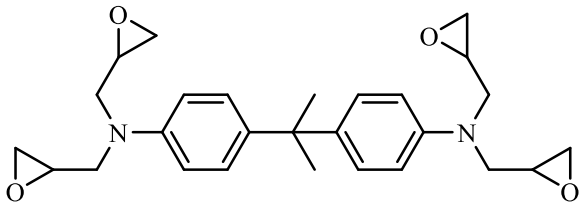

TGDDM

Schéma 2. Structures chimiques de résines époxydes glycidyl éther tétrafonctionnelles.

2.2. Les résines époxydes cycloaliphatiques

L'UVACURE 1500 ou **EPOX (Schéma 3)** est un monomère cationique cycloaliphatique dont le polymère issu de la réaction de durcissement présente une grande stabilité aux UV et une grande résistance thermique. Par ailleurs, l'augmentation de la longueur de la chaîne apporte plus de flexibilité, ce qui augmente la réactivité du système **(Schéma 3) [16].**

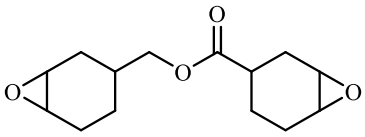

UVACURE 1500
EPOX

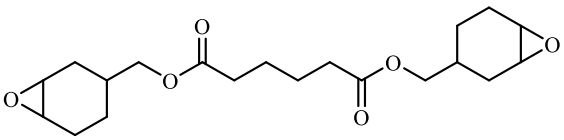

UVR6110

Schéma 3. Structures chimiques de deux résines époxydes cycloaliphatiques

Comme déjà évoqué, la polymérisation des monomères époxydes génère moins de retrait que la polymérisation des résines (méth)acrylates. Concernant les résines époxydes, les monomères cycloaliphatiques présentent un retrait plus faible que leurs homologues glycidyl éther.

3. Photoamorceurs cationiques UV

La photopolymérisation cationique par ouverture de cycle est une réaction en chaîne qui nécessite l'utilisation de photogénérateurs d'acides (PGA) qui ne sont activés que par utilisation des rayonnements UV-C (les plus dangereuses) **[17].** Dans les années 70, la capacité des sels d'onium à générer des acides en solution et par suite amorcer la polymérisation cationique a été mise en évidence par Crivello **[18].** Parmi eux, les sels d'iodonium **[19]** et les sels de sulfonium **[20-22]** avaient la capacité, après absorption d'une énergie lumineuse, de produire des acides de Bronsted responsables de l'amorçage de la CP. Généralement, les sels d'oniums sont constitués d'une partie cationique portée par un atome central chargé positivement, et d'une partie anionique qui constitue le contre-ion **(Schéma 4)**. La partie cationique est responsable de l'absorption lumineuse, alors que le fragment anionique contrôle la force des espèces cationiques générées. D'autre part, la nucléophilie de l'anion associé à la partie cationique contrôle l'efficacité d'amorçage et de propagation (addition du monomère sur le centre réactif) de sorte qu'une conversion finale élevée sera obtenue avec des anions moins nucléophiles **[23,24].**

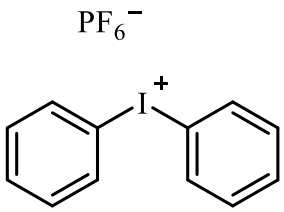

Hexafluorophosphate de Diaryliodonium

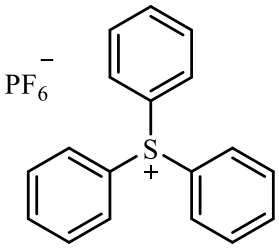

Hexafluorophosphate de Triarylsulfonium

Schéma 4. Structures des sels d'oniums

Cependant, les sels de diaryliodonium possèdent un spectre d'absorption limité à la zone UV (<320 nm), c'est pour cela que l'intérêt des chercheurs s'est orienté vers le développement de nouvelles stratégies pouvant décaler le spectre d'absorption de ces PA vers le proche-UV ou le visible, en introduisant des groupements chromophore à la structure du sel d'onium **[24-29].** D'autres stratégies ont été aussi utilisées avec l'incorporation dans la résine photosensible d'un photosensibilisateur (PS) capable d'absorber dans des domaines plus décalés (visible par exemple). Ce PS provoque la décomposition du sel d'onium soit par transfert d'énergie **[30]** soit par transfert d'électron **[31-35].**

Une autre stratégie prometteuse a été suivie pour surmonter la sensibilité spectrale des PA cationique, elle implique l'utilisation des PA radicalaires classiques qui produisent des radicaux suite à une absorption lumineuse. Les radicaux générés seront oxydés par le sel d'onium et donnent naissance à des espèces cationiques **(R^+)** capables d'amorcer la CP. Ce mode de polymérisation est connu par le nom 'Photopolymérisation cationique sensibilisés par les radicaux' (FRPCP). Ainsi, le choix du système PA contrôle les propriétés d'absorption ainsi que l'efficacité du processus de photopolymérisation cationique. Les oxydes de phosphine et les éthers de benzoïne sont des PA qui peuvent être utilisés dans ce mode de polymérisation. La recherche de nouveaux systèmes PA cationique hautement efficace représente actuellement un grand défi dans le domaine de la photopolymérisation.

Cependant, la FRPCP est fortement inhibée par l'oxygène de l'air **[36-38]** puisque les radicaux formés constituent un intermédiaire principal dans le mécanisme réactionnel de la production des cations. Les stratégies déjà citées auparavant qui visent à diminuer l'inhibition par l'oxygène peuvent également être utilisées afin d'augmenter l'efficacité des systèmes en Photopolymérisation cationique sensibilisée par les radicaux.

4. Mécanismes Réactionnels

4.1. Amorçage

La création des états excités par absorption d'un rayonnement UV ou visible permet la génération des espèces cationiques ou acides par coupure homolytique ou hétérolytique. Ces espèces sont capables d'amorcer la polymérisation cationique des monomères époxydes par activation électrophile du premier motif époxyde. Dans les sels d'iodonium, les acides de Bronsted sont produits par coupure hétérolytique alors que leurs homologues sont produits par une coupure homolytique **(Schéma 5).**

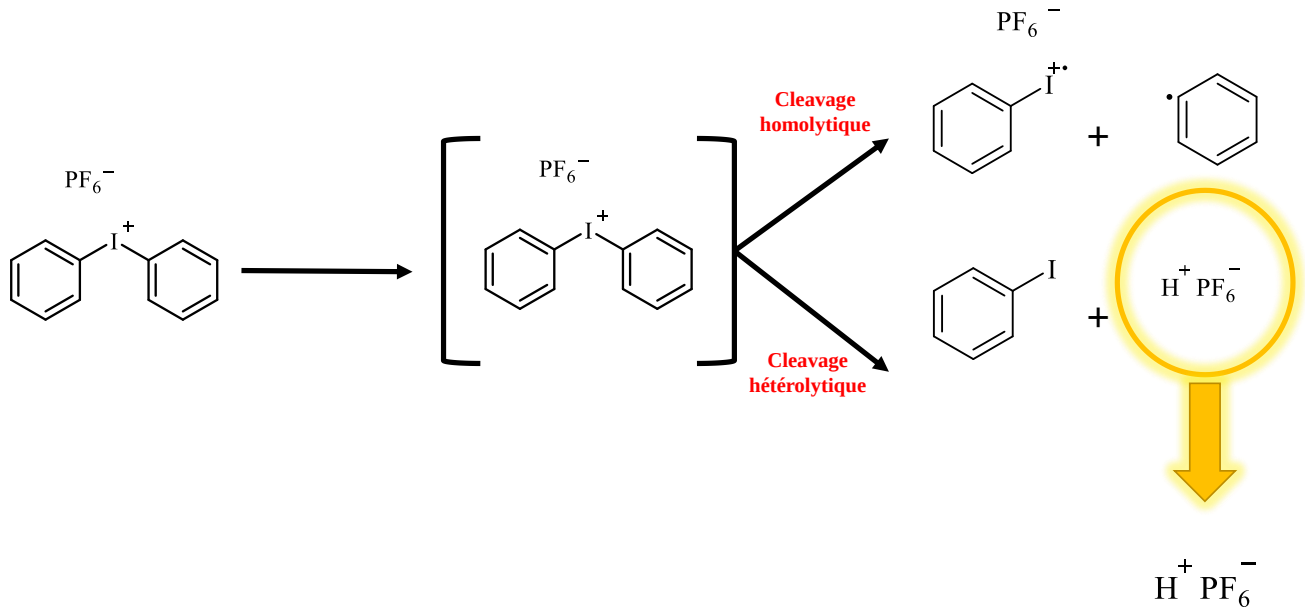

Schéma 5. Formation des espèces cationiques par photolyse du sel d'iodonium.

4.2 Propagation et Terminaison

L'ouverture du cycle époxyde et par suite la propagation de la photopolymérisation cationique se fait par addition successive du monomère cationique. Cette addition suit un mécanisme d'attaque nucléophile (doublet non liant porté par l'atome d'Oxygène du monomère) sur le site électrophile activé par l'acide de Bronsted ou de Lewis. Le caractère vivant de la CP permet d'atteindre de taux de conversion élevés en fonction époxydes et des épaisseurs plus profondes.

Cependant, la présence des impuretés nucléophiles (l'eau) peut fortement désactiver les cations primaires générés ainsi qu'inhiber l'addition de monomères sur le centre actif ce qui limite la polymérisation cationique. Par ailleurs, la formation des cations stables ou des cations fortement encombrés par transfert de chaîne peuvent entrainer également l'arrêt de la croissance des chaînes.

Références

[1] Yagci, Y.; Reetz, I. Externally stimulated initiator systems for cationic polymerization. Prog.Polym.Sci. **1998**, 23, 1485.

[2] Bi, Y.; Neckers, D.C.A. Visible Light Initiating System for Free Radical Promoted Cationic Polymerization. Macromolecules. **1994**, 27, 3683.

[3] Lalevée, J.; Dumur, F.; Mayer, C.R.; Gigmes, D.; Nasr, G.; Tehfe, M.A.; Telitel, S.; Morlet-Savary, F.; Graff, B.; Fouassier, J.P. Photopolymerization of N-Vinylcarbazole Using Visible-Light Harvesting Iridium Complexes as Photoinitiators. Macromolecules. **2012**, 45, 4134.

[4] Liow, S.S.; Lipik, V.T.; Widjaja, L.K.; Abadie, M.J.M. Synthesis, Characterization and Photopolymerization of Vinyl Ether and Acrylate Functionalized Hybrid Oligo-Caprolactone. J.Polym.Res. **2011**, 19, 9748.

[5] Sangermano, M. Advances in cationic photopolymerization. Pure Appl.Chem. **2012**, 84, 2089.

[6] Vitale, A.; Sangermano, M.; Bongiovanni, R.; Burtscher, P.; Moszner, N. Visible light curable restorative composites for dental applications based on epoxy monomer. Materials. **2014**, 7, 554.

[7] Garra, P.; Dietlin, C.; Morlet-Savary, F.; Dumur, F.; Gigmes, D.; Fouassier, J.P.; Lalevée, J. Photopolymerization of thick films and in shadow areas: A review for the access to composites. Polym. Chem. **2017,** 8, 7088.

[8] Bongiovanni, R.; Sangermano, M. UV-curing science and technology. Encycl. Polym. Sci. Technol. **2014,** 1.

[9] Nelson, E.W.; Jacobs, J.L.; Scranton, A.B.; Anseth, K.S; Bowman, C.N. Photodifferential scanning calorimetry studies of cationic polymerizations of divinyl ethers. Polymer. **1995,** 36**,** 4651.

[10] Sipani, V.; Scranton, A.B. Kinetic studies of cationic photopolymerizations of phenyl glycidyl ether: Termination/trapping rate constants for iodonium photoinitiators. J. Photochem. Photobiol. A Chem. **2003,** 159, 189.

[11] Ficek, B.A.; Thiesen, A.M.; Scranton, A.B. Cationic photopolymerizations of thick polymer systems: Active center lifetime and mobility. Eur. Polym. J. **2008,** 44, 98.

[12] Huang, R.; Ficek, B.A.; Glover, S.O.; Scranton, A.B. Effect of Water in Cationic Photopolymerizations: Reversible Inhibition. Rad. Tech. Rep. **2007**, 21, 32.

[13] Kim, D.; Jessop, J.L.P. The role of water in photoinitiated cationic ring-opening photopolymerization of cyclohexane epoxides. USA. Rad. Tech. **2006**.

[14] Park, S.J.; Jin, F.L.; Lee, J.R. Thermal and mechanical properties of tetrafunctional epoxy resin toughened with epoxidized soybean oil. Mater. Sci. Eng. A. **2004**, 374, 109.

[15] Lee, M.C.; Ho, T.H.; Wang, C.S. Synthesis of tetrafunctional epoxy resins and their modification with polydimethylsiloxane for electronic application. J.Appl.Polym. Sci. **1996,** 62, 217.

[16] Voytekunas, V.Y.; Ng, F.L.; Abadie, M.J. Kinetics study of the UV-initiated cationic polymerization of cycloaliphatic diepoxide resins. Eur. Polym. J. **2008**, 44, 3640.

[17] Césarini, J.P. Rayonnement ultraviolet et santé. Radioprotection. **2007,** 42, 379.

[18] Crivello, J.V. The discovery and development of onium salt cationic photoinitiators. J. Polym. Sci. Part A Polym. Chem. **1999,** 37, 4241.

[19] Crivello, J.V.; Lee, J.L. The synthesis and characterization of polymer-bound diaryliodonium salts and their use in photo and thermally initiated cationic polymerization. Polym. Bull. **1986,** 16, 243.

[20] Pappas, S.P.; Pappas, B.C.; Gatechair, L.R.; Jilek, J.H.; Schnabel, W. Photoinitiation of Cationic Polymerization. IV. Direct and Sensitized Photolysis of Axyl lodonium and Sulfonium Salts. Polym. Photochem. **1984,** 5, 1.

[21] Crivello, J.V.; Lam, J.H.W. Photoinitiated cationic polymerization with triarylsulfonium salts. J. Polym. Sci. Part A: Pol. Chem. **1979**, 17, 977.

[22] Crivello, J.V. Cationic polymerization–Iodonium and sulfonium salt photoinitiators. Adv. Polym. Sci. **1984**, 62, 1.

[23] Yagci, Y.; Schnabel, W. New aspects on the photoinitiated free radical promoted cationic polymerization. Macromol. Symp. **1992**, 60, 133.

[24] Fouassier, J.P.; Burr, D.; Crivello, J.V. Photochemistry and Photopolymerization Activity of Diaryliodonium Salts. Macromol.Sci, Pure and Appl. Chem. **1994**, 31, 677.

[25] Takata, T.; Takuma, K.; Endo, T. Photoinitiated cationic polymerization of epoxide with phosphonium salts as novel photolatent initiators. Macromol. Rapid Commun. **1993**, 14, 203.

[26] Zivic, N.; Bouzrati-Zerelli, M.; Villote, S.; Morlet-Savary, F.; Dietlin, C.; Dumur, F.; Gigmes, D.; Fouassier, J.P.; Lalevee, J. A novel naphthalimide scaffold based iodonium salt as a one-component photoacid/photoinitiator for cationic and radical polymerization under LED exposure. Polym. Chem. **2016,** 7, 5873.

[27] Villote, S.; Gigmes, D.; Dumur, F.; Lalevee, J. Design of Iodonium Salts for UV or Near-UV LEDs for Photoacid Generator and Polymerization Purposes. Molecules, **2020,** 25, 149.

[28] Topa, M.; Hola, E.; Galek, M.; Petko, F.; Pilch, M.; Popielarz, R.; Morlet-Savary, F.; Graff, B.; Lalevee, J.; Ortyl, J. One-component cationic photoinitiators based on coumarin scaffold iodonium salts as highly sensitive photoacid generators for 3D printing IPN photopolymers under visible LED sources. Polym. Chem., **2020,** 11, 5261.

[29] Gu, H.; Zhang, W.; Feng, K.; Neckers, D.C. Photolysis of ((3 (Trimethylsilyl)propoxy)phenyl)phenyliodonium Salts in the Presence of 1-Naphtholand 1-Methoxynaphthalene. J.Org.Chem. **2000**, 65, 3484.

[30] Hizal, G.; Yagci, Y.; Schnabel, W. Charge-transfer complexes of pyridinium ions and methyl-and methoxy-substituted benzenes as photoinitiators for the cationic polymerization of cyclohexene oxide and related compounds. Polymer. **1994**, 35, 2428.

[31] Crivello, J.V.; Bulut, U. Curcumin: A naturally occurring long-wavelength photosensitizer for diaryliodonium salts. J.Polym.Sci. Part A: Pol. Chem. **2005**, 43, 5217-5231.

[32] Dossow, D.; Zhu, Q.Q.; Hizal, G.; Yagci, Y.; Schnabel, W. Photosensitized cationic polymerization of cyclohexene oxide : a mechanistic study concerning the use of pyridinium type salts. Polymer. **1996**, 37, 2821.

[33] Chen, Y.H.; Yamamura, T.; Igarashi, K. Photosensitization of carbazole derivatives in cationic polymerization with a novel sensitivity to near-UV light. J.Polym.Sci., Part A:Polym. Chem. **2000**, 38, 90.

[34] Nelson, E.W.; Carter, T.P.; Scranton. A.B. Fluorescence Monitoring of Cationic Photopolymerizations : Divinyl Ether Polymerizations Photosensitized by Anthracene Derivatives. Macromolecules. **1994**, 27, 1013.

[35] Rodrigues, M.R.; Neumann, M.G. Mechanistic Study of Tetrahydrofuran Polymerization Photoinitiated by a Sulfonium Salt/Thioxanthone System. Macromol. Chem. Phys. **2001**, 202, 2776.

[36] Lalevée, J.; Dirani, A.; El-Roz, M.; Allonas, X.; Fouassier, J.P. Germanes as efficient coinitiators in radical and cationic photopolymerizations. J. Polym. Sci. Part A: Pol. Chem. **2008**, 46, 3042.

[37] Crivello, J.V. Radical-Promoted Visible Light Photoinitiated Cationic Polymerization of Epoxides. J.Macromol.Sci. Part A: Pure. Appl. Chem. **2009**, 46, 474-483.

[38] Crivello, J.V. Redox Initiated Cationic Polymerization. J.Polym.Sci. Part A: Polym.Chem. **2009,** 47, 1825.

Chapitre III : les systèmes hybrides ; Réseaux Interpénétrés de polymères (RIP ou IPN)

1. Introduction

La polymérisation des systèmes hybrides est définie comme étant une combinaison de deux ou plusieurs réseaux de polymères dont au moins l'un des polymères est réticulé en juxtaposition de l'autre **[1].** Le but de ce mode de polymérisation est de combiner les propriétés chimiques, mécaniques et physiques des deux polymères au sein d'un même matériau et pallier certains inconvénients et limitations présentes pour les composants pris séparément. Ainsi, les propriétés finales d'un matériau obtenu par polymérisation d'un système hybride dépendent fortement des propriétés des polymères constituant ce mélange.

Thermodynamiquement, les polymères sont non miscibles et sont sujets de la séparation de phases, cependant la présence d'enchevêtrements entre les réseaux force la miscibilité des polymères ce qui améliorera efficacement le processus de polymérisation hybride.

En effet, les réseaux interpénétrés de polymères **(RIP ou IPN)** ont été élaborés, comme c'est souvent le cas en chimie macromoléculaire, avant la compréhension détaillée de leur morphologie. Le mélange du caoutchouc naturel avec du soufre dans un mélange de phénol et formaldéhyde a produit le premier RIP synthétisé et cela a eu lieu au début du XX^{ème} siècle **[2].** En 2007, Crivello a rapporté la photopolymérisation hybride d'un mélange radicalaire/cationique qui a montré une grande efficacité car la chaleur libérée lors du processus radicalaire a permis une réaction cationique plus efficace **[3].** D'autre part, des revêtements à base de **RIP** ayant un faible retrait et une meilleure adhésion par rapport aux polymères individuels, ont été synthétisés par Sangermano suivant le même procédé **[4].** La synergie radicalaire/cationique dans les systèmes hybrides a fait l'objet de nombreuses applications dans différents domaines : (1) les adhésifs, (2) les résines dentaires **[5]**, (3) les encres photopolymérisables **[6,7]**, (4) la stéréolithographie **[8].** Cette technique a été utilisée ces dernières années dans le but d'améliorer la résistance aux chocs, la flexibilité, la stabilité mécanique et thermique…

La polymérisation photoinduite constitue une méthode très utile pour la formation des réseaux interpénétrés de polymères. Le nouveau matériau est synthétisé rapidement par irradiation d'un mélange de deux monomères multifonctionnels qui entraine la formation de

réseaux réticulés ayant des propriétés spécifiques. L'association d'un monomère acrylique et un monomère époxyde conduit à un matériau combinant la flexibilité du réseau polyéther et la rigidité du polyacrylate. D'autre part, la forte sensibilité de la polymérisation radicalaire envers l'oxygène de l'air est compensée par l'insensibilité de la voie cationique à l'O_2, ainsi que la sensibilité des espèces cationiques à la présence des espèces nucléophiles est compensée par l'insensibilité des espèces radicalaires envers les nucléophiles. Cette caractéristique fournit souvent des formulations photosensibles qui peuvent durcir dans des conditions douces (sous air…).

2. Méthodes de synthèse des RIP

Il existe deux méthodes principales décrites dans la littérature pour la synthèse de réseaux interpénétrés de polymères **[9,10].** Lors d'une **synthèse séquentielle (Schéma 1)**, le premier réseau formé par une simple polymérisation est gonflé par l'amorceur (ou le réticulant) du second monomère non encore polymérisé. Une fois l'agent de gonflement (amorceur et réticulant) activé, la seconde polymérisation aura lieu et le second réseau est ainsi formé. Cette voie de synthèse conduit à des RIP contenant deux réseaux de polymères enchevêtrés dont les propriétés sont différentes de celles du réseau simple. En effet, l'étape de gonflement est limitée par la solubilité du second monomère dans le premier réseau.

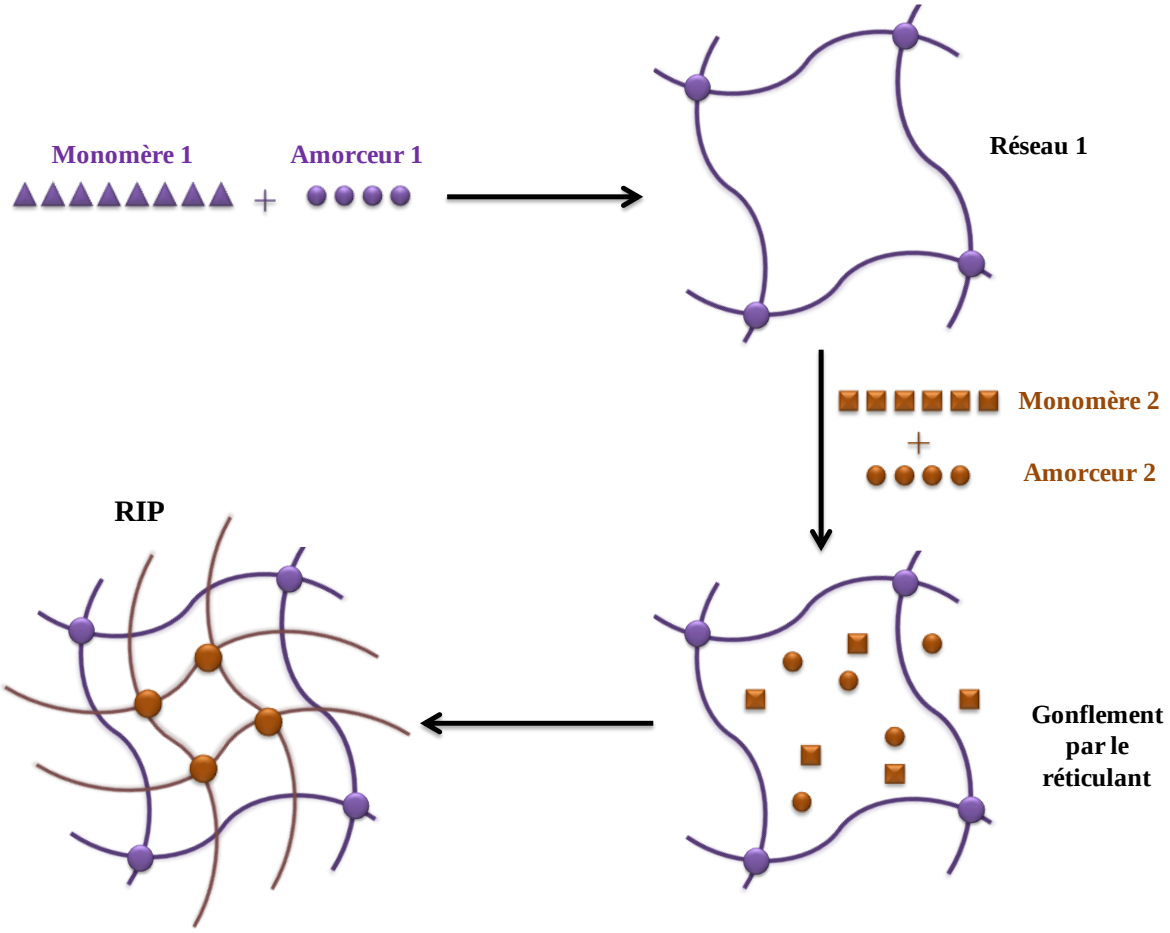

Schéma 1: Synthèse séquentielle de RIP

Lors d'une synthèse **in situ**, tous les composants (Monomère 1 et 2, amorceur 1 et 2) sont initialement mélangés, et les réactions de réticulation conduisant à la formation de RIP sont déclenchés simultanément **(Schéma 2)**. La formation d'un copolymère ou d'un co-réseau est un inconvénient majeur de ce mode de synthèse, de ce fait il est primordial que les mécanismes de formation des deux réseaux soient différents. Ainsi, la synthèse in situ et simultanée de RIP sera au cœur de notre travail de thèse.

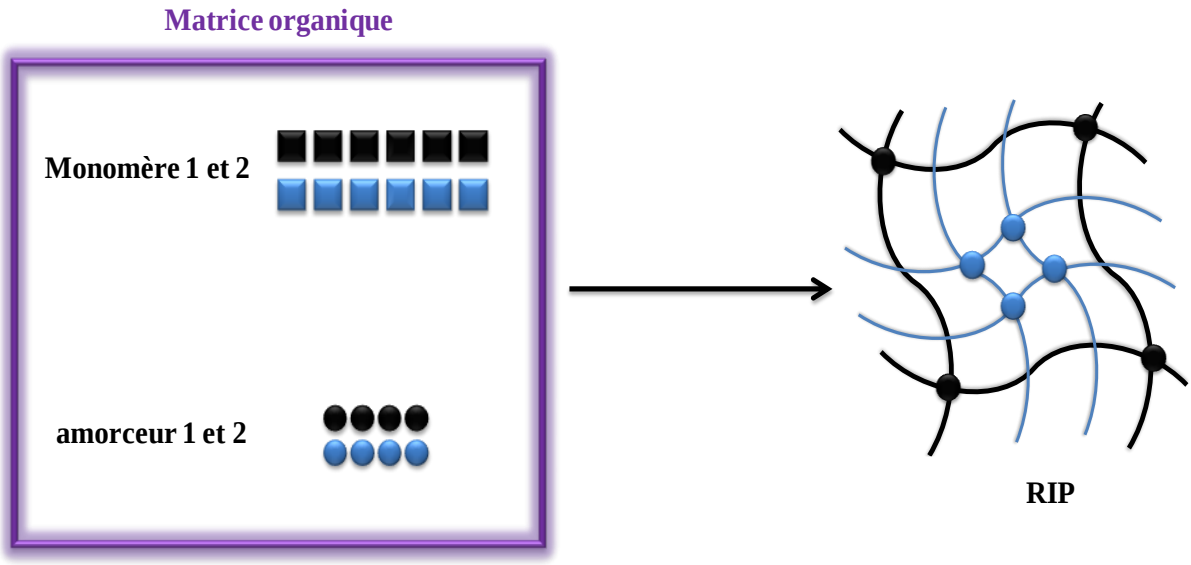

Schéma 2 : Synthèse in situ de RIP

3. Etat de l'art sur les réseaux interpénétrés

D'une manière intéressante de nombreuses combinaisons de résines photopolymérisables pour la synthèse des RIP ont été rapportées dans la littérature. Le tableau ci-dessous récapitule quelques combinaisons effectuées dans le but d'obtenir des réseaux interpénétrés de polymères. La nature ainsi que les propriétés finales des matériaux obtenus dépendent fortement du couple de monomères impliqués dans la synthèse de RIP **[11-13].** Les combinaisons époxydes/acrylates **[14],** vinyl éther/méthacrylate **[15],** thiol-ène/isocyanate **[16-18]** ont été largement utilisées pour la synthèse des matériaux par polymérisation hybride.

Tableau 1 : Exemples de RIP déjà synthétisés.

Polymère 1	Polymère 2
Phénol-formaldéhyde	Caoutchouc naturel
Caoutchouc naturel	PVC
Acrylique	Polyéther
Réseaux chargés positivement	Réseaux chargés négativement

Références

[1] Sperling, L.H. Interpenetrating Polymer Networks, D. Klemper, L.H. Sperling, L.A. Utracki, Adv. Chem. Ser. No 239, Ed. ACS, Washington DC, **1994**, 3.

[2] Aylsworth, J.W. U.S. Patent. **1914**, 1,111, 254.

[3] Crivello, J.V. Synergistic effects in hybrid free radical/cationic photopolymerizations. Polym. Sci., Part A: Polym. Chem. **2007**, 45,3759.

[4] Sangermano, M.; Carbonaro, W.; Malucelli, G.; Priola, A. UV-Cured Interpenetrating Acrylic-Epoxy Polymer Networks: Preparation and Characterization. Macromol. Mater. Eng. **2008**, 293, 515.

[5] Oxman, J.D.; Trom, M.C.; Jacobs, D.W. Compositions featuring cationically active and free radically active functional groups, and methods for polymerizing such compositions Minnesota Mining and Manufacturing Company USA, WOpatent 9, 962, 460, **1999**.

[6] Madhusoodhanan, S.; Nagvekar, D.S. Radiation curable inks. Hexion Specialty Chemicals Inc, USA; WO2, 008, 045, 480, **2008**.

[7] Nagvekar, D.S. HexionSpecialty Chemicals Inc, USA,WO2, 008, 002, 543, **2008**,

[8] Lawton, J.A.; Chawla, C.P. DSM Desotech Inc; USA, US patent 2, 005, 158, 660, **2005.**

[9] Kim, S.C.; Sperling, L.H. IPNs around the world : Science and engineering, New-York : Wiley. **1997**

[10] Sperling, L.H.; Klempner, D.; Utracki L.A. Eds. Interpenetrating Polymer Networks, Washington. ACS. **1991.**

[11] He, Y.; Xiao, M.; Wu, F.; Nie, J. Photopolymerization kinetics of cycloaliphatic epoxide–acrylate hybrid monome. Polym. Int. **2007,** 56, 1292.

[12]Ortiz, R.A; Sangermano, M.; Bongiovanni, R.; Garcia, Valdez A.E.; Duarte, L.B.; Saucedo, I.P.; Priola, A. Synthesis of hybrid methacrylate-silicone-cyclohexanepoxide monomers and the study of their UV induced polymerization. Prog. Org. Coat. **2006,** 57, 159.

[13] Decker, C.; Nguyen Thi Viet, T.; Decker, D.; Weber-Koehl, E. UV-radiation curing of acrylate/epoxide systems. Polymer. **2001,** 42, 5531.

[14] Hopff, H. Ger.Pat. **1935**, 623, 351.

[15] Lin, Y.; Stansbury, J.W. The impact of water on photopolymerization kinetics of methacrylate/vinyl ether hybrid systems. Polym. Adv.Technol. **2005**, 16, 195.

[16] Senyurt, A.F.; Wei, H.; Hoyle, C.E.; Piland, S.G.; Gould, T.E. Ternary Thiol-Ene/Acrylate Photopolymers: Effect of Acrylate Structure on Mechanical Properties. Macromolecules. **2007**, 40, 4901.

[17] Matsushima, H.; Shin, J.; Bowman, C.N.; Hoyle, C.E. Thiol-isocyanate-acrylate ternary networks by selective thiol-click chemistry. Polym.Sci., Part A : Polym.Chem. **2010**, 48, 3255.

[18] Shin, J.; Matsushima, H.; Comer, C.M.; Bowman, C.N.; Hoyle, C.E. Thiol-Isocyanate-Ene Ternary Networks by Sequential and Simultaneous Thiol Click Reactions. Chem.Mater. **2010**, 22, 2616.

Partie II : Colorants organiques comme photoamorceurs

Chapitre I : Colorants organiques à base de dérivés de coumarines comme photoamorceurs

Section I : Dérivés de coumarine en tant que photoamorceurs/photosensibilisateurs pour l'impression 3D et synthèse de photocomposites.

Dans ce premier chapitre de la partie II, des colorants organiques à base de dérivés de coumarines ont été utilisés comme photomaorceurs pour la polymérisation radicalaire sous lumière visible en utilisant des sources d'irradiation sûres tels que les Diodes Electroluminescentes. Deux familles de dérivés de coumarines seront présentées dans ce manuscrit. Ces composés agissent comme des photoamorceurs Type II en les combinant avec des additifs ou des co-amorceurs pour des réactions de polymérisation des acrylates.

Comme caractéristiques, les coumarines sont des composés naturels dérivant de la benzo-α-pyrone ; elles résultent de la lactonisation de l'acide ortho-hydroxycinnamique et elles sont largement distribuées dans le règne végétal (Rutacées, fève Tonka…). L'IUPAC considère la coumarine comme, étant, un dérivé de 2H-chromène (ou chrom-3-ène), un des deux isomères structuraux du produit d'insaturation de la chromane. Ces composés peuvent également être obtenus par différentes voies synthétiques (réaction de Pechmann, réaction de Wittig, réaction de Perkin…).

Les coumarines constituent une grande classe d'hétérocycles organiques. La plupart d'entre elles, sont douées d'activités biologiques variées. Parmi elles, on peut citer, l'activité antibiotique [1], l'activité anticancéreuse [2], l'activité anti-inflammatoire [3]. Par ailleurs, ces composés sont utilisés comme sondes fluorescentes [4], émetteurs pour les dispositifs électroluminescents [5], aussi elles entrent dans la fabrication de parfums [6-8].

Chimiquement parlant, ces composés dérivés de 2H-chromène se caractérisent par des rendements quantiques de transfert d'électron élevés [9], de bonnes solubilités [10] dans les solvants et les résines organiques, de grande capacité de réagir comme des donneurs et accepteurs d'électron [11], de bonnes propriétés d'absorption dans la zone UV-visible vue la facilité d'incorporer des groupements chromophores dans la fonction coumarine. En raison de ces propriétés photochimiques et redox intéressantes, deux familles de dérivés de coumarines

ont été synthétisées dans le but d'amorcer les réactions de photopolymérisation radicalaire sous lumière visible.

Dans ce chapitre, une série de trois composés de coumarines (Coum1, Coum2 et Coum3) a été développée pour la synthèse des polymères acryliques.

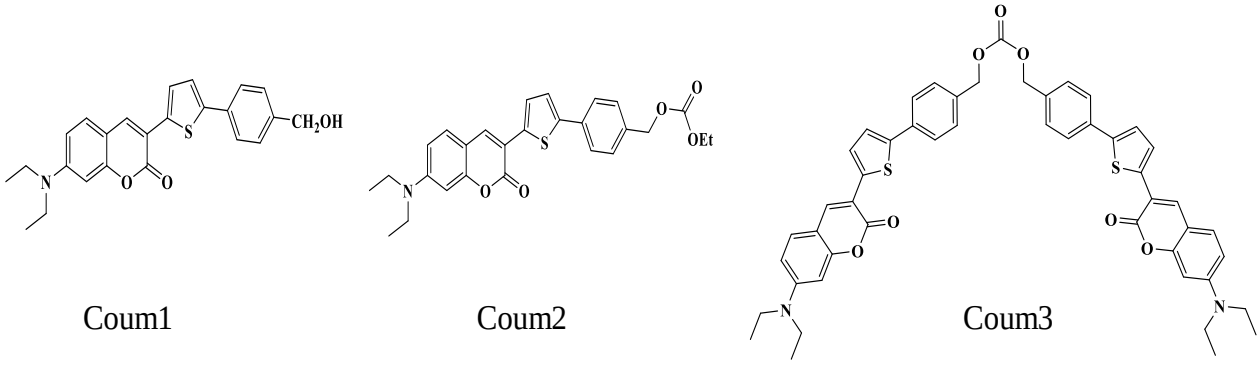

Schéma 1. Coumarines synthétisées en tant que photoamorceurs

Le but de cette étude est de comparer la capacité d'amorçage d'une coumarine monofonctionnel (Coum1 et Coum2) à une coumarine bifonctionnel (Coum3) résultant de la combinaison de Coum1 et Coum2 et ayant un poids moléculaire élevé. Comme prévu, cette molécule présente des capacités d'absorption supérieures à celles observées dans le cas des coumarines monofonctionnels. Cependant, la capacité de polymérisation des acrylates en utilisant Coum1 et 2 est plus importante que celle obtenue en utilisant la coumarine 3. Le pouvoir de photoamorçage des systèmes photoamorceurs utilisés (Coum/Iod ou Coum/Iod/amine) a été étudié en utilisant la spectroscopie infrarouge à transformée de Fourier en temps réel RT-FTIR. En fait, de faibles quantités de coumarine (0.05% et 0.1%) sont suffisantes pour amorcer efficacement la réaction de polymérisation des monomères acryliques. Ces résultats ont été expliqués par des expériences de spectroscopie UV-visible où la photolyse de la coumarine en présence d'additifs a été suivie en suivant la variation de l'intensité de la bande d'absorption du colorant. Des potentiels d'oxydation appropriés à l'état excité sont obtenus et des variations d'énergie libre favorable pour déclencher une polymérisation sont calculées en utilisant la voltammétrie cyclique. La synthèse des composites sous irradiation à 395 nm ainsi que la production de motifs polymères en 3D (sous diode laser à 405nm) et ayant une résolution spatial élevée ont également montrés la haute performance des dérivés de coumarine dans les processus de polymérisation. Ce travail a fait l'objet d'une **publication** dans **'Catalyst'** sous la citation suivante : Rahal, M.; Mokbel, H.;

Graff, B.; Toufaily, J.; Hamieh, T.; Dumur, F.; Lalevée, J. Mono vs. Difunctional Coumarin as Photoinitiatorsin Photocomposite Synthesis and 3D Printing. Catalyst. **2020**, 10, 1202.

Références

[1] Kayser, O.; Kolodziej, H. Antibacterial Activity of Extracts and Constituents of Pelargonium sidoides and Pelargonium reniforme. Planta medica. **1997**; 63, 508.

[2] Harvey, R.G.; Cortez, C.; Ananthanarayan, T.P.; Schmolka, S.A. New Coumarin Synthesis and Its Utilization for the Synthesis of Polycyclic Coumarin Compounds with Anticarcinogenic Properties. J. Org. Chem. **1988**, 53, 3936.

[3] Bansal, Y.; Sethi, P.; Bansal, G. Coumarin : A Potential Nucleus for Anti-Inflammatory Molecules. Med.Chem.Res. **2013**, 22, 3049-3060.

[4] Su, K.; Ming, J.; Zhang, L.; Xiang, S.; Cui, M.; Yang, H. A novel tricyclic heterocyclic fluorescent probe for Pd^{2+} in aqueous solution: Synthesis, properties and theoretical calculations. Opt. Mater. **2019**, 93, 25.

[5] Lee, M.T.; Yen, C.K.; Yang, W.P.; Chen, H.H.; Liao, C.H.; Tsai, C.H.; Chen, C.H. Efficient Green Coumarin Dopants for Organic Light-Emitting Devices. Org. Lett. **2004**, 6, 1241.

[6] Yourick, J.J.; Bronaugh, R.L. Percutaneous Absorption and Metabolism of Coumarin in Human and Rat Skin. J. Appl. Toxicol. **1997**, 17, 153.

[7] Weinmann, I. Coumarins: Biology, Applications, and Mode of Action; History of the Development and Applications of Coumarin and Coumarin-related Compounds. Eds. O'Kennedy, R.; Thornes, R.D. New York: John Wiley & Sons. **1997**.

[8] Nielson, B.E. Linnean Society of London. The Biology and Chemistry of the Umbelliferae.; Heywood, V.H. Published for the Linnean Society of London, by Academic Press: New York. **1971.**

[9] Satpati, A.K.; Kumbhakar, M.; Nath, S.; Pal, H. Photophysical Properties of Coumarin-7 Dye : Role of Twisted Intramolecular Charge Transfer State in High Polarity Protic Solvents. Photochem. Photobiol. **2009**, 85, 119.

[10] Ayyangar N. R.; Srinivasan K. V.; Daniel T. Polycyclic Compounds Part VII. Synthesis Laser Characteristics and Dyeing Behaviour of 7-Diethylamino-2H-l-Benzopyran-2-Ones. Dyes. Pigm. **1991**, 16, 197.

[11] Kielesiński, Ł.; Gryko, D.T.; Sobolewski, A.L.; Morawski, O.W. Effect of Conformational Flexibility on Photophysics of Bis-Coumarins. Phys. Chem. Chem. Phys. **2018**, 20, 14491.

Mono vs. Difunctional Coumarin as Photoinitiators in Photocomposite Synthesis and 3D Printing

Abstract:

This work is devoted to investigate three coumarin derivatives (Coum1, Coum2, and Coum3), proposed as new photoinitiators of polymerization when combined with an additive, i.e., an iodonium salt, and used for the free radical polymerization (FRP) of acrylate monomers under mild irradiation conditions. The different coumarin derivatives can also be employed in three component photoinitiating systems with a Iod/amine (ethyl 4-dimethylaminobenzoate (EDB) or N-phenylglycine (NPG)) couple for FRP upon irradiation with an LED @ 405 nm. These compounds showed excellent photoinitiating abilities, and high polymerization rates and final conversions (FC) were obtained. The originality of this work relies on the comparison of the photoinitiating abilities of monofunctional (Coum1 and Coum2) vs. difunctional (Coum3) compounds. Coum3 is a combined structure of Coum1 and Coum2, leading to a sterically hindered chemical structure with a relatively high molecular weight. As a general rule, a high molecular weight should reduce the migration of initiating molecules and favor photochemical properties such as photobleaching of the final polymer. As attempted, from the efficiency point of view, Coum3 can initiate the FRP, but a low reactivity was observed compared to the monofunctional compound (Coum1 and Coum2). Indeed, to study the photochemical and photophysical properties of these compounds, different parameters were taken into account, e.g., the light absorption and emission properties, steady state photolysis, and fluorescence quenching. To examine these different points, several techniques were used including UV-visible spectroscopy, real-time Fourier Transform Infrared Spectroscopy (RT-FTIR), fluorescence spectroscopy, and cyclic voltammetry. The photochemical mechanism involved in the polymerization process is also detailed. The best coumarins investigated in this work were used for laser writing (3D printing) experiments and also for photocomposite synthesis containing glass fibers.

Keywords: free radical polymerization; mild irradiation conditions; coumarins; composite materials; LED; 3D printing

Partie II : Colorants organiques comme photoamorceurs

1. Introduction

During the last decade, photochemical reactions showed a huge number of industrial and academic applications such as UV-curing, solar cells, and photopolymerization [1,2]. These reactions can advantageously replace thermally-based chemical processes due to their many advantages [3,4] such as low-cost reactions, low energy consumption, and very fast reaction (a few seconds) processes while exhibiting an eco-friendly character [5]. Therefore, the development of photosensitive systems with low toxicity will be preferably retained for the design of new initiating systems under mild irradiation conditions. Coumarin and its derivatives form a class of natural compounds that exhibit biological activity, e.g., cytotoxic activity against several human tumor cell lines [6,7], as well as spasmolytic, antiarrhythmic [8], and antioxidant [9] activities. Coumarins are also used in flavoring food and in cosmetic products such as fragrances [10,11]. These compounds are also characterized by high photoluminescence quantum yields and can therefore be used as fluorescent chromophores for various applications [12]. Recently, heterocyclic fluorescent compounds have been used in several research fields such as molecular probes for biochemical research [13], emitters for electroluminescent devices [14], fluorescent probes for heavy metal sensing [15], molecules exhibiting biological activities [16] or active layers for photovoltaic applications [17].

In fact, recent research devoted to photopolymerization aims at developing chromophores capable of strong absorption in the visible range [18-22]. For more safety and less harmfulness while reducing the energy consumption, light-emitting diodes (LEDs) [23] are now classically used in photopolymerization, enabling a good overlap between the emission of the LEDs and the absorption spectra of the photoinitiators (PIs).

In this work, three coumarins (Coum1, Coum2, and Coum3) bearing different substituents were synthesized and characterized (See Scheme 1). These coumarins were notably used in two (Coum/Iod (0.1%/1% *w*/*w*)) and three (Coum/Iod/amine (0.1%/1%/1% *w*/*w*/*w*)-component photoinitiating systems (PIS) to generate reactive species with the different additives presented in Scheme 2. Excellent polymerization initiating abilities were found at 405 nm during the free radical polymerization (FRP) of acrylates. In fact, the different substituents of coumarins could drastically affect the photochemical and/or electrochemical properties and absorption properties and thus their abilities to initiate the photopolymerization process. These coumarins were used in 3D printing application upon irradiation at 405 nm. The formation of composite materials using glass fibers was also provided. These different

applications clearly highlight the remarkable performances of the different coumarins reported in this work as photoinitiators.

Indeed, the reaction mechanisms can be explained using several techniques such as cyclic voltammetry, absorption, and photoluminescence techniques, or real-time Fourier transform infrared spectroscopy (RT-FTIR).

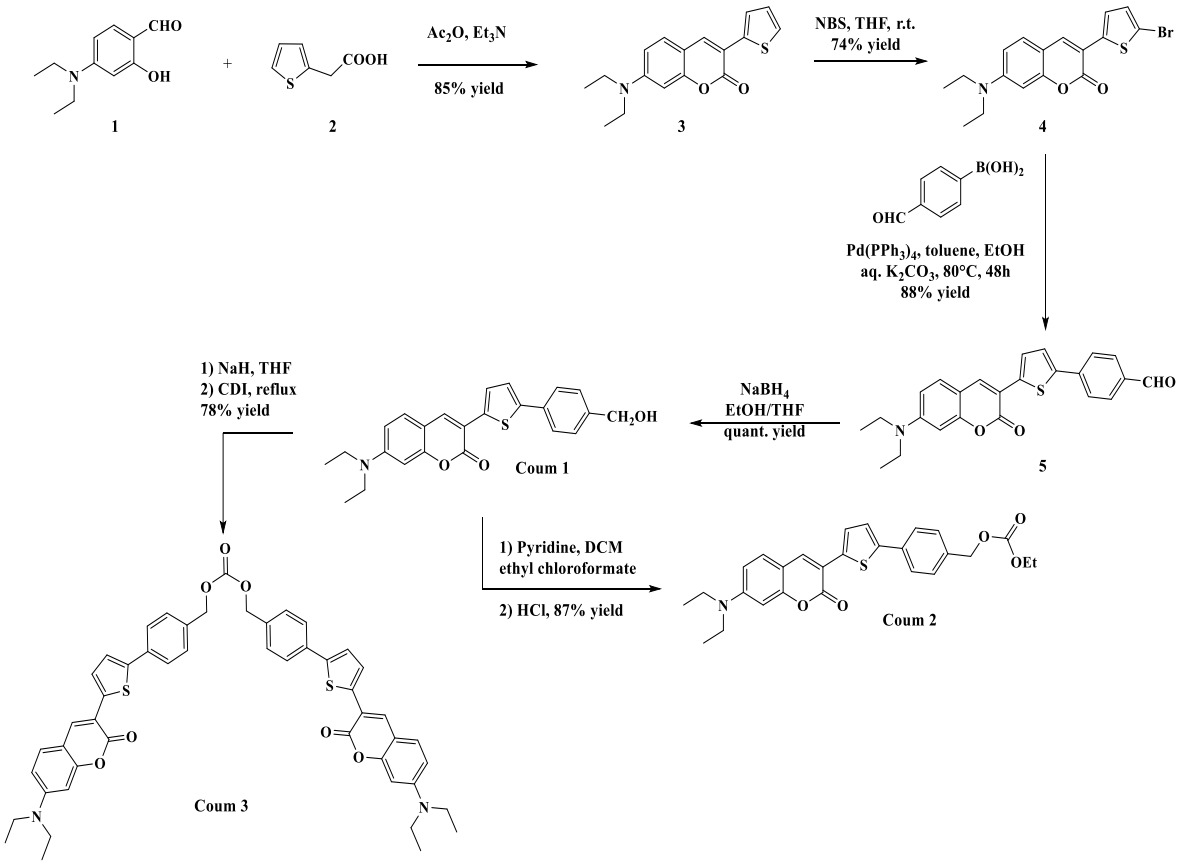

Scheme 1. The different coumarins (Coum1, Coum2, and Coum3) investigated in this study.

2. Experimental Part

2.1. Synthesis of Coumarins

Details concerning analyses of the different compounds (NMR machines, mass spectroscopy, etc…) described below have been reported in previous work [26].

2.1.1. Synthesis of 7-(Diethylamino)-3-(thiophen-2-yl)-2H-chromen-2-one 3

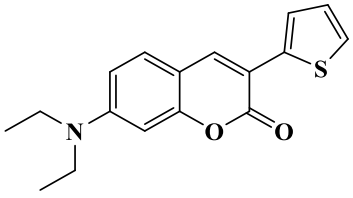

Thiopheneacetic acid **2**. (7.80 g, 55 mmol, M = 142.17 g/mol), 4-(diethylamino)salicylaldehyde 1 (16.4 g, 85 mmol, M = 193.24 g/mol) were dissolved in acetic anhydride (200 mL). Triethylamine (14.6 mL, 105 mmol) was added, and the solution was refluxed for three hours. After cooling, water was added. The aqueous phase was extracted several times with AcOEt. The organic layers were combined, dried over magnesium sulfate, and the solvent was removed under reduced pressure. The residue was purified by flash column chromatography (SiO_2, DCM: pentane 1:1) to yield coumarin 3 as a yellow solid (14.0 g, 85% yield). ^{1}H NMR ($CDCl_3$) δ: 1.18 (t, 6H, J = 7.1 Hz), 3.39 (q, 4H, J = 7.1 Hz), 6.50 (d, 1H, J = 2.4 Hz), 6.57 (dd, 1H, J = 8.8 Hz, J = 2.4 Hz), 7.04 (t, 1H, J = 3.8 Hz), 7.26–7.29 (m, 2H), 7.62 (d, 1H, J = 3.7 Hz), 7.83 (s, 1H); ^{13}C NMR ($CDCl_3$) δ: 12.5, 44.9, 97.2, 108.8, 109.3, 114.9, 124.9, 125.5, 127.2, 128.8, 136.8, 137.5, 150.5, 155.6, 160.5; HRMS (ESI MS) m/z: theor: 299.0980 found: 299.0982 (M^+. detected). Analyses were consistent with those reported in the literature [27–29].

2.1.2. Synthesis of 3-(5-Bromothiophen-2-yl)-7-(Diethylamino)-2H-chromen-2-one 4

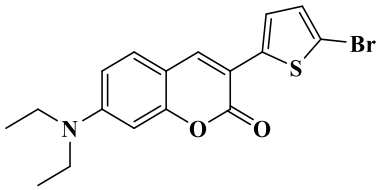

N-bromosuccinimide (NBS) (2.6 g, 14.69 mmol, M = 177.98 g/mol) was added to a solution of 7-(diethylamino)-3-(thiophen-2-yl)-2*H*-chromen-2-one 3 (4.0 g, 13.36 mmol, M = 299.39 g/mol) in THF (120 mL). The mixture was stirred at room temperature for 4 h, and water (20 mL) was added. The mixture was extracted with CH_2Cl_2 several times. The combined organic phases were combined, dried over magnesium sulfate, and the solvent removed under reduced pressure. The residue was purified by precipitation in a mixture diethyl ether/pentane. It was isolated as a yellow solid (3.74 g, 74% yield). ^{1}H NMR ($CDCl_3$) δ: 1.21 (t, 6H, J = 7.1 Hz), 3.43 (q, 4H, J = 7.1 Hz), 6.52 (d, 1H, J = 1.9 Hz), 6.62 (dd, 1H, J = 8.8 Hz, J = 1.9 Hz), 7.03 (d, 1H, J = 4.0 Hz), 7.30–7.33 (m, 2H), 7.82 (s, 1H); ^{13}C NMR ($CDCl_3$) δ: 12.5, 44.9, 97.2, 108.6, 109.5, 113.2, 114.1, 124.0, 129.7, 136.1, 138.7, 150.7, 155.5, 160.5; HRMS (ESI MS) *m/z:* theor: 377.0085 found: 377.0088 (M^+. detected). Analyses were consistent with those reported in the literature [30,31].

2.1.3. Synthesis of 4-(5-(7-(Diethylamino)-2-oxo-2H-chromen-3-yl) thiophen-2-yl) benzaldehyde 5

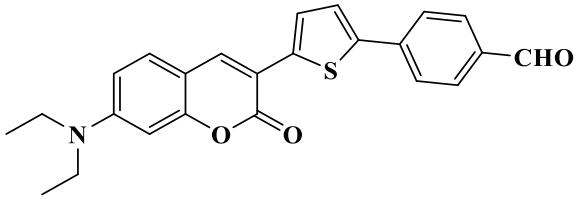

Tetrakis(triphenylphosphine)palladium (0) (0.46 g, 0.744 mmol, M = 1155.56 g.mol^{-1}) was added to a mixture of 3-(5-bromothiophen-2-yl)-7-(diethylamino)-2H-chromen-2-one 4 (2.31 g, 6.11 mmol, M = 378.28 g mol^{-1}), (4-formylphenyl)boronic acid (1.37 g, 9.16 mmol, M = 149.94 g mol^{-1}), toluene (54 mL), ethanol (26 mL), and an aqueous K_2CO_3 solution (2 M, 6.91 g in 25 mL water, 26 mL) under vigorous stirring. The mixture was stirred at 80 °C for 48 h under a nitrogen atmosphere. After cooling to room temperature, the reaction mixture was poured into water and extracted with ethyl acetate. The organic layer was washed with brine several times, and the solvent removed under reduced pressure. The residue was purified by filtration on a plug of silica gel using a mixture of DCM/ethanol as the eluent. The product was isolated with 88% yield (1.23 g). ^{1}H NMR ($CDCl_3$) δ: 1.24 (t, 6H, J = Hz), 3.44 (q, 4H, J = Hz), 6.54 (d, 1H, J = 2.2 Hz), 6.63 (dd, 1H, J = 8.8 Hz, J = 2.4 Hz), 7.34 (d, 1H, J = 8.8 Hz), 7.45 (d, 1H, J = 4.0 Hz), 7.65 (d, 1H, J = 4.0 Hz), 7.80 (d, 1H, J = 8.3 Hz), 7.88 (d, 1H, J = 8.3 Hz), 7.94 (s, 1H), 9.99 (s, 1H, CHO); ^{13}C NMR ($CDCl_3$) δ: 12.5, 44.9, 97.2, 108.7, 109.5, 114.1, 125.3, 125.7, 129.1, 130.4, 134.9, 136.8, 139.2, 140.2, 142.2, 150.8, 155.7, 160.4, 191.4; HRMS (ESI MS) m/z: theor: 403.1242 found: 403.1245 (M^+. detected).

2.1.4. Synthesis of 7-(Diethylamino)-3-(5-(4-(hydroxymethyl) phenyl) thiophen-2-yl)-2H-chromen-2-one Coum1

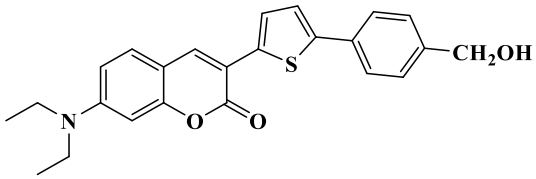

4-(5-(7-(Diethylamino)-2-oxo-2*H*-chromen-3-yl)thiophen-2-yl)benzaldehyde 5 (0.5 g, 1.24 mmol, 403.49 g/mol) was suspended in a mixture of ethanol/THF (100/200 mL), and sodium borohydride (100 mg) was added. The solution was stirred at room temperature for 1h30 (TLC control). The solution was quenched with HCl (1 mL, 1M), and the solvent was removed under reduced pressure. The residue was filtered on a plug of silica gel using THF as the eluent. The product (Coum1) was isolated in quantitative yield. ^{1}H NMR ($CDCl_3$) δ: 1.22 (t, 6H, J = 7.1 Hz), 3.44 (q, 4H, J = 7.1 Hz), 4.72 (d, 2H, J = 3.7 Hz), 5.00 (s, 1H), 6.54 (d,

1H, J = 2.4 Hz), 6.62 (dd, 1H, J = 8.8 Hz, J = 2.4 Hz), 7.30–7.40 (m, 4H), 7.63–7.67 (m, 3H), 7.90 (s, 1H); ^{13}C NMR ($CDCl_3$) δ: 12.5, 21.2, 30.3, 34.2, 44.9, 65.1, 97.2, 108.8, 109.3, 114.7, 123.4, 125.5, 125.81, 125.83, 127.5, 128.3, 128.8, 132.6, 133.9, 135.8, 136.3, 136.9, 140.1, 143.7, 150.5, 151.5, 155.6, 160.5; HRMS (ESI MS) m/z: theor: 405.1399 found: 405.1396 (M^+. detected).

2.1.5. Synthesis of 4-(5-(7-(Diethylamino)-2-oxo-2H-chromen-3-yl) thiophen-2-yl) benzyl ethyl carbonate Coum2

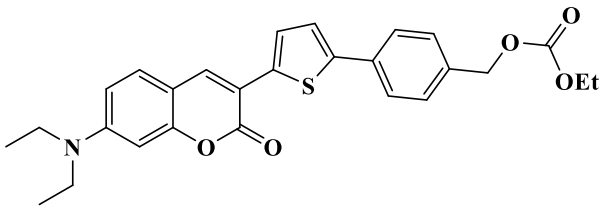

To a solution of 7-(diethylamino)-3-(5-(4-(hydroxymethyl) phenyl) thiophen-2-yl)-2*H*-chromen-2-one Coum1 (405 mg, 10 mmol, M = 405.51 g/mol) and pyridine (0.87 g, 0.89 mL, 11 mmol, M = 79.10 g/mol, d = 0.978) in dichloromethane (DCM) (60 mL), 0°C ethyl chloroformate (1.95 g, 1.72 mL, 18 mmol, M = 108.52 g/mol, d = 1.135)was added dropwise. The solution was stirred at room temperature for two hours. 1 M HCl (30 mL) was added to the solution, and the aqueous phase was extracted several times with dichloromethane. The organic phases were combined, dried over magnesium sulfate, and the solvent removed under reduced pressure. The residue was purified by column chromatography (SiO_2) using a gradient of eluent from pentane to DCM (415 mg, 87% yield). ^{1}H NMR ($CDCl_3$) δ : 1.22 (t, 6H, J = 7.1 Hz), 1.32 (t, 3H, J = 7.1 Hz), 3.42 (q, 4H, J = 7.1 Hz), 4.22 (q, 2H, J = 7.1 Hz), 6.52 (d, 1H, J = 2.4 Hz), 6.60 (dd, 1H, J = 8.8 Hz, J = 2.4 Hz), 7.27–7.30 (m, 2H), 7.39 (d, 2H, J = 8.2 Hz), 7.61–7.66 (m, 3H), 7.88 (s, 1H); ^{13}C NMR ($CDCl_3$) δ: 12.5, 14.3, 44.9, 64.2, 69.1, 97.1, 108.8, 109.3, 114.5, 123.7, 125.70, 125.72, 128.91, 128.93, 134.4, 134.6, 136.4, 137.2, 143.4, 150.6, 155.1, 155.5, 160.4; HRMS (ESI MS) m/z: theor: 477.1610 found: 477.1613 (M^+. detected)

2.1.6. Synthesis of bis (4-(5-(7-(Diethylamino)-2-oxo-2H-chromen-3-yl) thiophen-2-yl)benzyl) carbonate Coum3

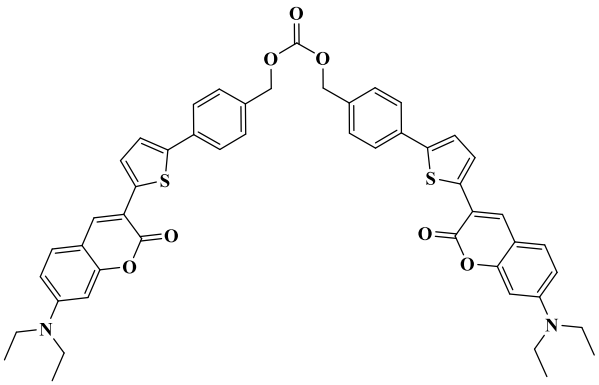

To a solution of 7-(Diethylamino)-3-(5-(4-(hydroxymethyl) phenyl)-thiophen-2-yl)-2*H*-chromen-2-one Coum2 (5.25 g, 12.95 mmol, 2.1 eq., M = 405.51 g/mol) in dry THF (50 mL) was added in small portions at 0°C sodium hydride 95% (0.32 g, 12.64 mmol, 2.05 eq., M = 24 g/mol). The solution was allowed to warm to room temperature and stirring was maintained for 2 h. Then, 1,1′-carbonyldiimidazole (CDI) (1 g, 6.17 mmol, 1 eq., M = 162.15 g/mol) was slowly added at 0°C, and the reaction was refluxed overnight. After cooling, the reaction was quenched by the addition of water, and THF was removed under reduced pressure. The aqueous phase was extracted with DCM several times. The organic phases were combined, dried over magnesium sulfate, and the solvent removed under reduced pressure. The residue was purified by column chromatography (SiO_2) using a gradient of eluent from pentane to DCM (4.03 g, 78% yield). ^{1}H NMR ($CDCl_3$) δ: 1.21 (t, 12H, J = 7.1 Hz), 3.43 (q, 8H, J = 7.1 Hz), 5.19 (s, 4H), 6.53 (d, 2H, J = 2.4 Hz), 6.62 (dd, 2H, J = 8.8 Hz, J = 2.4 Hz), 7.30–7.34 (m, 4H), 7.39 (d, 4H, J = 8.4 Hz), 7.63–7.67 (m, 6H), 7.89 (s, 2H); ^{13}C NMR ($CDCl_3$) δ: 12.5, 44.9, 69.5, 97.2, 108.8, 109.3, 114.6, 123.7, 125.7, 125.8, 128.9, 129.0, 134.2, 134.7, 136.4, 137.2, 143.4, 150.6, 155.1, 155.6, 160.4; HRMS (ESI MS) m/z: theor: 836.2590 found: 836.2595 (M^+. detected)

2.2. Other Chemicals

The different additives used in this work were purchased from Lambson Ltd (Wetherby, UK), country), Sigma Aldrich (St. Quentin Fallavier, France)or TCI Europe (Paris, France). The two monomers were obtained from Allnex. Chemical structures of monomers and additives are shown in Scheme 2.

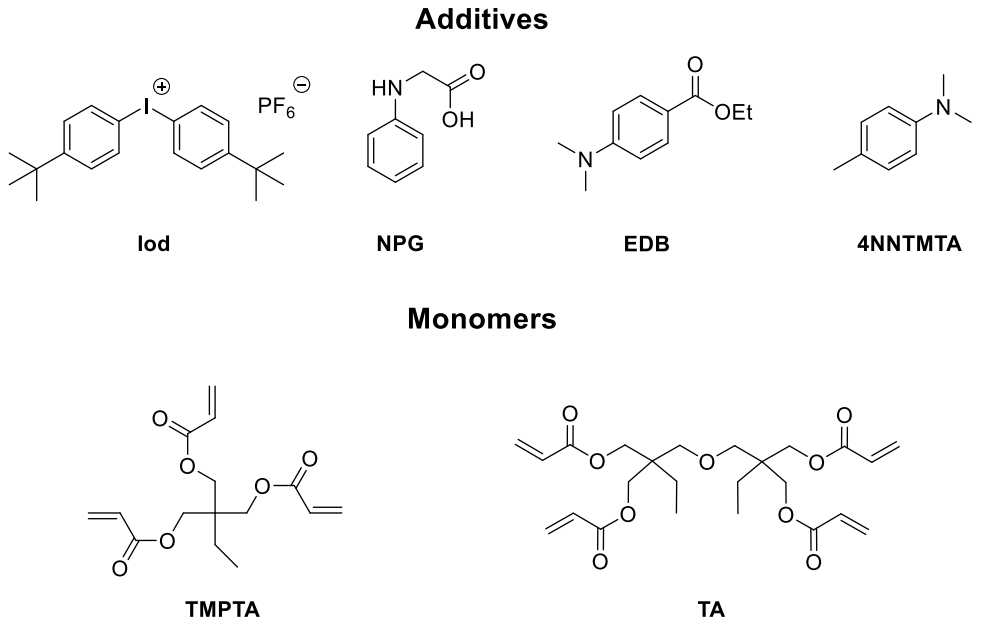

Scheme 2. Other chemical compounds used in this work

2.3. Light Sources

The following light sources were used in this work: (1) LED @ 375 nm (I = 40 mW.cm^{-2}) (2) LED @ 405 nm (I = 110 mW.cm^{-2}).

2.4. Free Radical Photopolymerization (FRP)

Coumarin/Iod (0.05-0.1%/1% w/w) or coumarin/Iod/additive (0.05-0.1%/1%/1 w/w/w) combinations were used as photoinitiating systems for the FRP of acrylates. Percentages mentioned for the different chemical compounds and used in the photoinitiating systems are related to the monomer weight.

FRP of TMPTA and TA was performed under laminated conditions (~25 µm thickness) to reduce O_2 inhibition. For thick samples (1.4 mm of thickness), the formulations were polymerized in a plastic mold ~ 1 cm in diameter. Monomer conversions (TMPTA or TA) were continuously followed by real-time FTIR spectroscopy. More details about photopolymerization monitoring are provided in [32,33].

2.5. Redox Potentials

Experimental conditions and equipment were previously detailed in Reference [34].

2.6. Fluorescence Experiments

Experimental conditions and equipment were previously detailed in Reference [34].

2.7. UV-Visible Absorption and Photolysis Experiments

Experimental conditions and equipment were previously detailed in Reference [34].

2.8. Computational Procedure

Theoretical calculations were carried out under the conditions previously detailed [35,36].

2.9. 3D printing Experiments

A diode laser (city, State Abbr. (if has), country) at 405 nm was used for 3D printing experiments, with light intensity similar to that used in the IR experiments. Polymerization was carried out under air. Analyses were performed with a numerical optical microscope (Shinjuku, Japan) (DSX-HRSU from OLYMPUS Corporation) [37].

2.10. Near-UV Conveyor

Photocomposite synthesis was carried out by impregnating the TMPTA or the TA-based resin with glass fibers (resin/fibers : 50%/50% w/w). Then, the glass fiber/resin system was irradiated using a dymax-LED conveyor. Other experimental conditions (belt speed, distance between the light source and the sample) were previously detailed in reference [34].

3. Results

3.1. Free Radical Photopolymerization (FRP) of Acrylate Monomers (TMPTA or Di(trimethylolpropane) Tetraacrylate (TA))

Thanks to their excellent absorption properties, these coumarins showed a very high performance (Figure 1, Table 1) in terms of final conversions and rates of polymerization upon exposure to the LED @ 405 nm. In fact, Iod alone, NPG alone, or Coum alone did not work. Conversely, two- or three-component systems such as Coum/Iod (0.1%/1% w/w) or Coum/Iod/amine (0.1%/1%/1% w/w/w) were quite efficient and could efficiently initiate the polymerization process. Obviously, this is related to the photooxidation process between Iod and coumarin (electron transfer from $Coum^*$ to Iod) and to the formation of a charge transfer complex (CTC) between Iod and NPG $[Iod\text{-}NPG]_{CTC}$.

For the photopolymerization of di(trimethylolpropane) tetraacrylate (TA) in thick samples in laminate (1.4 mm thickness), an excellent polymerization efficiency was found using Coum/Iod or Coum/Iod/NPG when irradiated with an LED @ 405 nm (See Figure 1A). High final conversions were obtained: the FC could increase up to 90 % for coum2/Iod/NPG

(0.1%/1%/1% w/w/w) compared to 83% using coum2/Iod (0.1%/1% w/w). These results show the superiority of the three-component systems over their two-component PIS analogues (See Figure 1C). Indeed, in the case of the three-component systems, the additional amines (NPG, EDB) are introduced in order to regenerate the photosensitizer, enabling a photocatalytic system. For the two-component systems, the photosensitizer is irreversibly oxidized upon photoexcitation, resulting from an electron transfer in the excited state from the photosensitizer to the photoinitiator (Iod) so that an irreversible consumption of the photosensitizer is observed [24,25]. This issue is addressed by the introduction of a sacrificial amine in the three-component systems. The same behavior is also observed with coum1 (Figure 1, curve 1 for the two-component PIS coum1/Iod (0.05%/1% w/w) and curve 10 for the three-component PIS coum1/Iod/NPG (0.05%1%/1% w/w/w)). Besides, it has to be noticed that a smaller enhancement of the final monomer conversion is observed with this second coumarin. Thus, if a monomer conversion of 84% is observed for the three-component system coum1/Iod/NPG (0.05%1%/1% w/w/w), the monomer conversion is in turn comparable to that obtained with the two-component system (83% monomer conversion (See Table 1). The crucial role of coumarins in the final monomer conversions is clearly evidenced through the different photopolymerization experiments.

In fact, in the case of Coum2 and 3, the increase in the concentration induces an increase in the final conversion rate (Figure 1A. Curve 3 and 4 for Coum2, and Curve 5 and 6 for Coum3); this can be explained by a greater generation of radicals. Conversely, a lower conversion rate is observed by increasing the concentration in the case of Coum1 (See Figure 1A Curve 1 and 2); this is due to an inner filter effect which prevents the penetration of light to the depth.

The performance of the different photoinitiating systems for the FRP of acrylates in thin films and under laminated conditions was also relatively good (See Figure 1B). In this case, the addition of NPG clearly showed an influence on the polymerization profile: the FC could increase up to 69.4% for Coum2/Iod/NPG compared to 53.4% with the two-component Coum2/Iod (0.1%/1% w/w) system. Similarly, the FC increased up to 63% with the three-component coum1/Iod/NPG (0.05%/1%/1% w/w/w) system, far from the result obtained with the two-component coum1/Iod (0.05%/1% w/w) system (41.3%).

The trend detected for the FRP of the acrylic monomers (TMPTA and TA) for thick samples and under laminated conditions followed relatively the same order: Coum1 and

Coum 2 are the best candidates for the FRP in three-component PIS; Coum/Iod/NPG. Interestingly, the reactivity of PIS comprising NPG as the amine was higher than that comprising EDB (e.g., Figure 1A. Curve 10 vs. Curve 7). Besides, the polymerization was still possible with this second amine. The difference in reactivity between NPG and EDB can be attributed to the fast decarboxylation of NPG when used as the sacrificial amine. This decreases the possibility of back electron transfer while jointly increasing the reactivity. Tack-free coatings were obtained in most of the cases, in full agreement with the increase in the characteristic acrylate peak at 1630 cm^{-1} for thin samples recorded before and after irradiation (See Figure 1D).

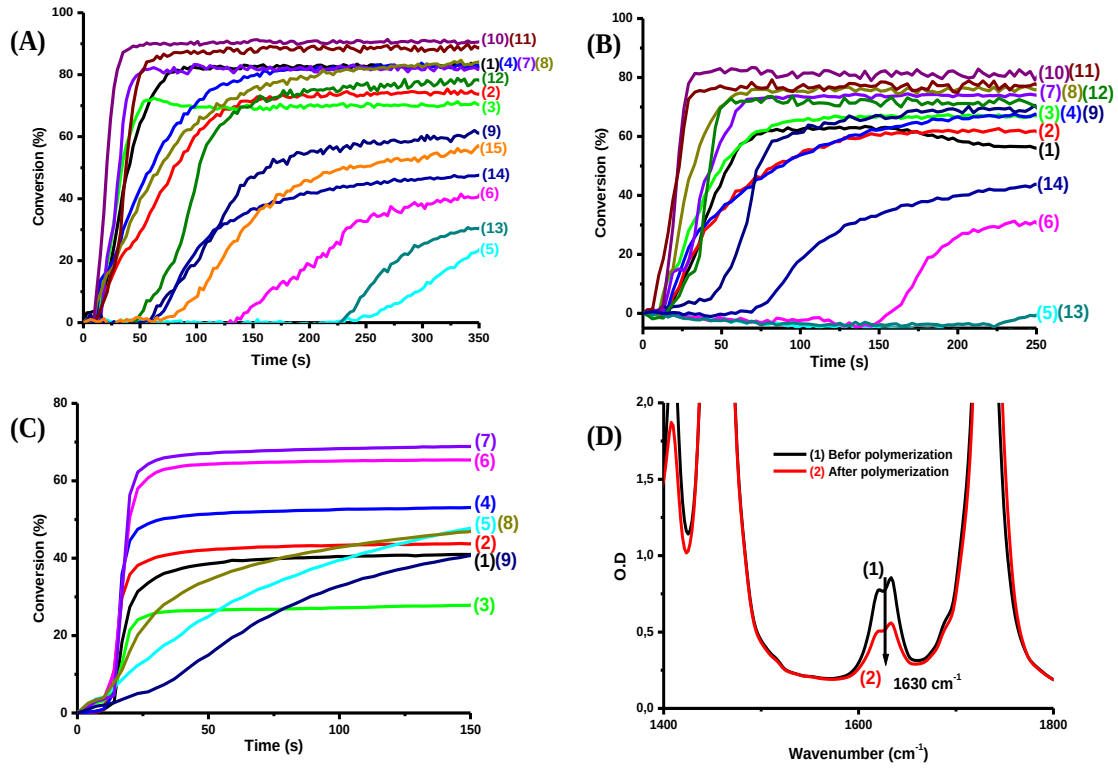

Figure 1. Polymerization profiles (acrylate function conversion vs. irradiation time) for TA **(A)** and TMPTA **(B)** (thickness = 1.4 mm in laminate) upon exposure to the LED @ 405 nm in the presence of the two- and three-component photoinitiating systems: **(1)** Coum 1/Iod (0.05%/1% w/w), **(2)** Coum 1/Iod (0.1%/1% w/w), **(3)** Coum 2/Iod (0.05%/1% w/w), **(4)** Coum 2/Iod (0.1%/1% w/w), **(5)** Coum 3/Iod(0.05%/1% w/w), **(6)** Coum 3/Iod (0.1%/1% w/w), **(7)** Coum 1/Iod/EDB (0.05%/1%/1% w/w/w), **(8)** Coum 2/Iod/EDB (0.05%/1%/1% w/w/w), **(9)** Coum 3/Iod/EDB (0.05%/1%/1% w/w/w), **(10)** Coum 1/Iod/NPG (0.05%/1%/1% w/w/w), **(11)** Coum2/Iod/NPG (0.05%/1%/1% w/w/w), **(12)** Coum3/Iod/NPG (0.05%/1%/1% w/w/w), **(13)** Iod/EDB (1%/1% w/w), **(14)** Iod/NPG (1%/1% w/w) and **(15)** Coum3/Iod (0.05%/1% w/w) with 5 drops of chloroform. **(C)** Polymerization profiles (acrylate function conversion vs. irradiation time) for TMPTA (thickness = 25 µm in laminate) upon exposure to the LED @ 405 nm in the presence of two- and three-component photoinitiating systems:

(1) Coum 1/Iod (0.05%/1% w/w), **(2)** Coum 1/Iod (0.1%/1% w/w), **(3)** Coum 2/Iod (0.05%/1% w/w), **(4)** Coum 2/Iod (0.1%/1% w/w), **(5)** Coum 3/Iod (0.1%/1% w/w), **(6)** Coum 1/Iod/NPG (0.1%/1%/1% w/w/w), **(7)** Coum 2/Iod/NPG (0.1%/1%/1% w/w/w), **(8)** Coum 3/Iod/NPG (0.1%/1%/1% w/w/w) and **(9)** Iod/NPG (1%/1% w/w). **(D):** IR spectra obtained before and after polymerization for Coum 1/Iod/NPG (0.05%/1%/1% w/w/w) in TMPTA (thickness = 25 µm).

Table 1. Final conversions of the acrylate function for TA using different PIS (400 s of irradiation, LED @ 405 nm, sample thickness = 1.4 mm).

Two-ComponentPhotoinitiating System Coum/Iod (0.05%/1% w/w) and Coum/Iod (0.1%/1% w/w)			**Three-Component Photoinitiating System Coum/Iod/EDB and Coum/Iod/NPG (0.1%/1%/1% w/w/w)**		
Coum1/Iod	Coum2/Iod	Coum3/Iod	Coum1/Iod/amine	Coum2/Iod/amine	Coum3/Iod/amine
83% [1]	71% [1]	n.p [1]	84% [3]	83% [3]	59% [3]
73% [2]	83% [2]	32% [2]	90% [4]	89% [4]	78% [4]
[1] Coum/Iod (0.05%/1% *w*/*w*); [2] Coum/Iod (0.1%/1% *w*/*w*); [3] Coum/Iod/EDB (0.1%/1%/1% *w*/*w*/*w*); [4] Coum/Iod/NPG (0.1%/1%/1% *w*/*w*/*w*); n.p.: no polymerization.					

3.2. 3D-Printing Experiments Using Coum/Iod or Coum/Iod/4-N,N,TMA Systems

Some examples of 3D patterns obtained by irradiation with a laser diode emitting at 405 nm (spot size: 50 µm) are presented in Figure 2. The three-component photoinitiating systems based on Coum1 and Coum2 (Coum1-2/Iod or coum1-2/Iod/amine) were very reactive to initiate the FRP of TMPTA and TA under air conditions. Remarkably, the high reactivity of the different resins allowed efficient polymerization in the irradiated zones; 3D patterns elaborated with remarkable precision were obtained using laser writing. In particular, these patterns were prepared in a relatively short space of time (~2 min) while enabling a high spatial resolution. 3D polymer patterns were characterized using a numerical optical microscope, as shown in Figure 2.

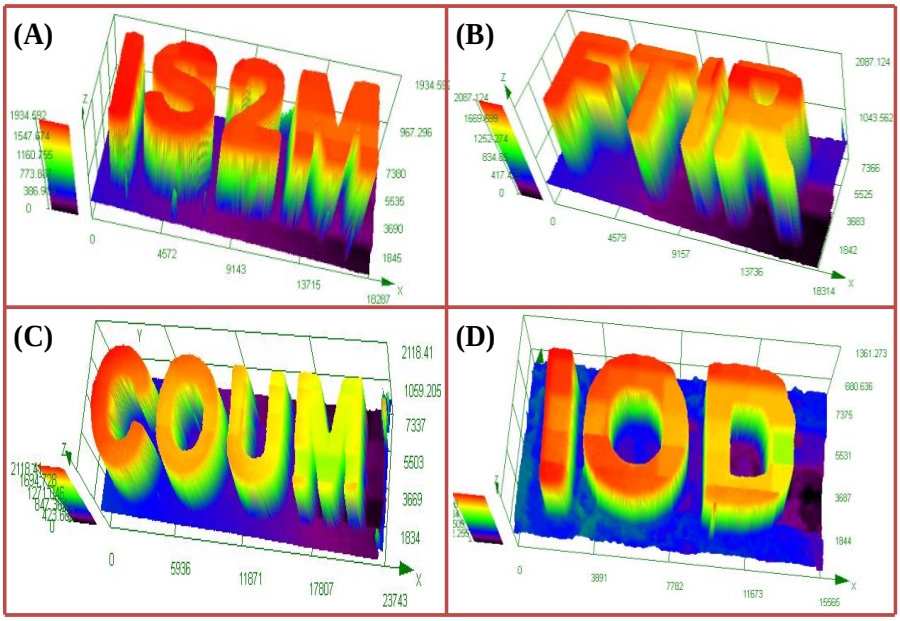

Figure 2. Characterization of the 3D patterns by numerical optical microscopy; (**A**) Coum2/Iod/4-N,N TMA (0.024%/0.4%/0.16% w/w/w) in TA; (**B**) Coum1/Iod/4-N,N TMA (0.02%/0.4%/0.16% w/w/w) in TA; (**C**) Coum2/Iod (0.02%/0.4% w/w) in TMPTA, (**D**) Coum1/Iod (0.02%/0.4% w/w) in TMPTA.

3.3. LED Conveyor Experiments for Composite Preparation

Photocomposite materials were produced by irradiation using an LED @ 385 nm (0.7 W/cm^2) using three-component PIS based on Coum2/Iod/NPG (0.1%/1%/1% w/w/w) or Coum1/Iod/NPG (0.1%/1%/1% w/w/w). Composite materials were prepared by impregnation of glass fibers (one layer, thickness = 2 mm) with an acrylic organic resin (50% organic resin/ 50% glass fibers). Interestingly, fast polymerization was observed using different PIS, where the surface and also the bottom became tack-free after only one pass using one layer of glass fibers. The results reported in Figure 3 show that coumarin derivatives have a high reactivity to produce photocomposite materials at 385 nm. In particular, an excellent depth of cure could be determined for all samples.

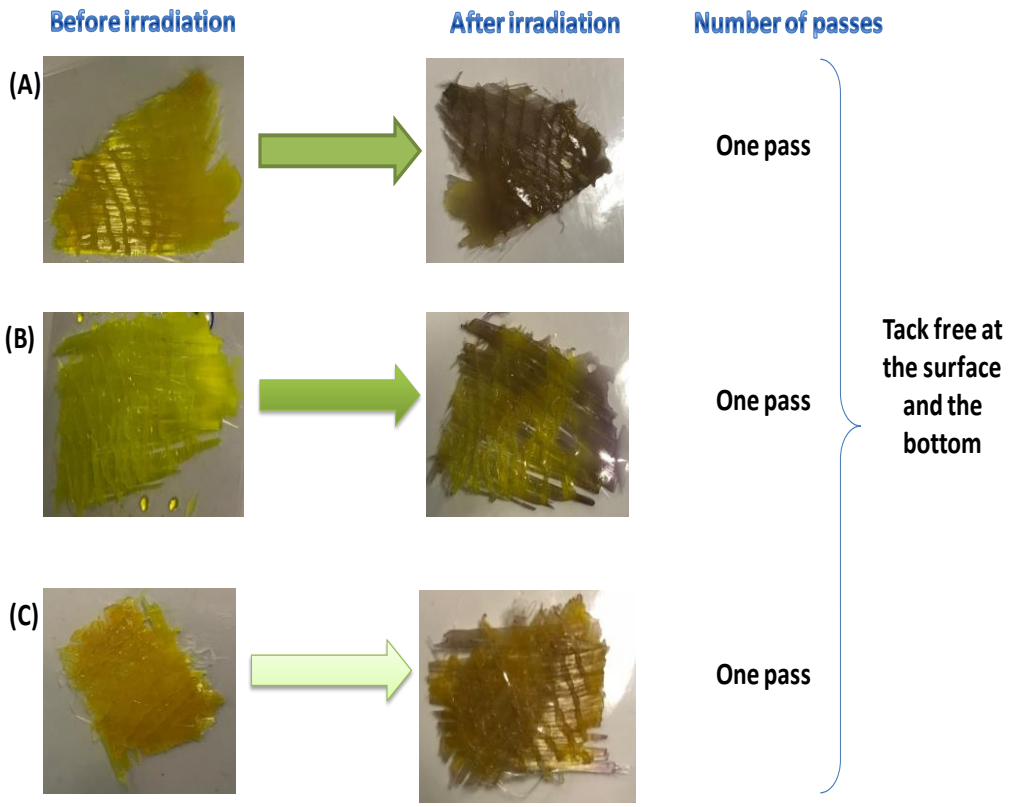

Figure 3. Photocomposite synthesis, Belt Speed = 2 m/min, using LED @ 385 nm: (**A**) Coum1/Iod/NPG (0.1%/1%/1% *w*/*w*/*w*) in TA, (**B**) Coum2/Iod/NPG (0.1%/1%/1% *w*/*w*/*w*) in TMPTA and (**C**) Coum1/Iod/NPG (0.1%/1%/1% *w*/*w*/*w*) in TMPTA.

4. Discussion

Based on the photochemical reactivity as well as the practical efficiency of the investigated coumarins that was clearly demonstrated, their associated chemical mechanisms have been investigated in detail.

4.1. Light Absorption Properties of the Different Dyes

Absorption spectra of coumarin derivatives investigated in this work are shown in Figure 4 (See Table 2). The different absorption spectra are characterized by two main absorption bands, one located in the near-UV range (<350 nm) and a second one with the highest molar extinction coefficient detected in the 350–550 nm range (e.g., Coum1 ~23,000 M^{-1} cm^{-1} @ 405 nm and ~43 560 M^{-1} cm^{-1} @ λ_{max} i.e., (444 nm)). Molar extinction coefficients of coumarins followed this order at the absorption maxima: $\varepsilon_{Coum3} > \varepsilon_{Coum2} > \varepsilon_{Coum1}$. The difference between the extinction coefficients of these compounds is related to the substitution of the coumarin scaffold. Remarkably, their absorption range extends between 350 and 520 nm. Therefore, a good overlap of their absorption spectra with the emission

spectrum of the LED @ 405 nm used in this work could be achieved. Optimized geometries as well as the contour plots of the highest occupied molecular orbital (HOMO) and the lowest unoccupied molecular orbital (LUMO) are presented in Figure 5. As shown in Figure 5, HOMO and LUMO energy levels extend over the entire π-conjugated system. More precisely, the HOMO energy level comprises the coumarin moiety as well as the electron-rich thiophene.

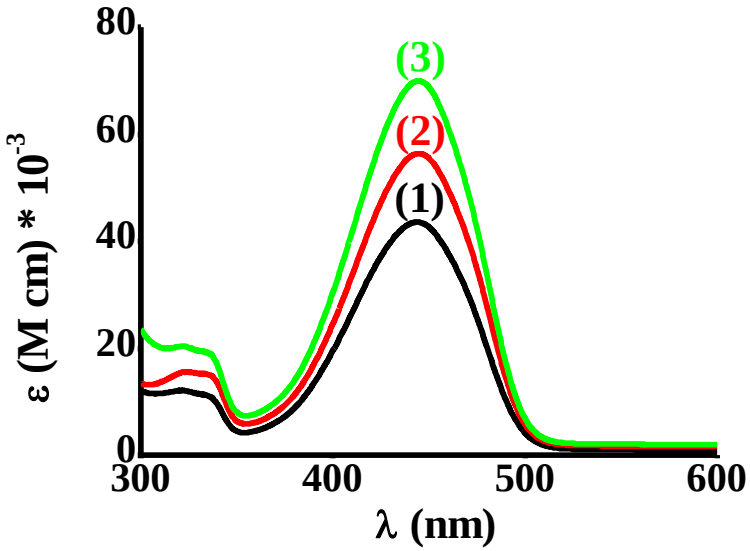

Figure 4 : UV-visible absorption spectra in chloroform: **(1)** Coum1, **(2)** Coum2 and **(3)** Coum3.

Table 2. Light absorption properties of coumarin compounds at **405 nm** and λ_{max}.

	λ_{max} (nm)	ε_{max} (M^{-1} cm^{-1})	$\varepsilon_{@\ 405\ nm}$ (M^{-1} cm^{-1})
Coum1	444	43 500	23 000
Coum2	444	56 400	28 900
Coum3	445	69 900	35 900

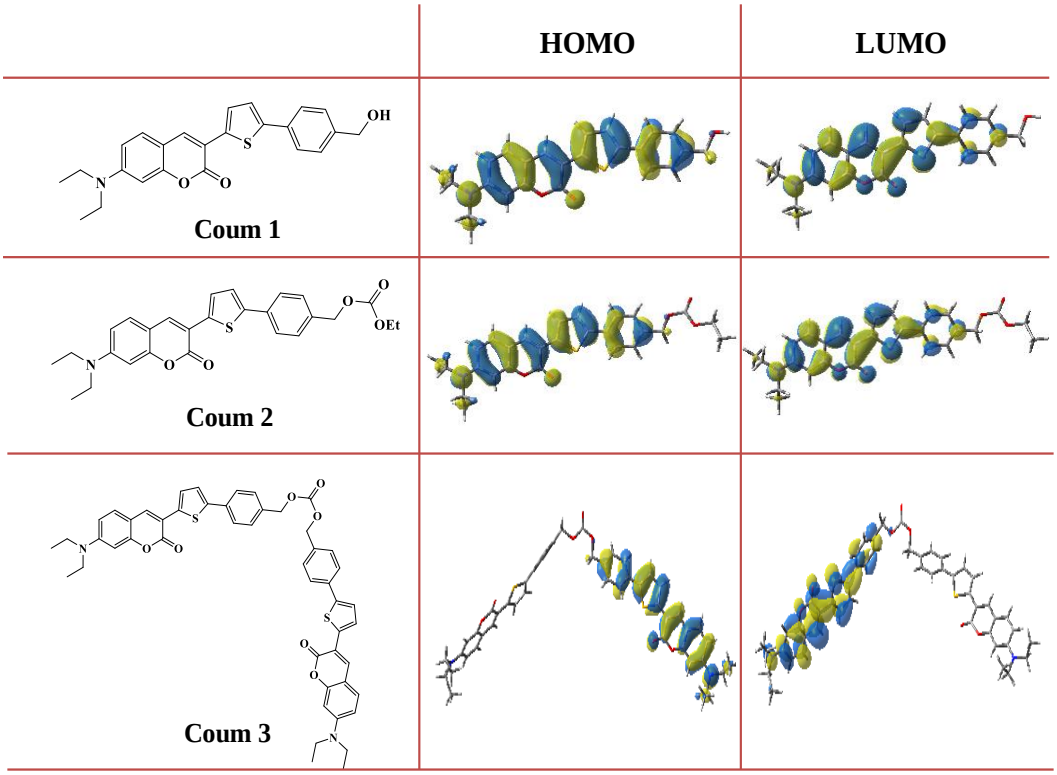

Figure 5. HOMO and LUMO energy levels of Coum1–Coum3 at the UB3 LYP/6–31G* level.

4.2. (Photo)Chemical Mechanisms

The chemical mechanisms were investigated more in detail for Coum3 used as a reference structure and compared to those of Coum1 and Coum2.

4.2.1. Photophysical and photochemical properties of Coum3

Steady-state photolysis experiments of Coum3 were carried out using UV-visible spectroscopy. The steady state photolysis of Coum3/Iod (10^{-2} M) in chloroform was very fast compared to the high photostability of Coum3 alone (e.g., Coum3/Iod in Figure. 6D.2 vs. Coum3 alone in Figure 6D.1) upon irradiation with the LED @ 375 nm. Indeed, the consumption of Coum3 with Iod (10^{-2} M) (Figure 6D.3 Consumption = 91%) was greater than that of Coum3/Iod/EDB (86%); these results are explained by a weaker regeneration of coum3 in the presence of the three-component PI. Fluorescence experiments of Coum3 in chloroform are shown in Figure 6A. The crossing point of the absorption and fluorescence spectra enables us to determine the first singlet excited state energies (E_{S1}) (e.g., estimation of E_{S1} for Coum3: 2.53 eV; Table 3, Figure 6C). As an indicator of interaction occurrence, fast fluorescence quenching processes of Coum3 by Iod were also detected (See Figure 6A and Table 3); this clearly shows a very important interaction of Coum3 (and even for Coum1 and

2) with Iod. These results show a very high quantum yield (for example, $\phi = 0.76$ for Coum3, Table 3).

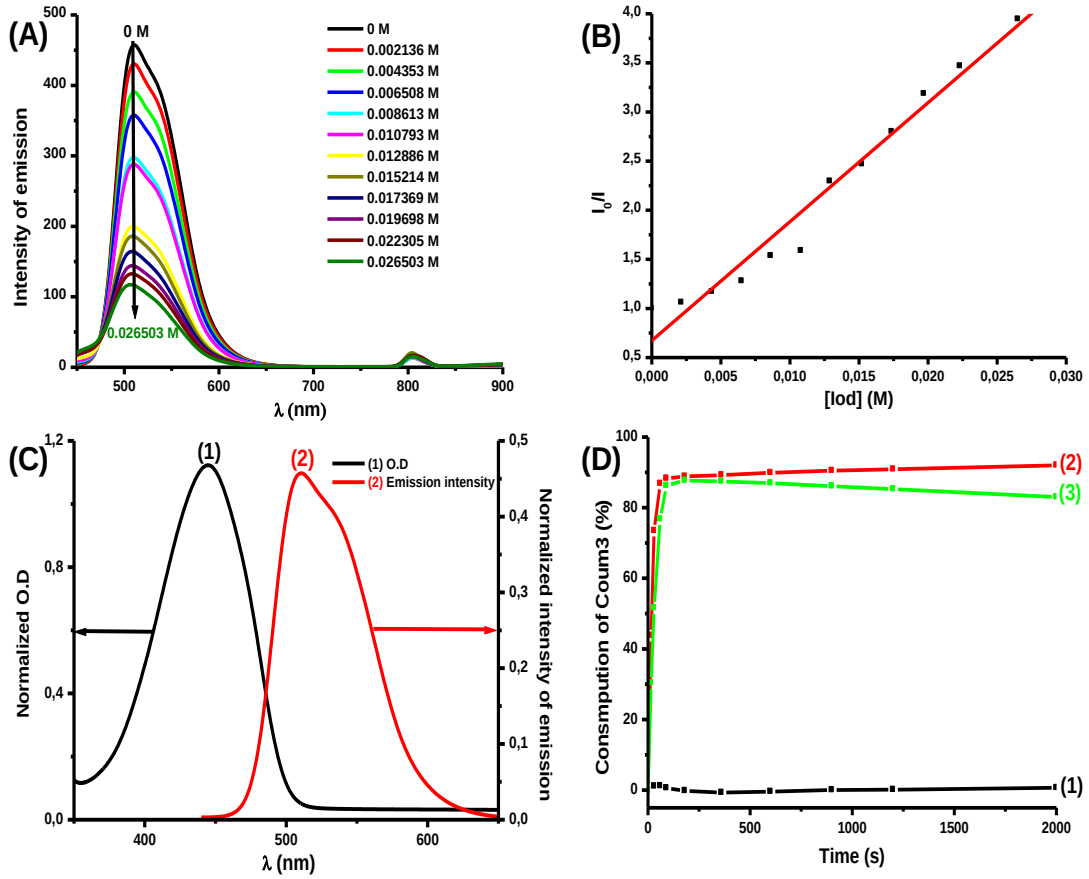

Figure 6. (**A**) Quenching of Coum3 by Iod, (**B**) Determination of the Stern–Volmer coefficient, (**C**) Determination of ES1, (**D**) Consumption of Coum3: (1) Without Iod, (2) With Iod (10^{-2} M), and (3) With Iod/EDB vs. irradiation time upon exposure to the LED @ 375 nm in chloroform.

4.2.2. Photophysical Properties of Coumarins Coum1 and Coum2

Steady-state photolysis experiments of coumarin derivatives (e.g., Coum2) alone, with Iod or Iod/EDB are reported in Figure 7. Interestingly, photolysis of the Coum2/Iod (See Figure 7B) system was faster than that determined for Coum2 alone (See Figure 7A), which proved to be highly photostable. The coum2/Iod interaction showed a photo-oxidation process (electron transfer from coum2 to Iod). In particular, the formation of a photoproduct exhibiting an absorption in the 500-650 nm range could be formed by the interaction of Coum2 with Iod (See Figure 7B). These results clearly show the effect of iodonium on the photolysis of coum2 and therefore on the generation of radicals, because once the Coum2 is irradiated, it reaches an excited state, where an electron transfer from Coum2 to iodonium salt can occur.

On the other hand, photolysis of Coum2 with Iod/EDB (See Figure 7C) was also very fast, but the percentage of consumption (vs. time of irradiation) was lower than that of Coum2/Iod; this result can be attributed to the regeneration of PI in the presence of the three-component PIS (See Figure 7D).

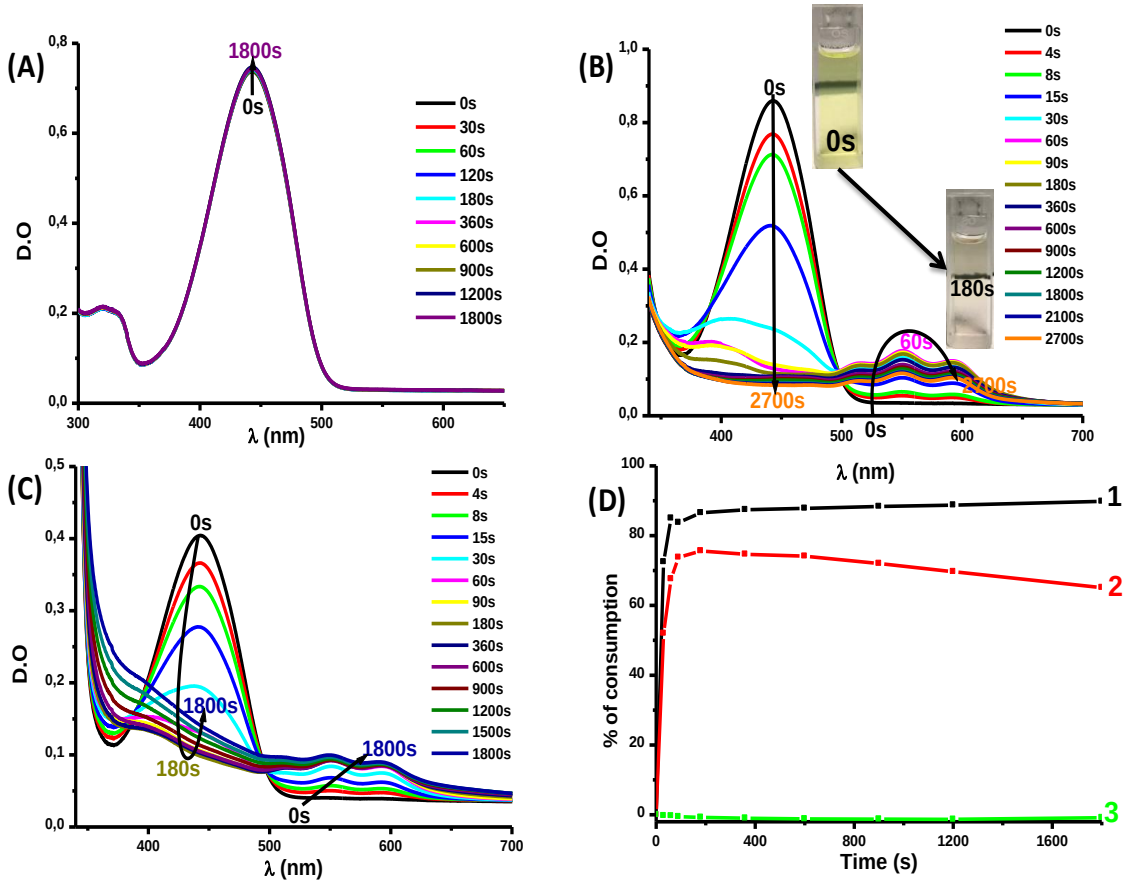

Figure 7. Photolysis of Coum2 in acetonitrile upon exposure to the LED @ 405 nm: (**A**) Coum2 alone (**B**): With Iod (10^{-2} M); and (**C**) With Iod/EDB (10^{-2} M). (**D**) Consumption of Coum2: (1) With Iod, (2) With Iod/EDB, and (3) Without Iod vs. irradiation time upon exposure to the LED @ 375 nm in chloroform.

The percentage of consumption was very high for the different coumarins in the presence of Iod (85% for Coum1, 91% for Coum2, and 93% for Coum3), but this percentage decreased remarkably in the presence of Iod/EDB (70% for Coum1, 72% for Coum2, and 83% for Coum3); this decrease was due to the partial regeneration of these coumarins in the three-component systems.

4.2.3. Fluorescence Quenching Experiments and Cyclic Voltammetry Measurements

Emission and fluorescence quenching spectra of coumarins in chloroform (e.g., Coum2) are presented in Figure 8. The crossing point of the emission and absorption spectra allows

the determination of Es_1 (singlet excited state energy), e.g., E_{S1} = 2.54 eV for Coum1, and 2.56 eV for Coum2. In fact, the fluorescence quenching of Coum2/Iod was very fast and was characterized by high Stern-Volmer coefficients. Thus, very high electron transfer quantum yields (ϕ_{et}= 0.37 for Coum1 and 0.87 for Coum2) were determined. While no quenching was observed in the presence of EDB, there was an increase of the emission intensity that can be ascribed to the formation of a complex between Coum and EDB. This result is totally in agreement with that of the photopolymerization process of Coum/EDB (or NPG). The electron transfer quantum yields (ϕ_{et}) were determined according to the following equation:

$$\phi_{S1} = K_{SV}[Iod]/(1 + K_{SV}[Iod]) \quad (1)$$

This term characterizes the formation of reactive species ($Ar^{\bullet}$ and $PI^{\bullet+}$) capable of initiating the FRP process. Electrochemical properties of the different coumarins were also examined by cyclic voltammetry (Figure 8D), and highly favorable free energy changes ΔG_{et} (which were calculated from Rhem–Weller equation using the oxidation potential between coumarin and Iod, and E_{S1}) could be determined, e.g., ΔG_{et} = −1.46 eV for Coum1 and −1.5 eV for Coum2.

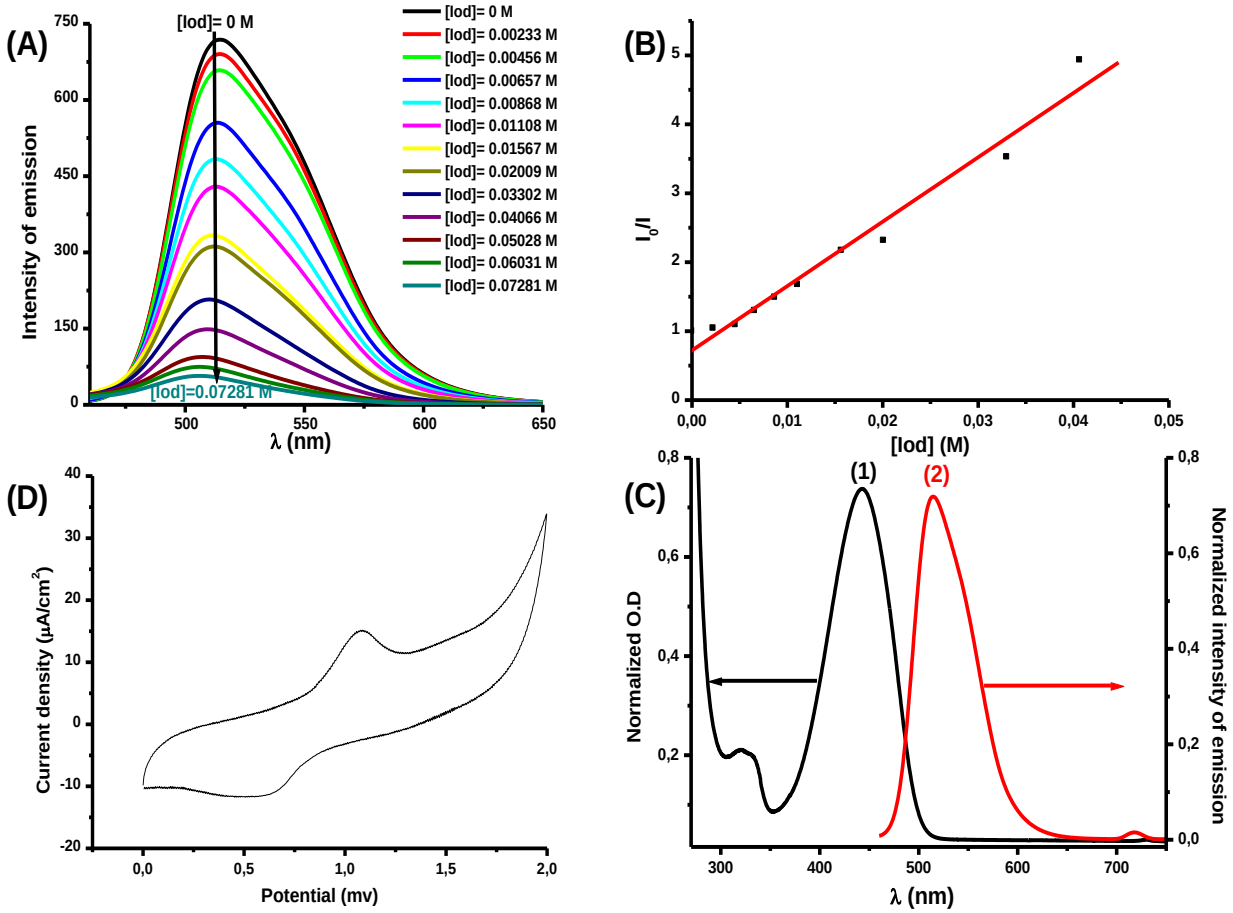

Figure 8. (**A**) Fluorescence quenching of Coum2 by Iod, (**B**) Determination of the Stern–Volmer coefficient, (**C**) ES1 determination, and (**D**) Cyclic voltammetry of Coum2 in acetonitrile.

Table 3. Parameters characterizing the chemical mechanisms associated with the ^{1}Coum/Iod interaction in acetonitrile.

	E_{ox} (eV)	E_{S1} (eV)	ΔG_{S1} (eV)	K_{SV} (Coum/Iod)	ϕ_{et} (Coum/Iod)
Coum1	0.87	2.54	−1.46	20	0.37
Coum2	0.86	2.56	−1.49	93	0.87
Coum3	n.o	2.53	-	121	0.76

E_{S1}: singlet excited state energy, ΔG_{S1}: Free energy change of the singlet state $\phi_{et(Coum/Iod):}$ electron transfer quantum yields

Photopolymerization results can be explained by a global chemical mechanism, based on the results obtained through the different experiments above including fluorescence

quenching, electrochemical, and photolysis experiments. Firstly, once the coumarins absorb the incident light, coumarins are promoted in an excited state PI*, and reactive species ($Ar^{\bullet}$ and $Coum^{+\bullet}$) are generated by the interaction between Coum* and Iod salt (r2). A charge transfer complex (CTC) can also be obtained due to the Iod/NPG interaction, so that $Ar^{\bullet}$ are formed (r3–r4). In addition, a hydrogen atom transfer from NPG to PI can also occur so that two different types of radicals can be generated (Coum-$H^{\bullet}$ and $NPG_{(-H)}{}^{\bullet}$). $NPG_{(-H,-CO2)}{}^{\bullet}$ is produced by decarboxylation of $NPG_{(-H)}{}^{\bullet}$; this decarboxylated compound can lead to the generation of reactive species ($Ar^{\bullet}$ and $NPG_{(-H,\ CO2)}{}^{+}$) by interaction with Iod salt (r6–r7). Therefore, the reactions r1–r7 are proposed for the three-component systems, and $Ar^{\bullet}$ and $NPG_{(-H,\ -CO2)}{}^{\bullet}$ are the main species responsible for FRP.

$$\text{Coumarin } (h\upsilon) \rightarrow {}^{1,3}\text{Coumarin}^{*} \quad (2)$$

$$^{1,3}\text{ Coumarin} + ArI^{+} \rightarrow Ar^{\bullet} + ArI + \text{Coumarin}^{\bullet+} \quad (3)$$

$$NPG + Iod \rightarrow [NPG\text{-}Iod]_{CTC} \quad (4)$$

$$[NPG\text{-}Iod]_{CTC} \rightarrow Ar^{\bullet} \quad (5)$$

$$^{1,3}\text{ Coumarin} + NPG \rightarrow \text{Coumarin—}H^{\bullet} + NPG_{(-H)}{}^{\bullet} \quad (6)$$

$$NPG_{(-H)}{}^{\bullet} \rightarrow NPG_{(-H;-CO2)}{}^{\bullet} + CO_2 \quad (7)$$

$$NPG_{(-H;-CO2)}{}^{\bullet} + Ar_2I^{+} \rightarrow NPG_{(-H;-CO2)}{}^{+} + Ar^{\bullet} + ArI \quad (8)$$

4.2.4. Structure/Reactivity/Efficiency Relationship

During the FRP process, Coum1 and Coum2 proved to be efficient photoinitiators, as demonstrated by the remarkable polymerization profiles evidencing the high rates of reaction and the high final conversions of the acrylate functions. However, this was not the case for Coum3, which showed a lower efficiency during the FRP experiments despite the high molar extinction coefficient and the high electron transfer quantum yields of this coumarin. These counter-intuitive results can be related to the poor solubility of Coum3 in the monomers, as the addition a few drops of chloroform was required to increase the final conversion rate and the polymerization rate, resulting from the higher solubility of Coum3. Therefore, in light of the polymerization efficiency, Coum3 seems to have a low reactivity compared to Coum1 and

Coum2. From the chemical structure point of view, Coum3 is a combination of Coum1 and Coum2, and the steric hindrance in Coum3 can clearly explain the poor reactivity of coum3. Thus, when using Coum3 in bulk, the diffusion is less favorable for all reactions in the multicomponent systems.

The better reactivity of Coum2 compared to Coum1 using two- or three-component photoinitiating systems for the photopolymerization of acrylate functions in thin samples can be explained by their differences in absorption properties. In fact, Coum2 exhibited a higher molar extinction coefficient at 405 nm compared with Coum1 (M^{-1} cm^{-1} vs. 23000 M^{-1} cm^{-1}).

5. Conclusions

In this paper, a series of coumarins have been proposed as efficient photoinitiators for the free radical polymerization of acrylates at 405 nm. Interestingly, the third coumarin (Coum3) examined as a photoinitiator proved to be a poor candidate, mainly attributable to its lack of solubility in the photocurable resins and its bulky character. Here again, the crucial role of molecular engineering for the design of highly efficient photoinitiators has been clearly evidenced. The best coumarins were tested for 3D printing experiments at 405 nm and for the synthesis of photocomposites with significant hardening of the surface and on the bottom using an LED @ 385 nm. In light of the high efficiency of coumarins, future development will consist of designing coumarins absorbing in the near infrared range, where light penetration is more important than that in the near UV/visible range.

References

[1] Ueno, K.; Oshikiri, T.; Sun, Q.; Shi, X.; Misawa, H. Solid-State Plasmonic Solar Cells. Chem. Rev. **2018**, 118, 2955.

[2] Fouassier, J.P.; Morlet-Savary, F.; Lalevée, J.; Allonas, X.; Ley, C. Dyes as photoinitiators or photosensitizers of polymerization reactions. Materials **2010**, 3, 5130.

[3] Fouassier, J.P.; Lalevee, J. Photoinitiators for Polymer Synthesis, Scope, Reactivity, and Efficiency; Wiley-VCH Verlag GmbH & Co.KGaA: Weinheim, Germany, 2012.

[4] Fouassier, J.P. Photoinitiator, Photopolymerization and Photocuring: Fundamentals and Applications; Hanser Gardner: New York, NY, USA, 1995.

[5] Xiao, P.; Zhang, J.; Dumur, F.; Tehfe, M.A.; Morlet-Savary, F.; Graff, B.; Gigmes, D.; Fouassier, J.P.; Lalevée, J. Photoinitiating systems: Recent progress in visible light induced cationic and radical photopolymerization reactions under soft conditions. Prog. Polym. Sci. **2015**, 41, 32.

[6] Trykowska Konc, J.; Hejchman, E.; Kruszewska, H.; Wolska, I.; Maciejewska, D. Synthesis and pharmacological activity of O-aminoalkyl derivatives of 7-hydroxycoumarin. Eur. J. Med. Chem. **2011**, 46, 2252.

[7] Wattenberg, L.W.; Low, L.K.T.; Fladmoe, A.V. Inhibition of chemical carcinogeninduced neoplasia by coumarins and a-angelicalactone. Cancer Res. **1979**, 39, 1651.

[8] Manolov, I.; Kostova, I.; Netzeva, T.; Konstantinov, S.; Karaivanova, M. Cytotoxic activity of cerium complexes with coumarin derivatives. Molecular modeling of the ligands. Archiv. Pharm. Med. Chem. **2000**, 333, 93.

[9] Lake, B.G. Coumarin metabolism, toxicity and carcinogenicity: Relevance for human risk assessment. Food Chem. Toxicol. **1999**, 37, 423.

[10] Manojkumar, P.; Ravi, T.K.; Subbuchettiar, G. Synthesis of coumarin heterocyclic derivatives with antioxidant activity and in vitro cytotoxic activity against tumour cells. Acta Pharm. **2009**, 59, 159.

[11] Mayekar, S.A.; Chaskar, A.C.; Mulwad, V.V. Facile synthesis of coumarinyl isothiocyanate from amino coumarin. Synth. Commun. **2009**, 40, 46.

[12] Jiang, Z.J.; Lv, H.S.; Zhu, J.; Zha, B.X. New fluorescent chemosensor based on quinoline and coumarin for Cu^{2+}. Synth. Met. **2012**, 162, 2112.

[13] Aldakov, D.; Anzenbacher, P. Dipyrrolyl quinoxalines with extended chromophores are efficient fluorimetric sensors for pyrophosphate. Chem. Commun. **2003**, 12, 1394.

[14] Hunger, K. Industrial Dyes, WILEY-VCH Verlag; Gmbh & Co. KGaA: Weinheim, Germany, 2003.

[15] Su, K.; Ming, J.; Zhang, L.; Xiang, S.; Cui, M.; Yang, H. A novel tricyclic heterocyclic fluorescent probe for Pd^{2+} in aqueous solution: Synthesis, properties and theoretical calculations. Opt. Mater. **2019**, 93, 25.

[16] Nasser Mabkhot, Y.; Barakat, A.; Mohammed Al-Majid, A.; Alshahrani, S.; Yousuf, S.; Iqbal Choudhary, M. Synthesis, reactions and biological activity of some new bis-heterocyclic ring compounds containing sulphur atom. Chem. Cent. J. **2013**, 7, 112.

[17] Cabanetos, C.; Blanchard, P.; Roncali, J. Arylamine Based Photoactive Push-Pull Molecular Systems: A Brief Overview of the Chemistry "Made in Angers". Chem. Rec. **2019**, 19, 1123-1130.

[18] Tehfe, M.A.; Dumur, F.; Graff, B.; Morlet-Savary, F.; Gigmes, D.; Fouassier, J.P.; Lalevée, J. Push-pull (thio)barbituric acid derivatives in dye photosensitized radical and cationic polymerization reactions under 457/473 nm Laser beams or blue LEDs. Polym. Chem. **2013**, 4, 3866.

[19] Xiao, P.; Dumur, F.; Graff, B.; Vidal, L.; Gigmes, D.; Fouassier, J.P.; Lalevée, J. Structural effects in the indanedione skeleton for the design of low intensity 300-500 nm light sensitive initiators. Macromolecules **2014**, 47, 26.

[20] Xiao, P.; Dumur, F.; Tehfe, M.A.; Gigmes, D.; Fouassier, J.P.; Lalevée, J. Red-light-induced cationic photopolymerization: Perylene derivatives as efficient photoinitiators Macromol. Rapid Commun. **2013**, 34, 1452.

[21] Dumur, F.; Gigmes, D.; Fouassier, J.P.; Lalevée, J. Organic Electronics: An El Dorado in the quest of new photoCatalysts as photoinitiators of polymerization. Acc. Chem. Res. **2016**, 49, 1980.

[22] Xiao, P.; Hong, W.; Li, Y.; Dumur, F.; Graff, B.; Fouassier, J.P.; Gigmes, D.; Lalevée, J. Green light sensitive diketopyrrolopyrrole derivatives used in versatile photoinitiating systems for photopolymerizations. Polym. Chem. **2014**, 5, 2293.

[23] Dietlin, C.; Schweizer, S.; Xiao, P.; Zhang, J.; Morlet-Savary, F.; Graff, B.; Fouassier, J.P.; Lalevée, J. Photopolymerization upon LEDs: New photoinitiating systems and strategies. Polym. Chem. **2015**, 6, 3895.

[24] Telitel, S.; Dumur, F.; Campolo, D.; Poly, J.; Gigmes, D.; Fouassier, J.P.; Lalevée, J. Iron complexes as potential photocatalysts for controlled radical photopolymerizations: A tool for modifications and patterning of surfaces. J. Polym. Sci. A Polym. Chem. **2016**, 54, 702.

[25] Gualandi, A.; Rodeghiero, G.; Della Rocca, E.; Bertoni, F.; Marchini, M.; Perciaccante, R.; Jansen, T.P.; Ceroni, P.; Cozzi, P.G. Application of coumarin dyes for organic photoredox catalysis. Chem. Commun. **2018**, 54, 10044.

[26] Liu, L.; Huang, D.; Draper, S.M.; Yi, X.; Wu, W.; Zhao, J. Visible light-harvesting trans bis(alkylphosphine)platinum(II)-alkynyl complexes showing long-lived triplet excited states as triplet photosensitizers for triplet-triplet annihilation upconversion. Dalton Trans. **2013**, 42, 10694.

[27] Kotchapadist, P.; Prachumrak, N.; Sunonnam, T.; Namuangruk, S.; Sudyoadsuk, T.; Keawin, T.; Jungsuttiwong, S.; Promarak, V. Synthesis, characterisation, and electroluminescence properties of n-coumarin derivatives containing peripheral triphenylamine. Eur. J. Org. Chem. **2015**, 3, 496.

[28] Yu, T.; Zhu, Z.; Bao, Y.; Zhao, Y.; Liu, X.; Zhang, H. Investigation of novel carbazole-functionalized coumarin derivatives as organic luminescent materials. Dyes Pigm. **2017**, 147, 260.

[29] Kochapradist, P.; Sunonnam, T.; Prachumrak, N.; Namuangruk, S.; Keawin, T.; Jungsuttiwong, S.; Sudyoadsuk, T.; Promarak, V. Synthesis, characterization, and properties of novel bis(aryl)carbazole-containing N-coumarin derivatives. Tetrahedron Lett. **2014**, 55, 6689.

[30] Al Mousawi, A.; Kermagoret, A.; Versace, D.L.; Toufaily, J.; Hamieh, T.; Graff, B.; Dumur, F.; Gigmes, D.; Fouassier, J.P.; Lalevée, J. Copper photoredox catalysts for polymerization upon near UV or visible light: Structure/reactivity/efficiency relationships and use in LED projector 3D printing resins. Polym. Chem. **2016**, 8, 568.

[31] Al Mousawi, A.; Dietlin, C.; Graff, B.; Morlet-Savary, F.; Toufaily, J.; Fouassier, J.P.; Chachaj-Brekiesz, A.; Ortyl, J.; Lalevée, J. Meta- terphenyl derivative/iodonium salt/9H-carbazole-9-ethanol photoinitiating systems for free radical promoted cationic polymerization upon visible lights. Macromol. Chem. Phys. **2016**, 217, 1955.

[32] Abdallah, M.; Hijazi, A.; Graff, B.; Fouassier, J.P.; Rodeghiero, G.; Gualandi, A.; Dumur, F.; Cozzi, P.G.; Lalevée, J. Coumarin derivatives as versatile photoinitiators for 3D printing, polymerization in water and photocomposite synthesis. Polym. Chem. **2019**, 10, 872.

[33] Bonardi, A.H.; Bonardi, F.; Noirbent, G.; Dumur, F.; Dietlin, C.; Gigmes, D.; Fouassier, J.P.; Lalevée, J. Different NIR dye scaffolds for polymerization reactions under NIR light. Polym. Chem. **2019**, 10, 6505.

[34] Tehfe, M.A.; Dumur, F.; Xiao, P.; Delgove, M.; Graff, B.; Gigmes, D.; Fouassier, J.P.; Lalevée, J. Chalcone derivatives as highly versatile photoinitiators for radical, cationic, thiol-ene and IPN polymerization reactions upon visible lights. Polym. Chem. **2014**, 5, 382.

[35] Zhang, J.; Dumur, F.; Xiao, P.; Graff, B.; Bardelang, D.; Gigmes, D.; Fouassier, J.P.; Lalevée, J. Structure design of naphthalimide derivatives: Toward versatile photoinitiators for near-UV/visible LEDs, 3D printing, and water-soluble photoinitiating systems. Macromolecules **2015**, 48, 2054.

[36] Zhang, J.; Zivic, N.; Dumur, F.; Guo, C.; Li, Y.; Xiao, P.; Graff, B.; Gigmes, D.; Fouassier, J.P.; Lalevée, J. Panchromatic photoinitiators for radical, cationic and thiol-ene polymerization reactions: A search in the diketopyrrolopyrrole or indigo dye series Mater. Today Commun. **2015**, 4, 101.

[37] Al Mousawi, A.; Poriel, C.; Dumur, F.; Toufaily, J.; Hamieh, T.; Fouassier, J.P.; Lalevée, J. Zinc tetraphenylporphyrin as high performance visible-light photoinitiator of cationic photosensitive resins for LED projector 3D printing applications. Macromolecules **2017**, 50, 746.

Chapitre I : Colorants organiques à base de dérivés de coumarines comme photoamorceurs

Section II : Recherche autour de la coumarine : colorants pour la polymérisation des acryliques

La photopolymérisation radicalaire (FRP) des monomères acryliques est largement rencontrée dans le domaine du séchage UV [1]. De nombreux systèmes mono et même multicomposants ont déjà été reportés dans la littérature [2-6]. Ces systèmes sont principalement basés sur des photoamorceurs sensibles au rayonnement électromagnétique UV.

Dans le cadre d'une recherche continue de nouveaux systèmes photoamorceurs hautement réactifs et efficaces, de nouveaux colorants organiques basés sur des dérivés de coumarines pour la polymérisation des résines acryliques et méthacryliques sont présentés dans cette section. Ces systèmes sont la suite des systèmes à base de coumarine déjà présentés dans la section précédente. En raison de leurs propriétés électrochimiques et photochimiques ces composés ont reçu beaucoup d'attention. Pour cela, neuf dérivés de coumarine ont été synthétisés par nos collaborateurs de l'université d'Aix-Marseille dans le but d'étudier leur capacité de photoamorçage des acrylates sous lumière visible. En effet, ces colorants possèdent d'excellentes propriétés d'absorption dans le proche UV et le visible (300-525 nm), des bonnes propriétés d'émission par fluorescence mais également des énergies des états excités élevées ce qui mène à des réactivités photochimiques élevées.

Comme la plupart des composés étudiés dans cette thèse, ces nouvelles coumarines développées ont été évaluées comme photoamorceurs Type II nécessitant l'utilisation d'un additif (sel d'iodonium) ou un co-amorceur (amine) afin d'amorcer efficacement le processus de polymérisation radicalaire. En raison de leurs propriétés d'absorption, ces colorants permettent un recouvrement favorable avec le spectre d'émission de la LED à 405nm utilisée, et sont ainsi très efficaces dans les réactions de polymérisation des acrylates une fois associés à un additif (ou un co-amorceur). De ce fait, des conversions finales élevées et des vitesses de polymérisation intéressantes ont été observées suite à une interaction oxydative ou réductive en présence du sel d'iodonium ou une amine (NPG) (systèmes bicomposants **Coum/Iod** ou **Coum/NPG).** Des systèmes à trois composants ont également été évalués, de sorte qu'une

forte amélioration du profil de polymérisation a été constatée une fois que le 3eme composant est ajouté à la formulation photosensible. Ce comportement a été expliqué par l'étude des propriétés électrochimiques, photochimiques et photophysiques des colorants utilisés (Quenching par Iod et NPG, photolyse en présence d'Iod et Iod/NPG, calcul des potentiels redox…).

Par ailleurs, ces dérivés sont utilisés dans des formulations photodurcissables pour la génération de motifs polymères en 3D épais par impression 3D sous une diode laser à 405nm. Les polymères obtenus présentent une bonne résolution spatiale reflétant la forte réactivité des systèmes étudiés. La synthèse de photocomposite a été accomplie avec succès par imprégnation de plusieurs couches de fibre de verre en se basant sur les systèmes dérivés de coumarine.

Les différentes applications ainsi que la capacité de photoamorcage des coumarines ont permis la proposition d'un **schéma générique** sur cette famille. Ce travail présenté dans cette section a été publié dans **'molecules'** sous la citation suivante : Rahal, M.; Graff, B.; Toufaily, J.; Hamieh, T.; Noirbent, G.; Gigmes, D.; Dumur, F.; Lalevee, J. Molecules 3-Carboxylic Acid and Formyl-Derived Coumarins as Photoinitiators in Photo-oxidaton or Photo-reduction Processes for Photopolymerization upon Visible Light : Photocomposite Synthesis and 3D printing Applications. Molecules, **2021**, 26, 1753.

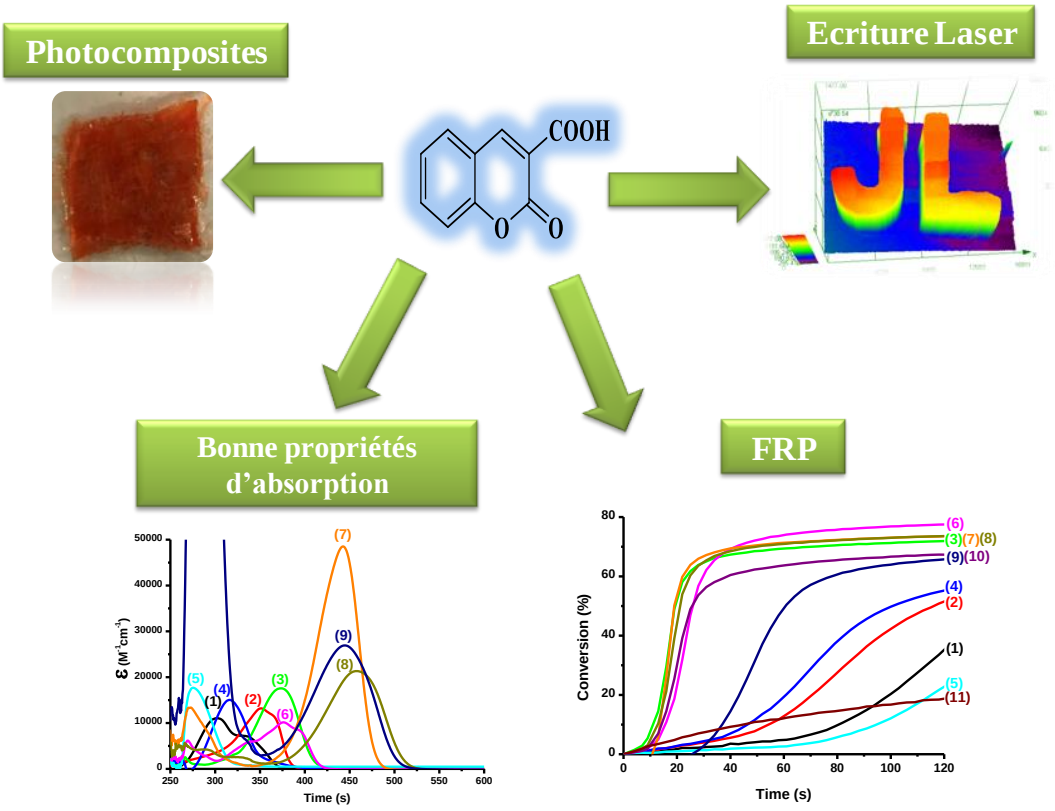

Schéma 1. Les coumarines, leurs applications et leurs caractéristiques

Références

[1] a) Fouassier, J.P. Photoinitiation; photopolymerization; photocuring : Fundamental and Applications, Munich: Hanser, **1995**; b) Fouassier, J.P. Photochemistry and UV Curing, Eds.; Research Signpost: Trivandrum, India, **2006**; c) Belfied, K.D.; Crivello, J.V. Photoinitiated polymerization, ACS Symposium series: American Chemical Society, Washington, DC, USA, vol. 847, **2003**.

[2] Tehfe, M.A.; Dumur, F.; Graff, B.; Morlet-Savary, F.; Gigmes, D.; Fouassier, J.P.; Lalevée, J. Design of new Type I and Type II photoinitiators possessing highly coupled pyrene–ketone moieties. Polym.Chem. **2013**, 4, 2313.

[3] Doğruyol, S.K.; Doğruyol, Z.; Arsu, N. A thioxanthone-based visible photoinitiator J.Polym.Sci., PartA : Polym.Chem. **2011**, 49, 4037.

[4] Xiao, P.; Dumur, F.; Graff, B.; Fouassier, J.P.; Gigmes, D.; Lalevée, J. Cationic and Thiol-Ene Photopolymerization upon Red Lights Using Anthraquinone Derivatives as Photoinitiators. Macromolecules, **2013**, 46, 6744.

[5] Xiao, P.; Dumur, F.; Graff, B.; Morlet-Savary, F.; Vidal, L.; Gigmes, D.; Fouassier, J.P.; Lalevée, J. Structural Effects in the Indanedione Skeleton for the Design of Low Intensity 300-500 nm Light Sensitive Initiators. Macromolecules, **2014**, 47, 26.

[6] Xiao, P.; Dumur, F.; Frigoli, M.; Tehfe, M.A.; Morlet-Savary, F.; Graff, B.; Fouassier, J.P.; Gigmes, D.; Lalevée, J. Naphthalimide based methacrylated photoinitiators in radical and cationic photopolymerization under visible light. Polym.Chem. **2013**, 4, 5440.

3-Carboxylic Acid and Formyl-Derived Coumarins as Photoinitiators in Photo-Oxidation or Photo-Reduction Processes for Photopolymerization upon Visible Light: Photocomposite Synthesis and 3D Printing Applications

Abstract:

In this paper, nine organic compounds based on the coumarin scaffold and different substituents were synthesized and used as high-performance photoinitiators for free radical photopolymerization (FRP) of meth(acrylate) functions under visible light irradiation using LED at 405 nm. In fact, these compounds showed a very high initiation capacity and very good polymerization profiles (both high rate of polymerization (Rp) and final conversion (FC)) using two and three-component photoinitiating systems based on coum/iodonium salt (0.1%/1% w/w) and coum/iodonium salt/amine (0.1%/1%/1% w/w/w), respectively. To demonstrate the efficiency of the initiation of photopolymerization, several techniques were used to study the photophysical and photochemical properties of coumarins, such as: UV-visible absorption spectroscopy, steady-state photolysis, real-time FTIR, and cyclic voltammetry. On the other hand, these compounds were also tested in direct laser write experiments (3D printing). The synthesis of photocomposites based on glass fiber or carbon fiber using an LED conveyor at 385 nm (0.7 W/cm^2) was also examined.

Keywords : coumarin; free radical polymerization; LED; photocomposites; direct laser write.

1. Introduction

The development of new low-cost, environmentally friendly, and energy-efficient polymer synthesis remains more than ever at the heart of academic and industrial concerns and the subject of many new research strategies. In fact, thanks to technological development, light sources which are at the same time inexpensive, efficient, and with low energy consumption have been developed recently to induce photopolymerization reactions [1–4]. Nowadays, photopolymers are present in several fields such as coatings [5], dentistry [6], automotive [7], cosmetics [8], 3D printing, and holography [9], etc. For most of these industrial fields, photochemical polymerization uses ultraviolet radiation, a technique widely known as UV curing. However, this pathway based on UV lamps (Hg lamps) remains energy-consuming.

Moreover, the ultraviolet light is harmful to human health (carcinogenic) and characterized by particularly low light penetration, which is a challenge for the photopolymerization of thick and filled samples [10]. Therefore, alternatives to UV lamps and the use of longer wavelengths (near UV or visible) can be advantageous. The use of light-emitting diodes (LEDs) perfectly fit this requirement for safer/cheaper, and more efficient irradiation devices than UV lamps or UV lasers [11–14]. In parallel, it is important to develop new photoinitiating systems able to absorb in the near UV or the visible range where their absorption spectrum overlaps that of the LED emission. To obtain this type of system, it is necessary to develop new organic molecules carrying chromophore groups capable of shifting their absorption spectrum towards the near-UV-visible range. These molecules will be called photoinitiator (PI), which can absorb the light and generate reactive species (in combination with additives) able to initiate the photopolymerization process.

In this paper, nine coumarin derivatives (noted Coum in Scheme 1) varying by the substitution pattern at the 3- and 7-positions of the coumarin core were synthesized and evaluated as photoinitiators for the FRP of acrylate and methacrylate monomers. In fact, coumarin derivatives have already been tested as photoinitiators of FRP and they have shown good polymerization profile (Rp and FC) as well as good photochemical and photophysical properties [15–19].

However, in the present work, coumarin-3-carboxylic acids, coumarin-3-aldehydes varying by the substitution pattern of the coumarin core and a coumarin of extended aromaticity have been studied as photoinitiators. Comparisons of the three families of coumarins have revealed that the substitution of the 3-position by electron-withdrawing groups such as a formyl group could improve the reactivity. The presence of a strong electron-donating group at the 7-position, such as diethylamine or a naphthalene group, could reinforce the electronic delocalization and the photoinitiating ability of the different systems. An optimum situation was found when electron-donating and electron-accepting groups were attached at both extremities of the coumarin core. Considering that the nitro group is among the most electron-withdrawing group, a coumarin bearing this electron acceptor was also designed and synthesized.

In fact, coumarin derivatives are usually characterized by very high fluorescence emission and can be used as fluorescent chromophores for several applications [20]. They are also characterized by high molar extinction coefficients in the near-UV and the visible range [19].

These novel coumarin-based photoinitiators were tested in photopolymerization of acrylate functions (TMPTA or TA) in both Thick (1.4 mm) and Thin sample (25 µm) using two and three-component photoinitiating systems PISs based on Coum/Iodonium salt (0.1%/1% w/w) and Coum/Iodonium salt/amine (NPG) (0.1%/1%/1% w/w/w). These systems were also used in 3D printing and photocomposite synthesis. These dyes are characterized by very high extinction coefficients with a broad absorption extending over the near UV/visible and high quantum yields were determined by fluorescence quenching. It is important to note that coumarin shows a dual photo-oxidation and photo-reduction character.

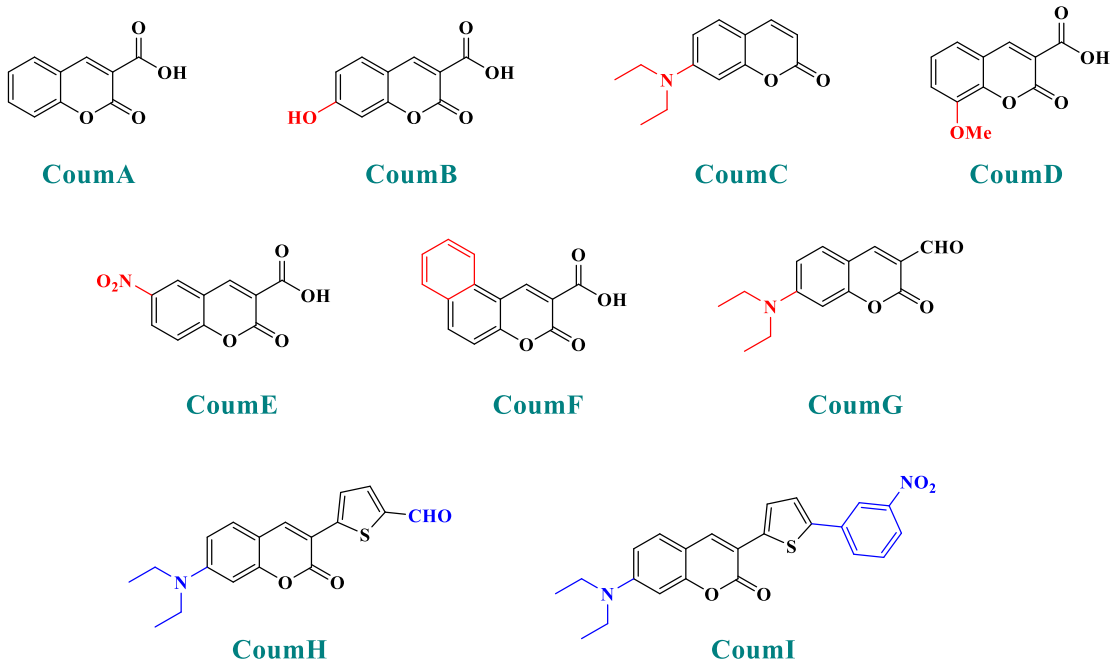

Scheme 1. The new series of Coumarins (CoumA - CoumI) examined as photoinitiators of polymerization.

2. Experimental part

2.1. Synthesis of the Different Dyes

As mentioned in the introduction section, three families of coumarins have been examined as photoinitiators of polymerization. The first family concerned coumarin-3-carboxylic acids. The five dyes were prepared in solution by condensation of diethyl malonate with ortho-hydroxyarylaldehydes [21]. After hydrolysis of esters in acidic conditions (a mixture of hydrochloric acid and acetic acid), the solution was neutralized to provide the different dyes with reaction yields ranging from 75% for CoumA to 86% yield for CoumE. A similar

procedure was used for CoumC except that the hydrolysis of the intermediate ester coumarin resulted in a decarboxylation reaction, providing CoumC in 72% yield. The presence of the dimethylamino group in CoumC is essential to activate the decarboxylation reaction since this reaction was not observed for the other coumarins, maintaining the acidic function on the coumarins (See Scheme 2) [22]. Using the Vilsmeier Haack reaction, CoumC could be converted as CoumG in a 77% yield.

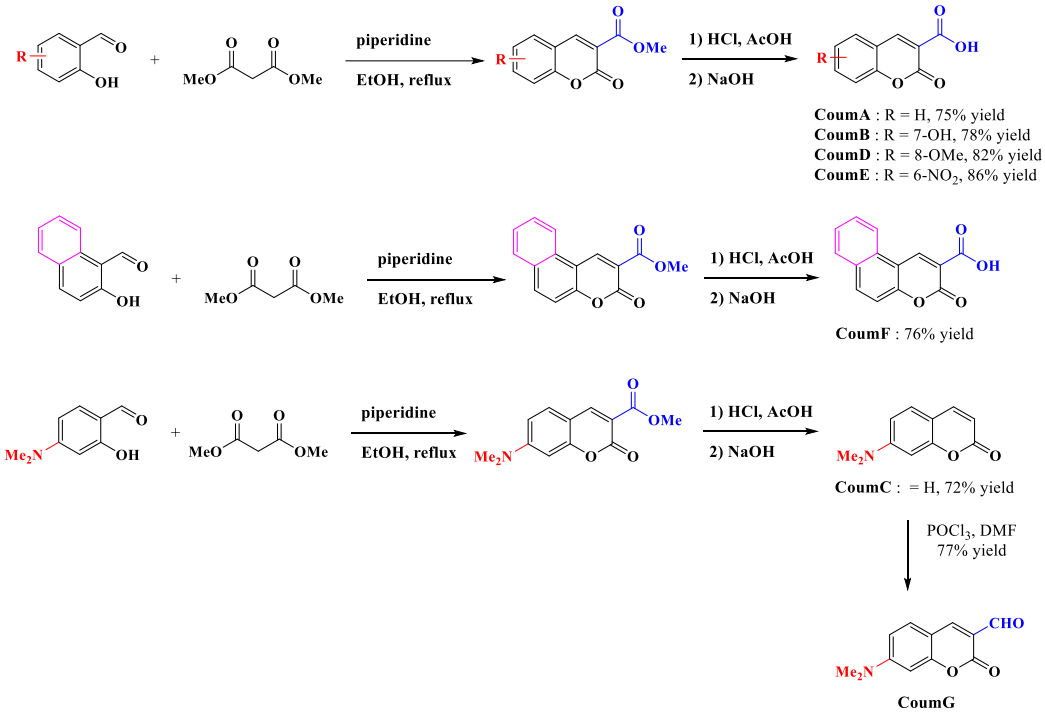

Scheme 2. Synthetic routes to CoumA-CoumG.

Finally, CoumH and CoumI could be prepared starting from 2-thiopheneacetic acid and 4-diethylamino-2-hydroxybenzaldehyde. By Knoevenagel reaction, 7-(diethylamino)-3 (thiophen-2-yl)-2H-chromen-2-one could be obtained in 58% yield and by means of a Vilsmeier Haack reaction, CoumH was isolated in pure form in 88% yield. Conversely, CoumI was prepared in two steps, first by bromination of 7-(diethylamino)-3-(thiophen-2-yl) 2H-chromen-2-one in 86% yield, followed by a Suzuki cross-coupling reaction with 3 nitrophenylboronic acid. Using this procedure, CoumI was obtained in 67% yield (See Scheme 3).

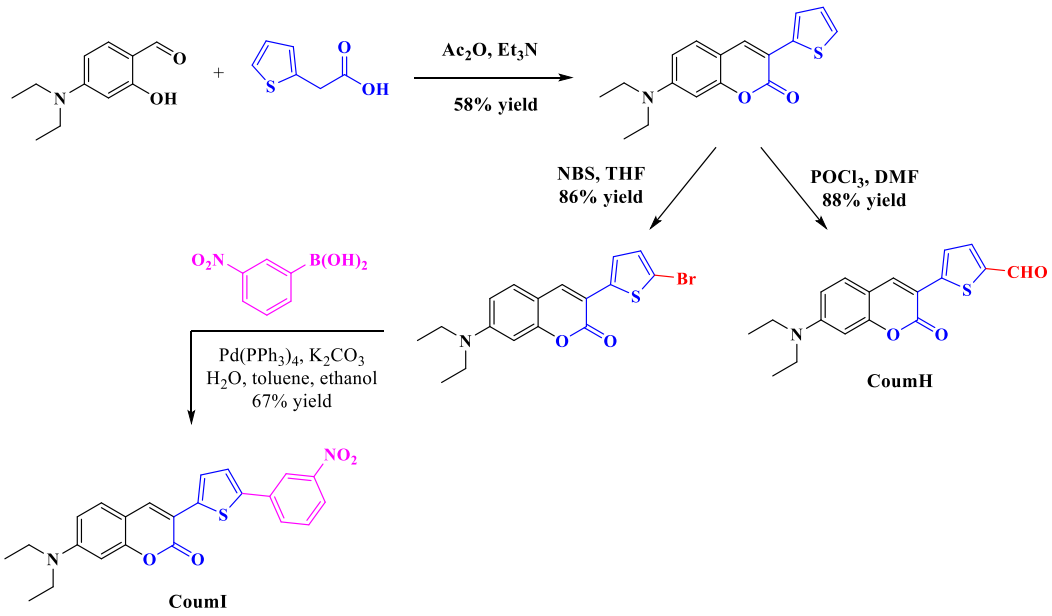

Scheme 3. Synthetic routes to CoumH and CoumI.

Synthesis of the Coumarins

All reagents and solvents were purchased from Aldrich, Alfa Aesar, or TCI Europe and used as received without further purification. Mass spectroscopy was performed by the Spectropole of Aix-Marseille University. ESI mass spectral analyses were recorded with a 3200 QTRAP (Applied Biosystems SCIEX) mass spectrometer. The HRMS mass spectral analysis was performed with a QStar Elite (Applied Biosystems SCIEX) mass spectrometer. Elemental analyses were recorded with a Thermo Finnigan EA 1112 elemental analysis apparatus driven by the Eager 300 software. ^{1}H and ^{13}C NMR spectra were determined at room temperature in 5 mm o.d. tubes on a Bruker Avance 400 spectrometer and on a Bruker Avance 300 spectrometer of the Spectropole: The ^{1}H chemical shifts were referenced to the solvent peak $CDCl_3$ (7.26 ppm), and the ^{13}C chemical shifts were referenced to the solvent peak $CDCl_3$ (77 ppm). 7-(Diethylamino)-3-(thiophen-2-yl)-2H-chromen-2-one and 3-(5-bromothiophen-2-yl)-7-(diethylamino)-2H-chromen-2-one used as intermediates of reaction have been synthesized according to procedures previously reported in the literature, without modifications and in similar yields [18]

Synthesis of 2-oxo-2H-chromene-3-carboxylic acid (CoumA)

Dimethyl malonate (2.64 g, 20 mmol, M = 132.11 g/mol) and piperidine (1 mL, 10 mmol) were mixed and added to a solution of salicylaldehyde (1.22 g, 10 mmol, M = 122.12 g/mol) dissolved in absolute ethanol (30 mL). After stirring and heating to reflux for 6 hours, the

solvent was removed under reduced pressure. Then, concentrated HCl (20 mL) and acetic acid (20 mL) were added for hydrolysis and the solution was refluxed overnight. After cooling, the solution was poured onto ice and aq. 40% NaOH was added until pH = 5. A pale precipitate formed. After stirring for another 30 min, the mixture was filtered, washed with water, pentane, and dried under vacuum (1.43 g, 75% yield). ^{1}H NMR (400 MHz, DMSO-d_6) δ 8.75 (s, 1H), 7.91 (dd, J = 7.7, 1.2 Hz, 1H), 7.80–7.68 (m, 1H), 7.42 (dd, J = 15.4, 7.9 Hz, 2H). Analyses were consistent with those previously reported in the literature [23]

Synthesis of 7-hydroxy-2-oxo-2H-chromene-3-carboxylic acid (CoumB)

Dimethyl malonate (2.64 g, 20 mmol, M = 132.11 g/mol) and piperidine (1 mL, 10 mmol) were mixed and added to the solution of 2,4-dihydroxybenzaldehyde (1.38 g, 10 mmol, M = 138.12 g/mol) dissolved in absolute ethanol (30 mL). After stirring and heating to reflux for 6 hours, the solvent was removed under reduced pressure. Then, concentrated HCl (20 mL) and acetic acid (20 mL) were added for hydrolysis, and the solution was refluxed overnight. After cooling, the solution was poured onto ice and aq. 40% NaOH was added until pH = 5. A pale precipitate formed. After stirring for another 30 min, the mixture was filtered, washed with water, pentane, and dried under vacuum (1.61 g, 78% yield). ^{1}H NMR (400 MHz, DMSO-d_6) δ 8.68 (s, 1H), 7.75 (d, J = 8.6 Hz, 1H), 6.85 (dd, J = 8.6, 2.3 Hz, 1H), 6.74 (d, J = 2.1 Hz, 1H). Analyses were consistent with those previously reported in the literature [23].

Synthesis of 7-(diethylamino)-2H-chromen-2-one (CoumC)

Dimethyl malonate (2.64 g, 20 mmol, M = 132.11 g/mol) and piperidine (1 mL, 10 mmol) were mixed and added to the solution of 4-(Diethylamino)-salicylaldehyde (1.93 g, 10 mmol) dissolved in absolute ethanol (30 mL). After stirring and heating to reflux for 6 hours, the solvent was removed under reduced pressure. Then, concentrated HCl (20 mL) and acetic acid (20 mL) were added for hydrolysis and the solution was refluxed overnight. After cooling, the solution was poured onto ice and aq. 40% NaOH was added until pH = 5. A pale precipitate formed. After stirring for another 30 min, the mixture was filtered, washed with water, pentane, and dried under vacuum (1.56 g, 72% yield). ^{1}H NMR (400 MHz, $CDCl_3$) δ 7.53 (d, J = 9.3 Hz, 1H), 7.24 (d, J = 8.8 Hz, 1H), 6.60–6.44 (m, 2H), 6.03 (d, J = 9.3 Hz, 1H), 3.41 (q, J = 7.1 Hz, 4H), 1.21 (t, J = 7.1 Hz, 6H). Analyses were consistent with those previously reported in the literature [24].

Synthesis of 8-methoxy-2-oxo-2H-chromene-3-carboxylic acid (CoumD)

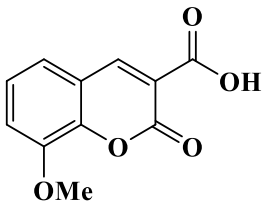

Dimethyl malonate (2.64 g, 20 mmol, M = 132.11 g/mol) and piperidine (1 mL, 10 mmol) were mixed and added to the solution of 3-methoxysalicylaldehyde (1.52 g, 10 mmol, M = 152.15 g/mol) dissolved in absolute ethanol (30 mL). After stirring and heating to reflux for 6 hours, the solvent was removed under reduced pressure. Then, concentrated HCl (20 mL) and acetic acid (20 mL) were added for hydrolysis and the solution was refluxed overnight. After cooling, the solution was poured onto ice and aq. 40% NaOH was added until pH = 5. A pale precipitate formed. After stirring for another 30 min, the mixture was filtered, washed with water, pentane, and dried under vacuum (1.80 g, 82% yield). ^{1}H NMR (400 MHz, DMSO-d_6) δ 8.50 (s, 1H), 7.42–7.26 (m, 3H), 3.91 (s, 3H). Analyses were consistent with those previously reported in the literature [25].

Synthesis of 6-nitro-2-oxo-2H-chromene-3-carboxylic acid (CoumE)

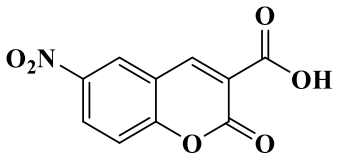

Dimethyl malonate (2.64 g, 20 mmol, M = 132.11 g/mol) and piperidine (1 mL, 10 mmol) were mixed and added to the solution of 2-hydroxy-5-nitrobenzaldehyde (1.67 g, 10 mmol, M = 167.12 g/mol) dissolved in absolute ethanol (30 mL). After stirring and heating to reflux for 6 hours, the solvent was removed under reduced pressure. Then, concentrated HCl (20 mL) and acetic acid (20 mL) were added for hydrolysis and the solution was refluxed overnight. After cooling, the solution was poured onto ice and aq. 40% NaOH was added until pH = 5. A pale precipitate formed. After stirring for another 30 min, the mixture was filtered, washed with water, pentane, and dried under vacuum (2.02 g, 86% yield). ^{1}H NMR (400 MHz, DMSO-d_6) δ 8.81 (d, J = 2.8 Hz, 1H), 8.51–8.33 (m, 2H), 7.59 (d, J = 9.1 Hz, 1H) Analyses were consistent with those previously reported in the literature [26].

Synthesis of 3-oxo-3H-benzo[f]chromene-2-carboxylic acid (CoumF)

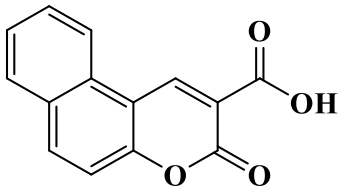

Dimethyl malonate (2.64 g, 20 mmol, M = 132.11 g/mol) and piperidine (1 mL, 10 mmol) were mixed and added to the solution of 2-hydroxy-1-naphthaldehyde (1.72 g, 10 mmol, M = 172.18 g/mol) dissolved in absolute ethanol (30 mL). After stirring and heating to reflux for 6 hours, the solvent was removed under reduced pressure. Then, concentrated HCl (20 mL) and acetic acid (20 mL) were added for hydrolysis and the solution was refluxed overnight. After cooling, the solution was poured onto ice and aq. 40% NaOH was added until pH = 5. A pale precipitate formed. After stirring for another 30 min, the mixture was filtered, washed with water, pentane, and dried under vacuum (1.82 g, 76% yield). ^{1}H NMR (400 MHz, DMSO-d_6) δ 9.37 (s, 1H), 8.60 (d, J = 8.3 Hz, 1H), 8.31 (d, J = 9.0 Hz, 1H), 8.09 (d, J = 7.8 Hz, 1H), 7.77 (ddd, J = 8.3, 7.0, 1.3 Hz, 1H), 7.65 (dt, J = 12.9, 2.9 Hz, 1H), 7.60 (d, J = 9.1 Hz, 1H). Analyses were consistent with those previously reported in the literature [27].

Synthesis of 7-(diethylamino)-2-oxo-2H-chromene-3-carbaldehyde (CoumG)

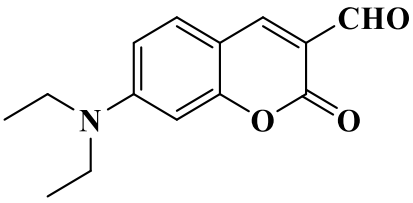

20 mL of $POCl_3$ was added dropwise to 20mL of dry DMF at 0 °C under Argon and stirred during 30 minutes at 50 °C. Then 7-(diethylamino)-2H-chromen-2-one (15,0 g, 69.1 mmol, M = 217.27g/mol) in 100 mL of DMF was added to the mixture and the mixture was heated to 60 °C overnight. Afterward, the mixture was poured into 500 mL of ice water and a solution of NaOH 20% was added. The precipitate was filtered and washed with water. (13.12 g, 77% yield). ^{1}H NMR (300 MHz, $CDCl_3$) δ 10.08 (s, 1H), 8.21 (s, 1H), 7.46–7.32 (m, 1H), 6.61 (dd, J = 9.0, 2.5 Hz, 1H), 6.45 (d, J = 2.3 Hz, 1H), 3.46 (q, J = 7.1 Hz, 4H), 1.23 (t, J = 7.1 Hz, 6H). Analyses were consistent with those previously reported in the literature [24].

Synthesis of 5-(7-(diethylamino)-2-oxo-2H-chromen-3-yl) thiophene-2-carbaldehyde (CoumH)

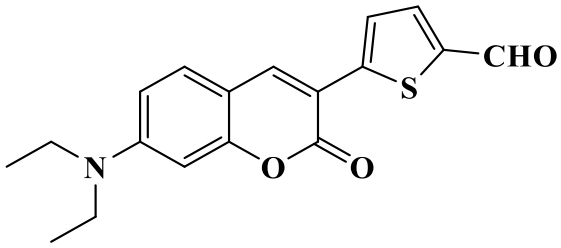

7-(Diethylamino)-3-(thiophen-2-yl)-2H-chromen-2-one (3.00 g, 10 mmol, M = 299.39 g/mol) was dissolved in DMF (7 mL) and $POCl_3$ (1.8 mL, 20 mmol) was slowly added at 0 °C. The mixture was heated up to 80 °C overnight. After cooling, the solution was quenched with water. The mixture was extracted with DCM several times. The organic phases were combined, dried over magnesium sulfate and the solvent removed under reduced pressure. It was used without any further purification (2.88 g, 88% yield). ^{1}H NMR (400 MHz, $CDCl_3$) δ 9.90 (s, 1H), 8.02 (s, 1H), 7.77 (d, J = 4.1 Hz, 1H), 7.73 (d, J = 4.1 Hz, 1H), 7.38 (d, J = 8.9 Hz, 1H), 6.69 (dd, J = 8.9, 2.5 Hz, 1H), 6.56 (d, J = 2.4 Hz, 1H), 3.46 (q, J = 7.1 Hz, 4H), 1.25 (t, J = 7.1 Hz, 6H). Analyses were consistent with those previously reported in the literature [28].

Synthesis of 7-(diethylamino)-3-(5-(3-nitrophenyl)thiophen-2-yl)-2H-chromen-2-one (CoumI)

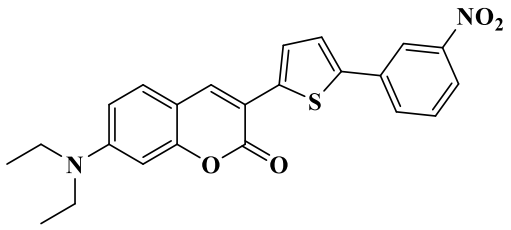

Tetrakis(triphenylphosphine)palladium (0) (0.46 g, 0.744 mmol, M = 1155.56 g.mol^{-1}) was added to a mixture of 3-(5-bromothiophen-2-yl)-7-(diethylamino)-2H-chromen-2-one (2.31 g, 6.11 mmol, M = 378.28 g.mol^{-1}), 3-nitrophenylboronic acid (1.53 g, 9.16 mmol, M = 166.93 g.mol^{-1}), toluene (54 mL), ethanol (26 mL) and an aqueous potassium carbonate solution (2 M, 6.91 g in 25 mL water, 26 mL) under vigorous stirring. The mixture was stirred at 80 °C for 48 h under a nitrogen atmosphere. After cooling to room temperature, the reaction mixture was poured into water and extracted with ethyl acetate. The organic layer was washed with brine several times, and the solvent was then evaporated. The residue was purified by filtration on a plug of silicagel using a mixture of DCM/ethanol as the eluent (67% yield, 1.72 g). ^{1}H NMR (400 MHz, $CDCl_3$) δ 8.49 (t, J = 1.9 Hz, 1H), 8.10 (ddd, J = 8.2, 2.2, 1.0 Hz,

1H), 7.98–7.92 (m, 2H), 7.64 (d, J = 4.0 Hz, 1H), 7.56 (d, J = 8.0 Hz, 1H), 7.43 (d, J = 4.0 Hz, 1H), 7.35 (d, J = 8.9 Hz, 1H), 6.64 (dd, J = 8.8, 2.5 Hz, 1H), 6.55 (d, J = 2.4 Hz, 1H), 3.45 (q, J = 7.1 Hz, 4H), 1.24 (t, J = 7.1 Hz, 6H); HRMS (ESI MS) m/z: theor: 420.1144 found: 420.1147 ($M^{+\cdot}$ detected); Anal. calc. for $C_{23}H_{20}N_2O_4S$: C, 65.7, H, 4.8, O, 15.2; found: C 65.5, H 4.7, O 15.4

2.2. Others chemical compounds

All the other chemicals (Figure 9) were selected with the highest purity available and used as received. Di-tert-butyl-diphenyliodonium hexafluorophosphate (Iod) and TMA (4,N,N-Trimethylaniline) were obtained from Lambson Ltd. (UK). Trimethylolpropane triacrylate (TMPTA), di(trimethylolpropane) tetraacrylate (TA), Mix-MA, N-Phenylglycine (NPG) were obtained from Allnex or Sigma Aldrich. TMPTA, TA, and Mix-MA were selected as benchmark monomers for the radical polymerizations.

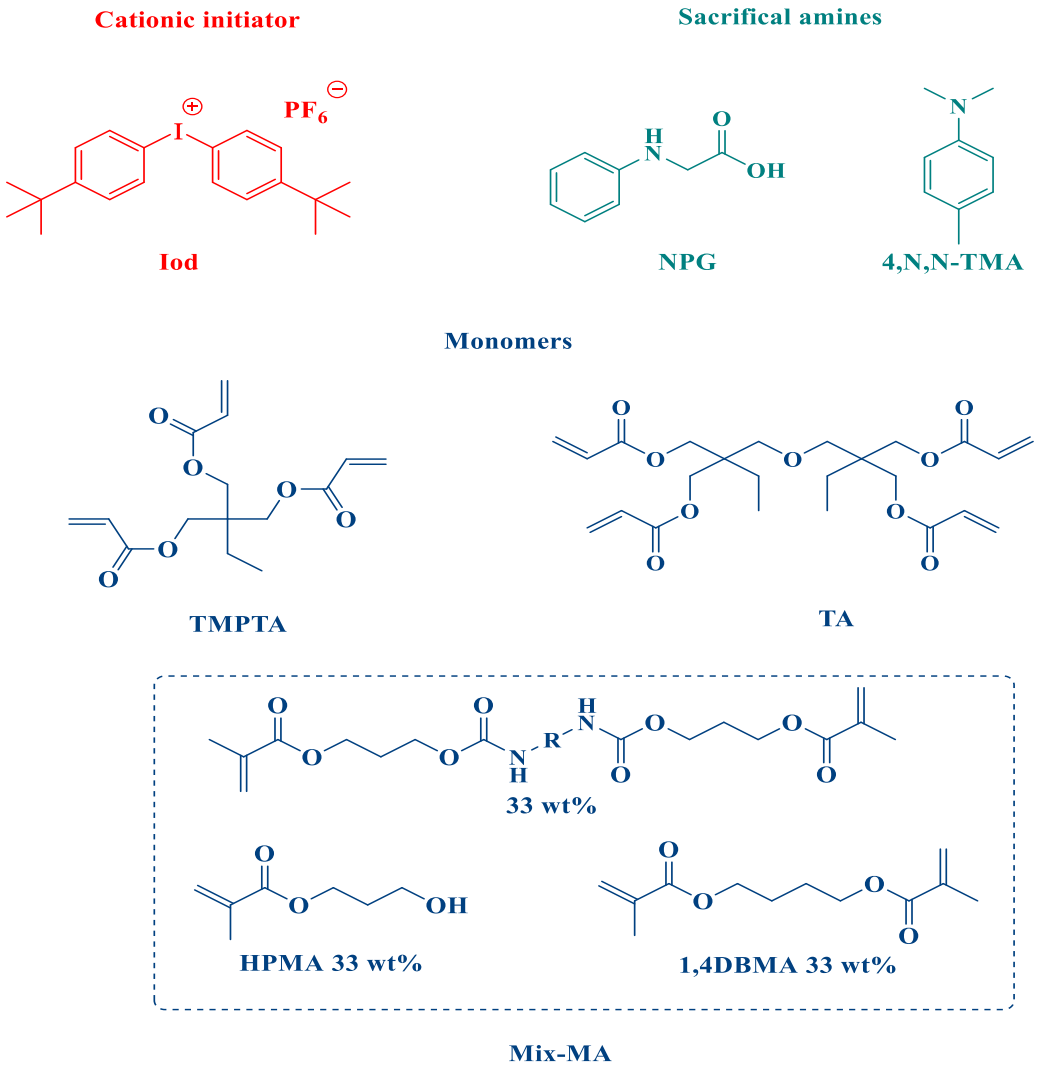

Figure 1. Other chemical compounds used in this paper.

2.3. Irradiation Light sources

We used different light-emitting diodes (LEDs) as light sources: (1) at 405 nm (I = 110 mW/cm^2) for the photopolymerization experiments, (2) at 375 nm (I = 40 mW/cm^2) for the photolysis of Coumarins and (3) at 385 nm (I = 0.7 W/cm^2) for the photocomposite synthesis.

2.4. Real-Time Fourrier Transform Infrared spectroscopy (RT-FTIR): Kinetic Followed and Final conversion (FC) determination for the Photopolymerisation

In this research, the ability of coumarins to initiate the photopolymerization of (meth)acrylate functions (FRP) was studied using two and three-component photoinitiating systems based on Coum/Iod salt (or NPG) (0.1%/1% w/w) and Coum/Iod/NPG (0.1%/1%/1% w/w/w). The percentage of the different chemical compounds is calculated according to the monomer weight. Kinetic study, as well as the reactive function conversion, were monitored

by the evolution of the double bond vs. time. In fact, the polymerization experiments were performed in both thick (1.4 mm) and thin (25 µm) samples, they were obtained by deposition of the formulation into the mold (1.4 mm) or between two propylene films in order to reduce O2 inhibition, respectively. In addition, excellent solubility of all coumarin derivatives (excluding the CoumE) were observed. For the thick and thin samples, the evolution of the (meth)acrylate functions for TMPTA or Mix-MA were followed by RT-FTIR spectroscopy (JASCO FTIR 6600) at about 6150 cm^{-1} and 1630 cm^{-1}, respectively. The procedure used to monitor the photopolymerization profile was described in detail in [29,30].

2.5 Redox potentials

The reduction (E_{red}) or oxidation (E_{ox}) potentials for the different coumarin derivatives were determined by cyclic voltammetry in ACN using tetrabutylammonium hexafluorophosphate as the supporting electrolyte (potential vs. saturated calomel electrode–SCE). The free energy change (ΔG_{et}) for an electron transfer reaction was calculated using equation (2) [25], where E_{ox}, E_{red}, E*, and C represent the oxidation potential of the electron donor, the reduction potential of the electron acceptor, the excited state energy level (determined from luminescence experiments) and the coulombic term for the initially formed ion pair, respectively. Here, C was neglectedm as usually done for polar solvents.

$$\Delta G_{et} = E_{ox} - E_{red} - E^* + C \qquad \text{eq.2}$$

2.6. UV-vis Absorption and photolysis experiments

The absorption properties (UV-visible absorption spectrum and molar extinction coefficient) as well as the steady state photolysis of the investigated Coumarin derivatives (CoumA - CoumI) in acetonitrile have been investigated using a JASCO V730 spectrometer.

2.7. Fluorescence experiments

The fluorescence properties of these organic compounds in ACN were studied using a JASCO FP-6200 spectrofluorimeter. The fluorescence quenching of ^{1}Coumarin by Iod or NPG were examinated from the classical Stern-Volmer treatment [31] ($I_0/I = 1 + kq\ \tau_0[Q]$, where I_0 and I stand for the fluorescent intensity of Coumarin in the absence and the presence of Iod or NPG, respectively; τ_0 stands for the lifetime of Coumarin in the absence of Iod and [Q] stand for the concentration of quencher, in our study Iod or NPG).

2.8. Computational Procedure

Molecular orbital calculations were carried out with the Gaussian 03 suite of programs [32,33]. Electronic absorption spectra for the different compounds were calculated with the time-dependent density functional theory at the MPW1PW91-FC/6-31G* level of theory on the relaxed geometries calculated at the UB3LYP/6-31G* level of theory.

2.9. Near-UV conveyor for photocomposite synthesis

Photocomposites have been achieved using glass fibers for the reinforcement and an organic resin based on acrylates (50%/50% w/w). The photosensitive resin has been deposited on glass fibers, then the mixture was irradiated using a LED conveyor at 385 nm(0.7 $W.cm^{-2}$). A Dymax-UV conveyor was used, the distance between the belt and the LED was fixed to 15 mm, and the belt speed was fixed to 2 $m.min^{-1}$.

2.10. Laser writing and 3D patterns characterization

For the direct laser write experiments, a computer-controlled the laser diode at 405 nm (spot size = 50 μm) was used, and the 3D patterns obtained were characterized by a numerical optical microscope (DSX-HRSU from OLYMPUS Corporation) [34].

3. Results

Photoinitiation ability, the performance of photopolymerization, photophysical and photochemical properties as well as chemical mechanisms associated with the photopolymerization processes will be discussed in detail.

3.1. Light Absorption Properties

UV-visible absorption spectra of the different coumarins in acetonitrile are depicted in Figure 1 (See also Table 1). These organic compounds are characterized by a high molar extinction coefficient in both near-UV and visible range (e.g., CoumC ε ~ 18000 $M^{-1}cm^{-1}$ at 374 nm and 3500 $M^{-1}cm^{-1}$ at 405 nm, and CoumF ε ~ 10200 $M^{-1}cm^{-1}$ at 376 nm and 4800 $M^{-1}cm^{-1}$ at 405 nm). So, these absorption properties afford a good overlap with the emission spectrum of the LEDs used in this work (LED at 405 nm for FRP, LED at 375 nm for the photolysis experiments and LED at 385 nm for the photocomposites synthesis).

In fact, the presence of different substituents on the coumarin scaffold can affect the absorption properties (Figure 2) of these compounds and their molar extinction coefficients can be affected. For example, taking CoumA as a standard structure among these 10 compounds, we observed a shift towards higher absorption range (e.g., CoumB, CoumD, and

CoumF are strongly shifted), and towards lower absorption range (e.g., CoumE), so a bathochromic effect is observed by introduction of electron donor group (such as OH, OMe, and NR_2) and a hypsochromic effect is observed by introduction of electron acceptor group (e.g., NO_2 in case of CoumE).

The electron-donating effect of these substituents is presented by ascending order: CoumH > CoumI > CoumG > CoumF > CoumC > CoumD > CoumB.

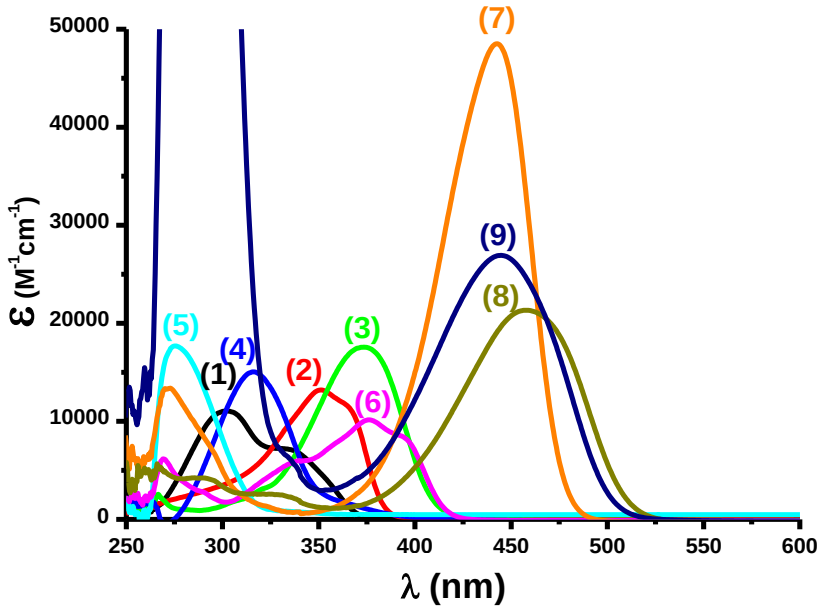

Figure 2. UV-visible absorption spectra of the investigated compounds based on Coumarin derivatives in ACN: **(1)** CoumA, **(2)** CoumB, **(3)** CoumC, **(4)** CoumD, **(5)** CoumE, **(6)** CoumF, **(7)** CoumG, **(8)** CoumH and **(9)** CoumI.

Table 1. Light absorption properties of coumarins at 405 nm and at λ_{max}; singlet state energy (E_{S1}) determined from the crossing point of absorption and fluorescence spectra.

	λ_{max} (nm)	ε_{max} (M^{-1} cm^{-1})	ε_{405nm} (M^{-1} cm^{-1})	E_{S1} (eV)
CoumA	302	11,000	40	3.35
CoumB	351	13,000	80	3.24
CoumC	374	18,000	3500	3.01
CoumD	322	14,000	100	3.12
CoumE	275	18,000	60	3.91
CoumF	376	10,000	4800	2.98
CoumG	442	48,000	19,000	2.62
CoumH	458	21,000	6500	2.48
CoumI	445	27,000	14000	2.55

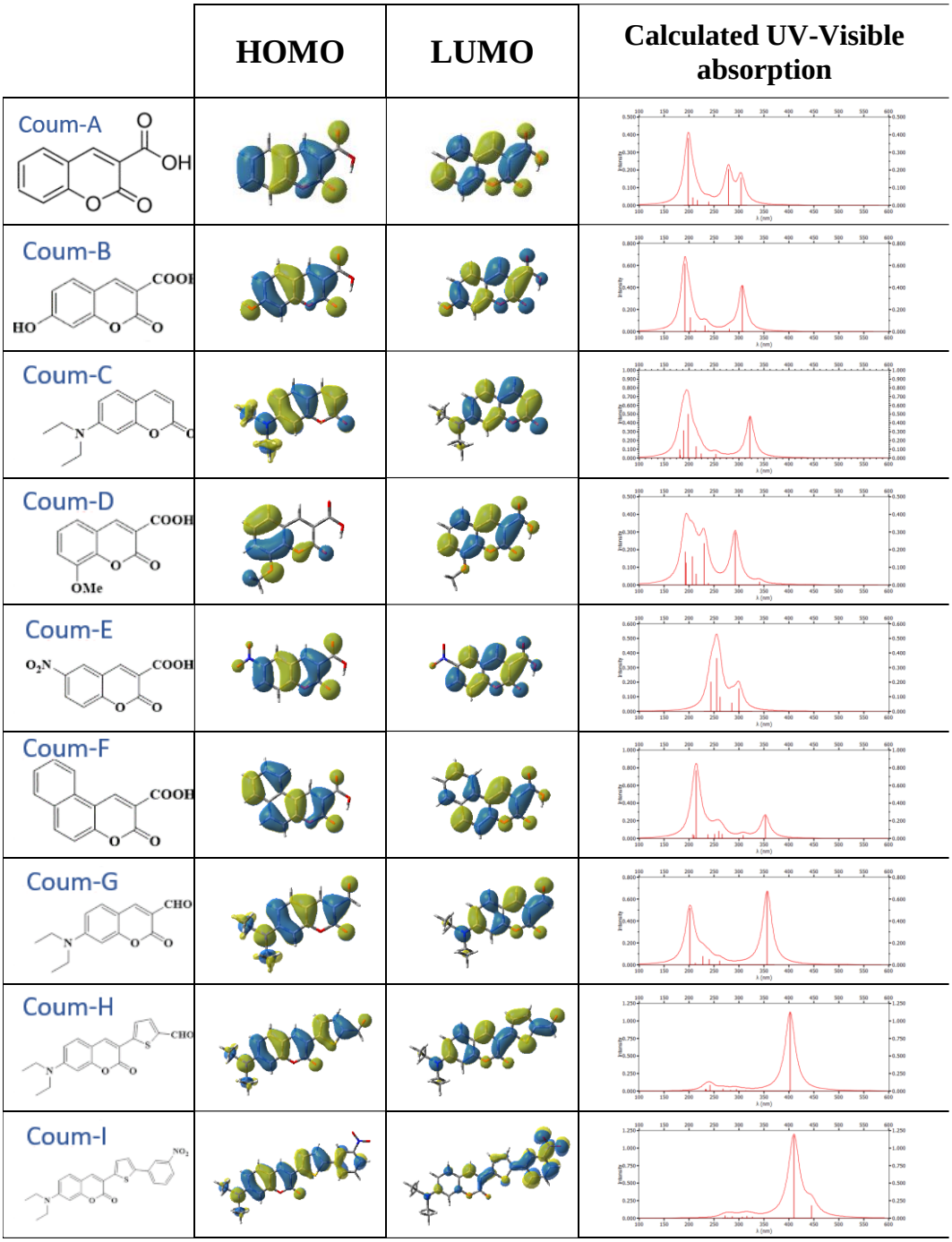

Figure 3. HOMO and LUMO frontier orbitals and their respective calculated UV-Visible absorption spectra for the different investigated compounds at the UB3LYP/6- 31G* level.

3.2. Free Radical Photopolymerization

3.2.1. Photopolymerization of Methacrylate Function of Mix-MA

The FRP profiles of methacrylate functions using Mix-MA as the benchmark monomer was performed in thick sample and in the presence of two or three-component PISs based on

Coum/Iod (or NPG) (0.1%/1% w/w) or Coum/Iod/NPG (0.1%/1%/1% w/w/w) respectively, upon visible light irradiation with a LED at 405nm are given in Figure 4 (See also Table 2).

The obtained results show that Coum/Iod (or NPG) is less reactive than three-component PISs (Coum/Iod/NPG), this result can be explained by a higher yield of reactive species (radicals) in the presence of Iod/NPG which is not able, alone, to initiate the FRP (e.g., FC = 24% for CoumI/Iod vs. 76% for CoumI/Iod/NPG, and FC = 0% for CoumA/Iod vs. 76% for CoumA/Iod/NPG; show Figure 4A and C curve 1). In fact, CoumB, CoumD, CoumF and CoumG showed a photoreduction process rather than a photo-oxidation process (e.g., FC = 0% for CoumB/Iod vs. 67% for CoumB/NPG, and FC = 0% for CoumD/Iod vs. 75% for CoumD/NPG), but CoumC and Coum8 show an opposite behavior with a photo-oxidation process probably more favorable than the photoreduction (FC = 70% for CoumC/Iod vs. 28% for CoumC/NPG; Figure 4A and B curve 3). The FRP profiles also show a low rate of polymerization, this can be due to the high oxygen inhibition effect.

.

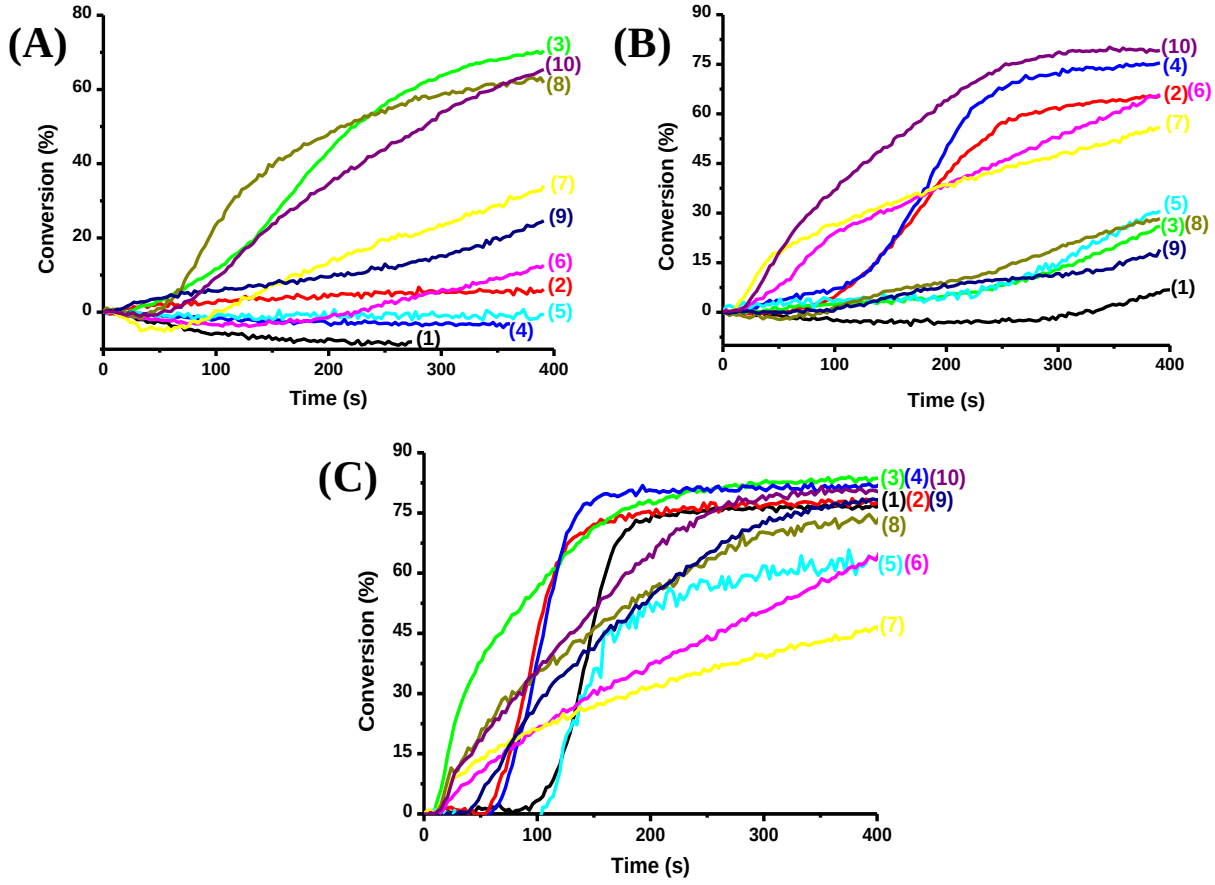

Figure 4. Photopolymerization profiles of methacrylate functions (conversion vs. irradiation time) using MIX-MA in thick sample (1.4 mm) under visible light irradiation using a LED at

405nm: **(A)** Coum/Iod (0.1%/1% w/w), **(B)** Coum/NPG (0.1%/1% w/w) and **(C)** Coum/Iod/NPG (0.1%/1%/1% w/w/w) : (1) CoumA, (2) CoumB, (3) CoumC, (4) CoumD, (5) CoumE, (6) CoumF, (7) CoumG, (8) CoumH, (9) CoumI and (10) Iod/NPG (1%/1% w/w). Irradiation starts at t = 10 s.

3.2.2. Photopolymerization of Acrylates (TMPTA or TA)

In fact, iodonium salt or NPG alone cannot initiate the FRP of acrylate at 405 nm due to their absorption in the UV range [17,23]. Therefore, the coumarins derivatives are introduced in order to improve the absorption properties of photosensitive formulations.

Firstly, the most of Coumarin derivatives show high extinction coefficients at 405 nm. The photopolymerization profiles of acrylate functions in thick (1.4 mm) or thin (25 µm) samples (conversion vs. irradiation time) using TMPTA (or TA) as benchmark monomers are depicted in Figure 5 (see also Table 2 and Table 3). The obtained results show that the two-component PISs based on Coum/Iod (0.1%/1% w/w) (or Coum/NPG) are able to strongly initiate the FRP, but a very higher performance [Final conversion (FC) and polymerization rate (Rp)] was acquired using the three-component PISs based on Coum/Iod/NPG which is quite efficient in the FRP of acrylate functions upon LED at 405 nm (e.g., FC = 60% for CoumC/Iod (0.1%/1% w/w) vs. 80% for CoumC/Iod/NPG (0.1%/1%/1% w/w/w), Figure 5A and B curve 3).

Moreover, the Iod/NPG (1%/1% w/w) couple weakly initiates the FRP (FC = 47%). This is ascribed to the formation of a charge transfer complex (CTC) between Iod and NPG [27] which is able to generate reactive species when it absorbs light. Clearly, the presence of Coumarin as photoinitiator is improving the performance of the photopolymerization processes.

Some of the coumarins can show both photoreduction (electron transfer from NPG to Coumarin) and photoxidation (electron transfer from Coumarin to Iod) processes, while other derivatives show only photoreduction process, such as CoumA, CoumB and CoumE (e.g., FC = 0% for CoumB/Iod (0.1%/1% w/w) vs. FC = 78% for CoumB/NPG (0.1%/1% w/w)).

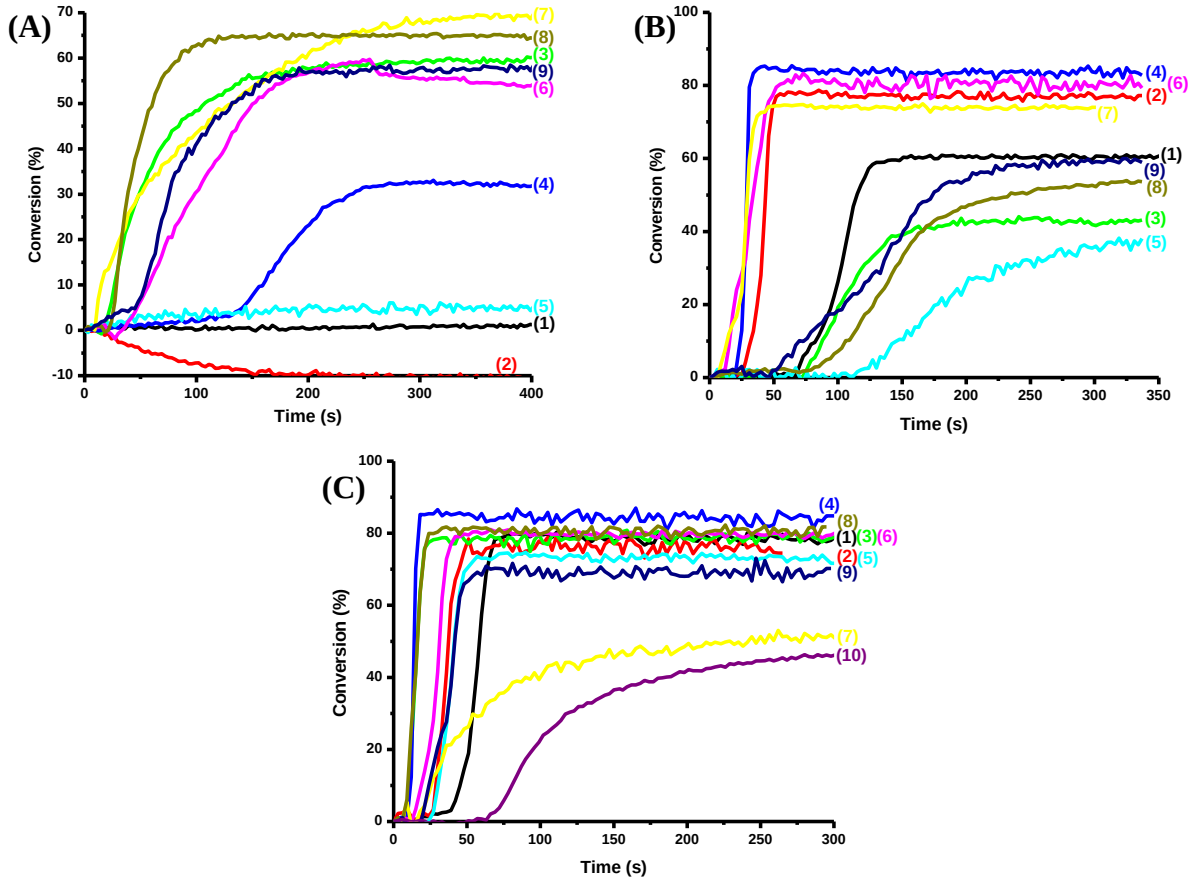

Figure 5. Photopolymerization profiles of acrylate functions (conversion vs irradiation time) using TMPTA in thick sample (1.4 mm) under visible light irradiation using a LED at 405 nm: (A) Coum/Iod (0.1%/1% w/w), (B) Coum/NPG (0.1%/1% w/w) and (C) Coum/Iod/NPG (0.1%/1%/1% w/w/w) : (1) CoumA, (2) CoumB, (3) CoumC, (4) CoumD, (5) CoumE, (6) CoumF, (7) CoumG, (8) CoumH, (9) CoumI and (10) Iod/NPG (1%/1% w/w). The molar concentrations for 0.1 % w/w are 0.0055, 0.0051, 0.0049, 0.0048, 0.0045, 0.0044, 0.0043, 0.0032, and 0.0025M for CoumA, CoumB, CoumC, CoumD, CoumE, CoumF, CoumG, CoumH, CoumI, respectelievly. The irradiation starts at t = 10 s.

Table 2. Final reactive functions conversion (FC%) for different monomers and different PISs upon visible light irradiation using a LED at 405 nm (400 s of irradiation and thickness = 1.4 mm).

	Two-Component PISs Coum/Additives (0.1%/1% w/w)			**Three-Component PISs Coum/Iod/NPG (0.1%/1%/1% w/w/w)**		
	TMPTA	**TA**	**Mix-MA**	**TMPTA**	**TA**	**Mix-MA**
CoumA	n.p [a] 61% [b]	n.p [a] 30% [b]	n.p [a] n.p [b]	80%	85%	76%
CoumB	n.p [a] 78% [b]	n.p [a] 81% [b]	n.p [a] 67% [b]	78%	88%	76%
CoumC	60% [a] 42% [b]	80% [a] 56% [b]	70% [a] 28% [b]	80%	88%	80%
CoumD	33% [a] 83% [b]	74% [a] 90% [b]	n.p [a] 75% [b]	86%	92%	79%

CoumE	n.p [a] 36% [b]	n.p [a] 25% [b]	n.p [a] 30% [b]	73%	75%	64%
CoumF	60% [a] 81% [b]	86% [a] 88% [b]	13% [a] 63% [b]	80%	88%	64%
CoumG	70% [a] 75% [b]	80% [a] 82% [b]	35% [a] 55% [b]	50%	40%	46%
CoumH	65% [a] 53% [b]	84% [a] 59% [b]	62% [a] 29% [b]	81%	87%	75%
CoumI	58% [a] 60% [b]	78% [a] 31% [b]	24% [a] 18% [b]	70%	75%	76%
[a] Coum/Iod (0.1%/1% w/w); [b] Coum/NPG (0.1%/1% w/w).						

Table 3. Final reactive functions conversion (FC%) for different monomers and different PISs upon visible light irradiation using a LED at 405 nm (150 s of irradiation and thickness = 25 µm).

	Two-Component PISs Coum/Additives (0.1%/1% w/w)			**Three-Component PISs Coum/Iod/NPG (0.1%/1%/1% w/w/w)**		
	TMPTA	**TA**	**Mix-MA**	**TMPTA**	**TA**	**Mix-MA**
CoumA	n.p [a] 32% [b]	n.p [a] n.p [b]	n.p [a] 22% [b]	25%	38%	36%
CoumB	49% [a] 13% [b]	32% [a] 24% [b]	14% [a] 15% [b]	28%	44%	52%
CoumC	25% [a] 25% [b]	53% [a] 15% [b]	n.p [a] 17% [b]	50%	75%	72%
CoumD	42% [a] 34% [b]	42% [a] 45% [b]	17% [a] 22% [b]	42%	70%	57%
CoumE	n.p [a] n.p [b]	n.p [a] n.p [b]	n.p [a] n.p [b]	30%	40%	n.p
CoumF	11% [a] 47% [b]	42% [a] 65% [b]	18% [a] 70% [b]	51%	73%	79%
CoumG	38% [a] 48% [b]	68% [a] 67% [b]	43% [a] 64% [b]	55%	81%	74%
CoumH	19% [a] 14% [b]	43% [a] 45% [b]	36% [a] 48% [b]	46%	68%	74%
CoumI	15% [a] 25% [b]	37% [a] 45% [b]	12% [a] 29% [b]	42%	58%	66%
[a] Coum/Iod (0.1%/1% w/w); [b] Coum/NPG (0.1%/1% w/w).						

3.3. 3D Printing Experiments Using Coum/Iod/amine PISs and Optical Microscopy Characterization

New 3D patterns were obtained by direct laser write experiments of Coum/Iod/amine PISs using a laser diode at 405 nm and characterized by optical microscopy. These 3D patterns were obtained under air using different PISs based on Coum/Iod/TMA (0.05%/0.5%/0.235% w/w/w) in TA or TMPTA (See Figure 6). In fact, the high photosensitivity of this resin

allowed an efficient polymerization process in the irradiated area so a high spatial resolution is observed. Markedly, a great thickness is obtained (~2090 µm) and these patterns were carried out in a very short irradiation time (~ 2-3 minutes). Using a well-established Type I photoinitiator (diphenyl(2,4,6-trimethylbenzoyl)phosphine oxide-TPO) in similar direct laser write conditions; similar performances can be reached but requiring a higher content (0.5% w/w). This latter result demonstrates the interest in using Coum derivatives. It is important to note that the 3D patterns based on CoumC exhibit a blue fluorescence when these structures are characterized by the light of the microscope.

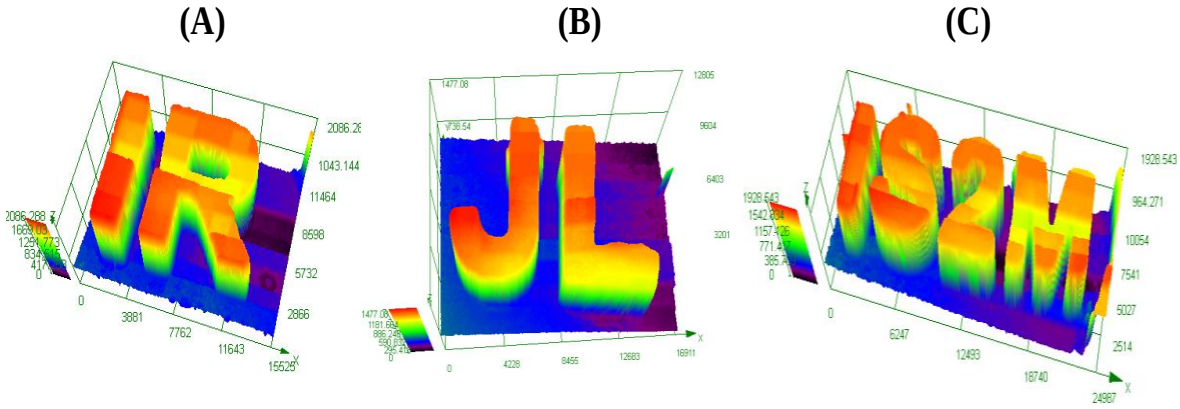

Figure 6. Characterization of 3D patterns by numerical optical microscopy obtained by Free Radical photopolymerization experiment (using TA or TMPTA as benchmark monomer) using a diode laser at 405nm: **(A)** CoumC/Iod/4,N-N-TMA (0.05%/0.5%/0.235% w/w/w) in TA, **(B)** CoumH/Iod/TMA (0.05%/0.5%/0.19% w/w/w) in TMPTA and **(C)** CoumD/Iod/4,N-N-TMA (0.05%/0.5%/0.275% w/w/w) in TMPTA.

3.4. Near-UV Conveyor Experiments for the Synthesis of Photocomposites Using Coum/Iod/NPG (0.1%/1%/1% w/w/w)

Generally, photocomposites are materials composed of at least two components: matrix and reinforcement. The mixture of these two components leads to new interesting properties that the two components separately do not have. The production of composites in the last decades and until today represents a very dynamic market in different fields such as aeronautics, automotive, wind power, and buildings. So, due to their very high mechanical resistance and chemical resistance, the glass fibers are used in this work as a matrix for the photocomposite synthesis.

In this work, the proposed coumarin derivatives were tested for access to photocomposites upon near-UV light using a LED conveyor at 385 nm (0.7 W/cm^2). The curing results obtained are summarized in Figure 7. Firstly, photocomposites were prepared by

impregnation of glass fibers with an acrylic resin (TMPTA) (50% glass fibers/50% acrylic resin) and irradiated upon a LED at 385 nm. Remarkably, a very fast polymerization was observed using Coum/Iod/NPG (0.1%/1%/1% w/w/w), where both the surface and the bottom are tack-free after some passes.

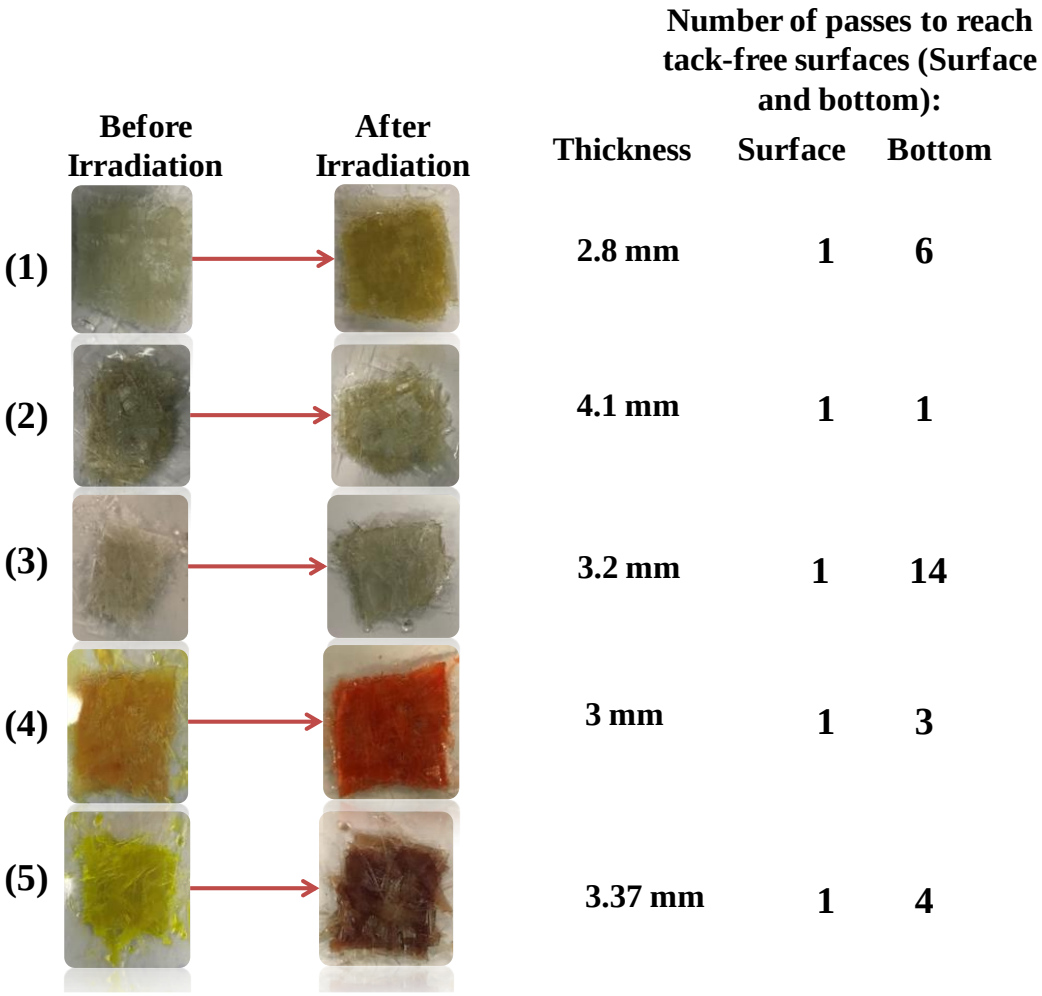

Figure 7. Photocomposites manufactured upon near-UV irradiation at 385 nm (0.7 W/cm^2) using glass fiber/resin (50%/50% w/w) in the presence of three-component PISs based on Coum/Iod/NPG (0.1%/1%/1% w/w/w): (1) CoumC, (2) CoumD, (3) CoumF, (4) CoumG, and (5) CoumH.

4. Discussion

For a better understanding of the photoinitiation ability, the photochemical properties of the studied coumarins were investigated. More particularly, their photolysis behaviors, fluorescence quenchings, and redox properties were investigated in the presence of additives (amine/iodonium salt), allowing to establish the photochemical mechanisms (see Scheme 4 below).

$$\text{Coumarin } (h\nu) \rightarrow {}^{1,3}\text{Coumarin} \quad \text{r1}$$
$${}^{1,3}\text{Coumarin} + \text{ArI}^{+} \rightarrow \text{Ar}^{\bullet} + \text{ArI} + \text{Coumarin}^{\bullet+} \quad \text{r2}$$
$$\text{NPG} + \text{Iod} \rightarrow [\text{NPG-Iod}]_{CTC} \quad \text{r3}$$
$$[\text{NPG-Iod}]_{CTC}\,(h\nu) \rightarrow \text{Ar}^{\bullet} \quad \text{r4}$$
$${}^{1,3}\text{Coumarin} + \text{NPG} \rightarrow \text{Coumarin-H}^{\bullet} + \text{NPG}_{(-H)}{}^{\bullet} \quad \text{r5}$$
$$\text{NPG}_{(-H)}{}^{\bullet} \rightarrow \text{NPG}_{(-H;-CO2)}{}^{\bullet} + CO_2 \quad \text{r6}$$
$$\text{NPG}_{(-H;-CO2)}{}^{\bullet} + \text{Ar}_2\text{I}^{+} \rightarrow \text{NPG}_{(-H;-CO2)}{}^{+} + \text{Ar}^{\bullet} + \text{ArI} \quad \text{r7}$$
$$\text{Coumarin}^{\bullet+} + \text{NPG} \rightarrow \text{Coumarin} + \text{NPG}^{\bullet+} \quad \text{r8}$$
$$\text{Coumarin-H}^{\bullet} + \text{Ar}_2\text{I}^{+} \rightarrow \text{Coumarin} + \text{Ar}^{\bullet} + \text{ArI} + \text{H}^{+} \quad \text{r9}$$

Scheme 4. Proposed chemical mechanisms.

4.1. Steady-State Photolysis of Coumarins

Steady-state photolysis of coumarins derivatives in ACN and under irradiation light using a LED at 375 nm have been performed to explain the obtained results in FRP. So, the photolysis of one of these compounds (CoumC) is presented in Figure 8. First of all, the photolysis of CoumC alone upon irradiation at 375 nm is very slow compared to that obtained with Iod, which is very fast. In fact, the appearance of a weak peak between 425 and 500 nm and the evolution of the absorption peak of CoumC shows that a high interaction between CoumC and Iod took place by an electron transfer process, this process induced, during the irradiation, a photolysis of the CoumC and generation of new photoproducts. On the other hand, the photolysis of CoumC with Iod/NPG couple was very slow (Figure 8D curve 3) and poor consumption was obtained; these results can be explained by a high regeneration of CoumC in three-component PISs.

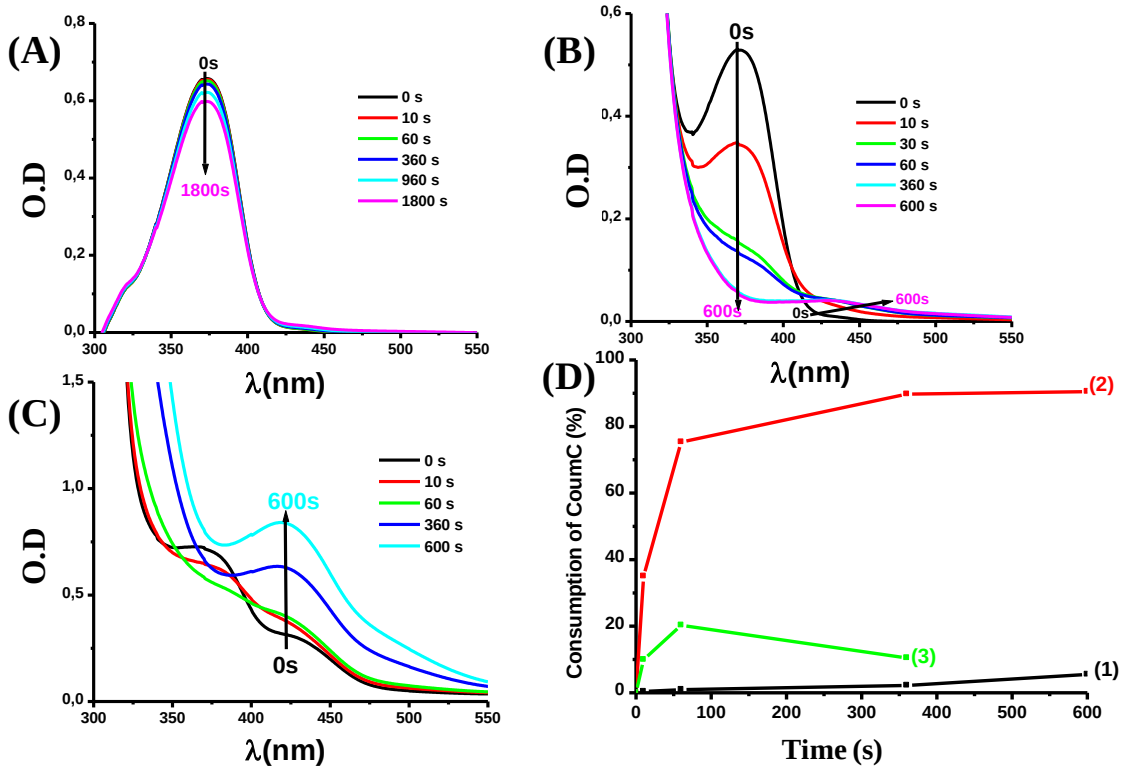

Figure 8. (A) Photolysis of CoumC alone in ACN, (B) photolysis of CoumC with Iod (10-2 M) in ACN, (C) photolysis of CoumC with Iod/NPG (10-2M) couple, (D) percentage of consumption of CoumC (1) without Iod, and with (2) with Iod (10-2 M), and (3) with Iod/NPG vs. irradiation time – upon exposure to the LED@375 nm in ACN.

4.2. Fluorescence Quenching and Cyclic Voltammetry Experiments for the Coumarins

Fluorescence quenching and emission spectra of the different coumarins (e.g CoumC) have been carried out in ACN and reported in Figure 9. Firstly, where the emission intensity of CoumC decreases when we added Iod or NPG, so an interaction between ^{1}Coum-C and Iod (or NPG) occurs, this result is in full agreement with FRP and photolysis experiments shown above. To compare the reactivity of different coumarin with Iod or NPG, the Stern-Volmer coefficient (Ksv) have been calculated according to Equation (1). For example, a very high quenching of CoumF with NPG and poor quenching of CoumC with NPG were observed, so Ksv for CoumF is higher than that of CoumC (Ksv = 44 M^{-1} for CoumC and 400 M^{-1} for CoumF), therefore a high electron transfer quantum yield is obtained for CoumF ϕ =0.9) compared to that obtained for CoumC (ϕ = 0.6) (Table 4).

$$\phi_{S1} = K_{SV}[Iod]/(1 + K_{SV}[Iod]) \qquad \textbf{(1)}$$

The free energy change (ΔG) for the electron transfer between coumarins and Iod or NPG is an important parameter to evaluate the feasibility of this process. ΔG can be extracted from the E_{S1} and the electrochemical properties (E_{ox} and E_{red}) (using Equation (1)) e.g., ΔG = −2.39 eV for CoumF/Iod which is more reactive in FRP of acrylate functions (TA monomer) (FC = 86%). All these data are gathered in Table 4

. Finally, the FRP results of acrylate functions can be explained by a global mechanism based on the different results obtained by the characterization techniques (steady-state photolysis, Fluorescence quenching and cyclic voltammetry). First of all, the photoinitiator (Coumarin) goes to its excited state once it absorbs suitable light energy, and as it is notable to give reactive species alone, the Iod salt (or NPG), therefore, interacts with its excited state and will be able to dissociate and give reactive species responsible to initiate the FRP (r1-r2). The addition of NPG to the photosensitive formulation is very important because of the formation of a charge-transfer complex between Iod salt and NPG $[Iod\text{-}NPG]_{CTC}$ able to generate reactive species (r3-r4). Moreover, a hydrogen transfer process from NPG to Coumarins can occur which generates two types of radicals (Coum-H$^{\bullet}$,NPG(-H)$^{\bullet}$) (r5). In fact, a decarboxylation of $NPG_{(-H)}{}^{\bullet}$ can take place and leads to the radical formation ($NPG_{(-H, -CO2)}{}^{\bullet}$), which react with Iod salt to produce reactive species (Ar$^{\bullet}$ and $NPG_{(-H, CO2)}{}^{+}$) (r6-r7). Ar$^{\bullet}$ and $NPG_{(-H,-CO2)}{}^{\bullet}$) (r1-r9) radicals are assumed as the reactive species responsible to the FRP of the (meth)acrylate functions. The coumarins consumption is reduced in three-component PIS (Figure 8); this can be explained by a regeneration of the photoinitiator, which is in agreement on r8-r9 (See Scheme 4).

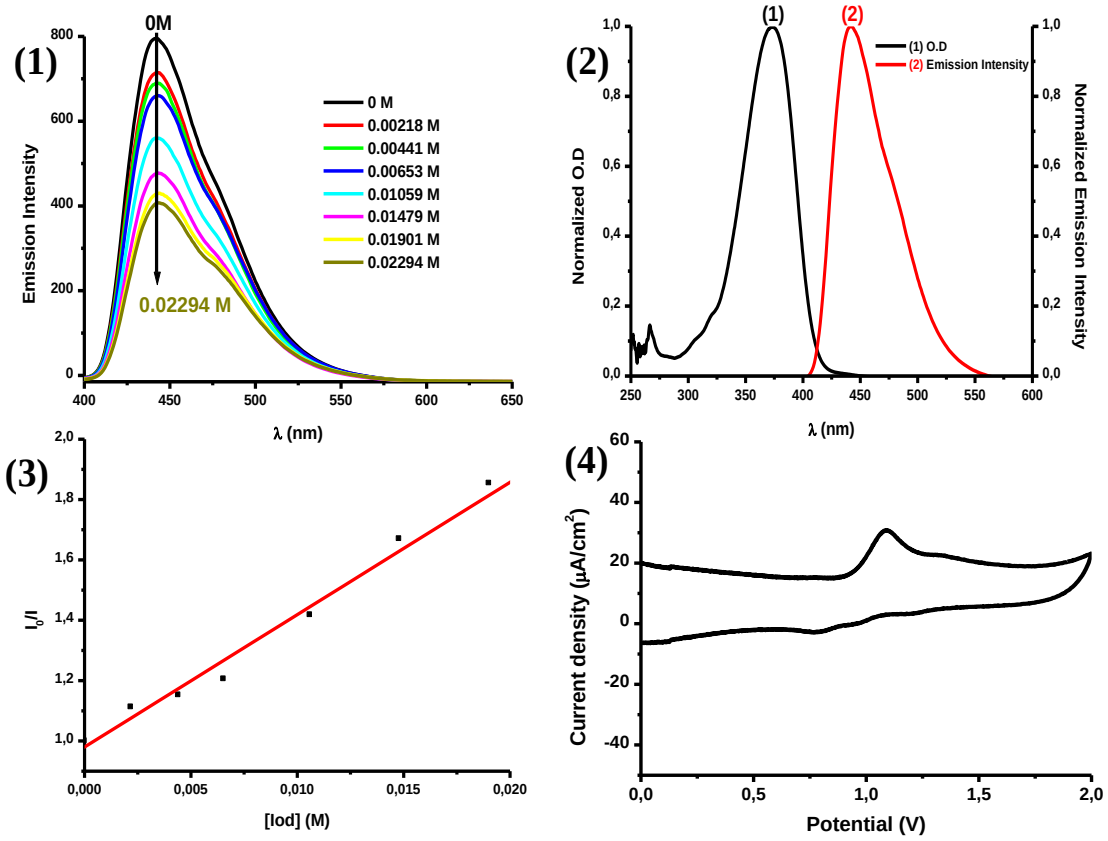

Figure 9. (1) Fluorescence quenching of CoumC by Iod, **(2)** E_{S1} determination, **(3)** Determination of K_{SV} (Stern-Volmer coefficient), and **(4)** Oxidation potential (E_{ox}) determination of CoumC.

Table 4. Parameters characterizing the chemical mechanisms associated with ^{1}Coum/Iod or ^{1}Coum/NPG interaction in acetonitrile. For Iod and NPG, a reduction and oxidation potential of -0.2 and 1.03 eV were used respectively for the ΔGet calculation.

	E_{ox} (V)	E_{red} (V)	ΔG (eV) (Coum/Iod)	ΔG (eV) (Coum/NPG)	K_{SV} (M^{-1}) (Coum/Iod)	K_{SV} (M^{-1}) (Coum/NPG)	Φ (Coum/Iod)	Φ (Coum/NPG)
CoumA	-	−0.61	-	−1.71	7.25	104	0.35	0.78
CoumB	-	-	-	-	21	174	0.39	0.82
CoumC	1	-	−1.81	-	44	44	0.5	0.6
CoumD	0.6	−0.98	−2.32	−1.11	14	46.5	0.3	0.5
CoumE	-	-	-	-	5297	773	0.972	0.9
CoumF	0.39	−1.01	−2.39	−0.94	9	400	0.3	0.9
CoumG	0.46	−1.35	−1.96	−0.24	6	16	0.2	0.5
CoumH	0.96	−1.40	−1.32	−0.05	48	22	0.6	0.6
CoumI	-	−1.06	-	−0.460	4	-	0.25	-

Finally, the FRP results of acrylate functions can be explained by a global mechanism based on the different results obtained by the characterization techniques (steady-state photolysis, Fluorescence quenching and cyclic voltammetry). First of all, the photoinitiator

(Coumarin) goes to its excited state once it absorbs suitable light energy, and as it is not able to give reactive species alone, the Iod salt (or NPG), therefore, interacts with its excited state and will be able to dissociate and give reactive species responsible to initiate the FRP (r1–r2). The addition of NPG to the photosensitive formulation is very important because of the formation of a charge-transfer complex between Iod salt and NPG $[Iod\text{-}NPG]_{CTC}$ able to generate reactive species (r3–r4). Moreover, a hydrogen transfer process from NPG to Coumarins can occur which generates two types of radicals ($Coum\text{-}H^{\bullet}$, $NPG_{(-H)}^{\bullet}$) (r5). In fact, a decarboxylation of $NPG_{(-H)}^{\bullet}$ can take place and leads to the radical formation ($NPG_{(-H,\ -CO2)}^{\bullet}$), which react with Iod salt to produce reactive species ($Ar^{\bullet}$ and $NPG_{(-H,\ CO2)}^{+}$) (r6–r7). $Ar^{\bullet}$ and $NPG_{(-H,-CO2)}^{\bullet}$) (r1–r9) radicals are assumed as the reactive species responsible to the FRP of the (meth)acrylate functions. The coumarins consumption is reduced in three-component PIS (Figure 6C); this can be explained by a regeneration of the photoinitiator, which is in agreement on r8-r9 (See Scheme 4).

The photoinitiation ability is a strong interplay between these different reactions (r1-r9), but their light absorption properties and intersystem crossing behavior (singlet vs. triplet state pathways, lifetimes) must also be taken into account. Therefore, a deeper characterization of their structure/reactivity/efficiency relationship is beyond the scope of the present work.

5. Conclusions

Nine coumarins varying by the substitution pattern at the 3- and 7-positions of the coumarin core have been tested and proposed as highly efficient photoinitiators for the FRP of meth(acrylates) functions under visible light irradiation using a LED at 405 nm. Remarkably, these photoinitiators can be used in 3D printing experiments and these dyes showed a very high efficiency in the photocomposite synthesis (significant curing of the surface and the bottom) using a LED conveyor at 385 nm. The challenge remains, therefore, to develop new coumarins absorbing at longer wavelengths e.g., in the near-infrared rangefor a better penetration of light into thick/filled samples.

References

[1] Fouassier, J.P.; Lalevée, J.Photoinitiators for Polymer Synthesis, Scope, Reactivity, and Efficiency; Wiley-VCH Verlag GmbH &Co.KGaA: Weinheim, Germany, **2012**.

[2] Fouassier, J.P.Photoinitiator, Photopolymerization and Photo-curing: Fundamentals and Applications; Gardner Publications: New York,NY, USA, **1995**.

[3] Dietliker, K.A.Compilation of Photoinitiators Commercially Available for UV Today; Sita Technology Ltd.: Edinbergh, London, **2002**.

[4] Davidson, S.Exploring the Science, Technology and Application of UV and EB Curing; Sita Technology Ltd.: Edinbergh, London, **1999**.

[5] Wu, L.; Baghdachi, J.Functional Polymer Coatings: Principles, Methods, and Applications; Wiley Series on Polymer Engineering andTechnology: New York, NY, USA, **2015**.

[6] Bouzrati-Zerelli, M.; Maier, M.; Dietlin, C.; Morlet-Savary, F.; Fouassier, J.P.; Klee, J.E.; Lalevée, J. A novel photoinitiating systemproducing germyl radicals for the polymerization of representative methacrylate resins: Camphorquinone/R3GeH/iodoniumsalt.Dent. Mater. **2016**, 32, 1226.

[7] Garcès, J.M.; Moll, D.J.; Bicerano, J.; Fibiger, R.; McLeod, D.G. Polymeric Nanocomposites for Automotive Applications.Adv.Mater. **2000**, 12, 1835.

[8]Morgan, S.E.; Havelka, K.O.; Lochhead, R.Y.Cosmetic Nanotechnology: Polymers and Colloids in Cosmetics in Person Care; ACSSymposium Series: Washington, DC, USA, 2007; 961p.

[9]Lawrence, J.R.; O'Neill, F.T.; Sheridan, J.T. Photopolymer holographic recording material.Optik. **2001**, 112, 449.

[10] Lee, J.H.; Prud'Homme, R.K.; Aksay, I.A. Cure Depth in Photopolymerization: Experiments and Theory.J. Mater. Res. **2001**, 16,3536.

[11] Fouassier, J.P.; Lalevée, J. Recent Advances in Photoinduced Polymerization Reactions under 400-700 nm Light.Photochemistry. **2014**, 42, 215.

[12] Dumur, F.; Gigmes, D.; Fouassier, J.-P.; Lalevée, J. Organic Electronics: An El Dorado in the Quest of New Photocatalysts forPolymerization Reactions.Acc. Chem. Res. **2016**, 49, 1980.

[13] Dietlin, C.; Schweizer, S.; Xiao, P.; Zhang, J.; Morlet-Savary, F.; Graff, B.; Fouassier, J.P.; Lalevée, J. Photopolymerization uponLEDs: New Photoinitiating Systems and Strategies.Polym. Chem. **2015**, 6, 3895.

[14] Zivic, N.; Bouzrati-Zerelli, M.; Kermagoret, A.; Dumur, F.; Fouassier, J.P.; Gigmes, D.; Lalevée, J. Photocatalysts in PolymerizationReactions.Chem. Cat. Chem. **2016**, 8, 1617.

[15] Abdallah, M.; Hijazi, A.; Graff, B.; Fouassier, J.P.; Rodeghiero, G.; Gualandi, A.; Dumur, F.; Cozzi, P.G.; Lalevée, J. Coumarin derivatives as versatile photoinitiators for 3D printing, polymerization in water and photocomposite synthesis.Polym. Chem. **2019**, 10, 872.

[16] Abdallah, M.; Hijazi, A.; Dumur, F.; Lalevée, J. Coumarins as Powerful Photosensitizers for the Cationic Polymerization ofEpoxy-Silicones under Near-UV and Visible Light and Applications for 3D Printing Technology.Molecules. **2020**, 25, 2063.

[17] Abdallah, M.; Hijazi, A.; Graff, B.; Fouassier, J.-P.; Dumur, F.; Lalevée. In-silico based development of photoinitiators for 3Dprinting and composites: Search on the coumarin scaffold.J. Photochem. Photobiol. A Chem. **2020**, 400, 112698.

[18] Abdallah, M.; Hijazi, A.; Lin, J.-T.; Graff, B.; Dumur, F.; Lalevée. Coumarin Derivatives as Photoinitiators in Photo-Oxidation andPhoto-Reduction Processes and a Kinetic Model for Simulations of the Associated Polymerization Profiles.ACS Appl. Polym.Mater. **2020**, 2, 2769.

[19] Rahal, M.; Mokbel, H.; Graff, B.; Toufaily, J.; Hamieh, T.; Dumur, F.; Lalevée, J. Mono vs. Difunctional Coumarin as Photoinitiatorsin Photocomposite Synthesis and 3D Printing.Catalyst. **2020**, 10, 1202.

[20] Jiang, Z.J.; Lv, H.S.; Zhu, J.; Zha, B.X. New fluorescent chemosensor based on quinoline and coumarin for Cu2+.Synth. Met. **2012**, 162, 2112.

[21] Loncaric, M.; Gašo-Sokac, D.; Jokic, S.; Molnar, M. Recent Advances in the Synthesis of Coumarin Derivatives from DifferentStarting Materials.Biomolecules. **2020**, 10, 151.

[22] Zeydi, M.M.; Kalantarian, S.J.; Kazeminejad, Z. Overview on developed synthesis procedures of coumarin heterocycles.J. Iran.Chem. Soc. **2020**, 17, 3031.

[23] Jiang, X.; Guo, J.; Lv, Y.; Yao, C.; Zhang, C.; Mi, Z.; Shi, Y.; Gu, J.; Zhou, T.; Bai, R.; et al. Rational design, synthesis and biologicalevaluation of novel multitargeting anti-AD iron chelators with potent MAO-B inhibitory and antioxidant activity, Bioorg.Med.Chem. **2020**, 28, 115550.

[24] Markad, D.; Khullar, S.; Mandal, S.K. A Primary Amide-Functionalized Heterogeneous Catalyst for the Synthesis of Coumarin-3-carboxylic Acids via a Tandem Reaction.Inorg. Chem. **2020**, 59, 11407.

[25] Wang, X.; Bai, X.; Su, D.; Zhang, Y.; Li, P.; Lu, S.; Gong, Y.; Zhang, W.; Tang, B. Simultaneous Fluorescence Imaging RevealsN-Methyl-D-aspartic Acid Receptor Dependent Zn2+/H+Flux in the Brains of Mice with Depression.Anal. Chem. **2020**, 92, 4101.

[26] Qiu, W.; Zhu, J.; Dietliker, K.; Li, Z. Polymerizable Oxime Esters: An Efficient Photoinitiator with Low Migration Ability for 3DPrinting to Fabricate Luminescent Devices.Chem. Photo. Chem. **2020**, 4, 5296.

[27] Liu, H.; Xia, D.G.; Chu, Z.W.; Hu, R.; Cheng, X.; Lv, X.H. Novel coumarin-thiazolyl ester derivatives as potential DNA gyraseInhibitors: Design, synthesis, and antibacterial activity.Bioorg. Chem. **2020**, 100, 103907.

[28] Bhagwat, A.A.; Avhad, K.C.; Patil, D.S.; Sekar, N. Design and Synthesis of Coumarin–Imidazole Hybrid Chromophores:Solvatochromism, Acidochromism and Nonlinear Optical Properties.Photochem. Photobiol. **2019**, 95, 740.

[29] Lalevée, J.; Blanchard, N.; Tehfe, M.A.; Peter, M.; Morlet-Savary, F.; Gigmes, D.; Fouassier, J.P. Efficient Dual Radical/CationicPhotoinitiator under Visible Light: A New Concept.Polym. Chem. **2011**, 2, 1986.

[30] Lalevée, J.; Blanchard, N.; Tehfe, M.A.; Peter, M.; Morlet-Savary, F.; Fouassier, J.P. A Novel Photopolymerization Initiating SystemBased on an Iridium Complex Photocatalyst. Macromol.Rapid Commun. **2011**,32, 917.

[31] Rehm, D.; Weller, A. Kinetics of Fluorescence Quenching by Electron and H-Atom Transfer. Isr. J. Chem. **1970**, 8, 259.

[32] Foresman, J.B.; Frisch, A. Exploring Chemistry with Electronic Structure Methods. In Exploring Chemistry with Electronic Structure Methods, 2nd ed.; Gaussian Inc.: Pittsburgh, PA, USA, **1996**.

[33] Frisch, M.J.; Trucks, G.W.; Schlegel, H.B.; Scuseria, G.E.; Robb, M.A.; Cheeseman, J.R.; Zakrzewski, V.G.; Montgomery, J.A.; Stratmann, J.R.E.; Burant, J.C.; et al.Gaussian 03, Revision B-2; Gaussian Inc.: Pittsburgh, PA, USA, **2003**.

[34] Zhang, J.; Dumur, F.; Xiao, P.; Graff, B.; Bardelang, D.; Gigmes, D.; Fouassier, J.P.; Lalevée, J. Structure Design of Naphthalimide Derivatives: Toward Versatile Photoinitiators for Near-UV/Visible LEDs, 3D Printing, and Water-Soluble Photoinitiating Systems. Macromolecules. **2015**, 48, 2054.

[35] Mousawi, A.A.; Dumur, F.; Garra, P.; Toufaily, J.; Hamieh, T.; Graff, B.; Gigmes, D.; Fouassier, J.P.; Lalevée, J. Carbazole Scaffold Based Photoinitiator/Photoredox Catalysts: Toward New High-Performance Photoinitiating Systems and Application in LED Projector 3D Printing Resins. Macromolecules. **2017**, 50, 2747.

Chapitre II : De nouveaux composés organiques à base de céto-coumarine pour l'impression 3D, l'écriture laser et la synthèse des photocomposites.

Les procédés de photopolymérisation connaissent actuellement un développement important avec des applications considérables au niveau industriel (croissance de l'ordre 10% par an). Ce processus photochimique, comparé aux procédés thermiques traditionnels, permet de réaliser une réaction de durcissement potentiellement rapide, avec une faible consommation d'énergie et une résolution spatiale élevée. Cependant, ce procédé de synthèse exige la recherche de molécules photosensibles à la lumière visible émise par les diodes électroluminescentes (LED) pour pouvoir déclencher le processus de photopolymérisation.

Les 3-cétocoumarines représentent une famille de coumarines, dont un groupement carbonyle est directement lié à la position 3 du noyau coumarine. Elles ont été reportées pour la première fois dans les années 80 dans les processus de photopolymérisation [1]. Photochimiquement parlant, ces composés possèdent des spectres d'absorption localisés dans la zone comprise entre 330 et 450 nm [2], ils sont caractérisés par un rendement quantique de croisement intersystème (ICS) très élevé [3,4] ainsi qu'une longue duré de vie de leur état excité triplet assurant des processus de désactivation efficaces. Toutes ces caractéristiques font des cétocoumarines un photoamorceur potentiellement efficace pour les processus de polymérisation. Cependant, ces composés souffrent d'une mauvaise solubilité dans les monomères acryliques.

Dans ce chapitre, dix nouveaux dérivés de la cétocoumarine (MeO-Coum1 – MeO-Coum10) ont été synthétisés afin de remédier aux problèmes de solubilité. Remarquablement, ces composés absorbent fortement dans la zone UV-visible, de ce fait, l'effet des différents substituants a été discuté en se basant sur des calculs de modélisation moléculaire.

La capacité d'amorçage de ces dérivés a été suivie en utilisant la RT-FTIR et en les combinant soit avec des additifs (sel d'iodonium) soit avec un co-amorceur (EDB, NPG). De même, des systèmes à trois composants ont également été étudiés (MeO-Coum/Iod/amine). Des profils de polymérisation performants ont été observés avec la combinaison MeO-Coum/Iod et MeO-Coum/amine, ce qui reflète une interaction efficace par photo-oxydation et photo-réduction, respectivement. Ces interactions sont mises en évidence par des expériences

de désactivation de fluorescence où des constantes de Stern-Volmer très élevées sont obtenues, ainsi que des potentiels d'oxydation et de réduction favorables observés par voltampérométrie cyclique. La forte réactivité des systèmes dérivés des cétocoumarines est fortement démontrée par la synthèse des photocomposites épais (3mm), l'écriture laser, ainsi que l'impression 3D sous irradiation visible à 405nm et à faible intensité.

Ce travail a fait l'objet d'une **publication** dans **'European Polymer Journal'** sous la citation suivante : Rahal, M.; Graff, B.; Toufaily, J.; Hamieh, T.; Dumur, F.; Lalevee, J. Design of keto-coumarin based photoinitiator for Free Radical Photopolymerization: Towards 3D printing and photocomposites applications. Eur. Polym. J., **2021**, 154, 110559.

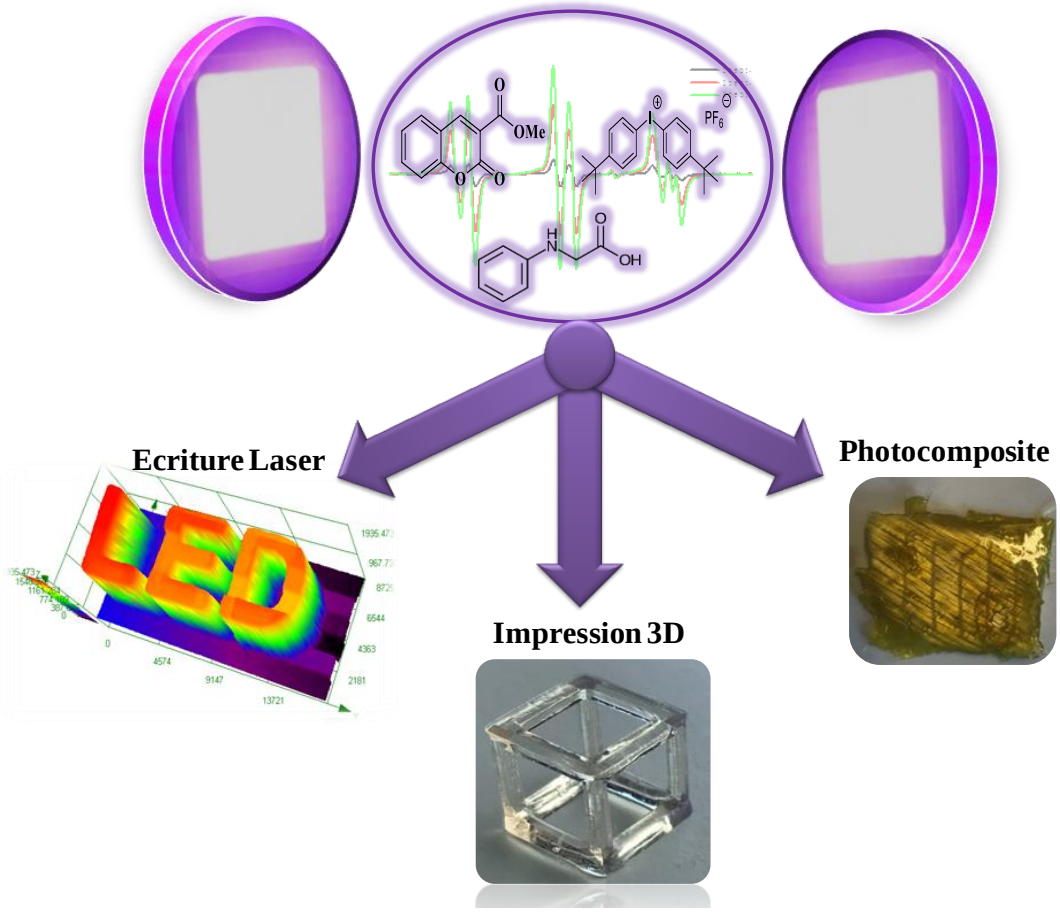

Références

[1] Specht, D.P.; Matric, P.A.; Farid, S. Ketocoumarins: A new class of triplet sensitizers. Tetrahedron. **1982**, 38, 1203.

[2] Bernini Freddi, A.; Morone, M.; Norcini, G. Design of New 3-ketocoumarins for UV-LED Curing. Rad. Tech. **2016**.

[3] Nazir, R.; Danilevicius, P.; Ciuciu, A.I.; Chatzinikolaidou, M.; Gray, D.; Flamigni, L.; Farsari, M.; Gryko, D.T. π-Expanded Ketocoumarins as Efficient, Biocompatible Initiators for Two-Photon-Induced Polymerization. Chem. Mater. **2014**, 26, 3175.

[4] Niu, G.; Liu, W.; Xiao, H.; Zhang, H.; Chen, J.; Dai, Q.; Ge, J.; Wu, J.; Wang, P. Keto-benzo[h]-Coumarin-Based Near-Infrared DyesWith Large Stokes Shifts for Bioimaging Applications.Chem. Asian J. **2016**, 11, 498.

Design of keto-coumarin based photoinitiator for Free Radical Photopolymerization: Towards 3D printing and photocomposites applications

Abstract

In this article, ten organic dyes based on keto-coumarin (KC) derivatives (MeO-Coum1, MeO-Coum10) have been synthesized and characterized as high performance photoinitiators for the Free Radical Photopolymerization (FRP) of acrylates upon visible light exposure using a Light emitting diode (LED) @405nm. The addition of Iodonium salt (Iod), amine [ethyl dimethylaminobenzoate (EDB) or *N*-phenylglycine (NPG)] and Iod/NPG couple in the photocurable resins have been carried out in order to prove their influences on the improvement on the photoinitiating abilities of keto-coumarins. The different dyes showed a very high ability to initiate the Free Radical Photopolymerization by introduction of these additives, using Two or Three-component photoinitiating systems based on MeO-Coum/Iod or amine (0.1% or 0.4%/1% w/w) or MeO-Coum/Iod/NPG (0.1% or 0.4%/1%/1% w/w/w) respectively. In fact, these photoinitiators have been tested in different applications. For example: in direct laser write to generate 3D patterns using a laser diode @405nm, or for the photocomposite synthesis based on glass fibers. To characterize the initiation ability and to explain the reaction mechanisms in the photoinitiation step, several techniques have been used, such as UV-visible spectroscopy and steady state photolysis, fluorescence emission, RT-FTIR and cyclic voltammetry experiments.

1. Introduction

The search for new synthetic strategies that can give access to polymer materials while consuming less energy, less costly, with a fast monomer conversion and with a lower environmental impact, is one of the most worrying challenges today. For this, the production of polymers by photochemical means is more and more used at the academic and industrial levels given their advantages compared to the thermal processes [1-5]. One of these chemical processes used is the Free Radical photopolymerization (FRP) or the Cationic photopolymerization (CP), which consists in the transformation of a liquid resin to a solid material in the presence of a photoinitiating system. Depending on the morphology, the nature

as well as their mechanical, chemical and physical properties, these polymers will be used in different sectors of our daily life [6-11]. Thus, the most important step in this process is the initiation, where a photosensitive molecule absorbs light and will thus be able to generate reactive species (radicals or cations) able to produce photopolymerization process. Considering their harmfulness, their high energy consumption as well as the danger for the operator, the use of a UV irradiation source can be limited and thus replaced by the visible source using light-emitting diodes (LED) which are safer, compact, lightweight and with a long lifetime. These equipments give also a greater light penetration in thick samples (for longer wavelengths) and these light sources are usually associated with better monochromatic behavior (bandwidth of ~ 20 nm centered on the maximal emission wavelength) [12-17]. So, the challenge remains to develop new molecules photosensitive to visible light. In fact, a rather limited number of organic molecules are capable to absorb in the visible region. Hence, the use of Keto-coumarins (KCs) as photoinitiators of photopolymerization is justified by the fact that these compounds are characterized by a very high visible light absorption ability (very high molar extinction coefficient), high triplet state lifetime, a rather low singlet-triplet energy gap. This family of dyes has already been largely tested as photoinitiating systems for Free Radical Photopolymerization and Cationic Photopolymerization; see examples in ref [18-21]. However, previous works were mostly devoted to 3-phenyl-2*H*-chromen-2-ones and 3-benzoyl-2*H*-chromen-2-ones that are highly polyaromatic structures. Conversely, reduction of the aromaticity on methyl 2-oxo-2H-chromene-3-carboxylate derivatives can be greatly beneficial for the solubility of the photosensitizers in resins, especially in acrylic resins [22]. Indeed, hydrogen bonds can form between the monomer and the carbonyl and carboxyl groups of methyl 2-oxo-2H-chromene-3-carboxylate derivatives, improving its solubility. These products are also good fluorophores.

In our work, keto-coumarin derivatives (Ester functions bonded at the 3-position of the coumarin scaffold – noted MeO-Coum in Scheme 1) characterized by a strong visible (and near UV) light-absorbing ability with the molar extinction coefficient of ~16000 M^{-1} cm^{-1} for MeO-Coum9 for example, have been tested in two and three-component photoinitiating systems based on MeO-Coum/Iod or amine (EDB or NPG) (0.1%/1% w/w) and MeO-Coum/Iod/NPG (0.1%/1%/1% w/w/w) for the FRP of acrylates in thick and thin samples under visible irradiation using a LED @ 405nm. These organic compounds showed a very high initiation ability so that high performances (final conversions and polymerization rates) could be obtained. As a result of this, the dyes have been tested in laser write experiments as

well as in the synthesis of photocomposites using glass fibers for reinforcement purposes. Finally, absorption and emission properties, photochemical properties as well as the redox properties, ability of MeO-Coum to initiate the FRP are directly affected by the impact of these different substituents on the KC scaffold.

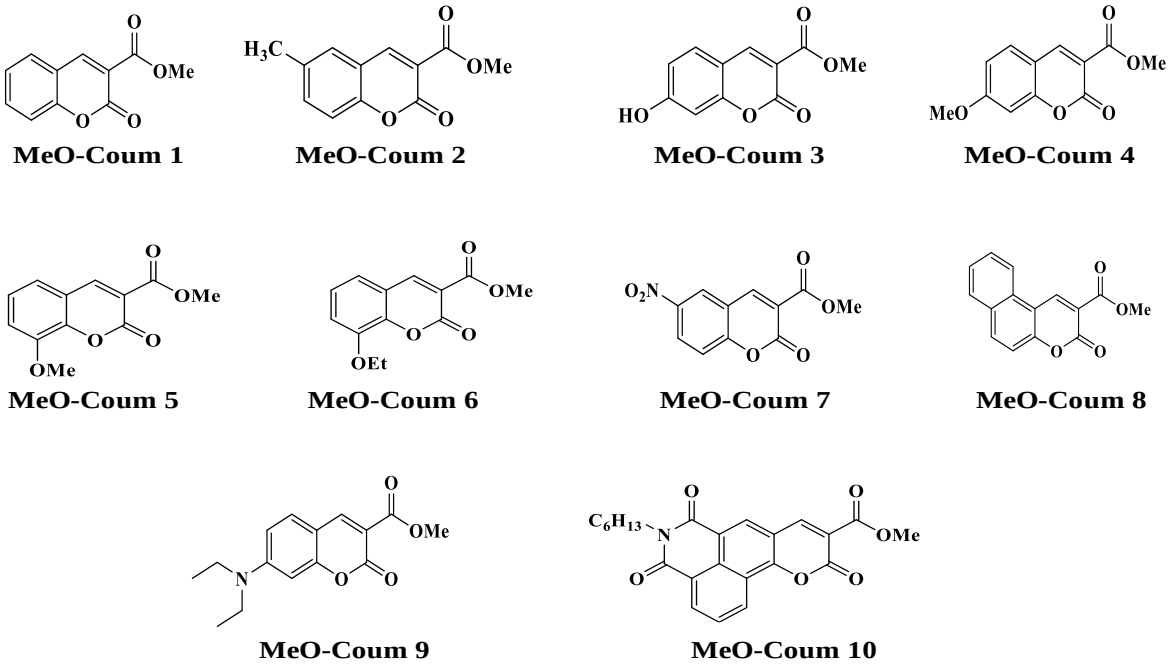

Scheme 1: Chemical structures of the KCs used in this work.

2. Experimental part

2.1 Chemical compounds used in this work

The synthesis of the ketocoumarins is described in detail in supporting information. All reagents and solvents used were purchased from Aldrich or Alfa Aesar and used as received without further purification. The purification procedures were similar to those presented in [18].

All the other chemicals (See Scheme 2) were selected with the highest purity available and used as received. The storage inhibitors of the monomers were not removed prior to the experiments. Di-*tert*-butyl-diphenyl iodonium hexafluorophosphate (Iod) and ethyl 4-(dimethylamino)benzoate (EDB) were obtained from Lambson Ltd (UK). Trimethylolpropane triacrylate (TMPTA), di(trimethylolpropane) tetraacrylate (TA), *N*-phenylglycine (NPG) were obtained from Allnex or Sigma Aldrich. TMPTA and TA were selected as benchmark

monomers for the radical polymerizations (these monomers were used without inhibitor removal).

Additives

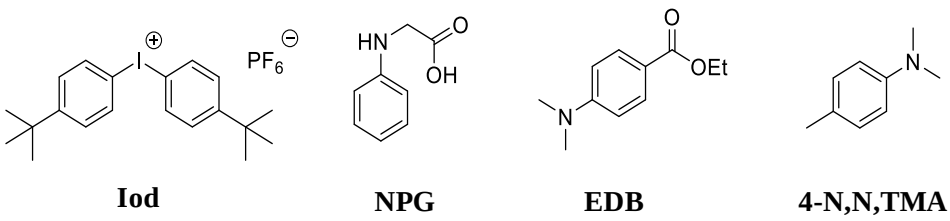

Iod **NPG** **EDB** **4-N,N,TMA**

Monomers

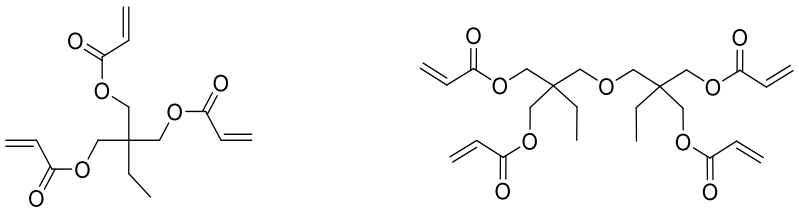

TMPTA **TA**

Scheme 2: Other chemical compounds used in this work

2.2 Irradiation sources

Light Emitting Diodes (LEDs) were used in this work as safe irradiation sources for different experiments: **(1)** Steady state photolysis for the different KCs have been carried out using a LED @375nm with an incident light intensity at the sample surface I_0 = 40 mW/cm^2, **(2)** Photopolymerization experiments have been performed using a LED@ 405nm with I_0 = 110 mW/cm^2, **(3)** Photocomposites were obtained using a LED conveyor @395nm with I_0 = 4 W/cm^2.

2.3 Free Radical Photopolymerization (FRP) of acrylate functions: Kinetic followed and final conversion (FC) determination by RT-FTIR

The FRP experiments of acrylate functions for the different Keto-Coumarins have been achieved using two or three-component photoinitiating systems based on MeO-Coum/Iod salt or amine (EDB or NPG) (0.1% or 0.4%/1% w/w) or MeO-Coum/Iod/NPG (or EDB) (0.1% or 0.4%/1%/1% w/w/w) upon visible light irradiation using a LED @405nm. The weight percent of the different compounds (Photoinitiators and additives) is calculated from the monomer content.

The photopolymers are obtained by two different treatments: **(1)** in thick sample (Thickness = 1.4 mm) using a circular mold (1.4 mm), where the photosensitive resin (Acrylate and EPOX) is deposited, and **(2)** in thin sample (Thickness = 25 μm), where the photopolymerizable resin is deposited in sandwich between two polypropylene films (to reduce oxygen inhibition). In fact, the kinetics tracking as well as the final reactive function conversions (FC) of different photoinitiating systems are obtained using a JASCO 6600 FTIR spectrometer. The monomer conversions were determined by following the evolution of the C=C peak located at 6160 cm^{-1} and 1630 cm^{-1} for the Thick and Thin samples respectively [23].

2.4. Redox potentials: Free energy change determination

Oxidation potential and reduction potential for KCs (E_{ox} and E_{red}) were determined by cyclic voltammetry experiments using tetrabutylammonium hexafluorophosphate as the supporting electrolyte (potentials vs. Saturated Calomel Electrode – SCE) in acetonitrile (ACN). The free energy change (ΔG_{et}) for an electron transfer reaction was calculated from eq.1 [24], where E_{ox}, E_{red}, E*, and C represent the oxidation potential of the electron donor, the reduction potential of the electron acceptor, the excited state energy level (obtained from the crossing point of the UV–visible and fluorescence spectra) and the coulombic term for the initially formed ion pair, respectively. Here, C is neglected as usually done for polar solvents.

$$\Delta G_{et} = E_{ox} - E_{red} - E^* + C \qquad \text{eq.1}$$

2.5. UV-Visible absorption, photolysis experiments and fluorescence spectroscopy to suggest the chemical mechanism

A JASCO V730 UV-visible spectrometer was used to study the UV-visible absorption, the molar extinction coefficients and the steady state photolysis experiments of the different Keto-coumarins compounds in acetonitrile (ACN). In the other hand, luminescence properties as well as the fluorescence quenching experiments of the different KCs were investigated using a JASCO FP-6200 spectrofluorimeter. According to the classical Stern−Volmer treatment [25] ($I_0/I = 1 + kq\ \tau_0[Iod]$, where I_0 and I stand for the fluorescent intensity of keto-coumarins in the absence and the presence of Iod, respectively; τ_0 stands for the lifetime of keto-coumarins in the absence of Iod), the quantum yields of the PI quenched by Iod in ACN could be determined.

2.6. Computational Procedure

Molecular orbital calculations were carried out with the Gaussian 03 suite of programs [26,27]. Electronic absorption spectra for the different compounds were calculated with the time-dependent density functional theory at the MPW1PW91-FC/6-31G* level of theory on the relaxed geometries calculated at the B3LYP/6-31G* level of theory.

2.7. Photocomposites synthesis using a LED Near-UV conveyor

A Dymax-UV conveyor was used to synthesize photocomposites. First of all, the photosensitive resin was deposited on the glass fibers (50%/50% w/w), then the photocomposites were obtained by irradiation of the sample using a LED conveyor @395 nm (4 W/cm^2). The distance between the belt and the LED was fixed at 15 mm, and the belt speed was fixed at 2 m/min (3s of irradiation per pass).

2.8. Direct laser write and 3D printing experiments

3D patterns were obtained using a computer-controlled diode laser at 405 nm (spot size = 50 μm), which were performed under air and analysed by a numerical optical microscope (DSX-HRSU from OLYMPUS Corporation) [28]**.**

3. Result and discussion

In this part, we discuss the impact of different substituents, linked to the Keto-Coumarins core, on the absorption properties, photochemical and photophysical properties as well as the FRP efficiency.

3.1 Investigation of UV-Visible spectra of Keto-Coumarins derivatives

The UV-visible spectra of the new investigated Keto-Coumarins in acetonitrile (ACN) are presented in Figure 1 (See also Table 1). These compounds are characterized by a very high molar extinction coefficient in both, near-UV and visible range (e.g. MeO-Coum8 41000 $M^{-1}.cm^{-1}$ @344 nm and 3100 $M^{-1}.cm^{-1}$ @405nm, and MeO-Coum9 17500 $M^{-1}.cm^{-1}$ @416nm and 15900 $M^{-1}.cm^{-1}$ @405nm). More specifically, their absorptions are very interesting in the 300-480 nm spectral range, so a good overlap is ensured with the emission spectra of the LEDs used in this work (LED@ 405 nm for the photopolymerization experiments, 375 nm for the steady state photolysis experiments and 395 nm for the photocomposites synthesis).

The absorption properties of the keto-coumarins are directly related to the presence of a donor or acceptor groups linked to the KC scaffold (see in Figure 2 for the frontier orbitals of the KCs). Remarkably, a bathochromic effect is observed due to the presence of the donor

groups on the Keto-Coumarin core which destabilizes the π-π* transition, while a hypsochromic effect is observed upon introduction of an accepting group which stabilizes the π-π* transition (in the case of MeO-Coum7 which shows a blue-shifted absorption due to the presence of an electron accepting group NO_2). Therefore, MeO-Coum8, MeO-Coum9 and MeO-Com10 have the most red-shifted absorption spectra due to the presence of the donating groups (Ar, $N(CH_2CH_3)_2$ and Naphthalimide group respectively). Taking MeO-Com1 as the original structure, the UV-visible spectra of MeO-Coum2, 3 and 4 are slightly red shifted due to the presence of a weak donor group (CH_3, OH and OCH_3 respectively), MeO-Coum3 and 4 have high extinction coefficients due to the presence of auxochrome group which is not present in MeO-Coum2 (absence of a heteroatom). On the other hand, the UV-visible spectra of MeO-Coum5 and 6 show a hypsochromic effect despite the presence of the donor group (OH and OCH_3). This result can be explained by the (OH and OMe) group in position 7 that induce a delocalization of electrons over the totality of the Keto-Coumarins scaffold in the case of MeO-Coum3 and 4, but OMe and OEt groups in position 8 induce a delocalization just in the aromatic part (phenyl) in the case of MeO-Coum5 and 6 (MeO in position 8), so more the delocalization is elongated, more the absorption is shifted towards red range, therefore MeO-Coum3,4 are more shifted to the red range then MeO-Coum5 and 6. This behavior is well observed by the computational results on HOMO and LUMO frontier orbitals (Figure 2).

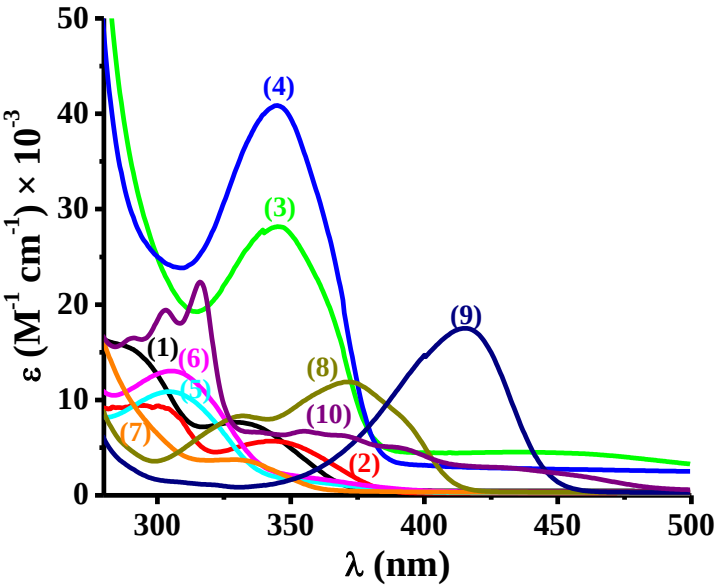

Figure 1: UV-visible spectra of the KCs in ACN: **(1)** MeO-Coum1, **(2)** MeO-Coum2, **(3)** MeO-Coum3, **(4)** MeO-Coum4, **(5)** MeO-Coum5, **(6)** MeO-Coum6, **(7)** MeO-Coum7, **(8)** MeO-Coum8 and **(9)** MeO-Coum9 and (**10)** MeO-Coum10.

Table 1: Light absorption properties of Keto-Coumarins at 405 nm and at λ_{max}

	λ_{max} (nm)	ε_{max} (M^{-1} cm^{-1})	ε_{405nm} (M^{-1} cm^{-1})	ε_{375nm} (M^{-1} cm^{-1})
MeO-Coum1	330	15900	480	700
MeO-Coum2	343	10000	190	1700
MeO-Coum3	345	28200	4440	9600
MeO-Coum4	344	40900	3060	11600
MeO-Coum5	304	10900	300	880
MeO-Coum6	305	13000	440	1150
MeO-Coum7	328	3700	350	430
MeO-Coum8	372	11900	3000	11700
MeO-Coum9	416	17500	15800	600
MeO-Coum10	316	22400	3600	5900

	HOMO	LUMO
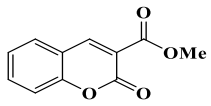 MeO-Coum1	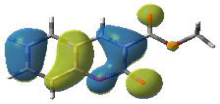	
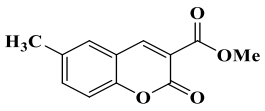 MeO-Coum 2		
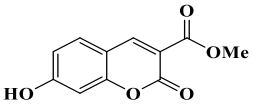 MeO-Coum 3	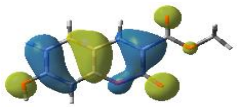	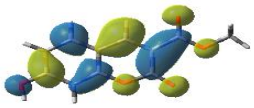
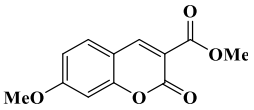 MeO-Coum 4	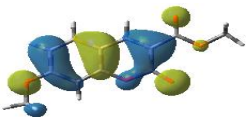	
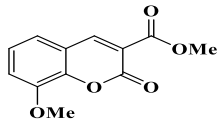 MeO-Coum 5	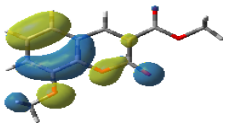	
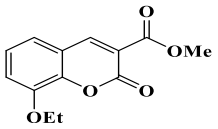 MeO-Coum6	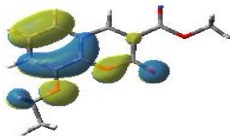	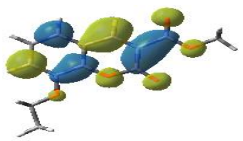
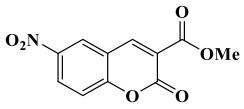 MeO-Coum 7	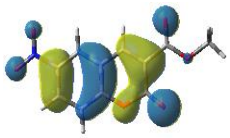	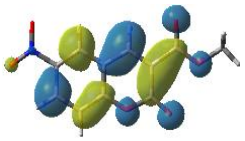
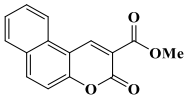 MeO-Coum 8	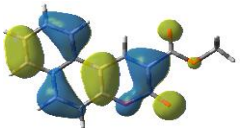	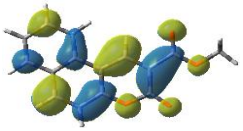
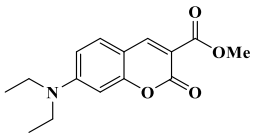 MeO-Coum 9	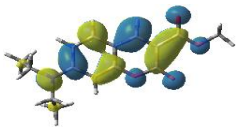	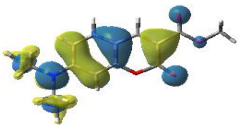
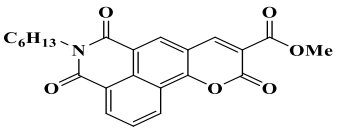 MeO-Coum 10	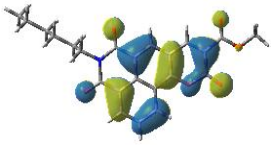	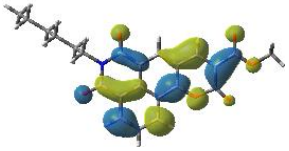

Figure 2: HOMO and LUMO frontier orbitals for the different investigated compounds at the UB3LYP/6- 31G* level.

3.2 Free Radical Photopolymerization (FRP) of acrylate functions of TMPTA and TA

The FRP using TMPTA or TA as benchmark acrylate monomers have been performed for both thick (1.4 mm) or thin (25 μm) samples using two or three-component photoinitiating systems upon visible light irradiation with a LED @405nm (I = 110 mW/cm^2). The polymerization profiles are depicted in Figure 3 (See also Table 2). First of all, Keto-Coumarins alone or additives alone (e.g. Iod, EDB and NPG) cannot initiate the FRP. These results clearly shows the importance of introducing a PI able to absorb a near-UV or visible light, since the additives are not able to absorb near UV or visible light. In fact, MeO-Coum8, 9 and 10 are very effective where they coupled with Iod or NPG (0.1%/1% w/w) using TA (final acrylate function conversion (FC) = 81%, 70% and 61% respectively with Iod and 86%, 83% and 87% respectively with NPG), but all other compounds (except MeO-Coum2 and 7) initiates effectively the FRP of acrylate functions in the presence of NPG (0.4%/1% w/w) (e.g. FC= 71%, 70%, 75% and 74% for MeO-Coum3,4,5,6). These results clearly show that MeO-Coum8,9 and 10 presents a photo-oxidation and photo-reduction process, and that MeO-Coum3,4,5,6 show mainly a photo-reduction process. In order to improve the performance of FRP, a three-component photoinitiating system PIS was prepared by introduction of NPG into the photosensitive formulation. In fact, a charge transfer complex (CTC) could be obtained by interaction between Iod and NPG. This CTC could weakly initiate the FRP of acrylates (FC = 47% in TMPTA and 77% in TA). The performance (final reactive function conversion and rate of polymerization) was improved by addition of Keto-Coumarin into the photocurable resin.

Remarkably, MeO-Coum/Iod/NPG (0.1% or 0.4%/1%/1% w/w/w) was more efficiency compared to MeO-Coum/Iod or NPG (0.1% or 0.4%/1% w/w) (e.g. FC = 86% for MeO-Coum8/NPG vs. 91% for MeO-Coum8/Iod/NPG Figure 3B vs. 3C curve 8, 74% for MeO-Coum6/NPG vs. 87% for MeO-Coum6/Iod/NPG Figure 3B vs. 3C curve 6).

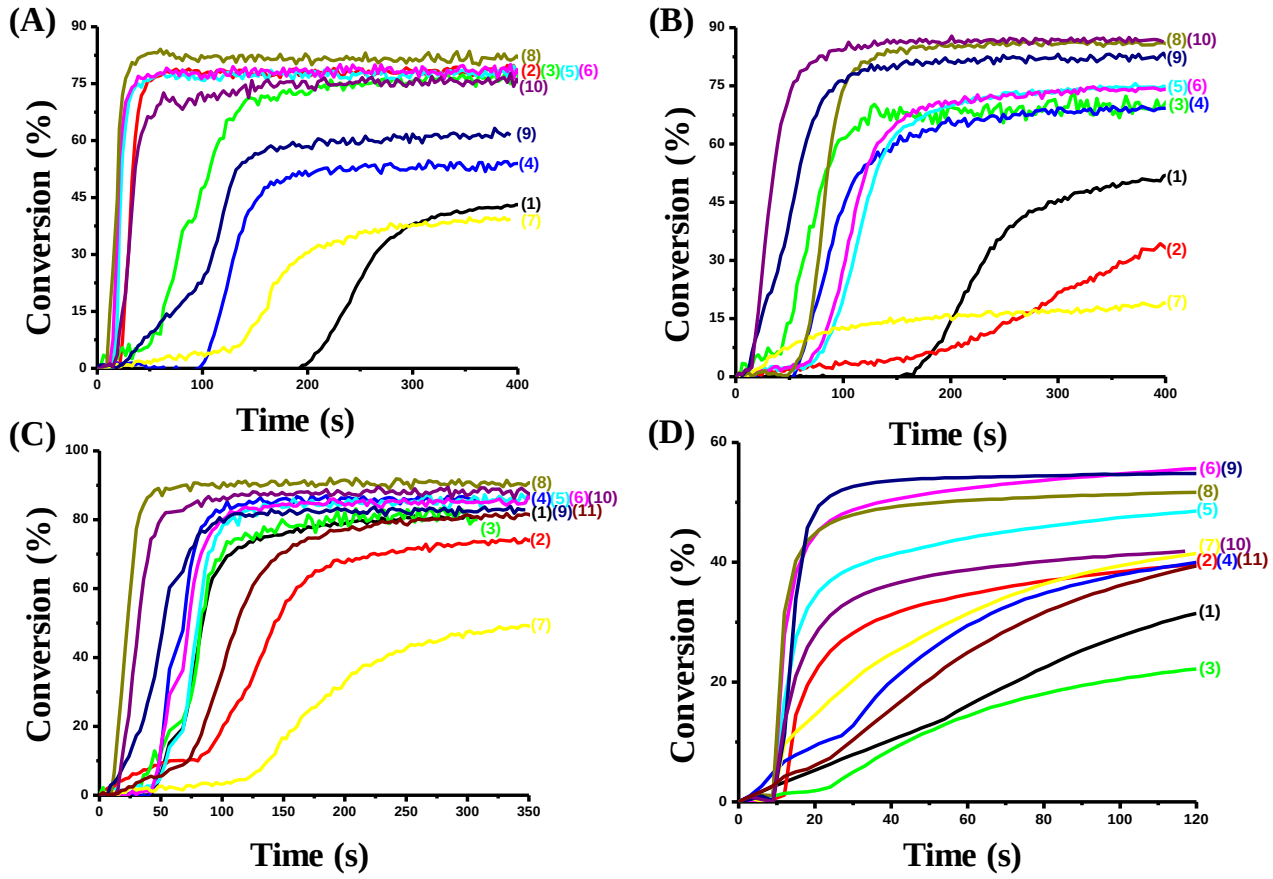

Figure 3: Free Radical photopolymerization profiles of acrylate functions (conversion vs irradiation time) in thick (A,B and C) and thin sample (D) upon visible light irradiation using a LED@405nm: (A,B) using two-component PIS based on MeO-Coum/NPG, (C,D) using three-component PIS based on MeO-Coum/Iod/NPG (0.1% or 0.4%/1% w/w): **(1)** MeO-Coum1 (0.4%), **(2)** MeO-Coum2 (0.4%), **(3)** MeO-Coum3 (0.4%), **(4)** MeO-Coum4 (0.4%), **(5)** MeO-Coum5 (0.4%), **(6)** MeO-Coum6 (0.4%), **(7)** MeO-Coum 7 (0.4%), **(8)** MeO-Coum8 (0.1%), **(9)** MeO-Coum9 (0.1%), **(10)** MeO-Coum10 (0.1%) and **(11)** Iod/NPG (1%/1% w/w). **(A,D)** in TMPTA and **(B,C)** in TA. Irradiation starts at t = 10s.

Table 2: Final reactive function conversions (FC%) for different monomers and different PISs upon visible light irradiation using a LED @405nm (400 s of irradiation and thickness = 1.4 mm).

	Two-component photoinitiating systems					**Three-component photoinitiating systems**	
	TMPTA			**TA**		**TMPTA**	**TA**
	1% Iod	**+1%EDB**	**1%NPG**	**1%Iod**	**1%NPG**	**Iod/NPG (1%/1% w/w)**	**Iod/NPG (1%/1% w/w)**
MeO Coum1	n.p[1]	n.p	36%	n.p	52%	73%	81%
MeO Coum2	n.p	48%	39%	n.p	34%	83%	76%
MeO Coum3	n.p	n.p	41%	n.p	71%	70%	83%
MeO Coum4	n.p	n.p	18%	n.p	70%	71%	87%
MeO Coum5	23%	57%	52%	12%	75%	84%	87%
MeO Coum6	18%	61%	50%	13%	74%	86%	87%

MeO Coum7	32%	41%	38%	10%	19%	70%	52%
MeO Coum8	18%	60%	51%	81%	86%	86%	91%
MeO Coum9	34%	n.p	45%	70%	83%	74%	84%
MeO Coum10	38%	49%	32%	65%	87%	78%	89%

[1] n.p : no polymerization

3.3 Direct laser write and 3D printing using MeO-Coum/Iod/amine system

A diode laser @405nm was used for the generation of 3D polymers patterns which were characterized by optical microscopy. This experiment was carried out under air and using different PISs based on MeO-Coum/Iod/TMA in TMPTA or TA (See Figure 4). Remarkably, a great thickness could be obtained (~1900 µm), with a high spatial resolution (polymerization process is produced in the irradiated area) and very short irradiation times were necessary to generate the 3D patterns. Some 3D printing experiments were also carried out using a low light intensity 3D printer (LCD-based 405 nm 3D Printer Anycubic Photon S) (Figure 4E) showing the high photosensitivity of the proposed systems.

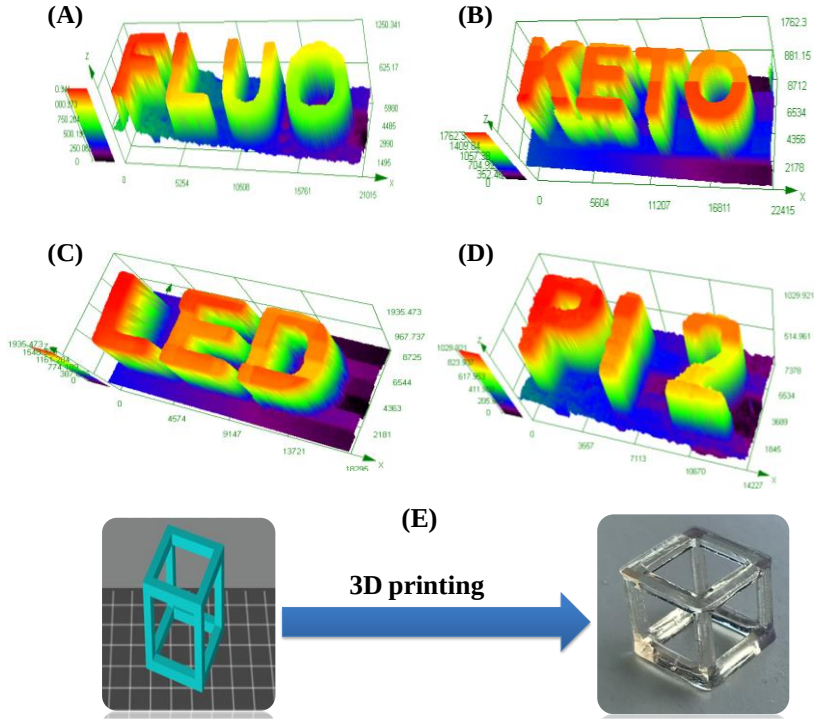

Figure 4: Free Radical Photopolymerization experiments using a laser diode @405nm for the generation of 3D patterns characterized by numerical optical microscopy: **(A)** MeO-Coum2/Iod/TMA (0.15%/0.5%/0.175% w/w/w) in TA, **(B)** MeO-Coum5/Iod/TMA (0.15%/0.5%/0.23% w/w/w) in TMPTA, **(C)** MeO-Coum6/Iod/NPG (0.266%/0.667%/0.667 w/w/w) in TMPTA, **(D)** MeO-Coum8/Iod/TMA (0.05%/0.5%/0.18% w/w/w) in TMPTA and **(E)** 3D printing experiments using MeO-Coum8/Iod/NPG (0.1%/1%/1% w/w/w) in TMPTA.

3.4 Photopolymerization of acrylate monomer for the access to photocomposite

Partie II : Colorants organiques comme photoamorceurs

In view of their costs/performance ratios, glass fibres are widely used in reinforcement applications in composite preparation. Due to their ability to initiate Free Radical Photopolymerization, some KCs were selected for the synthesis of photocomposites using TMPTA as the organic matrix and glass fibres as reinforcement (50%/50% w/w) upon near-UV light using a LED conveyor @ 395 nm (4 W/cm^2). The obtained results are depicted in the Figure 5. Firstly, the glass fibres were impregnated by the photosensitive resin, then this sample was irradiated, and a very fast curing was obtained using MeO-Coum/Iod/NPG (0.1% or 0.4%/1%/1% w/w/w). It is important to note that both the surface and the bottom are tack-free after 1 pass only (for MeO-Coum 2,5,6) and 1 pass only at their surfaces and 2 passes on the bottom for MeO-Coum 8,9,10. A tack-free character is observed by touching the two polymerized surfaces, once the two surfaces are smooth and non-sticky, we speak of a tack-free character.

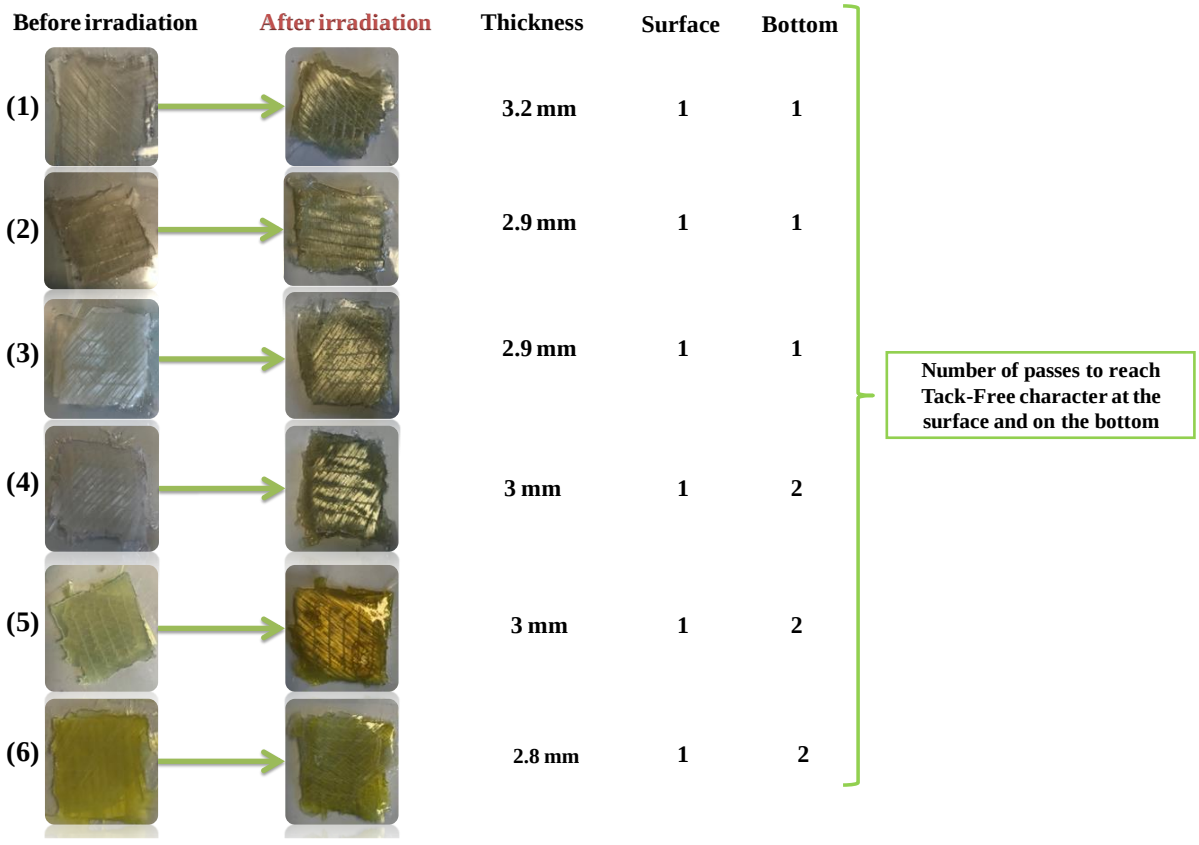

Figure 5: FRP experiments of acrylates (TMPTA) for photocomposites curing using a LED conveyor @395nm: **(1)** MeO-Coum2 /Iod /NPG (0.4%/1%/1% w/w/w) , **(2)** MeO-Coum5/Iod/NPG (0.4%/1%/1% w/w/w), **(3)** MeO-Coum6/Iod/NPG (0.4%/1%/1% w/w/w), **(4)** MeO-Coum8/Iod/NPG (0.1%/1%/1% w/w/w), **(5)** MeO-Coum9/Iod/NPG (0.1%/1%/1% w/w/w) and **(6)** MeO-Coum10/Iod/NPG (0.1%/1%/1% w/w/w).

4. Discussion: Photochemical mechanisms

The photochemical and photophysical properties of Keto-Coumarins in solution will be discussed in this part.

4.1 Steady state photolysis of Keto-Coumarin derivatives

Photolysis experiments of the different KCs in ACN have been carried out using a LED @375nm. One of these compounds (MeO-Coum8) was chosen and presented in Figure 6 to explain the results obtained by FRP. First of all, no photolysis occurs for MeO-Coum8 alone (Figure 6A), but a very fast photolysis of this compound is observed in the presence of Iod (10^{-2} M). These results clearly show that MeO-Coum8 is photostable. Decrease of the absorption peak of MeO-Coum8 and the increase in the optical density between 420 nm and 500 nm show that an interaction between the KC and Iod occurs. This interaction can be explained by an electron transfer process which generates a radical and a photoproduct when they are irradiated. The consumption percentage obtained by KC/Iod photolysis (56%) is very high compared to that in the presence of KC alone (no consumption occurs) (Figure 6C curve 1 vs. 2).

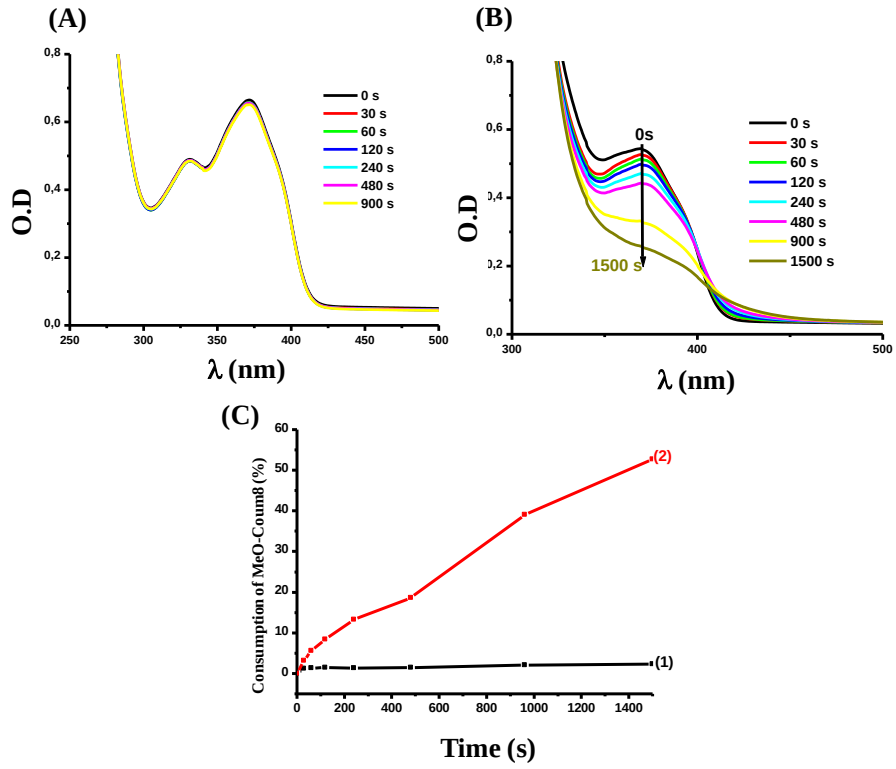

Figure 6: Steady state photolysis experiments of MeO-Coum8 in ACN: **(A)** alone, **(B)** with Iod (10^{-2} M). **(C)** Consumption (%) of MeO-Coum8 vs. Irradiation time (s) : **(1)** alone, and **(2)** with Iod.

4.2 Excited state reactivity and redox behaviour

Emission spectra and fluorescence quenching experiments in ACN for one of the KCs (MeO-Coum8) are reported in Figure 7. First of all, singlet excited state energy (E_{S1}) could be calculated from the crossing point of the absorption and emission spectra (See Figure 7A) (E_{S1} = 3.05 eV). A decrease of the emission intensity for MeO-Coum8 was observed by addition of Iod, EDB and NPG clearly showing an interaction between ^{1}MeO-Coum8 and Iod (EDB or NPG). The decrease in intensity in the presence of NPG is fast compared to that obtained in the presence of Iod or EDB. This result is in agreement with the FRP results which show a high reactivity of MeO-Coum8 with NPG (FC = 83%) compared to that obtained with EDB (FC = 60%) and Iod (FC = 60%). The Stern-Volmer coefficient (Ksv) was determined in the aim to compare the KCs reactivity with different additives (Iod, EDB and NPG). Thus, if Ksv is higher, the interaction between KC and the additives is higher, then the electron transfer quantum yields (ϕ) (calculated from the eq.2) will be higher, for example MeO-Coum8 is more quenched with NPG compared to MeO-Coum9, so Ksv of MeO-Coum8 are higher compared to MeO-Coum9 (Ksv = 217 for MeO-Coum8 vs. 10 for MeO-Coum9) (See Table 3)

$$\phi_{S1} = K_{SV}[Iod] / (1+K_{SV}[Iod]) \qquad \text{eq. 2}$$

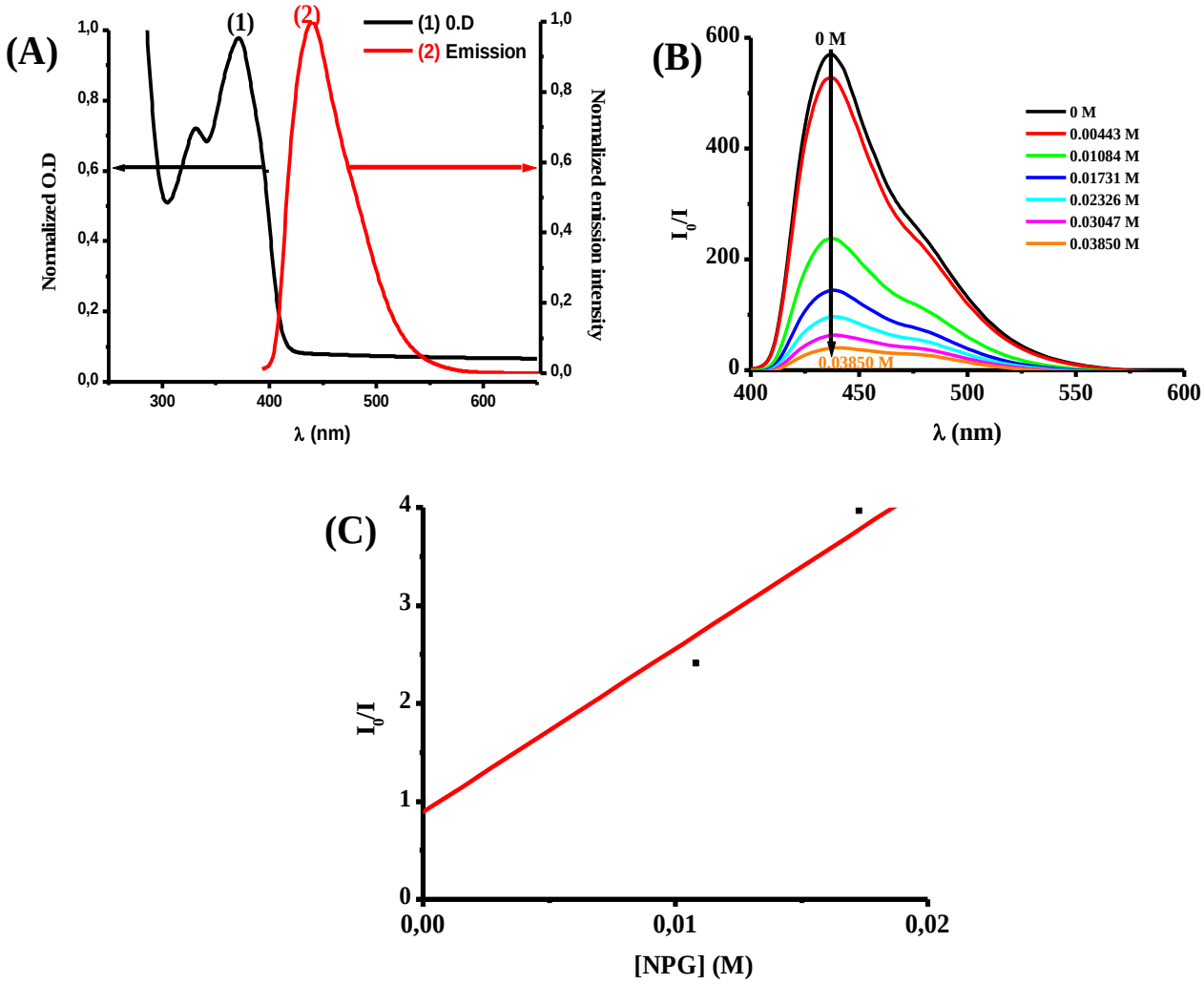

Figure 7 : (A) E_{S1} determination of MeO-Coum8 in ACN, **(B)** Fluorescence quenching of MeO-Coum8 by NPG in ACN, **(C)** Stern-Volmer coefficient determination of MeO-Coum8.

Cyclic voltammetry experiments were carried out in ACN to calculate the free energy change (ΔG) for the electron transfer between Keto-Coumarins and Iod or NPG, which is a very important parameter to evaluate the reaction spontaneity of FRP. ΔG is calculated from E_{S1} and the electrochemical properties (E_{ox} and E_{red}) (using eq. 1), for example $\Delta G_{S1\ (PI/NPG)}$ = -0.19 eV for MeO-Coum1 vs. -0.53 eV for MeO-Coum8 which is more reactive in the FRP process (FC = 43% vs. 83% for MeO-Coum1 and 8 respectively). All these data are summarized in Table 3.

Table 3: Parameters characterizing the chemical mechanisms associated with ^{1}Keto-Coum/Iod (EDB or NPG) interaction in acetonitrile. For Iod and NPG, a reduction and oxidation potential of -0.7 and 1.03 eV were used respectively for the ΔGet calculation.

	E_{ox} (eV)	E_{red} (eV)	E_{S1} (eV)	ΔG_{S1} (PI/NPG) (eV)	ΔG_{S1} (PI/Iod) (eV)	K_{SV} (M^{-1}) (MeO-Coum/Iod)	K_{SV} (M^{-1}) (MeO-Coum/EDB)	K_{SV} (M^{-1}) (MeO-Coum/NPG)	Φ_{et} (MeO-Coum/Iod)	Φ_{et} (MeO-Coum/EDB)	Φ_{et} (MeO-Coum/NPG)
MeO-Coum1		-2.1	3.32	-0.19		8.83	5	51	0.13	0.38	0.65
MeO-Coum2		-1.38	3.20	-0.79		6.5	9.5	51	0.12	0.3	0.68
MeO-Coum3		-1.77	3.24	-0.44			23	55		0.47	0.6
MeO-Coum4		-1.82	3.23	-0.38		15	45	102	0.34	0.6	0.75
MeO-Coum5		-1.37									
MeO-Coum6		-1.38	3.08	- 0.67			14	22		0.39	0.64
MeO-Coum7		-1.22									
MeO-Coum8	0.41	-1.52	3.05	-0.5	-1.94	18	116	180	0.33	0.76	0.76
MeO-Coum9	1.11	-1.62	2.72	- 0.07	-0.91	10	8	9	0.18	0.15	0.24
MeO-Coum10	0.72	-0.7	2.61	-0.88	-1.19	497		735	0.68		0.9

$KC\ (h\nu) \rightarrow {}^{1,3}KC$ r1

${}^{1,3}KC + Ar_2I^+ \rightarrow Ar^\bullet + ArI + KC^{\bullet+}$ r2

$NPG + Iod \rightarrow [NPG\text{-}Iod]_{CTC}$ r3

$[NPG\text{-}Iod]_{CTC} \rightarrow Ar^\bullet$ r4

${}^{1,3}KC + NPG \rightarrow KC\text{-}H^\bullet + NPG_{(-H)}{}^\bullet$ r5

$NPG_{(-H)}{}^\bullet \rightarrow NPG_{(-H;-CO2)}{}^\bullet + CO_2$ r6

$NPG_{(-H;-CO2)}{}^{\bullet+} + Ar_2I^+ \rightarrow NPG_{(-H;-CO2)}{}^+ + Ar^\bullet + ArI$ r7

Scheme 3. Proposed chemical mechanisms

A global mechanism can be proposed to explain the FRP results based on the different characterization techniques (Steady state photolysis, fluorescence quenching, cyclic voltammetry experiments). Firstly, the KC is promoted in its excited state when the dye absorbs a suitable light energy. Since KC is mainly a Type II PI, KC cannot give reactive species alone, but reacts with other additives (Iod, EDB or NPG). The photoinitiating systems will be able to generate initiating radicals able to initiate the FRP (r1-r2). Addition of a third additive (e.g. NPG) in the photosensitive formulation resulted in a very high performance of FRP profile. This can be explained by the more efficient generation of radicals due to the formation of a charge transfer complex between Iod salt and NPG $[Iod\text{-}NPG]_{CTC}$ which generates reactive species (r3-r4). NPG can also react with the excited state of KC by a hydrogen transfer process from amine to KC (r4-r5) which generates two new type of radicals

(KC-H$^{\bullet}$, $NPG_{(-H)}^{\bullet}$). This reaction explains the high performance of the FRP of acrylate functions using Keto-Coum/NPG as PISs. By decarboxylation of $NPG_{(-H)}^{\bullet}$, a new radical ($NPG_{(-H;-CO2)}^{\bullet}$) is generated which can react with Iod to generate also aryl radical (Ar$^{\bullet}$) (r6-r7).

5. Conclusion

In this research, ten organic compounds based on Keto-Coumarin derivatives have been synthesized and proposed as new photoinitiating systems (PISs) able to initiate the FRP of acrylate functions using TMPTA or TA as benchmark acrylic resins under mild irradiation conditions. The FRP results were discussed and explained by a proposed global mechanism using different characterization techniques such as: steady state photolysis, fluorescence quenching, and cyclic voltammetry experiments. These KCs have been tested in direct laser write and 3D printing as well as in the synthesis of thick glass fiber photocomposites. The different photoinitiating systems showed a very high efficiency. Development of new high-performance PISs capable to be activated at longer wavelengths (e.g. Near-Infrared) for a better light penetration into thick samples remains a great challenge and it deserves to be investigated in the future with (keto)coumarins, after modification by chemical engineering.

References

[1] Fouassier, J.P.; Lalevée, J. Photoinitiators for Polymer Synthesis, Scope, Reactivity, and Efficiency; Wiley-VCH Verlag, Weinheim, **2012**.

[2] Fouassier, J.P. Photoinitiator, Photopolymerization and Photo-curing: Fundamentals and Applications; Gardner Publications: New York, **1995**.

[3] Dietliker, K.A. Compilation of Photoinitiators Commercially Available for UV Today; Edinbergh. Sita Technology Ltd.: London, **2002**.

[4] Davidson, S. Exploring the Science, Technology and Application of UV and EB Curing, Sita Technology Ltd, London, **1999**.

[5] Crivello, J.V.; Dietliker, K.; Bradley, G. Photoinitiators for Free Radical Cationic & Anionic Photopolymerisation; John Wiley &Sons: Chichester, U.K., **1999**.

[6] Neckers, D.C.; Jager, W. SITA Technology Limited Chemistry &Technology for UV & EB Formulation for Coatings, Inks &Paints, Photoinitiation for Polymerization: UV & EB at the Mill-enium; Wiley : Chichester, **1999**.

[7] Moraes, R.R.; Fariae-Silva, A.L.; Ogliari, F.A; Correr-Sobrinho, L.; Demarco, F.F; Piva, E. Impact of immediate and delayed light activation on self-polymerization of dual-cured dental resin luting agents. Acta Biomater. **2009**, 5, 2095.

[8] Palin, W.M.; Leprince, J.G.; Hadis, M.A. Shining a light on high volume photocurable materials Dent. Mater., **2018**, 34, 695.

[9] Garra, P.; Dietlin, C.; Morlet-Savary, F.; Dumur, F.; Gigmes, D.; Fouassier, J.P.; Lalevée. Photopolymerization processes of thick films and in shadow areas : a review for the access to composites J.Polym.Chem. 2017, 8, 7088.

[10] Garra, P.; Bonardi, A.H.; Baralle, A.; Al Mousawi, A.; Bonardi, F.; Dietlin, C.; Morlet-Savary, F.; Fouassier, J.P.; Lalevée, J. Monitoring photopolymerization reactions through thermal imaging: A unique tool for the real-time follow-up of thick samples, 3D printing, and composites Polym.Sci. Part A: Polym. Chem. **2018**, 56, 889.

[11] Lalevee, J.; Fouassier, J.P. Photopolymerisation Initiating Systems, The Royal Society of Chemistry, London, **2018**.

[12] Dietlin, C.; Schweizer, S.; Xiao, P.; Zhang, J.; Morlet-savary, F.; Graff, B.; Fouassier, J.P.; and Lalevée, J. Photopolymerization upon LEDs: new photoinitiating systems and strategies Polym. Chem. **2015**, 6, 3895.

[13] Schmitt, M. Method to analyse energy and intensity dependent photo-curing of acrylic esters in bulk. RSC Adv. **2015**, 5, 67284.

[14] Schmitt, M.; Lalevée, J. ZnO nanoparticles as polymerisation photo-initiator: Levulinic acid/NaOH content variation. Colloids Surf. A, **2017**, 532, 189.

[15] Fouassier, J.P.; Lalevée, J. Recent Advances in Photoinduced Polymerization Reactions under 400-700 nm Light. Photochem. **2014**, 42, 215.

[16] Dumur, F.; Gigmes, D.; Fouassier, J.P.; Lalevée, J. Organic Electronics: An El Dorado in the Quest of New Photocatalysts for Polymerization Reactions. Acc. Chem. Res. **2016**, 49, 1980.

[17] Zivic, N.; Bouzrati-Zerelli, M.; Kermagoret, A.; Dumur, F.; Fouassier, J.P.; Gigmes, D.; Lalevée, J. Photocatalysts in Polymerization Reactions. ChemCatChem. **2016**, 8, 1617.

[18] Abdallah, M.; Dumur, F.; Hijazi, A.; Rodeghiero, G.; Gualandi, A.; Cozzi, P.G ; Lalevée, J. Keto-coumarin scaffold for photoinitiators for 3D printingand photocomposites. J Polym. Sci., **2020**, 58, 1115.

[19] Salmi, H.; Tar, H.; Ibrahim, A.; Ley, C.; Allonas, X. Ketocoumarin/triazine/thiol as new high speed photoinitiating system for free radical polymerization under visible light in aerated media. Eur. Polym. J. **2013**, 49, 2275.

[20] Lalevée, J.; Zadoina, L.; Allonas, X.; Fouassier, J.P. New sulfur-centered radicals as photopolymerization initiating species. J. Polym. Sci.A Polym. Chem. **2007**, 45, 2494.

[21] Fouassier, JP. Photochemistry and UV curing : new trends 2006. Ed.,Research Signpost: Trivandrum, Kerala, India, **2006**.

[22] Rahal, M.; Mokbel, H.; Graff, B.; Toufaily, J.; Hamieh, T.; Dumur, F.; Lalevée, J. Mono vs. Difunctional Coumarin as Photoinitiatorsin Photocomposite Synthesis and 3D Printing.Catalyst, **2020**, 10, 1202

[23] Mousawi, A.; Kermagoret, A.; Versace, D.L.; Toufaily, J.; Hamieh, T.; Graff, B.; Dumur, F.; Gigmes, D.; Fouassier, J.P.; and Lalevee. L. Polym. Chem., **2016**, 8, 568.

[24] Wang, X.; Bai, X.; Su, D.; Zhang, Y.; Li, P.; Lu, S.; Gong, Y.; Zhang, W.; Tang, B. Simultaneous Fluorescence Imaging Reveals N-Methyl-D-aspartic Acid Receptor Dependent Zn^{2+}/H^{+} Flux in the Brains of Mice with Depression, Anal. Chem. **2020**, 92, 4101.

[25] Rehm, D; Weller, A. Kinetics of Fluorescence Quenching by Electron and H-Atom Transfer. Isr. J. Chem. **1970**, 8, 259.

[26] Foresman, J.B; Frisch, A. Exploring Chemistry with Electronic Structure Methods, second ed., Gaussian Inc., Pittsburgh, PA, **1996**.

[27] Frisch, M.J.; Trucks, G.W.; Schlegel, H.B.; Scuseria, G.E.; Robb, M.A.; Cheeseman, J.R.; Zakrzewski, V.G.; Montgomery, J.A.; Stratmann, J.R.E.; Burant, J.C.; Dapprich, S.; Millam, J.M.; Daniels, A.D.; Kudin, K.N.; Strain, M.C.; Farkas, O.; Tomasi, J.; Barone, V.; Cossi, M.; Cammi, R.; Mennucci, B.; Pomelli, C.; Adamo, C.; Clifford, S.; Ochterski, J.; Petersson, G.A.; Ayala, P.Y.; Cui, Q.; Morokuma, K.; Salvador, P.; Dannenberg, J.J.; Malick, D.K.; Rabuck, A.D.; Raghavachari, K.; Foresman, J.B.; Cioslowski, J.; Ortiz, J.V.; Baboul, A.G.; Stefanov, B.B.; Liu, G.; Liashenko, A.; Piskorz, P.; Komaromi, I.; Gomperts, R.; Martin, R.L.; Fox, D.J.; Keith, T.; Al-Laham, M.A.; Peng, C.Y.; Nanayakkara, A.; Challacombe, M.; Gill, P.M.W.; Johnson, B.; Chen, W.; Wong, M.; Andres, J.L.; Gonzalez, C.; Head-Gordon, M.; Replogle, E.S.; Pople, J.A.; Gaussian 03, Revision B-2, Gaussian Inc., Pittsburgh, PA, **2003**.

[28] Zhang, J.; Dumur, F.; Xiao, P.; Graff, B.; Bardelang, D.; Gigmes, D.; Fouassier, J.-P.; Lalevée, J. Structure Design of Naphthalimide Derivatives: Toward Versatile Photoinitiators for Near-UV/Visible LEDs, 3D Printing, and Water-Soluble Photoinitiating Systems. Macromolecules. **2015**, 48, 2054.

Partie III : Nouveaux photoamorceurs à base de colorants pour la polymérisation radicalaire (FRP) et Cationique (CP)

Partie III : Nouveaux photoamorceurs à base de colorants pour la polymérisation radicalaire (FRP) et Cationique (CP)

Chapitre I : Des dérivés de phénothiazine comme photoamorceurs Type II pour la polymérisation radicalaire et cationique

De nos jours les colorants organiques sont de plus en plus utilisés dans l'industrie des cosmétiques, aliments, peintures, en biologie, et certains d'entre eux ont été utilisés comme agents pharmaceutiques et photosensibilisateur/photoamorceur pour la synthèse des polymères réticulés par photopolymérisation radicalaire ou cationique [1-5]. Cependant, la recherche de nouveaux photoamorceurs plus sensibles à la lumière visible, et capables d'induire le processus de polymérisation radicalaire et ou/cationique avec une faible consommation d'énergie et un coût relativement faible, représente un défi majeur dans les recherches actuelles.

De ce fait, quatre nouveaux dérivés de phénothiazine ont été synthétisés et proposés comme photoamorceurs pour l'élaboration des photopolymères réticulés. Ces composés se caractérisent par un noyau tricyclique : deux cyclique benzéniques couplés par des atomes de soufre et d'azote, ils sont facilement oxydables, avec une décomposition rapide en solution. Ils sont aussi faiblement solubles dans l'eau. La plupart des études menées sur les phénothiazines portent sur l'utilisation de ces composés pour l'amorçage de la photopolymérisation cationique avec une capacité d'absorption limitée à la zone UV [6]. Ainsi, la recherche de nouveaux dérivés de phénothiazine capables sous irradiation visible de générer des espèces actives pour l'amorçage des processus de polymérisation est au cœur de ce travail.

Dans ce contexte, la synthèse de ces dérivés a été réalisée suivant la réaction d'acylation Friedel-Crafts catalysée une fois par l'acide de Lewis ($AlCl_3$) pour la synthèse de PT3 et PT4, et autre fois par le réactif de Vilsmeier pour la synthèse de PT1 et PT2. En fait, PT3 et PT4 n'ont jamais été synthétisés avant, et ont de bonnes propriétés d'absorption dans le visible. Ces quatre colorants diffèrent par la nature du substituant lié au le noyau phénothiazine affectant ainsi leur capacité d'absorption et d'amorçage ainsi que leur propriétés photophysique/photochimique. L'amorçage du processus de photopolymérisation porte sur la combinaison de ces nouveaux dérivés avec le sel d'iodonium. Le potentiel d'oxydation

approprié de ces colorants conduit à des valeurs très favorables en énergie libre (ΔG) pour les réactions de transfert d'électron PT/Iod. Ce transfert d'électron est bien observé sous photolyse (sous irradiation avec une LED à 375 nm) avec une réaction très rapide des dérivés de phénothiazine en solution. Les constantes de vitesse de désactivation de leur fluorescence par leur le sel d'iodonium sont aussi très élevées.

De ce fait, les photopolymérisations radicalaire et cationique ont été réalisées dans des conditions d'irradiation douce en utilisant la LED à 405nm pour le système PT/Iod. Effectivement, des bons profils de polymérisation en échantillons épais ou minces ont été observés dans chaque type de polymérisation. La FRP des acrylates en utilisant un système à trois composants par l'introduction d'une amine dans la résine photosensible a été également testée. La vitesse de réaction ainsi que le taux de conversion final sont alors fortement augmentés par ajout de l'amine. Cela a pu démontrer que la PT a été régénérée suivant un cycle catalytique. Les photoamorceurs ainsi développés sont caractérisés comme **des catalyseurs photoredox.**

Pour finir, des motifs polymères en 3D ont été obtenus par impression 3D d'acrylates en utilisant une diode laser à 405nm. La synthèse des photocomposites représente aussi une des applications les plus intéressantes dans le domaine de photopolymérisation qui a été accomplie avec succès dans ce travail qui a fait l'objet d'une **publication** dans **'Polymer Chemistry'** sous la citation suivante : Rahal, M.; Abdallah, M.; Bui, TT.; Goubard, F.; Graff, B.; Dumur, F.; Toufaily, J.; Hamieh, T.; Lalevee, J. Design of new phenothiazine derivatives as visible light photoinitiators Polym.Chem., **2020**, 11, 3349.

Références

[1] Zivic, N.; Bouzrati-Zerelli, M.; Villote, S.; Morlet-Savary, F.; Dietlin, C.; Dumur, F.; Gigmes, D.; Fouassier, J.P.; Lalevee, J. A novel naphthalimide scaffold based iodonium salt as a one-component photoacid/photoinitiator for cationic and radical polymerization under LED exposure. Polym. Chem. **2016,** 7, 5873.

[2] Lalevée, J.; Dumur, F.; Mayer, C.R.; Gigmes, D.; Nasr, G.; Tehfe, M.A.; Telitel, S.; Morlet-Savary, F.; Graff, B.; Fouassier, J.P. Photopolymerization of N-Vinylcarbazole Using

Visible-Light Harvesting Iridium Complexes as Photoinitiators. Macromolecules. **2012**, 45, 4134.

[3] Zhang, J.; Dumur, F.; Xiao, P.; Graff, B.; Bardelang, D.; Gigmes, D.; Fouassier, J.-P.; Lalevée, J. Structure Design of Naphthalimide Derivatives: Toward Versatile Photoinitiators for Near-UV/Visible LEDs, 3D Printing, and Water-Soluble Photoinitiating Systems. Macromolecules. **2015**, 48, 2054.

[4] Mousawi, A.A.; Dumur, F.; Garra, P.; Toufaily, J.; Hamieh, T.; Graff, B.; Gigmes, D.; Fouassier, J.P.; Lalevée, J. Carbazole Scaffold Based Photoinitiator/Photoredox Catalysts: Toward New High-Performance Photoinitiating Systems and Application in LED Projector 3D Printing Resins. Macromolecules. **2017**, 50, 2747.

[5] Hammoud, F.; Lee, Z.H.; Graff, B.; Hijazi, A.; Lalevee, J.; Chen Y.C. Novel phenylamine-based oxime-ester photoinitiators for LED-induced free radical, cationic, and hybrid polymerization. J.Polym.Sci. **2021,** 59, 1711.

[6] Rodrigues, M.R.; Neumann, M.G. Cationic photopolymerization of tetrahydrofuran: A mechanistic study on the use of a sulfonium salt–phenothiazine initiation system. J. Polym. Sci. Part. A: Pol. Chem. **2001**, 39, 46.

Design of New Phenothiazine Derivatives as Visible Light Photoinitiators

Abstract

In this article, four new phenothiazine derivatives (noted PT1, PT2, PT3 and PT4) are specifically in-silico designed by molecular modelling for good light absorption properties @405nm. The most interesting structures showing both intense violet/blue light absorption and high potential photochemical reactivity were synthesized for detailed investigations as photoinitiators/photosensitizers in the presence of an iodonium salt for the free radical photopolymerization of (meth)acrylates and the cationic polymerization of epoxides upon near-UV or visible light irradiation. Remarkably, two of the proposed structures (PT3 and PT4) from this in-silico design were never synthesized prior to this work and were thus specifically designed for this work. Three-component photoinitiating systems based on PT/Iodonium/Amine (*N*-phenylglycine or Ethyl 4-dimethylaminobenzoate) are also developed for the free radical polymerization of acrylates. Both excellent polymerization rates and high final reactive function conversions were obtained. A full picture of the photochemical mechanisms is provided using different techniques: Real-Time Fourier Transform InfraRed Spectroscopy, UV-visible spectroscopy, fluorescence spectroscopy, and cyclic voltammetry. Finally, the high performance of the phenothiazine derivatives is also shown in 3D printing experiments as well as in photocomposite synthesis using glass fibres (thick sample; using a LED@395nm conveyor).

1. Introduction

Cationic (CP) and Free Radical (FRP) polymerization reactions induced by UV light have been widely encountered since decades in the field of irradiation hardening and it constitutes a powerful tool for the preparation of functional coatings [1]. Nowadays, light emitting diodes (LEDs) are classically used as irradiation sources, because of their numerous advantages compared to the traditional UV mercury lamps or lasers (low heat generation, low energy consumption, low operating costs, long lifetime, portability, simple and safe handling, possible integration in compact 3D printers, etc.) [2-4]. A photoinitiator (PI) is required to convert light to initiating species. Therefore, one of the most important purposes is the good

matching between the emission spectrum of the LED with the absorption of the PI [5-6]. For that reason, it is important to develop new photoinitiating systems (PISs) for both types (radical and cationic) of polymerization under mild near-UV or visible light irradiation sources. In this context, many works were focused on the development of new PIs or PISs see in e.g. [7-12].

Phenothiazine and their derivatives are nitrogen and sulfur-containing heterocycles which are used in a wide range of applications, going from pharmacological to biological applications [13-14]. But their range of applicability is not only limited to pharmacology and these structures have also been examined in various fields such as energy conversion [15], for their intense photoluminescence or their electrochemical properties [16-17]. Some phenothiazine derivatives have also shown a good ability to initiate the cationic photopolymerization and even the copolymerization of different monomers [18]. However, due to their low absorption in the visible range, these compounds are only able to initiate polymerization processes upon excitation with a UV light [19]. More recently, a new series of phenothiazine has been synthesized and studied as high performance photoinitiators to initiate both the FRP and CP under visible irradiation [20]; these compounds were also examined for 3D printing applications. Phenothiazine derivatives were also elegantly developed as photoredox catalysts for controlled polymerization processes [21].

In this new work, four phenothiazine derivatives (PT: PT1, PT2, PT3 and PT4 in Scheme 1) were specifically in-silico designed by molecular modelling and used as photoinitiators/photosensitizers of polymerization due to their excellent light absorption properties. As examples, completely new structures (e.g. PT3 and PT4) with excellent predicted light absorption properties @405 nm were selected for synthesis and more detailed photochemical investigations; this is a completely different strategy than a classical “trial-error” approach. The different phenothiazine derivatives were incorporated into two and three-component (PI/Iodonium (Iod) and PI/Iod/amine) photoinitiating systems PISs in order to induce the formation of reactive species (radicals, radical cations or acids) for both free radical (FRP) and cationic (CP) polymerizations upon visible light while using a LED@405nm. The different substituents specifically introduced on the phenothiazine core can affect the absorption properties as well as the photochemical/electrochemical properties of the targeted molecules. The photochemical properties are studied by using different methods such as: photolysis, UV-Visible absorption, fluorimetry and cyclic voltammetry. The new

PISs will be compared to benchmark initiating systems. To finish, remarkable performances of these derivatives are especially shown during 3D printing experiments carried out with the (PT/Iod/NPG) systems as well as during the preparation of photocomposites using glass fibers.

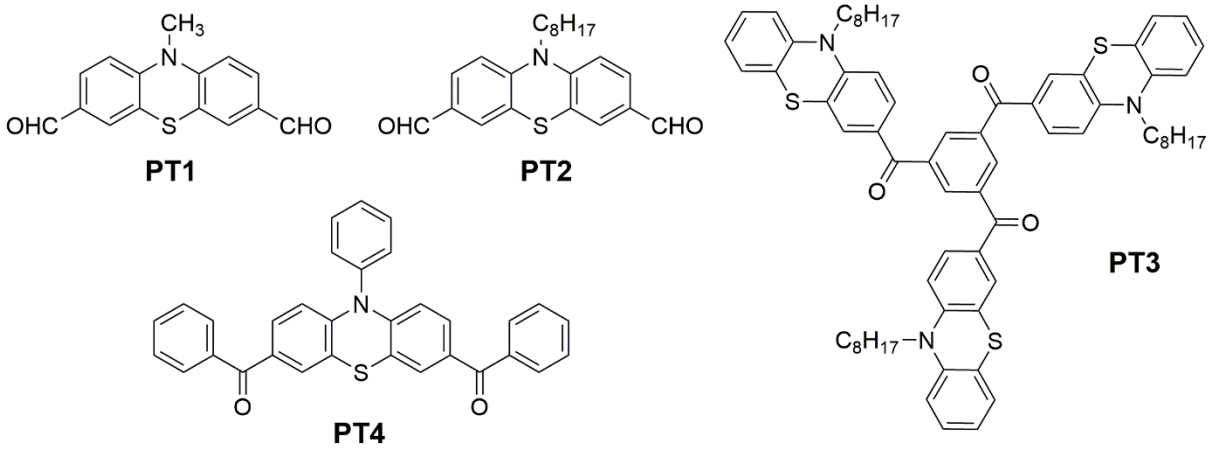

Scheme 1. The different phenothiazine derivatives investigated in this work.

2. Experimental part

2.1. Synthesis of phenothiazine derivatives:

N-Octyl phenothiazine (**1a**) [21], *N*-Phenyl phenothiazine (**1b**)[21], 10-methyl-10*H*-phenothiazine-3,7-dicarbaldehyde (**PT1**)[22] and 10-octyl-10*H*-phenothiazine-3,7-dicarbaldehyde (**PT2**) [21] are known compounds and were prepared according to procedures previously reported in the literature. **PT3** and **PT4** were prepared as described below.

Synthesis of PT3: In a dry round-bottom flask, *N*-octyl phenothiazine (**1a)** (8.9 g, 28.57 mmol), 1,3,5-benzenetricarbonyl trichloride (1.265 g, 4.76 mmol) and dry CH_2Cl_2 (40 mL) were charged yielding yellow solution. $AlCl_3$ (3.8 g, 28.52 mmol) was then added in one portion leading to violet/purple solution. The reaction mixture was stirred overnight. Water was added slowly and then the mixture was extracted by dichloromethane (3×75 mL). The organic layers were combined, washed with water, dried over anhydrous $MgSO_4$, filtered, and concentrated under reduced pressure. The crude product was purified by column chromatography eluting with pure dichloromethane then dichloromethane/ethyl acetate (95/5 to 90/10 v/v). The desired fractions were then collected and evaporated under reduced pressure to yield the title compound as a reddish powder (1.71 g, 33 % yield). **^{1}H NMR** (400

MHz, $CDCl_3$, δ_{ppm}): 8.15 (s, 3H), 7.55 (m, 6H), 7.07 (m, 3H), 7.01 (m, 3H), 6.87 (m, 3H), 6.78 (dd, *J* = 4.0-9.0 Hz, 6H), 3.79 (t, *J* = 7.0 Hz, 6H), 1.71 (m, 6H), 1.37 (m, 6H), 1.16 (m, 24 H), 0.78 (t, *J* = 7.0 Hz, 9H). **^{13}C NMR** (75 MHz, $CDCl_3$, δ_{ppm}): 192.9, 149.9, 143.5, 138.7, 133.0, 130.7, 130.3, 129.2, 127.5, 124.6, 123.7, 123.4, 115.8, 114.3, 48.0, 31.8, 29.2, 26.9, 26.7, 22.6, 14.1. **HRMS** (ESI+): Calculated for $C_{69}H_{75}N_3O_3S_3^{\bullet+}$ ($[M]^{\bullet+}$): 1089.4965/found: 1089.4954

Synthesis of PT4: In a dry round-bottom flask, *N*-Phenyl phenothiazine (**1b**) (1.403 g, 5.1 mmol), benzoyl chloride (3.6 g, 25.5 mmol) and dry CH_2Cl_2 (40 mL) were charged yielding yellow solution. $AlCl_3$ (3.4 g, 25.5 mmol) was then added in one portion leading to violet/purple solution. The reaction mixture was stirred overnight. Water was added slowly and then the mixture was extracted by dichloromethane (3×75 mL). The organic layers were combined, washed with water, dried over anhydrous $MgSO_4$, filtered, and concentrated under reduced pressure. The crude product was purified by column chromatography eluting with dichloromethane. The desired fractions were then collected, evaporated under reduced pressure and precipitated into petroleum ether to yield the title compound as a bright yellow powder (1.4 g, 57% yield). **^{1}H NMR** (400 MHz, $CDCl_3$, δ_{ppm}): 7.74 (m, 5H), 7.60 (m, 5H), 7.50 (m, 4H), 7.47 (s, 2H), 7.45 (s, 1H), 7.41 (d, *J* = 7.6 Hz, 2H), 6.15 (d, *J* = 8.0 Hz, 2H). **^{13}C NMR** (75 MHz, $CDCl_3$, δ_{ppm}): 194.3, 137.7, 133.0, 132.1, 131.4, 130.2, 130.1, 129.6, 128.3, 115.2. **HRMS** (ESI+): Calculated for $C_{32}H_{22}NO_2S^{\bullet+}$ ($[M+H]^{\bullet+}$): 484.1366/found: 484.1368.

2.2. Other chemical compounds

All the other chemicals (Scheme 2) were selected with the highest purity available and used as received. Di-*tert*-butyl-diphenyl iodonium hexafluorophosphate hexafluorophosphate (Iod or SpeedCure 938) and ethyl-4-(dimethylamino) benzoate (EDB) were obtained from Lambson Ltd (UK). (3,4 Epoxycyclohexane)methyl 3,4-epoxycyclohexylcarboxylate (EPOX; Uvacure 1500), trimethylolpropane triacrylate (TMPTA), Ebecryl 40 were obtained from Allnex. *N*-Phenylglycine (NPG) was obtained from Sigma Aldrich. TMPTA (or Ebecryl 40) and EPOX were selected as benchmark monomers for radical and cationic polymerization, respectively.

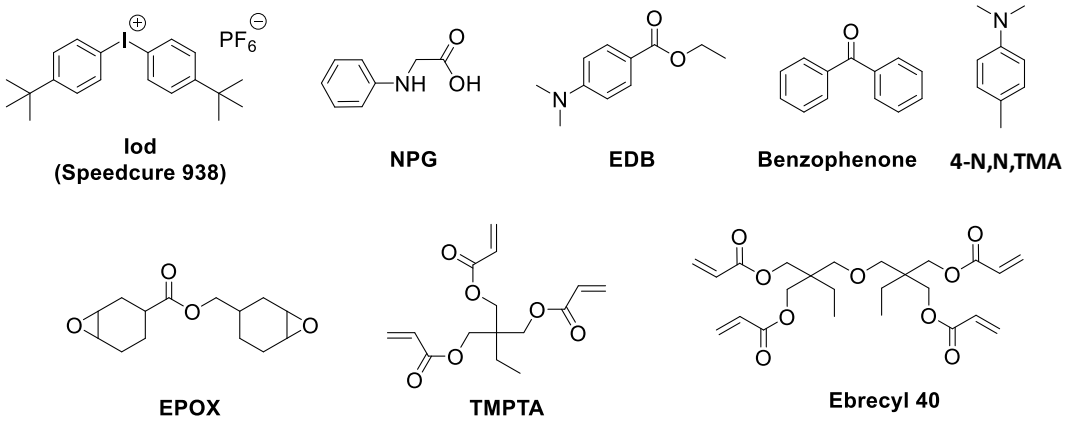

Scheme 2. Other used chemical compounds (initiators: Iod, Benzophenone; amine co-initiators: EDB, NPG, 4NNTMA; monomers: EPOX, TMPTA, Ebecryl40).

2.3. Irradiation sources

Different irradiation sources were used for the polymerization of the photocurable samples and for the photolysis experiment: (1) LED@ 375nm with an incident light intensity at the sample surface I_0 =40 mW.cm^{-2}; (2) LED@ 405nm with I_0=110 mW.cm^{-2}.

2.4. Free radical photopolymerization (FRP) and cationic photopolymerization (CP)

In this work, phenothiazine/Iod salt couples (0.1%/1% w/w) have been used as two-component photoinitiating systems PIS to initiate FRP or CP processes. The percentages for the different chemicals are related to the monomer weight. Then, these phenothiazine derivatives have been used in three-component photoinitiating systems (PT/Iod/amine (EDB or NPG)) (0.1%/1%/1% w/w/w) for the FRP.

The FRP of 1.4 mm thick samples of TMPTA or Ebecryl 40 was carried out under air into a rounded plastic mold ~ 1 cm in diameter and 1.4 mm thickness, and the FRP of 25 μm thin formulation was performed in laminate conditions (between two propylene film to reduce O_2 inhibition). For CP processes, the photosensitive resin was spread on a BaF_2 pellet (thickness = 25 μm) and the photopolymerization carried out under air.

The evolution of acrylate functions in TMPTA (or Ebecryl 40) and epoxy groups in EPOX were continuously followed by real time FTIR spectroscopy (JASCO FTIR 6100) at about 1630 and 790 cm^{-1} for thin samples and 6160 and 3600 cm^{-1} for thick samples. The procedure used to monitor the photopolymerization profiles has been already described in detail [23-24].

2.5. Redox potentials

The redox potentials for PT compounds (E_{ox} and E_{red}) were measured in acetonitrile by cyclic voltammetry with tetrabutylammonium hexafluorophosphate as the supporting electrolyte (potentials vs. Saturated Calomel Electrode – SCE). The free energy change (ΔGet) for an electron transfer reaction was calculated from eq. 1 [25], where Eox, Ered, E*, and C represent the oxidation potential of the electron donor, the reduction potential of the electron acceptor, the excited state energy level (determined from luminescence experiments) and the coulombic term for the initially formed ion pair, respectively. Here, C is neglected as usually done for polar solvents.

$$\Delta G_{et} = E_{ox} - E_{Red} - E^{*} + C \qquad \text{eq.1}$$

2.6. UV-Visible absorption and photolysis experiments

Both the UV-Visible absorption properties and the steady state photolysis of these compounds were studied using JASCO V730 UV-visible spectrometer.

2.7. Fluorescence experiments

The fluorescence properties of the different compounds in chloroform were investigated using a JASCO FP-6200 spectrofluorimeter. The fluorescence quenching experiments of PT by Iod were investigated from the classical Stern−Volmer treatment [26] ($I_0/I = 1 + kq\ \tau_0[Iod]$, where I_0 and I stand for the fluorescent intensity of PT in the absence and the presence of Iod, respectively; τ_0 stands for the lifetime of PT in the absence of Iod).

2.8. Computational Procedure

Molecular orbital calculations were carried out with the Gaussian 03 suite of programs [27-28]. The electronic absorption spectra for the different compounds were calculated with the time-dependent density functional theory at the MPW1PW91-FC/6-31G* level of theory on the relaxed geometries calculated at the UB3LYP/6-31G* level of theory. The triplet state energy levels were calculated at this latter level of theory.

2.9. Near-UV conveyor

A Dymax-LED conveyor was used to cure the composites. The glass fibers were impregnated with an organic resin (50%/50% w/w) and then irradiated. The LED conveyor is equipped with a 120 mm wide Teflon coated belt and one LED lamp (@395nm; 4 $W.cm^{-2}$). The belt speed was fixed at 2 $m.min^{-1}$.

2.10. 3D printing experiments

For 3D printing experiments, a laser diode @405 nm (spot size around 50 μm) was used for the spatially controlled irradiation. The photosensitive resin was polymerized under air and the generated 3D patterns were analysed using a numerical optical microscope (DSX-HRSU from OLYMPUS Corporation) as presented in [29-30].

3. Results

3.1. Light harvesting dyes synthesis

10-methyl-10*H*-phenothiazine-3,7-dicarbaldehyde (**PT1**) [23] and 10-octyl-10*H* phenothiazine-3,7-dicarbaldehyde (**PT2**) [21] have been reported by us and others. Two other novel compounds (**PT3** and **PT4**) have been readily synthetized from the corresponding *N*-substituted phenothiazine and the acyl chloride under classical Friedel Crafts acylation conditions (Scheme 3). *N*-octyl phenothiazine (**1a**) [21] reacted with 1,3,5-benzenetricarbonyl trichloride giving **PT3** in 33% yield. In this reaction, **1a** has been used in large excess (6.2 molar equivalence in respect of 1,3,5-benzenetricarbonyl trichloride) in order to favorite the threefold benzoylation of the 1,3,5-benzenetricarbonyl central core. The excess of **1a** has been easily recovered during the chromatography purification of the targeted compound (**PT3**). On the other hand, the treatment of *N*-phenyl phenothiazine (**1b)** [22] with of benzoyl chloride led to **PT4** in suitable yield (57%). In contrast to **PT3**, herein benzoyl chroride has been used in large excess (5.0 molecular equivalence with respect to **1b**) to force the twofold acylation on the two active sides of **1b**. Both compounds have a good solubility in common organic solvents, facilitating their purifications by column chromatography. Both final compounds have been characterized by NMR and HRMS analysis.

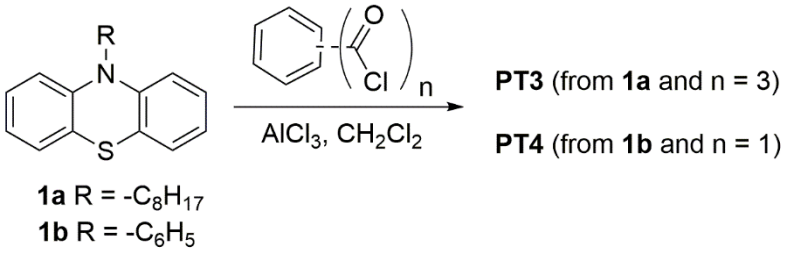

Scheme 3. Synthesis of **PT3** and **PT4**.

3.2. Light absorption properties of the investigated compounds

Partie III : Nouveaux photoamorceurs à base de colorants pour la polymérisation radicalaire (FRP) et Cationique (CP)

The UV-Visible absorption spectra of the proposed PTs in chloroform are gathered in Figure 1 and in Table 1. These compounds are characterized by high extinction coefficients (ε) in the near UV and visible range (e.g. ε(PT2) = 8290 $M^{-1}.cm^{-1}$ @405nm and 9570 $M^{-1}.cm^{-1}$ @ λ_{max}). Their good absorption properties ensure a good matching with the emission spectrum of the near UV or visible LEDs. Interestingly, the new synthesized compounds (PT3 and PT4) exhibit a better absorption than PT1 and PT2 (Figure 1).

From molecular modelling data, the frontier orbitals (Highest Occupied Molecular Orbital - HOMO and Lowest Unoccupied Molecular Orbital - LUMO) involved in the lowest energy transition are depicted in Figure 2. It can be noted that both the HOMO and LUMO are delocalized all over the π-system clearly showing a π → π* lowest energy transition. For PT3 and PT4, a charge transfer transition is also observed i.e. HOMO and LUMO located at different places of the molecular structure.

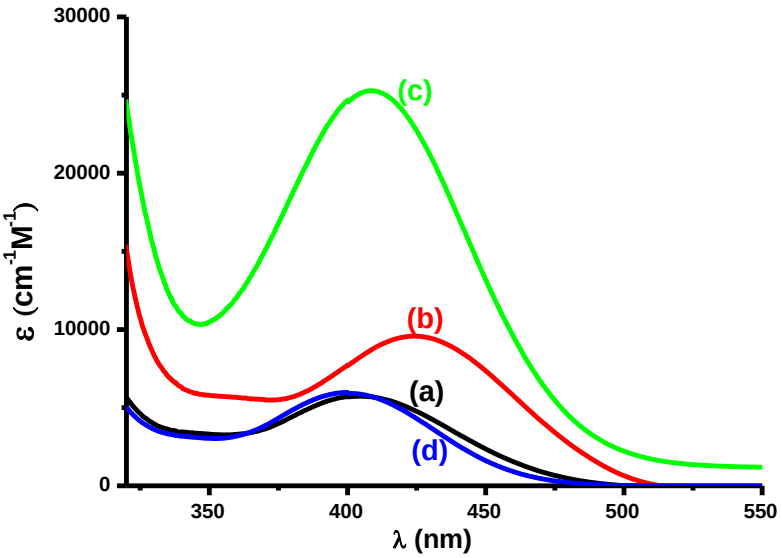

Figure 1. Absorption spectra of the investigated compounds in chloroform: **(a)** PT2, **(b)** PT4, **(c)** PT3 and **(d)** PT1.

Table 1. Light absorption properties of PT compounds at **405** nm and $\lambda_{max.}$

	λ_{max} (nm)	ε_{max} (M^{-1} cm^{-1})	$\varepsilon_{@405nm}$ (M^{-1} cm^{-1})
PT1	400	5910	5850

PT2	405	5730	5730
PT3	408	25280	25150
PT4	424	9570	8290

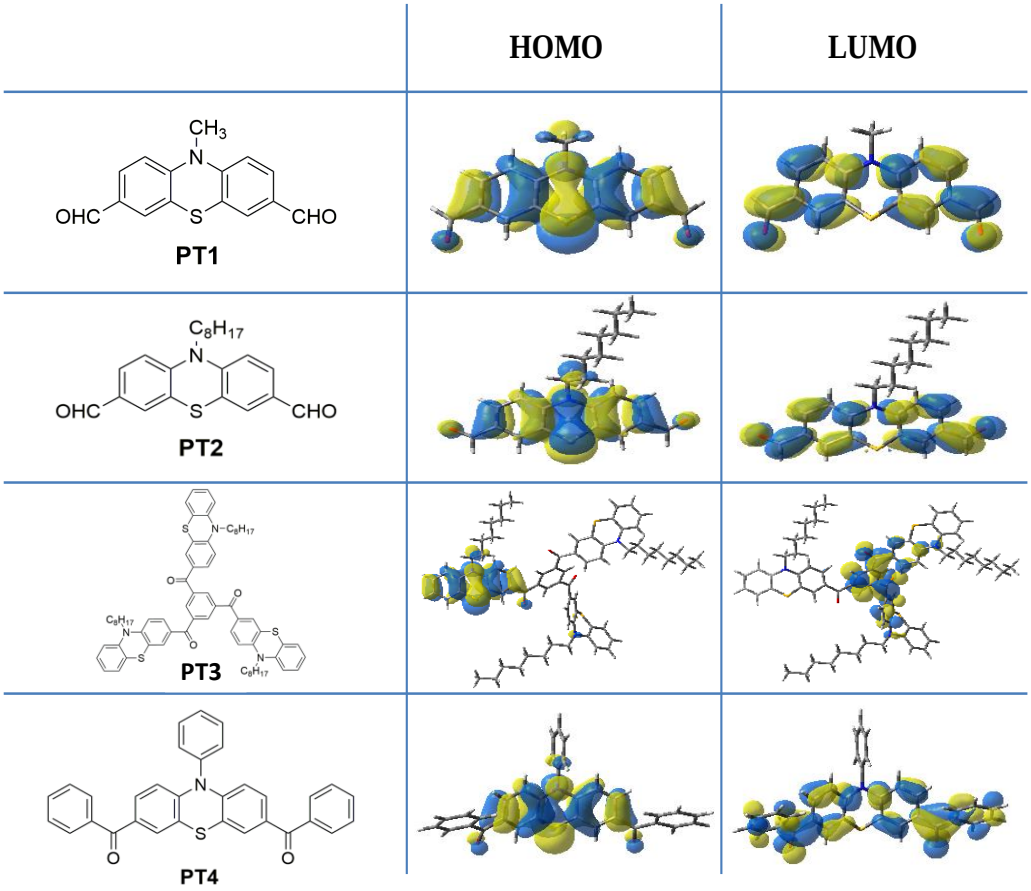

Figure 2. Contour plots of the frontier orbitals (HOMO/LUMO) for PTs; structures optimized at the B3LYP/6-31G* level of theory.

3.3. Free radical photopolymerization (FRP) of acrylates (TMPTA or Ebecryl 40):

The photopolymerization profiles of the acrylate functions are reported in Figure 3 for the benchmark monomers and the final reactive function conversions (FC) are gathered in the Table 2. Different systems including PT/Iod/NPG or PT/Iod/EDB were studied. No polymerization occurs using PT alone. The different additives alone were tested before studying the effect of phenothiazine. In fact, the Iod/EDB system cannot initiate the FRP of acrylates upon exposure to LED at 405 nm (Figures 3A,3B and 3C). However, the Iod/NPG (1%/1% w/w) couples shows a rather good efficiency for the FRP of Ebecryl 40 in thin and

thick samples upon exposure to LED at 405 nm (FC= 81% curve 14 in Figure 3B for the thick samples, and FC= 32% curve 14 in Figure 3C for the thin samples) but also for the FRP of TMPTA (FC= 48% curve 14 in Figure 3A). This result is probably due to a charge transfer complex formation CTC between Iod and NPG [31], and will be discussed in the chemical mechanism part. However, in all cases, much better polymerization rates are obtained in the presence of PT derivatives than without (curves 5-8 vs. curve 13 (Iod/EDB) and curve 14 (Iod/NPG) in Figure 3A, B and C). This clearly shows the crucial role of phenothiazine derivative to improve the polymerization initiating ability.

For the two-component systems, PT1/Iod (0.1%/1% w/w) system is the most efficient one for the FRP of Ebecryl 40 or TMPTA (thickness= 1.4 mm, curve 4 in Figure 3B and 3A, respectively). While, PT2/Iod is the most efficient one for the FRP of Ebecryl 40 in thin samples (curve 1 in Figure 3C). This is in agreement with the very fast photolysis of these derivatives in the presence of Iod. The structure/ reactivity /efficiency relationships will be discussed in the chemical mechanism part.

On the other hand, the PT/EDB (0.1%/1% w/w) system shows an absence of polymerization except for PT1 which has a poor performance in terms of polymerization rate. These results can be ascribed to the weak interaction between PT and EDB.

Remarkably, very high performances were obtained with the introduction of the iodonium salt into the PT/EDB system which shows the huge role of the three-component systems (PT/amine/Iod) to reach good polymerization efficiencies e.g. FC = 62% for the PT1/EDB (0.1%/1% w/w) system after 400s of irradiation and 72% for the PT1/Iod/EDB (0.1%/1%/1% w/w/w) system after 150s of irradiation.

Compared to the well-established benzophenone/EDB system (Figure 3D), both the PT/Iod and PT/Iod/amine systems exhibit much higher polymerization rates and final conversions (Figure 3). For the benchmark 2-isopropylthioxanthone/Iod initiating system (0.1/1% wt), a final acrylate conversion of 55% is obtained vs. 62-71% for PT/Iod (Table 2) showing again the interest of the proposed PT/Iod initiating systems.

The ability of the different PT/Iod systems to initiate the FRP in laminate (thickness=25 μm) under exposure to LED at 405nm, follows the order: PT1 > PT2 > PT4 > PT3. These initiating abilities can be governed by different parameters such as their absorption properties,

the photolysis behavior, free-energy change for the electron transfer reaction (ΔG_{et}) and the electron transfer quantum yields. This point will be discussed below.

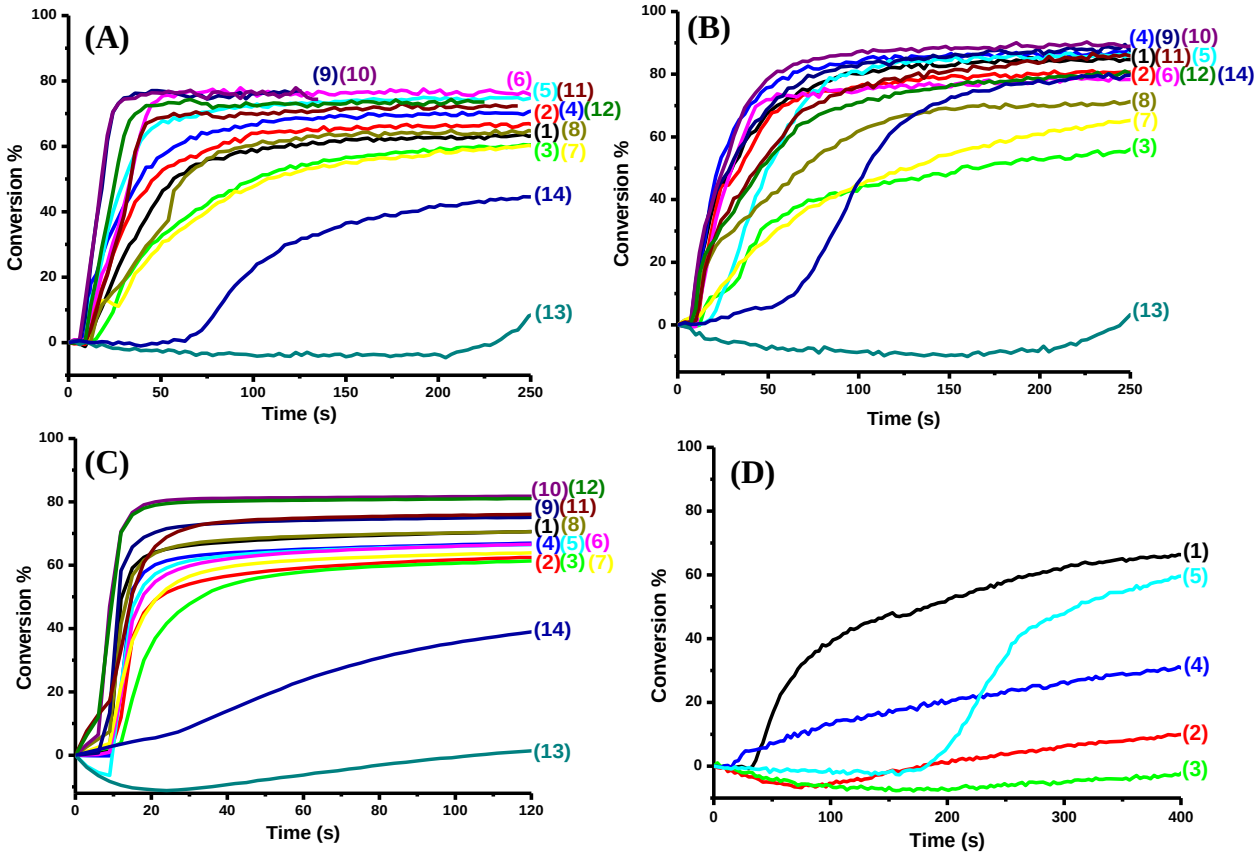

Figure 3. Polymerization profiles (Acrylate function conversion vs. irradiation time) for **(A)** TMPTA (thickness = 1.4 mm), **(B)** Ebecryl 40 (thickness = 1.4 mm), **(C)** Ebecryl 40 (thickness = 25µm) upon exposure to the LED @405 nm in the presence of the two or three photoinitiating systems: (1) PT2/Iod (0.1%/1% w/w), (2) PT4/Iod (0.1%/1% w/w), (3) PT3/Iod (0.1%/1% w/w), (4) PT1/Iod (0.1%/1% w/w), (5) PT2/Iod/EDB (0.1%/1%/1% w/w/w), (6) PT4/Iod/EDB (0.1%/1%/1% w/w/w),(7) PT3/Iod/EDB (0.1%/1%/1% w/w/w), (8) PT1/Iod/EDB (0.1%/1%/1% w/w/w), (9) PT2/Iod/NPG (0.1%/1%/1% w/w/w), (10) PT4/Iod/NPG(0.1%/1%/1% w/w/w), (11) PT3/Iod/NPG (0.1%/1%/1% w/w/w), (12) PT1/Iod/NPG (0.1%/1% /1% w/w/w), (13) Iod/EDB (1%/1% w/w), (14) Iod/NPG (1%/1% w/w). Irradiation starts at t=10s. **(D)** Polymerization profiles (Acrylate function conversion vs. irradiation time) for a Ebecryl 40 resin (thickness =1.4 mm) upon exposure to the LED @405nm in the presence of the two-photoinitiating systems: (1) PT2/EDB (0.1%/1% w/w), (2) PT4/EDB (0.1%/1% w/w), (3) PT3/EDB (0.1%/1% w/w), (4) PT1/EDB (0.1%/1% w/w), (5) Benzophenone/EDB (0.1%/1% w/w).

Table 2. Final Acrylate function conversion (FC) for TMPTA and Ebecryl 40 using different photoinitiating systems after 400 s of irradiation with the LED @405 nm (Thickness= 1.4mm).

TMPTA							
Two-component photoinitiating system PT/Iod (0.1%/1% w/w) and PT/Iod (0.2%/1% w/w)				**Three-component photoinitiating system PT/Iod/EDB and PT/Iod/NPG (0.1%/1%/1% w/w/w)**			
PT1/ Iod	PT2/Iod	PT3/Iod	PT4/Iod	PT1/Iod/amine	PT2/Iod/amine	PT3/Iod/amine	PT4/Iod/amine
71 %[a] 54 %[b]	64 %[a] 68%[b]	62 %[a] 32 %[b]	67 %[a] 67%[b]	74 %[c] 65 %[d]	77 %[c] 75 %[d]	72 %[c] 61 %[d]	78 %[c] 76 %[d]
Ebecryl 40							
PT1/ Iod	PT2/Iod	PT3/Iod	PT4/Iod	PT1/Iod/amine	PT2/Iod/amine	PT3/Iod/amine	PT4/Iod/amine
87 %[a] 63 %[b]	85 %[a] 68 %[b]	63 %[a] 48 %[b]	81 %[a] 72 %[b]	81%[c] 73 %[d]	90 %[c] 87 %[d]	88 %[c] 71 %[d]	90 %[c] 81 %[d]
a: PT/Iod (0.1%/ 1% w/w)				**c: PT/Iod/NPG (0.1%/1%/1% w/w/w)**			
b: PT/Iod (0.2%/1% w/w)				**d: PT/Iod/EDB (0.1%/1%/1% w/w/w)**			

3.4. Cationic photopolymerisation (CP) of epoxides

The CP of epoxides (EPOX) was studied in thick (under air, thickness = 1.4 mm) and thin (under air, 25 μm) samples using the different PTs in the presence of iodonium salt (PT/Iod system) upon irradiation with LED at 405 nm. Interestingly, these systems (0.15%/2% w/w) lead to good polymerization efficiency i.e. both high final conversions and also good polymerization rates were obtained in thick samples (FC = 42%; 40% and 39% for PT2, PT4 and PT1, respectively), and in thin samples (FC = 50%; 47% for PT2 and PT3, respectively) (Figure 4).

For these irradiation conditions, when using Iod or PT alone, no polymerization occurs, showing the key role of the PT/Iod systems when using LED@405 nm. A new peak ascribed to the polyether network can be easily observed at ~1080 cm^{-1} (Figure 4C). The efficiency for CP (i.e. for Rp) clearly follows the trend PT2> PT3> PT1> PT4. This behavior is not directly related to their respective light absorption properties because PT3 is less effective compared to PT2 but it has the highest extinction coefficient among the different PT. This may be due to their photochemical reactivity which also plays a very important role (see below in the chemical mechanisms part).

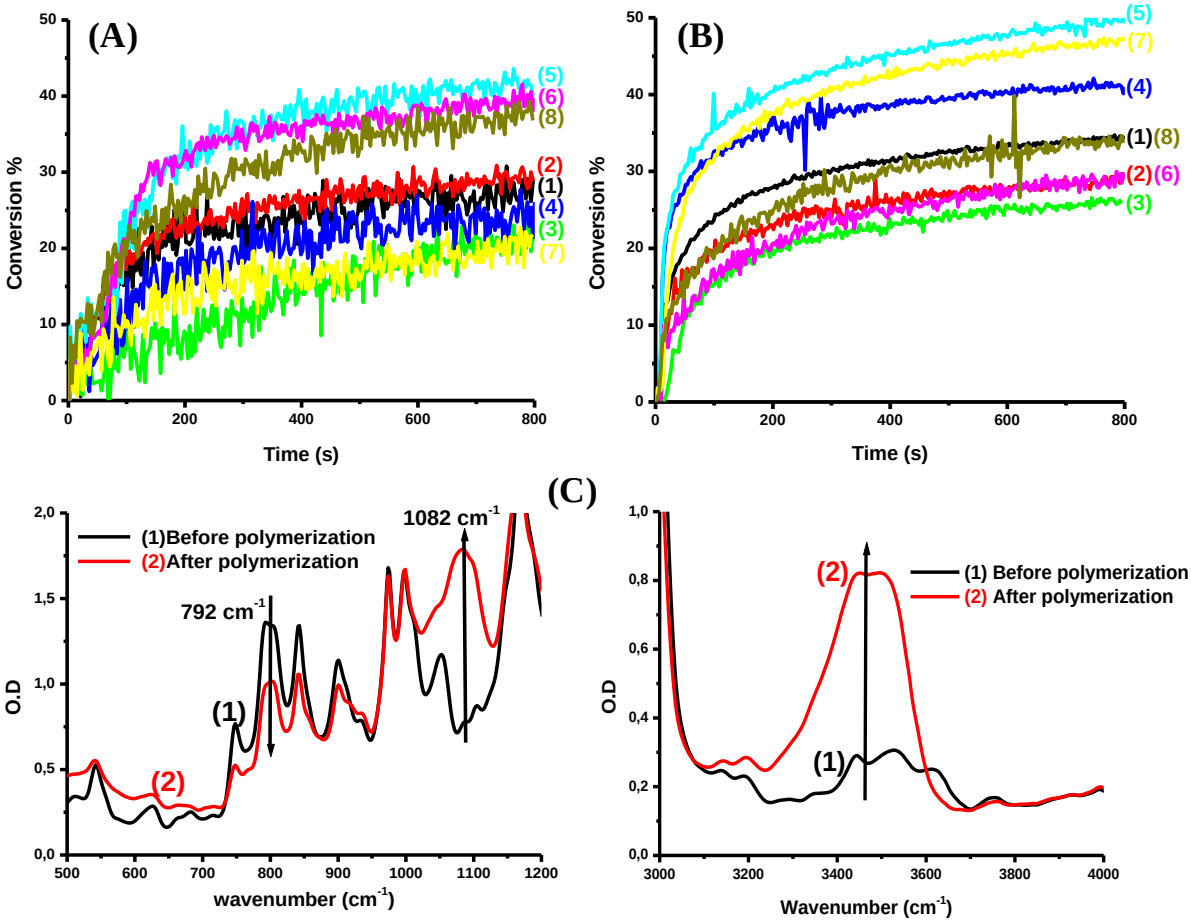

Figure 4. Polymerization profiles (Epoxy function conversion vs. irradiation time) for EPOX: **(A)** in thick sample (1.4 mm) and **(B)** thin sample upon exposure to the LED@405 nm in the presence of the two photoinitiating systems: (1) PT2/Iod (0.1%/1% w/w), (2) PT4/Iod (0.1%/1% w/w), (3) PT3/Iod (0.1%/1% w/w), (4) PT1/Iod (0.1%/1% w/w), (5) PT2/Iod (0.15%/2% w/w), (6) PT4/Iod (0.15%/2% w/w), (7) PT3/Iod (0.15%/2% w/w), (8) PT1/Iod (0.15%/2% w/w). Irradiation starts at t=10s. **(C)** IR spectra recorded before and after polymerization for PT2/Iod (0.15%/2% w/w) in EPOX

3.5. 3D printing experiments using PT/Iod or PT/Iod/amine systems

3D printing experiments were done in the presence of the PT/Iod/amine systems in Ebecryl 40 (Figure 5). Indeed, the high photosensitivity of these resins (see above) allows an efficient polymerization process in the irradiated area. Thick polymer samples were obtained in a short writing time (~2 min). Representative 3D patterns have been characterized by numerical optical microscopy (Figure 5). The spatial resolution is excellent (only limited by the size of the laser diode beam: spot of 50 µm). The thickness for one printed layer (900 µm in Figure 5A to 1.2mm in Figure 5C) is very high for 3D printing with this high spatial resolution.

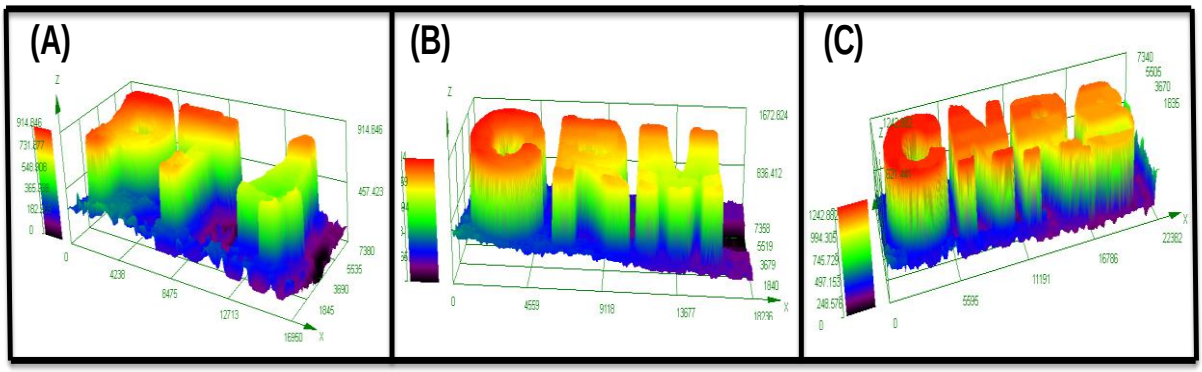

Figure 5. Characterization of the 3D patterns by numerical optical microscopy; **(A)** PT4/Iod (0.04%/0.4% w/w) in Ebecryl40; **(B)** PT1/Iod/amine (4-*N*,*N*-trimethylaniline) (0.04%/0.4%/0.11% w/w) in Ebecryl 40 and **(C)** PT2/Iod (0.04%/0.4% w/w) in Ebecryl 40.

3.6. Photocomposites preparation using the LED conveyor

Nowadays, photopolymerization of composites is used for different applications such as the curing of dental cements [32-33] or others [34-35]. The principal shortcoming of the photopolymerization process applied to composite formulations is the limited light penetration strongly reducing the potential depth of cure. However, the main advantages of composites are their high strength and relatively low weight. Therefore, efficient accesses to curing in depth are highly desired and new PISs are urgently required for such an application.

In this work, the glass fibers were impregnated with an organic resin in the presence of PIS (Ebecryl 40 or TMPTA) (50% glass fibers/50% resin; thickness of the composite = 2 mm) and were irradiated with a LED conveyor. Remarkably, only one pass need to be used to completely cure the composite in the presence of the PT/Iod/amine (amine=NPG) (0.1%/1%/1% w/w/w) systems (both the surface and the bottom are tack-free). The results are summarized in the Figure 6. This shows that the PT/Iod/amine (0.1%/1%/1% w/w/w) three-component systems can be used for curing composites upon near-UV light.

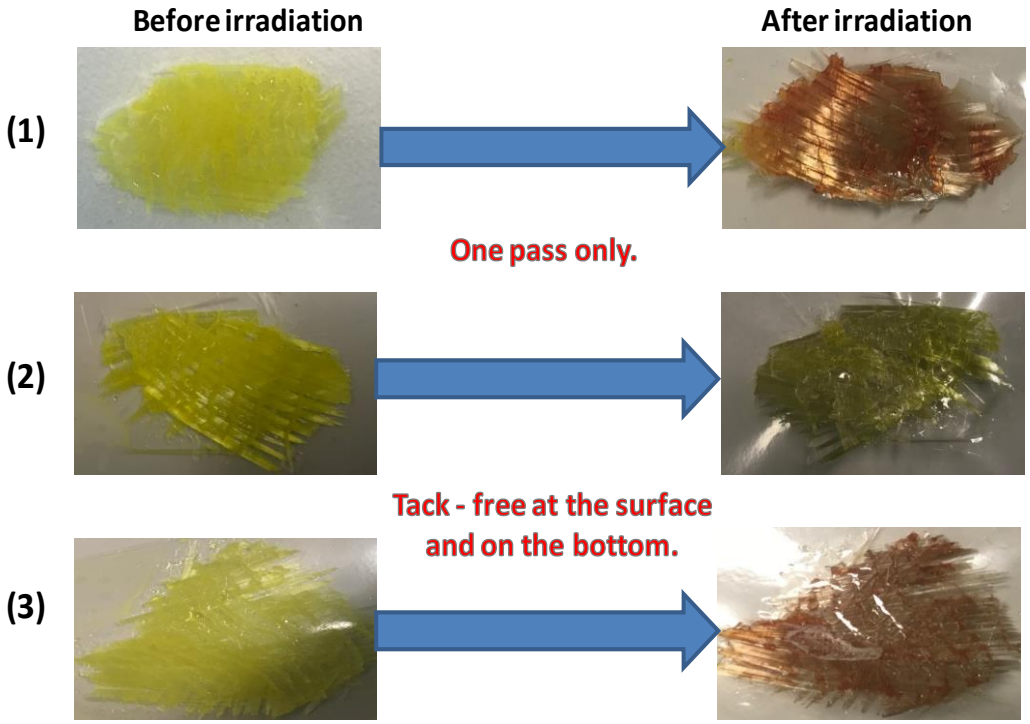

Figure 6. Photocomposites produced upon exposure to near-UV light (LED@395 nm), belt speed = 2 m/min, using free radical polymerization (FRP) in the presence of glass fibers/acrylate resin for different systems: **(1)** PT2/Iod/NPG (0.1%/1%/1% w/w/w); **(2)** PT4/Iod/NPG (0.1%/1%/1% w/w/w); and **(3)** PT2/Iod/NPG (0.1%/1%/1%) in TMPTA.

4. Discussion

To discuss the polymerization results obtained above, the chemical mechanisms must be established for a better understanding of the PT structure/reactivity/efficiency relationship.

4.1. Steady state photolysis

Different steady state photolysis experiments for the investigated PTs are shown in the Figure 7. Photolysis of the PT1/Iod system in chloroform upon irradiation with a LED @375nm is faster than for PT1 alone which is very photostable (Figure 7B vs. 7A, respectively) i.e. a strong interaction between PT1 and Iod clearly occurs. The same behaviour is observed with the other PTs. A new photoproduct (characterized by a significant new absorption between 300 and 390nm) is formed due to this PT1/Iod interaction. In the presence of both EDB and Iod, the photolysis of PT is slower than with Iod. Indeed, the percentage of consumption of the PT is depicted in Figure 7D where this percentage is measured as a function of the irradiation time in the presence of Iod, Iod/EDB or even for PT alone.

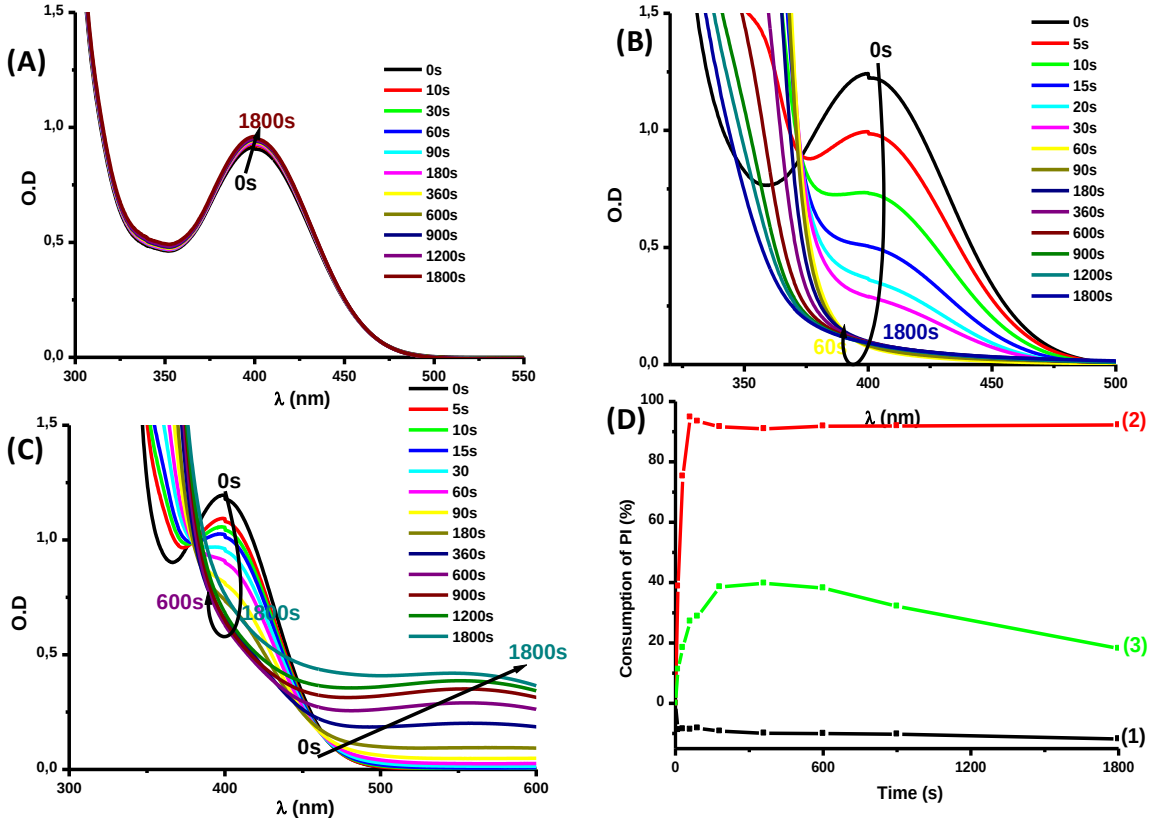

Figure 7. (A): Photolysis of PT1 in the absence of Iod; **(B):** PT1/Iod photolysis; and **(C):** PT1/Iod/EDB photolysis. **(D)** Consumption of PT1: **(1)** without Iod, **(2)** with Iod (10^{-2} M) and **(3)** with Iod and EDB (10^{-2} M) vs. irradiation time – upon exposure to the LED @375 nm in Chloroform**.**

4.2. Fluorescence quenching and Cyclic Voltammetry

Fluorescence and fluorescence quenching experiments were carried out for the different PTs in chloroform (See Figure 8A). The crossing point of the absorption and fluorescence spectra allows the evaluation of the first singlet excited state energy levels (E_{S1}) (e.g. for PT1: ~2.61 eV; Table 3, Figure 8B). In addition, an efficient fluorescence quenching of PT1 by Iod was observed with high value of the Stern-Volmer coefficient (Ksv) (for PT1/Iod interaction Ksv = 111.8 M^{-1}, Figure 8C). Therefore, very high electron transfer quantum yields from the excited singlet state ϕ_{S1} (e.g. ϕ_{etS1} = 0.70 for PT1/Iod) were calculated from the equation (eq. 2) (Table 3):

$$\phi_{et\,S1} = K_{SV}[Iod] / (1+K_{SV}[Iod]) \qquad \text{eq. 2}$$

The free energy changes (ΔGet) for the electron transfer reaction between PTs (as electron donors) and Iod (an electron acceptor) were calculated from eq.1 using the oxidation potentials E_{ox} (Figure 8D, Table 3) and the excited state energies (E_{S1}) of PTs. In full

agreement with the high Ksv determined above, these processes from S_1 are found favorable ($\Delta Get < 0$) e.g. PT1 with Iod ΔG_{etS1} = - 1.58 eV and PT4 with Iod ΔG_{etS1}= -1.57 eV (Table 3).

In contrast, no quenching was observed for PT/EDB interaction. These results are in full agreement with the photopolymerization results which show a much better initiating performance for the PT/Iod vs. the PT/EDB initiating systems. It should be noted that the PT/Iod interaction corresponds to a photo-oxidation process for the phenothiazine derivatives.

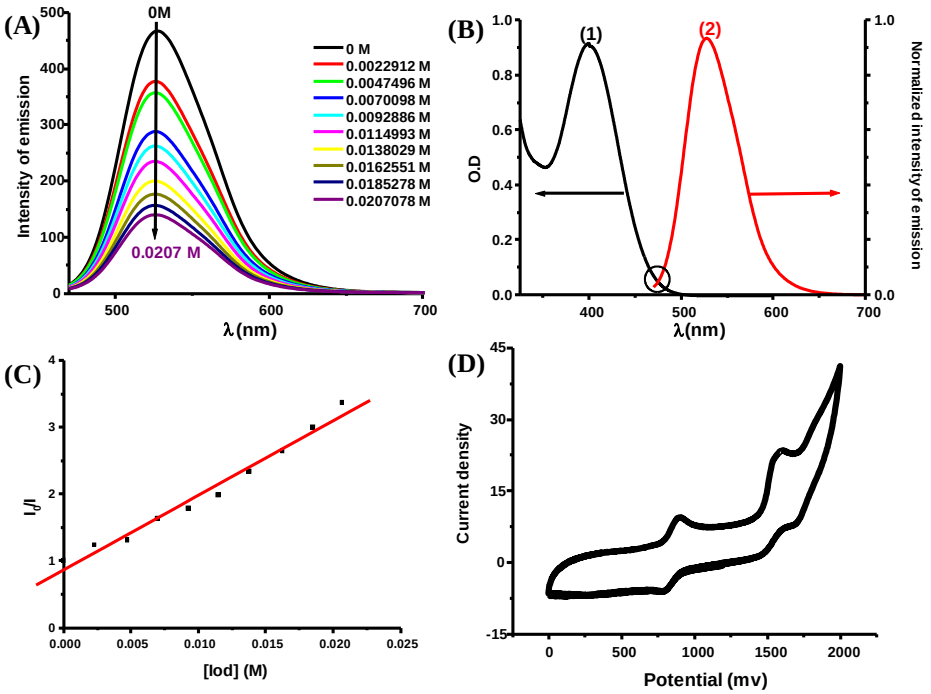

Figure 8. (A) Fluorescence quenching of PT1 by Iod, **(B)** singlet state determination in chloroform for PT1, **(C)** Stern-Volmer treatment for the PT1/Iod fluorescence quenching, **(D)** cyclic voltammetry for PT1 oxidation.

Table 3. Parameters characterizing the photochemical mechanisms associated with ^{1}Phenothiazine/Iod in chloroform.

	E_{ox} (V/SCE)	E_{S1} (eV)	ΔG_{S1} (eV)	K_{SV} (PT/Iod)	Φ_{et} (PT/Iod)
PT1	0.78	2.58	-1.6	250	0.8
PT2	0.75	2.52	-1.57	114	0.7
PT3	0.77	2.45	-1.48	5.7	0.25
PT4	0.83	2.61	-1.58	112	0.7

Based on these results, a global mechanism is proposed (r1-r8) (according to other dyes in dye/Iod/amine systems [6]) showing the formation of the reactive species for CP and FRP (^{1,3}PT stands for the singlet and triplet excited states of PT). A charge transfer complex CTC can be formed between the amine (electron donor) and Iod (electron acceptor), this complex leads to the formation of Ar$^{\bullet}$ (r3 and r4). r7 and r8 are proposed for the three-component systems regenerating the PT in agreement with a lower consumption of the PT for these three-component systems. This regeneration of PT suggests a partial photoredox catalysts behaviour. Overall, $NPG_{(-H,-CO2)}^{\bullet}$, Ar$^{\bullet}$ and $NPG_{(-H,\ -CO2)}^{+}$, $PT^{\bullet+}$ are the responsible species for FRP and CP, respectively.

$$PT \rightarrow {}^{1,3}PT^{*} \quad (h\nu) \qquad \text{r1}$$

$$^{1,3}PT^{*} + ArI^{+} \rightarrow Ar^{\bullet} + ArI + PT^{\bullet+} \qquad \text{r2}$$

$$NPG + Iod \rightarrow [NPG\text{-}Iod]_{CTC} \qquad \text{r3}$$

$$[NPG\text{-}Iod]_{CTC} \rightarrow Ar^{\bullet} \qquad \text{r4}$$

$$^{1,3}PT + NPG \rightarrow PT\text{-}H^{\bullet} + NPG_{(-H)}^{\bullet} \qquad \text{r5}$$

$$NPG_{(-H)}^{\bullet} \rightarrow NPG_{(-H;-CO2)}^{\bullet} + CO_2 \qquad \text{r6}$$

$$NPG_{(-H;-CO2)}^{\bullet} + Ar_2I^{+} \rightarrow NPG_{(-H;-CO2)}^{+} + Ar^{\bullet} + ArI \qquad \text{r7}$$

$$PT\text{-}H^{\bullet} + Ar_2I^{+} \rightarrow \text{Phenothiazine} + H^{+} + ArI + Ar^{\bullet} \qquad \text{r8}$$

4.3. Phenothiazine derivatives as photoredox catalysts in three-component systems

Interestingly, a photoredox catalyst behavior was observed, where a high performance of the FRP of TMPTA in thick or thin sample is shown, when an amine was introduced in the formulation in order to regenerate the phenothiazine derivative (r5, r8). The effect of EDB is clearly manifested by an increase of the final conversion for all phenothiazine-based systems. (75% for PT2/Iod/EDB (0.1%/1%/1% w/w/w) compared to 64.5% for PT2/Iod (0.1%/1% w/w), and 76% for PT4/Iod/EDB (0.1%/1%/1% w/w/w) compared to 67% PT4/Iod (0.1%/1% w/w). This photoredox catalyst behaviour for PT derivatives is also in agreement with a lower consumption of PT in the three-component system vs. the two-component ones (Figure 7D, curve 3 vs. curve 2) showing a regeneration through r8.

5. Conclusion:

In this article, four in-silico developed phenothiazine derivatives showed very high performance in FRP and CP upon irradiation with LED at 405 nm. Indeed, three of these phenothiazines have been classified as photoredox catalysts (they can be – at least – partly regenerated in three-component systems). These derivatives are very powerful for 3D printing as well as for the synthesis of photocomposites. In the future, it is important to develop new phenothiazine derivatives by shifting their absorption spectra towards the NIR region for a greater absorption for thick samples and consequently higher conversion rates.

References

[1] Zivic, N.; Bouzrati-Zerelli, M.; Kermagoret, A.; Dumur, F.; Fouassier, J.P.; Gigmes, D.; Lalevee. J. A novel naphthalimide scaffold based iodonium salt as a one-component photoacid/photoinitiator for cationic and radical polymerization under LED exposure Polym.Chem., **2016**, 7, 5873.

[2] Schmitt, M. Method to analyse energy and intensity dependent photo-curing of acrylic esters in bulk RSC Adv., **2015**, 5, 67284.

[3] Schmitt, M.; Lalevée, J. ZnO nanoparticles as polymerisation photo-initiator: Levulinic acid/NaOH content variation Colloids Surf., A, **2017**, 532, 189-194.

[4] Dietlin, C.; Schweizer, S.; Xiao, P.; Zhang, J.; Morlet-Savary, F.; Graff, B.; Fouassier, J.P.; Lalevée, J. Photopolymerization upon LEDs: New photoinitiating systems and strategies. Polym. Chem. **2015**, 6, 3895.

[5] Crivello, J.V. Photoinitiators for Free Radical, Cationic; Anionic Photopolymerization, John Wiley & Sons, Chichester, 2nd edn, **1998**.

[6] Fouassier, J.P.; Lalevée, J. Photoinitiators for Polymer Synthesis-Scope, Reactivity, and Efficiency, Wiley-VCHVerlag GmbH & Co. KGaA, Weinheim, **2012**.

[7] Neshchadin, D.; Rosspeintner, A.; Griesser, M.; Lang, B.; Mosquera-Vazquez, S.; Vauthey, E.; Gorelik, V.; Liska, R.; Hametner, C.; Ganster, B.; Saf, R.; Moszner, N.; Gescheidt, G. Acylgermanes : Photoinitiators and Sources for Ge-Centered Radicals. Insights into their Reactivity J.Am.Chem.Soc., **2013**, 135, 17314–17321.

[8] Kara, M.; Dadashi-Silab, S.; Yagci, Y. Phenacyl Ethyl Carbazolium as a Long Wavelength Photoinitiator for Free Radical Polymerization. Macromol.Rapid.Commun., **2015**, 36, 2070.

[9] Yagci, Y.; Jockusch, S.; Turro, N.J. Photoinitiated Polymerization: Advances, Challenges, and Opportunities. Macromolecules, **2010**, 43, 6245.

[10] Wang, J.; Stanic, S.; Altun, A.A.; Schwentenwein, M.; Dietliker, K.; Jin, L.; Stampfl, J.; Baudis, S.; Liska R.; Grützmacher, H. A highly efficient waterborne photoinitiator for visible-light-induced three-dimensional printing of hydrogels Chem.Commun., **2018**, 54, 920.

[11] Eren, T.N.; Graff, B.; Lalevee J.; Avci, D. Thioxanthone-functionalized 1,6-heptadiene as monomeric photoinitiator. Prog.Org.Coat., **2019**, 128, 148.

[12] Radebner, J.; Eibel, A.; Leypold, M.; Jungwirth, N.; Pickl, T.; Torvisco, A.; Fischer, R.; Fischer, U.K.; Moszner, N.; Gescheidt, G.; Stueger, H.; Haas, M. Tetraacylstannanes as Long-Wavelength Visible-Light Photoinitiators with Intriguing Low Toxicity. Chem.Eur.J., **2018**, 24, 8281.

[13] Jaouen, G.; Top, S.; Vessieres, A.; Leclercq, G.; McGlinchey, M.J. The First Organometallic Selective Estrogen Receptor Modulators (SERMs) and Their Relevance to Breast Cancer. Curr.Med.Chem., **2004**, 11, 2505.

[14] Pluta, K.; Morak-Mlodawska, B.; Jelen, M. Recent progress in biological activities of synthesized phenothiazines. Eur.J.Med.Chem., **2011**, 46, 3179.

[15] Albery, W.J.; Foulds, A.W.; Hall, K.J.; Hillman, A.R.; Edgell, R.G.; and Orchard, A.F. Thionine coated electrode for photogalvanic cells. Nature, **1979**, 282, 793.

[16] Okazaki, M.; Takeda, Y.; Data, P.; Pander, P.; Higginbotham, H.; Monkman, P.; Minakata, S. Thermally activated delayed fluorescent phenothiazine–dibenzo[a,j]phenazine–phenothiazine triads exhibiting tricolor-changing mechanochromic luminescence. Chem.Sci., **2017**, 8, 2677.

[17] Zhang, Z.Q.; Wu, Z.; Sun, J.B.; Yao, B.Q.; Zhang, G.H.; Xueand, P.C.; Lu, R. Mechanofluorochromic properties of β-iminoenolate boron complexes tuned by the electronic effects of terminal phenothiazine and phenothiazine-S,S-dioxide. J.Mater.Chem.C, **2015**, 3, 4921.

[18] Gomurashvili, Z.; Crivello, J.V. Monomeric and Polymeric Phenothiazine Photosensitizers for Photoinitiated Cationic Polymerization. Macromolecules, **2002**, 35, 2962.

[19] Chao, P.; Gu, R.; Ma, X.; Wang, T.; Zhao, Y. Thiophene-substituted phenothiazine-based photosensitisers for radical and cationic photopolymerization reactions under visible laser beams (405 and 455 nm). Polym.Chem., **2016**, 7, 5147.

[20] Abdallah, M.; Bui, T.T.; Goubard, F.; Theodosopoulou, D.; Dumur, F.; Hijazi, A.; Fouassier, J.P.; Lalevée. J. Phenothiazine derivatives as photoredox catalysts for cationic and radical photosensitive resins for 3D printing technology and photocomposite synthesis. Polym.Chem., **2019**, 10, 6145.

[21] Treat, N.J.; Sprafke, H.; Kramer, J.W.; Clark, P.G.; Barton, B.E.; Read De Alaniz, J.; Fors, B.P.; Hawker, C.J. Metal-Free Atom Transfer Radical Polymerization. J.Am.Chem.Soc., **2014**, 136, 16096.

[22] Marin, L.; Bejan, A.; Ailincai, D.; Belei, D. Poly(azomethine-phenothiazine)s with efficient emission in solid state. Eur.Polym.J., **2017**, 95, 127.

[23] Al Mousawi, A.; Kermagoret, A.; Versace, D.L.; Toufaily, J.; Hamieh, T.; Graff, B.; Dumur, F.; Gigmes, D.; Fouassier, J.P.; Lalevee, J. Copper photoredox catalysts for polymerization upon near UV or visible light : structure/reactivity/efficiency relationships and use in LED projector 3D printing resins. Polym. Chem., **2016**, 8, 568.

[24] Al Mousawi, A.; Dietlin, C.; Graff, B.; Morlet-Savary, F.; Toufaily, J.; Hamieh, T.; Fouassier, J.P.; Chachaj-Brekiesz, A.; Ortyl J.; Lalevee, J. Meta-Terphenyl Derivative/Iodonium Salt/9H-Carbazole-9-ethanol Photoinitiating Systems for Free Radical Promoted Cationic Polymerization upon Visible Lights. Macromol.Chem.Phys., **2016**, 217, 1955.

[25] Rehm, D.; Weller, A. Kinetics of Fluorescence Quenching by Electron and H-Atom Transfer. Isr. J. Chem. **1970**, 8, 259.

[26] Fouassier, J.P. Photoinitiator, Photopolymerization and Photocuring : Fundamentals and Applications, Hanser Publishers, Munich, **1995**.

[27] Foresman J.B.; Frisch, A. Exploring Chemistry with Electronic Structure Methods, Gaussian Inc., Pittsburgh, PA, 2nd edn, **1996**.

[28] Frisch, M.J.; Trucks, G.W.; Schlegel, H.B.; Scuseria, G.E.; Robb, M.A.; Cheeseman, J.R.; Zakrzewski, V.G.; Montgomery, J.A.; Stratmann, J.R.E.; Burant, J.C.; Dapprich, S.; Millam, J.M.; Daniels, A.D.; Kudin, K.N.; Strain, M.C.; Farkas, O.; Tomasi, J.; Barone, V.; Cossi, M.; Cammi, R.; Mennucci, B.; Pomelli, C.; Adamo, C.; Clifford, S.; Ochterski, J.; Petersson, G.A.; Ayala, P.Y.; Cui, Q.; Morokuma, K.; Salvador, P.; Dannenberg, J.J.; Malick, D.K.; Rabuck, A.D.; Raghavachari, K.; Foresman, J.B.; Cioslowski, J.; Ortiz, J.V.; Baboul, A.G.; Stefanov, B.B.; Liu, G.; Liashenko, A.; Piskorz, P.; Komaromi, I.; Gomperts, R.; Martin, R.L.; Fox, D.J.; Keith, T.; Al-Laham, M.A.; Peng, C.Y.; Nanayakkara, A.; Challacombe, M.; Gill, P.M.W.; Johnson, B.; Chen, W.; Wong, W.M.; Andres, J.L.;

Gonzalez, C.; Head-Gordon, M.; Replogle E.S.; Pople, J.A. Gaussian 03, Revision B-2, Gaussian Inc., Pittsburgh, PA, **2003**.

[29] Zhang, J.; Dumur, F.; Xiao, P.; Graff, B.; Bardelang, D.; Gigmes, D.; Fouassier, J.P.; Lalevee, J. Structure Design of Naphthalimide Derivatives: Toward Versatile Photoinitiators for Near-UV/Visible LEDs, 3D Printing, and Water-Soluble Photoinitiating Systems. Macromolecules, **2015**, 48, 2054.

[30] Xiao, P.; Dumur, F.; Zhang, J.; Fouassier, J.P.; Gigmes, D.; Lalevee, J. Copper Complexes in Radical Photoinitiating Systems : Applications to Free Radical and Cationic Polymerization upon Visible LEDs. Macromolecules, **2014**, 47, 3837.

[31] Garra, P.; Graff, B.; Morlet-Savary, F.; Dietlin, C.; Becht, J.M.; Fouassier, J.P.; Lalevée, J. Charge Transfer Complexes as Pan-Scaled Photoinitiating Systems : From 50 μm 3D Printed Polymers at 405 nm to Extremely Deep Photopolymerization (31 cm). Macromolecules, **2018**, 51,57.

[32] Bayou, S.; Mouzali, M.; Aloui, F.; Lecamp, L.; Lebaudy, P. Simulation of conversion profiles inside a thick dental material photopolymerized in the presence of nanofillers. Polymer, **2013**, 45, 863.

[33] Vreven, J.; Raskin, A.; Sabbagh, J.; Vermeersch, G.; Leloup, G. Résines composites EMC, Odontologie, **2005**.

[34] Kardar, P.; Ebrahimi, M.; Bastani, S. Influence of temperature and light intensity on the photocuring process and kinetics parameters of a pigmented UV curable system. J.Therm.Anal.Calorim., **2014**, 118, 541.

[35] Kardar, P.; Ebrahimi, M.; Bastani, S. Curing behaviour and mechanical properties of pigmented UV-curable epoxy acrylate coatings. Pigm.Resin.Technol., **2014**, 43, 177.

Chapitre II : Dérivés de Naphthalimide en tant que PA sous lumière visible pour la polymérisation radicalaire, la synthèse des Réseaux Polymères Interpénétrés (IPN) et la préparation des hydrogels.

L'application actuelle de la polymérisation amorcée par voie photochimique dans les domaines classiques tels que les adhésifs, les peintures pigmentées, l'impression 3D, la synthèse des photocomposites et bien d'autres domaines exige le développement de nouveaux systèmes photoamorceurs sensibles à la lumière visible. Cette technologie de radiations fournit plusieurs avantages à savoir la rapidité, l'exigence de basse énergie, l'absence de solvant. En fait, les composés hétérocycliques fluorescents ont trouvé leur intérêt dans des applications intéressantes tels que : les dispositifs électroluminescents [1], les matériaux conducteurs [2], et dans le domaine de photopolymérisation car ils offrent des rendements quantiques élevés et servent comme photoamorceurs dans le domaine du séchage des acrylates.

Dans ce contexte, notre recherche s'est orientée vers les dérivés de Naphthalimide : composés hétérocycliques organiques portant une fonction phthalimide liée à un groupement aromatique. Cette conformation implique un transfert de charge intramoléculaire aboutissant ainsi à des propriétés d'absorptions élevées dans le proche UV et visible. Ces colorants sont également caractérisés par des longues durées de vie de leur état excité singulet assurant des processus de désactivation très efficaces. Dans ce travail, six colorants à base de dérivés de Naphthalimide ayant de bonnes capacités d'absorption dans le visible ont été évalués comme photoamorceurs de la polymérisation radicalaire et la polymérisation hybride sous irradiation visible. Ces molécules diffèrent par la nature de substituant apporté au noyau naphthalimide, qui entraine une forte modification des propriétés photophysique/photochimique et électrochimique. Les colorants examinés ont montré des potentiels d'oxydation favorisant les réactions de transfert d'électron, d'où une forte interaction avec l'additif (Iod). Cette interaction par photo-oxydation assure un photoblanchiment lors de la photolyse de la

solution contenant le système Napht/Iod, et une accélération du déclin de fluorescence (Quenching) favorisant ainsi la formation des espèces réactives responsable du processus de polymérisation.

Il est à souligner qu'une bonne capacité de photoamorcage exige une synergie bicomposante ou tricomposante de ces colorants avec un additif (Iod) ou un co-amorceur. De ce fait, différentes combinaisons peuvent être à la base des systèmes photoamorceurs efficaces : Napht/Iod, Napht/Iod/amine (NPG, TMA…). En effet, de très hautes conversions finales en fonctions réactives (acrylate et méthacrylate) et des vitesses de polymérisation rapides ont été obtenues pour les différentes combinaisons utilisées. La polymérisation hybride (acrylate/époxyde) a pu aussi être examinée, par conséquent, des profils de polymérisation plus performantes ont été atteints. Ce pouvoir de polymérisation a ouvert la voie à l'utilisation de ces dérivés dans des expériences d'écriture laser où des résolutions spatiales élevées et de grandes épaisseurs ont été obtenues, ces caractéristiques sont améliorées dans un système hybride. La synthèse des photocomposites par imprégnations des fibres de verre représente aussi une application intéressante de ce travail. Un de ces photoamorceurs avait la capacité de former des hydrogels par polymérisation dans l'eau. Ce travail a été publié dans 'ChemphotoChem' sous la citation suivante : Rahal, M.; Mokbel, H.; Graff, B.; Pertici, V.; Gigmes D.; Toufaily, J.; Hamieh, T.; Dumur, F.; Lalevee, J. Naphthalimide-Baed Dyes as Photoinitiators under Visible Light Irradiation and their applications: Photocomposites synthesis, 3D printing and polymerization in Water. ChemPhotoChem, **2021**, 5, 1.

Références

[1] Hunger, K. Industrial Dyes : Chemistry, Properties, Applications.WILEY-VCH Verlag, GmbH & Co. KGaA, Weinheim, Germany. 2003.

[2] Kalle, A.G. British Patent 1962, 895 (001).

Partie III : Nouveaux photoamorceurs à base de colorants pour la polymérisation radicalaire (FRP) et Cationique (CP)

New Naphthalimides as Photoinitiators under Visible Light Irradiation and their Application: Photocomposite Synthesis, 3D printing and Polymerization in Water.

Abstract

In this work, six new fluorescent dyes derived from the Naphthalimide scaffold (Napht1 - Napht6) were synthesized and used as high-performance photoinitiating systems (PISs) in two and three-component systems (combined with iodonium salt (Iod) and / or an electron donor amine (such as *N*-phenylglycine - NPG) for the radical photopolymerization of the acrylate and methacrylate monomers under visible light using a light-emitting diode at 405 nm. Markedly, these dyes were never synthesized before. In fact, these PISs showed high initiation efficiency with both a high final reactive function conversions and high polymerization rates. Interest of our study is to determine the effect of the different substituents (chromophoric group) on the naphthalimide function, concerning the efficiency of initiation of the free radical polymerization. In order to improve the mechanical properties of the obtained polymers, these derivatives were also tested for the photopolymerization of a blend of acrylate / epoxy monomers (TA/EPOX); these latter properties were characterized by traction tests. To demonstrate the initiation efficiency of these dyes, several methods and characterization techniques were used, including steady state photolysis, real-time Fourier transform infrared spectroscopy, emission spectroscopy as well as cyclic voltammetry. In our study, these naphthalimides were used for the synthesis of photocomposites (one and multiple layers of glass fibres) using a UV@395 nm (4W/cm^2) conveyor, as well as in the preparation of 3D printed polymers. Markedly, one of the naphthalimide (Napht-4) can be used as a new high-performance water soluble photoinitiator for photopolymerization in water and hydrogel synthesis.

Keywords: Naphthalimide, LED, 3D printing, Photocomposite, IPN, water soluble photoinitiator.

Partie III : Nouveaux photoamorceurs à base de colorants pour la polymérisation radicalaire (FRP) et Cationique (CP)

1. Introduction

Industrial technological developments during the last decades have been largely influenced by the ability to synthesize high performance materials that are essential for our daily life but also with the aim at developing environmentally friendly materials. Therefore, it was necessary to introduce light into the creation of these polymer-based materials in order to reduce the harmful effects of the other industrial synthesis processes. The term photopolymerization therefore designates the transformation of a liquid formulation into a solid material under irradiation [1,2], it is, therefore, a green technology since the reaction takes place at room temperature [3-8]. Photopolymers thus obtained are used in different fields such as coatings, dentistry, automotive, cosmetics, composites as well as 3D printing. Considering the harmfulness, the high energy consumption as well as the danger for the operator related to the use of UV lamps (e.g. Hg based), these irradiation setups are now more and more widely discarded in favor of light-emitting diodes (LEDs) [8-11], which can be inexpensive, durable, ecological, exhibit a low energy consumption and be safe for the operator.

The challenge is, therefore, to develop new molecules, whose absorption zones match the emission spectrum of visible LEDs (for example 405 nm LEDs) as well as to improve their photophysical and photochemical properties to act as high-performance photoinitiators (PI) for the FRP. Hence, the use of dyes based on Naphthalimide is investigated in this study. Indeed, these compounds are composed of an aromatic ring group connected to a phthalimide group and the electron delocalization resulting from the presence of the electron-withdrawing phthalimide group can give rise to an intramolecular charge transfer whose absorption band is located in the near UV or visible range (350-500 nm). These compounds are also characterized by high photoluminescence quantum yields so that these fluorescent organic compounds [12,13] were ideal candidates for bioimaging [14] or the development of tumor-targeting drug-delivery systems (as DNA targeting, as cytotoxic agents, anticancer agent and as potential markers for cancers) [15]. Different naphthalimide derivatives have also been reported in the literature as high-performance PI for FRP and cationic polymerization (CP) of acrylate and epoxy functions, respectively [16 -17]. Importance of using this type of molecule as PI is that they are easily modifiable by introducing chromophore groups onto the naphthalimide part [see ref.17]. As a result of this, absorption properties of these dyes can be easily modified as well as their photochemical and physical properties. This structural change

can drastically affect the photoinitiation ability of the FRP reaction and therefore the final monomer conversions as well as the shape of the photopolymerization profiles.[18-26]

In this paper, six naphthalimides (Napht; Scheme 1) never reported in the literature were tested as photoinitiators for the photopolymerization of acrylates. These dyes showed good polymerization profiles when used in two and three-component photoinitiating systems (Napht/Iod or Napht/Iod/NPG). To provide a clear mechanistic picture, different characterization techniques were used in this work: UV-visible absorption spectroscopy and photolysis, emission spectroscopy, Fourier transform Infrared spectroscopy and cyclic voltammetry. Some applications in composites synthesis as well as in 3D printing are provided to highlight their high performances. Markedly, Napht-4 was also water-soluble and this compound could also be used for photopolymerization in water and for hydrogel synthesis.

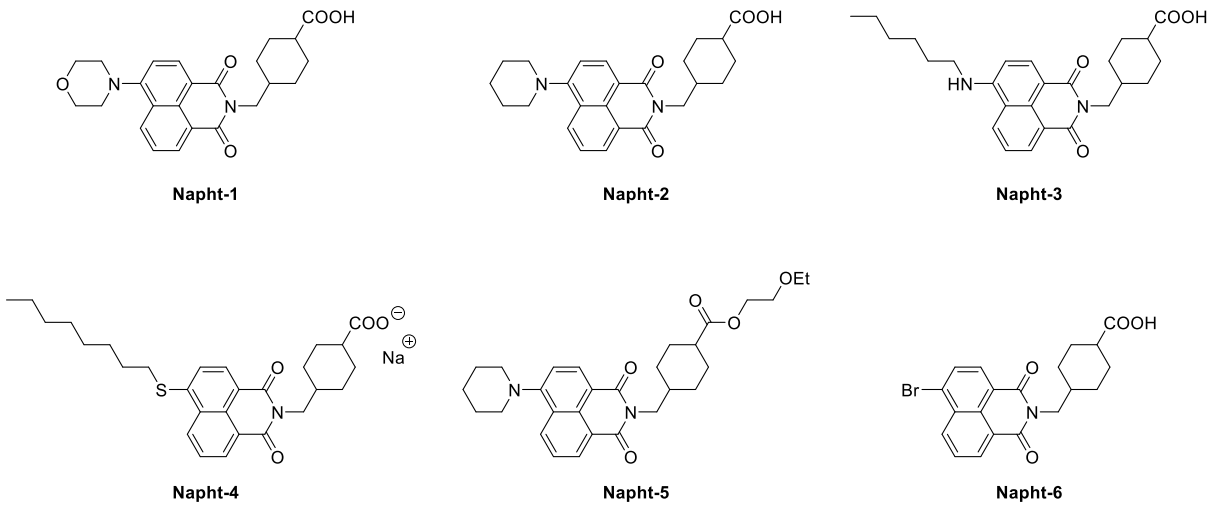

Scheme 1. New proposed Naphthalimides.

2. Experimental part

2.1. Synthesis of the Naphthalimides

All reagents and solvents were purchased from Aldrich or Alfa Aesar and used as received without further purification. Mass spectroscopy was performed by the Spectropole of Aix-Marseille University. ESI mass spectral analyses were recorded with a 3200 QTRAP (Applied Biosystems SCIEX) mass spectrometer. The HRMS mass spectral analysis was performed with a QStar Elite (Applied Biosystems SCIEX) mass spectrometer. Elemental analyses were

recorded with a Thermo Finnigan EA 1112 elemental analysis apparatus driven by the Eager 300 software. ^{1}H and ^{13}C NMR spectra were determined at room temperature in 5 mm o.d. tubes on a Bruker Avance 400 spectrometer of the Spectropole: ^{1}H (400 MHz) and ^{13}C (100 MHz). The ^{1}H chemical shifts were referenced to the solvent peaks DMSO (2.49 ppm), $CDCl_3$ (7.26 ppm) and the ^{13}C chemical shifts were referenced to the solvent peak DMSO (49.5 ppm), $CDCl_3$ (77.0 ppm). All photoinitiators were prepared with analytical purity up to accepted standards for new organic compounds (>98%) which was checked by high field NMR analysis.

Synthesis of 4-((6-morpholino-1,3-dioxo-1*H*-benzo[*de*]isoquinolin-2(3*H*)-yl)methyl)cyclohexane-1-carboxylic acid (Napht-1)

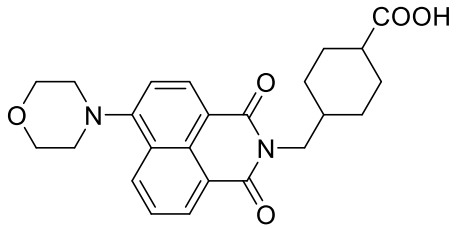

A mixture of 4-((6-bromo-1,3-dioxo-1*H*-benzo[*de*]isoquinolin-2(3*H*)-yl)methyl)cyclohexane-1-carboxylic acid (1.02 g, 2.45 mmol, M = 416.27 g.mol^{-1}) and morpholine (0.64 g, 0.64 mL, 7.34 mmol, 3 eq., M = 87.12 g.mol^{-1}, d = 1.007) in DMF (10 mL) was stirred at reflux for 16 h. After cooling to room temperature, the solvent was removed under reduced pressure using a rotary evaporator. The crude product was purified by column chromatography on silica gel (CH_2Cl_2/MeOH: 9/1) to provide an orange solid as the pure product (900 mg, 87 % yield). ^{1}H NMR ($CDCl_3$) δ : 8.55 (d, *J* = 7.1 Hz, 1H), 8.50 (d, *J* = 8.0 Hz, 1H), 8.40 (d, *J* = 8.4 Hz, 1H), 7.68 (t, *J* = 7.8 Hz, 1H), 7.21 (d, *J* = 8.0 Hz, 1H), 4.10-3.95 (m, 6H), 3.25-3.25 (m, 4H), 2.35 – 2.20 (m, 1H), 2.07 – 1.75 (m, 5H), 1.45-1.25 (m, 2H), 1.23-1.05 (m, 2H), COOH not detected; ^{13}C NMR ($CDCl_3$) δ : 163.69, 163.24, 154.61, 131.64, 130.29, 129.03, 128.89, 125.12, 124.84, 122.22, 116.06, 113.98, 65.94, 52.42, 44.55, 41.93, 35.10, 28.90, 27.29; HRMS (ESI MS) m/z: theor: 423.1914 found: 423.1918 ($[M+H]^+$ detected).

Synthesis of 4-((1,3-dioxo-6-(piperidin-1-yl)-1*H*-benzo[*de*]isoquinolin-2(3*H*)-yl)methyl) cyclohexane-1-carboxylic acid (Napht-2)

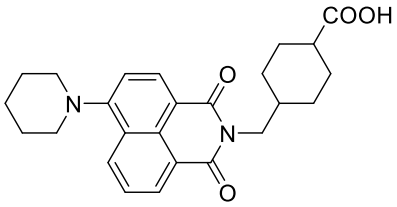

A mixture of 4-((6-bromo-1,3-dioxo-1*H*-benzo[*de*]isoquinolin-2(3*H*)-yl)methyl)cyclohexane-1-carboxylic acid (1.14 g, 2.74 mmol, M = 416.27 g.mol^{-1}) and piperidine (0.70 g, 0.81 mL, 8.21 mmol, 3 eq., M = 85.15 g.mol^{-1}, d = 0.861) in 2-ethoxyethanol (10 mL) was stirred at reflux for 16 h. After cooling to room temperature, the solvent was removed under reduced pressure. The crude product was purified by column chromatography on silica gel (CH_2Cl_2/MeOH: 9/1) to provide an orange solid as the pure product (1.66 g, 82 % yield). ^{1}H NMR ($CDCl_3$) δ : 8.55 (d, *J* = 5.8 Hz, 1H), 8.48 (d, *J* = 7.1 Hz, 1H), 8.38 (d, *J* = 7.1 Hz, 1H), 7.66 (s, 1H), 7.17 (d, *J* = 7.3 Hz, 1H), 4.05 (d, *J* = 4.2 Hz, 2H), 3.32-3.25 (m, 4H), 3.05-3.00 (m, 1H), 2.32-2.15 (m, 1H), 2.11 – 1.49 (m, 11H), 1.45-1.12 (m, 3H), COOH not detected; Anal. Calc. for $C_{25}H_{28}N_2O_4$: C, 71.4; H, 6.7; O, 15.2; Found: C, 71.0; H, 6.2; O, 15.5 %; HRMS (ESI MS) m/z: theor: 421.2122 found: 421.2124 ([M+H]$^+$ detected)

Synthesis of 4-((6-(hexylamino)-1,3-dioxo-1*H*-benzo[*de*]isoquinolin-2(3*H*)-yl)methyl) cyclohexane-1-carboxylic acid (Napht-3)

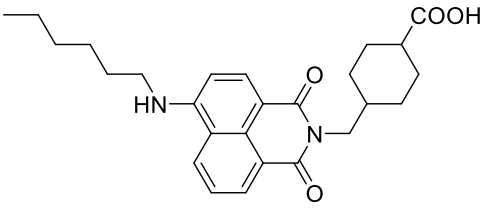

A mixture of 4-((6-bromo-1,3-dioxo-1*H*-benzo[*de*]isoquinolin-2(3*H*)-yl)methyl)cyclohexane-1-carboxylic acid (0.60 g, 1.44 mmol, M = 416.27 g.mol^{-1}) and hexylamine (0.44 g, 0.57 mL, 4.32 mmol, 3 eq., M = 101.19 g.mol^{-1}, d = 0.773) in 2-ethoxyethanol (5 mL) was stirred at reflux temperature for 16 h. After cooling to room temperature, the solution was concentrated under reduced pressure until most of the solvent was removed. The residue was poured into the water (30 mL) and extracted with $CHCl_3$ (3×50 mL). The combined organic layers were dried over $MgSO_4$ and concentrated. The crude product was purified by column chromatography on silica gel (CH_2Cl_2/MeOH: 25/1 to 10/1) to provide a yellow solid (478 mg, 76 % yield). ^{1}H NMR ($CDCl_3$) δ : 8.58 (dd, *J* = 7.3,

1.1 Hz, 1H), 8.54 – 8.47 (m, 2H), 7.67 (dt, *J* = 11.3, 5.6 Hz, 1H), 7.17 (d, *J* = 8.2 Hz, 1H), 4.20 – 4.11 (m, 2H), 1.79 – 1.65 (m, 6H), 1.47 – 1.23 (m, 14H), 0.91 (t, 8.6 Hz, 3H), COOH and NH not detected; Anal. Calc. for $C_{26}H_{32}N_2O_4$: C, 71.5; H, 7.4; O, 14.7; Found: C, 71.2; H, 7.2; O, 14.5 %; HRMS (ESI MS) m/z: theor: 437.2435 found: 437.2432 ($[M+H]^+$ detected)

Synthesis of 4-((6-(octylthio)-1,3-dioxo-1*H*-benzo[*de*]isoquinolin-2(3*H*)-yl)methyl)cyclohexane-1-carboxylic acid (Napht-4-H)

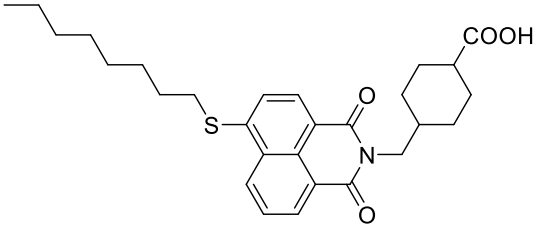

A mixture of 4-((6-bromo-1,3-dioxo-1*H*-benzo[*de*]isoquinolin-2(3*H*)-yl)methyl)cyclohexane-1-carboxylic acid (0.60 g, 1.44 mmol, M = 416.27 $g.mol^{-1}$), octanethiol (0.22 g, 0.26 mL, 1.51 mmol, 1.05 eq., M = 146.29 $g.mol^{-1}$, d = 0.843) and K_2CO_3 (0.13 g, 0.94 mmol, M = 138.2 $g.mol^{-1}$) in 2-ethoxyethanol (5 mL) was stirred at 50 °C for 16 h. After cooling to room temperature, the solution was poured into water (30 mL) and extracted with $CHCl_3$ (3×50 mL). The combined organic layers were dried over $MgSO_4$ and concentrated. The crude product was purified on silica thin layer with CH_2Cl_2 and collected with ethanol. After evaporation of the solvent, the pure product was obtained as yellow solid (391 mg, 0.95 mmol, 66 % yield). ^1H NMR ($CDCl_3$) δ : 8.60 (dd, *J* = 13.3, 7.8 Hz, 2H), 8.47 (d, *J* = 7.9 Hz, 1H), 7.75 (t, *J* = 7.9 Hz, 1H), 7.54 (d, *J* = 7.9 Hz, 1H), 4.07 (d, *J* = 7.0 Hz, 2H), 3.16 (s, 2H), 2.30 (t, *J* = 12.0 Hz, 1H), 2.02 (d, *J* = 11.5 Hz, 2H), 1.97 – 1.75 (m, 4H), 1.51 (dd, *J* = 14.5, 7.4 Hz, 2H), 1.46 – 1.11 (m, 13H), 0.88 (t, 8.6 Hz, 3H), COOH not detected; Anal. Calc. for $C_{28}H_{35}NO_4S$: C, 69.8; H, 7.3; O, 13.3; Found: C, 70.0; H, 7.2; O, 13.5 %; HRMS (ESI MS) m/z: theor: 482.2360 found: 482.2365 ($[M+H]^+$ detected)

Synthesis of sodium 4-((6-(octylthio)-1,3-dioxo-1*H*-benzo[*de*]isoquinolin-2(3*H*)-yl)methyl)cyclohexane-1-carboxylate (Napht-4)

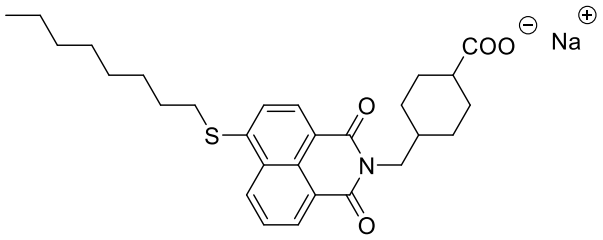

4-((6-(Octylthio)-1,3-dioxo-1*H*-benzo[*de*]isoquinolin-2(3*H*)-yl)methyl)cyclohexane-1-carbo-xylic acid (1 g, 2.08 mmol, M = 481.65 g/mol) was solubilized in THF (50 mL) and aq. NaOH solution (30 %, 2 mL) was added to the mixture. The solution was stirred under reflux for 3 h. After cooling, THF and part of water were removed under reduced pressure. A precipitate formed. It was filtered off, washed several times with pentane and dried under vacuum (963 mg, 92% yield). ^{1}H NMR (D_2O) δ : 7.95-7.89 (brs, 1H), 7.70-7.62 (brs, 1H), 7.58-7.50 (brs, 1H), 7.23-7.15 (brs, 1H), 6.85-6.77 (brs, 1H), 3.65-3.50 (brs, 2H), 2.85-2.65 (brs, 2H), 2.15-2.03 (brs, 1H), 1.95-1.80 (m, 2H), 1.75-1.50 (m, 4H), 1.48-1.11 (m, 15H), 0.92 (t, 8.6 Hz, 3H); Anal. Calc. for $C_{28}H_{34}NNaO_4S$: C, 66.8; H, 6.8; O, 12.7; Found: C, 66.2; H, 6.4; O, 12.8 %; HRMS (ESI MS) m/z: theor: 482.2360 found: 482.2358 ($[M+H]^+$ detected)

Synthesis of 2-ethoxyethyl 4-((1,3-dioxo-6-(piperidin-1-yl)-1*H*-benzo[*de*]isoquinolin-2(3*H*)-yl)methyl)cyclohexane-1-carboxylate (Napht-5)

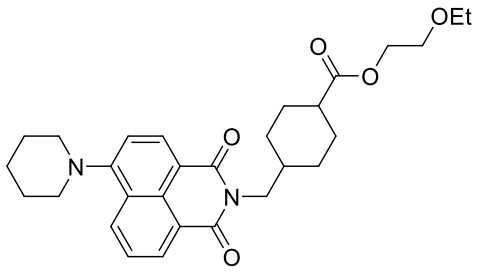

This compound was identified as a side-product formed during the synthesis of Napht-2. ^{1}H NMR ($CDCl_3$) δ : 8.57 (dd, *J* = 7.3, 1.0 Hz, 1H), 8.49 (d, *J* = 8.1 Hz, 1H), 8.41 (dd, *J* = 8.4, 1.0 Hz, 1H), 7.72 – 7.64 (m, 1H), 7.19 (d, *J* = 8.1 Hz, 1H), 4.07 (d, *J* = 6.9 Hz, 2H), 3.77 – 3.67 (m, 4H), 3.59 – 3.48 (m, 6H), 3.28 – 3.20 (m, 2H), 2.35 – 1.69 (m, 12H), 1.40 (ddd, *J* = 26.0, 13.1, 2.6 Hz, 2H), 1.23 (dd, *J* = 13.2, 6.3 Hz, 3H); Anal. Calc. for $C_{29}H_{36}N_2O_5$: C, 70.7; H, 7.4; O, 16.2; Found: C, 70.5; H, 7.4; O, 16.5 %; HRMS (ESI MS) m/z: theor: 493.2697 found: 493.2695 ($[M+H]^+$ detected)

Synthesis of 4-((6-bromo-1,3-dioxo-1*H*-benzo[*de*]isoquinolin-2(3*H*)-yl)methyl)cyclohexane-1-carboxylic acid (Napht-6)

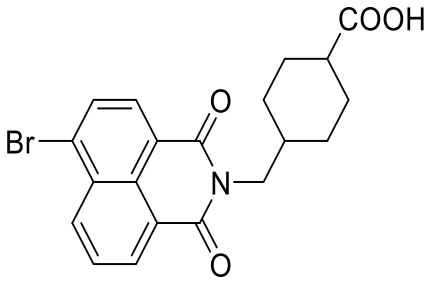

A mixture of 4-bromo-1,8-naphthalic anhydride (6.0 g, 21.65 mmol) and *trans*-4-(aminomethyl)cyclohexanecarboxylic acid (3.74 g, 23.82 mmol, 1.1 eq.) in DMF (70 mL) was stirred at reflux temperature for 4h. The reaction mixture was cooled to room temperature. The solvent was removed under reduced pressure. The residue was poured into ice cooled water and stirred for 15 min. An orange precipitate formed. It was filtered off, rinsed several times with cold water and dried under vacuum (7.93 g, 88 % yield). ^{1}H NMR ($CDCl_3$) δ : 8.66 (dd, *J* = 7.3, 1.1 Hz, 1H), 8.58 (dd, *J* = 8.5, 1.1 Hz, 1H), 8.41 (d, *J* = 7.9 Hz, 1H), 8.05 (d, *J* = 7.9 Hz, 1H), 7.85 (dd, *J* = 8.5, 7.3 Hz, 1H), 4.07 (d, *J* = 7.1 Hz, 2H), 2.29 (tt, *J* = 12.1, 3.5 Hz, 1H), 2.09 – 1.77 (m, 5H), 1.40 (ddd, *J* = 25.3, 13.1, 2.9 Hz, 2H), 1.28 – 1.11 (m, 2H), COOH not detected; Anal. Calc. for $C_{20}H_{18}BrNO_4$: C, 57.7; H, 4.4; O, 15.4; Found: C, 57.2; H, 4.2; O, 15.8 %; HRMS (ESI MS) m/z: theor: 416.0492 found: 416.0496 ($[M+H]^+$ detected)

2.2. Other chemical compounds

All the other chemicals (Scheme 2) were selected with the highest purity available and used as received without removing the storage inhibitors. Di-*tert*-butyl-diphenyl iodonium hexafluorophosphate (Iod) and ethyl 4-(dimethylamino)benzoate (EDB) were obtained from Lambson Ltd (UK). (3,4 Epoxycyclohexane)methyl 3,4-epoxycyclohexylcarboxylate (EPOX; Uvacure 1500), trimethylolpropane triacrylate (TMPTA), di(trimethylolpropane) tetraacrylate (TA), Mix-MA, *N*-Phenylglycine (NPG) were obtained from Allnex or Sigma Aldrich. TMPTA, TA, Mix-MA and EPOX were selected as benchmark monomers for the radical and cationic polymerizations, respectively.

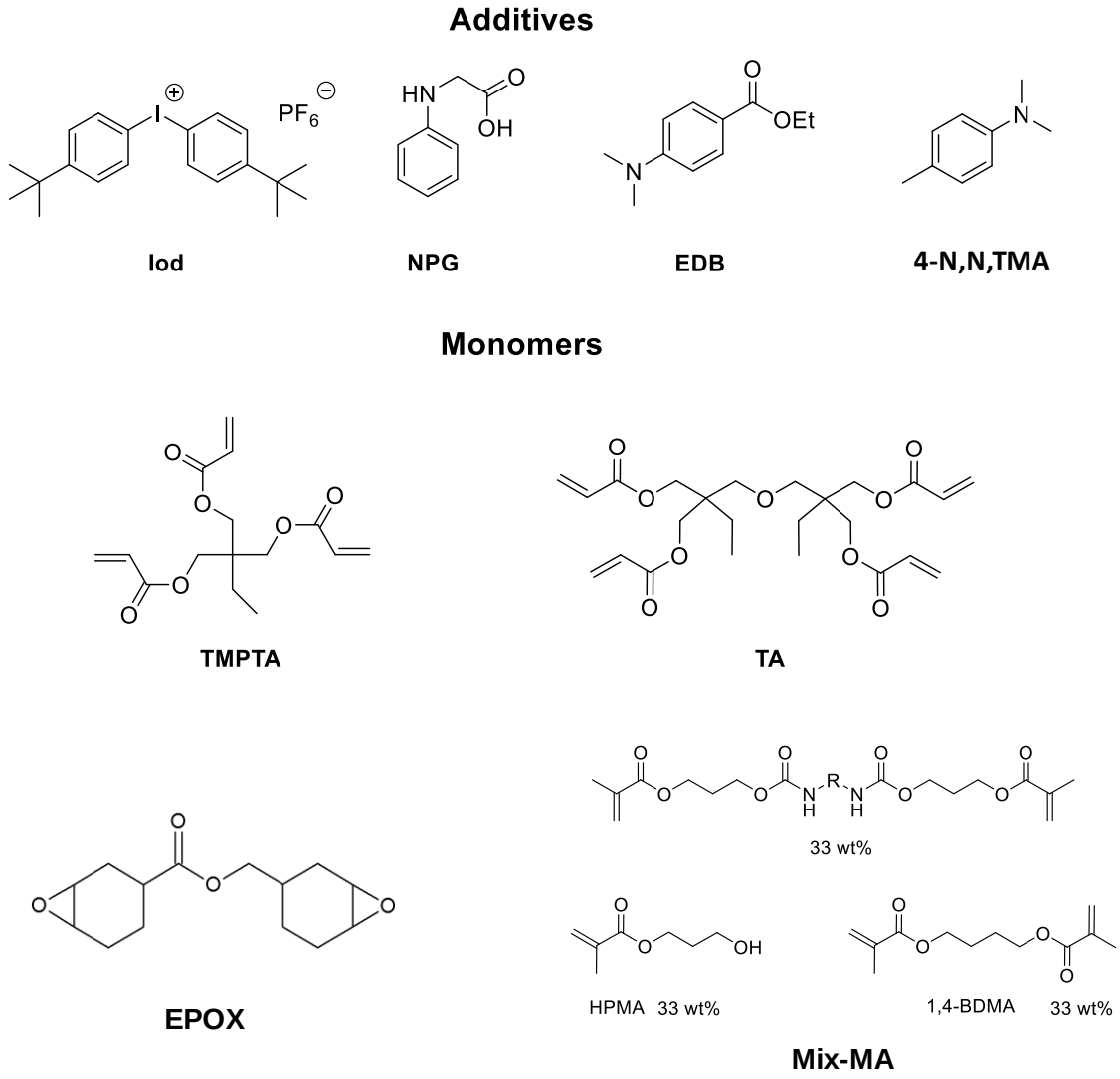

Scheme 2. Other used chemical compounds used in this work.

2.3. Irradiation sources

The different sources of irradiation used in this work (polymerization of the photocurable samples, photolysis experiments and photocomposites synthesis) were the following: **(1)** LED@ 375nm with an incident light intensity at the sample surface I_0 = 40 mW.cm^{-2}; **(2)** LED@ 405nm with I_0 = 110 mW.cm^{-2}, **(3)** LED conveyor @395nm with I_0 = 4 W/cm^2.

2.4. Free radical photopolymerization (FRP) and Interpenetrating polymer network (IPN) synthesis

FRP experiments were carried out using two and three-component photoinitiating systems based on: Napht/Iod (0.1%/1% w/w) and Napht/Iod/NPG (0.1%/1%/1% w/w/w). Conversely,

IPNs were only prepared using two-components PISs: Napht/Iod (0.1%/1% w/w). Higher percentages in PI were also studied (0.2% in Napht) in this last case. The percentages of the components in the photoinitiation system were calculated from the global monomer content.

Two types of samples were studied: i) thick samples: where the resin containing the reactive system was deposited in a circular mold (thickness = 1.4mm) in which the polymerization of the acrylate or epoxy functions could take place or ii) thin samples: where the photopolymerizable resin is sandwiched between 2 polypropylene films (thickness = 25μm) for the FRP and the IPN synthesis. In fact, the polymerization rate (Rp) as well as the final reactive functions conversion (FC) of FRP (TA and TMPTA) were monitored by following by evolution of the C=C peak located at 6160 cm^{-1} and 1630 cm^{-1} for the thick and thin samples respectively. For the epoxy functions, peaks at 3744 cm^{-1} and 790 cm^{-1} were selected for the thick and thin samples respectively. RT-FTIR experiments were carried out using a JASCO 6600 FTIR spectrometer.

2.5. Redox potentials

Redox potentials for Naphthalimide derivatives (E_{ox} and E_{red}) were determined by cyclic voltammetry using tetrabutylammonium hexafluorophosphate as the supporting electrolyte (potentials vs. Saturated Calomel Electrode – SCE) in acetonitrile. The free energy change (ΔG_{et}) for an electron transfer reaction was calculated from eq.1 [27], where E_{ox}, E_{red}, E*, and C represent the oxidation potential of the electron donor, the reduction potential of the electron acceptor, the excited state energy level (determined from luminescence experiments) and the coulombic term for the initially formed ion pair, respectively. Here, C is neglected as usually done for polar solvents.

$$\Delta G_{et} = E_{ox} - E_{red} - E^* + C \qquad \text{eq.1}$$

2.6. UV-Visible absorption and photolysis experiments

The UV-visible absorption spectra, the molar extinction coefficients and the steady state photolysis experiments of Naphthalimide derivatives (in acetonitrile) have been studied using a JASCO V730 UV-visible spectrometer.

2.7. Fluorescence experiments

Fluorescence properties of the different compounds in chloroform were investigated using a JASCO FP-6200 spectrofluorimeter. The fluorescence quenching of ^{1}Napht by Iod were

investigated from the classical Stern−Volmer treatment [1] ($I_0/I = 1 + kq\ \tau_0[Iod]$, where I_0 and I stand for the fluorescent intensity of Naphthalimide in the absence and the presence of Iod, respectively; τ_0 stands for the lifetime of Naphthalimide in the absence of Iod).

2.8. Computational Procedure

Molecular orbital calculations were carried out with the Gaussian 03 suite of programs [28,29]. Electronic absorption spectra for the different compounds were calculated with the time-dependent density functional theory at the MPW1PW91-FC/6-31G* level of theory on the relaxed geometries calculated at the UB3LYP/6-31G* level of theory. The triplet state energy levels were calculated at this level of theory.

2.9. Near-UV conveyor for photocomposite synthesis

For the synthesis of photocomposites, a Dymax-UV conveyor is used. Firstly, the photopolymerizable resin has been deposited on the glass fibres (50%/50% w/w) and then the samples were irradiated using a LED conveyor at 395 nm (4 W/cm^2). The distance between the belt and the LED was fixed at 15 mm, and the belt speed was fixed at 2 m/min.

2.10. 3D printing experiments

3D printing experiments were carried out using a computer-controlled diode laser at 405 nm (spot size = 50 μm), these experiments were performed under air. 3D patterns were analyzed using a numerical optical microscope (DSX-HRSU from OLYMPUS Corporation) [22].

2.11. Dynanometer experiments

A Dynamometer INSTRON 4505 modernized Zwick (speed = 10 mm/min) has been used to measure the shear stress (MPa) of material as a function of the elongation (mm). The materials were prepared in a silicone mold where the formulation was deposited and irradiated using an LED projector @395nm (0.3W/cm^2).

3. Results and discussion

Influence of the different groups attached to the Naphthalimide core on the photochemical and photophysical properties as well as the chemical mechanisms have been investigated in details.

3.1. Light absorption properties

Absorption spectra as well as the molar extinction coefficients of the naphthalimide derivatives in acetonitrile are depicted in Figure 1 (See also Table 1). In fact, these compounds are characterized by a main band and a high absorption capacity (e.g.: Napht-2: ε = 11300 $M^{-1}cm^{-1}$ at 405 nm; Napht-3: ε = 10860 $M^{-1}cm^{-1}$ at 405 nm) in the near UV as well as in the visible range (350-500 nm). These absorption properties provide an excellent overlap with the emission spectra of the near UV or visible LEDs used in this work (LED @ 375nm, 395nm and 405nm). UV-visible absorption spectra as well as the molar extinction coefficients are drastically impacted by the substituent linked to the naphthalimide scaffold. Notably, introduction of an electron donating group resulting in a bathochromic shift of the absorption spectra whereas introduction of an electron withdrawing group produced an hypsochromic shift of the intramolecular charge transfer band. The electron-donating effect of these substituents is presented as follows by ascending order: Napht-3 > Napht-2 and 5 > Napht-6 > Napht-1 > Napht-4. Optimized geometries as well as the frontier orbitals (Highest Occupied Molecular Orbital - HOMO - and Lowest Unoccupied Molecular Orbital - LUMO) are shown in Figure 2. The electron donating group strongly participates to the HOMO orbital (except Napht-4), while the LUMO one is localized onto the naphthalimide core, thus ensuring a partial charge character for this π-π^* transition. In fact, the alkyl group present in Napht-3 and Napht-4 also gives a fast solubility of these molecules in the photopolymerizable resin (see below).

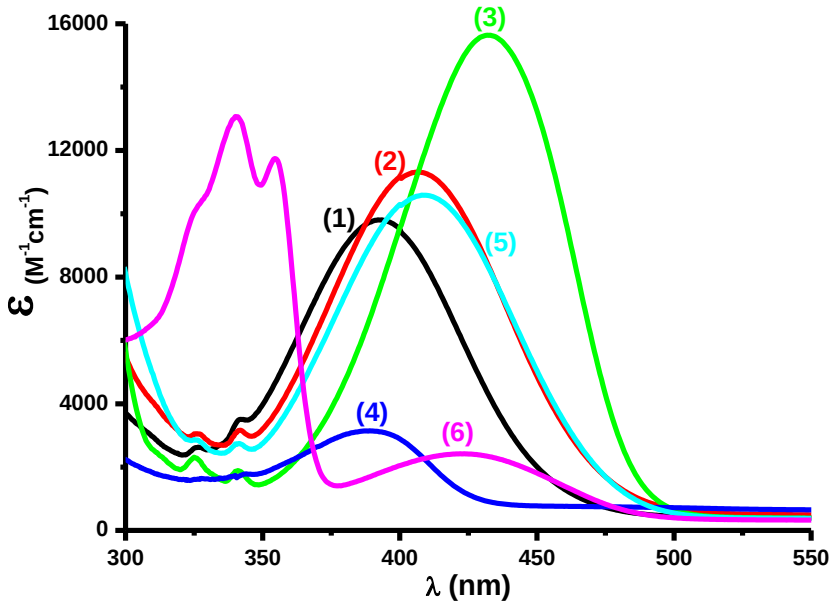

Figure 3. UV-visible absorption spectra of the investigated compounds in ACN: **(1)** Napht-1, **(2)** Napht-2, **(3)** Napht-3, **(4)** Napht-4, **(5)** Napht-5 and **(6)** Napht-6.

Table 1. Light absorption properties of Naphthalimide compounds at 405 nm and at λ_{max}.

	λ_{max} (nm)	ε_{max} (M^{-1} cm^{-1})	$\varepsilon_{@405nm}$ (M^{-1} cm^{-1})
Napht-1	392	9810	8960
Napht-2	406	11320	11300
Napht-3	432	15640	10860
Napht-4	389	3140	2570
Napht-5	408	10590	10510
Napht-6	423	2420	2180

	HOMO	LUMO
Napht-1 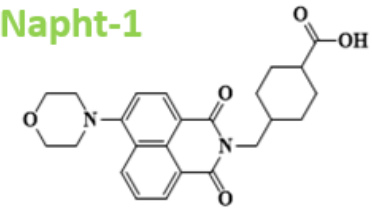	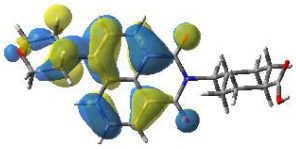	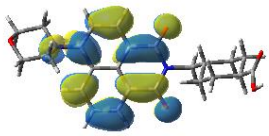
Napht-2 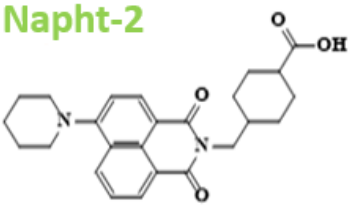	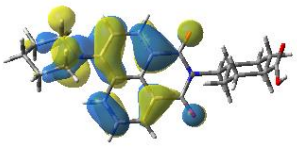	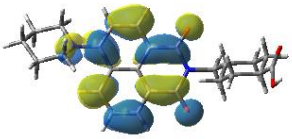
Napht-3 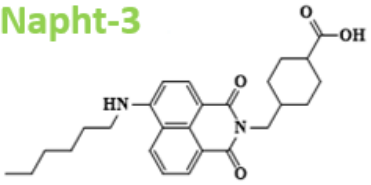	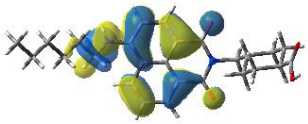	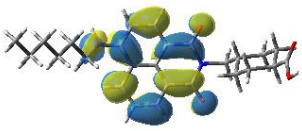
Napht-4 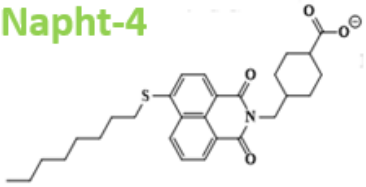	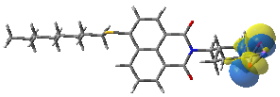	
Napht-5 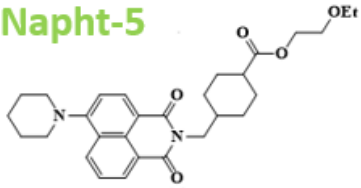	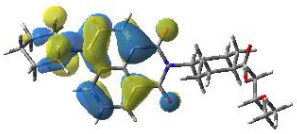	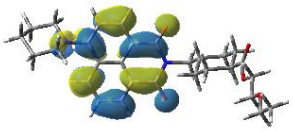
Napht-6 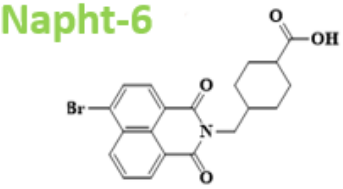	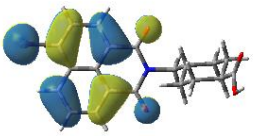	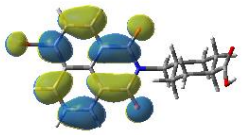

Figure 2. HOMO and LUMO frontier orbitals for the different investigated compounds at the UB3LYP/6- 31G* level.

Partie III : Nouveaux photoamorceurs à base de colorants pour la polymérisation radicalaire (FRP) et Cationique (CP)

3.2. Free Radical Photopolymerization (FRP)

3.2.1. Photopolymerization of methacrylate monomers (Mix-MA)

Since the different compounds showed a significant absorption in the near UV as well as in the visible range, the dyes were tested as photoinitiators for the FRP of methacrylate-based monomers.

In fact, these compounds showed very good photopolymerization profiles in thick samples and the results are depicted in Figure 3 (and see also Table 2). The use of a two-component PIS (Napht/Iod) enabled to get interesting photopolymerization profiles in terms of polymerization rates but the three-component PISs obtained by the introduction of an amine into the photosensitive resin showed a greater efficiency i.e. a better final methacrylate function conversion (FC) and a higher polymerization rate (e.g. FC= 68% for Napht-6/Iod (0.2%/1% w/w) vs. 86% for Napht-6/Iod/NPG (0.2%/1%/1% w/w/w)). Presence of the Naphthalimide-based photosensitizer is crucial for the global performance i.e. Napht/Iod/NPG being better PIS than Iod/NPG e.g. Figure 3, curve 12 vs. curve 13.

It is important to note that the polymerization profiles for Mix-MA were lower than those obtained with TMPTA or TA (see below). This may be due to the low viscosity of Mix-MA which causes a higher oxygen inhibition.

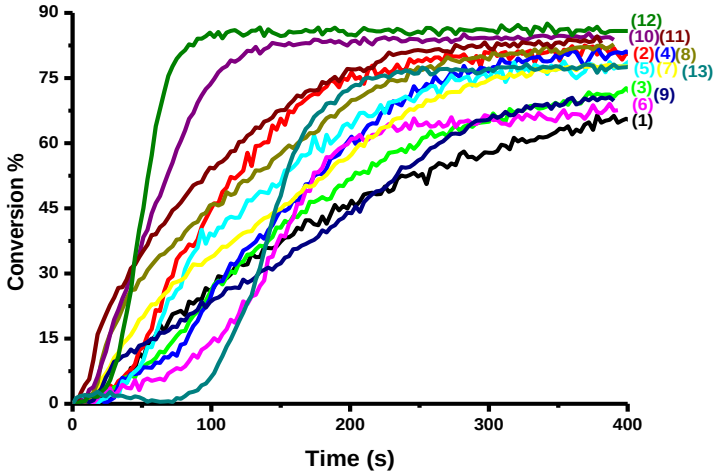

Figure 3. Photopolymerization profiles (methacrylate function conversion vs. irradiation time) for Mix-MA (thickness =1.4 mm) upon exposure to the LED @405 nm in the presence of **the two-component** photoinitiating systems: Napht/Iod (0.1% / 1% w/w) : **(1)** Napht-1, **(2)** Napht-2, **(3)** Napht-3, **(4)** Napht-4, **(5)** Napht-5, **(6)** Napht-6 (0.2%/1% w/w); and **three-component** PIS Napht/Iod/NPG (0.1%/1%/1% w/w/w) :**(7)** Napht-1, **(8)** Napht-2, **(9)** Napht-3, **(10)** Napht-4, **(11)** Napht-5, (**12)** Napht-6 (0.2%/1%/1% w/w/w) and **(13)** Iod/NPG (1%/1% w/w). Irradiation starts at t=10s.

3.2.2. Photopolymerization of acrylate monomers (TA and TMPTA)

Typical acrylate function conversion–time profiles are given in Figure 4, and the final acrylate function conversions (FC) are gathered in Table 2. The FRP of TMPTA and TA was investigated in both thick (1.4 mm) and thin (25 μm) samples using two and three component PISs. The FRP of acrylates in the presence of the two-component Napht/Iod (0.1%/1% w/w) and the three-component Napht/Iod/NPG (0.1%/1%/1% w/w/w) photoinitiating systems is very efficient compared to Napht, Iod or NPG considered alone which shows no polymerization of the acrylate functions. This latter result unambiguously confirms the role of the naphthalimide dyes as photoinitiators.

The obtained results clearly show that Napht-2 leads to a very efficient polymerization, compared to the other structures, in terms of FC and Rp for the FRP of TA, e.g. FC = 85% for Napht-2 vs 68%, 62%, 65%, 81% and 64% for Napht-1,3,4,5 and Napht-6 (Figure 4C curves 1-6). These results can be explained by a more efficient photo-oxidation interaction between Napht-2 and Iod. The efficiency of the FRP (i.e. for the FC) using a LED@405 nm clearly follows the trend Napht-2 > Napht-5 > Napht-1 > Napht-4 > Napht-6 > Napht-3. In fact, an increase of the PI concentration induced a decrease in the final conversion of the acrylate functions, this may be due to an inner filter effect which prevents the penetration of the incident light into the photosensitive resin (see Table 2).

On the other hand, an improvement in the performance of FRP was observed using NPG as a third component in the photosensitizable resin (Napht/Iod/NPG (0.1%/1%/1% w/w/w). In fact, the Iod/NPG (1%/1% w/w) couple showed a quite efficient polymerization in the FRP of the acrylate functions (FC = 79%; Figure 4D curve 7). It has to be noticed that Iod alone or NPG alone cannot induce a polymerization, this may be due to the formation of a charge transfer complex $[Iod\text{-}NPG]_{CTC}$ that can be activated under visible light irradiation. The addition of PI to the Iod/NPG couple effectively improved the polymerization profile, e.g. FC = 90% for Napht-1/Iod/NPG (0.1%/1%/1% w/w/w vs. 68% for Napht-1/Iod (0.1%/1% w/w) (Figure 4D curve 1 vs 4C curve 1).

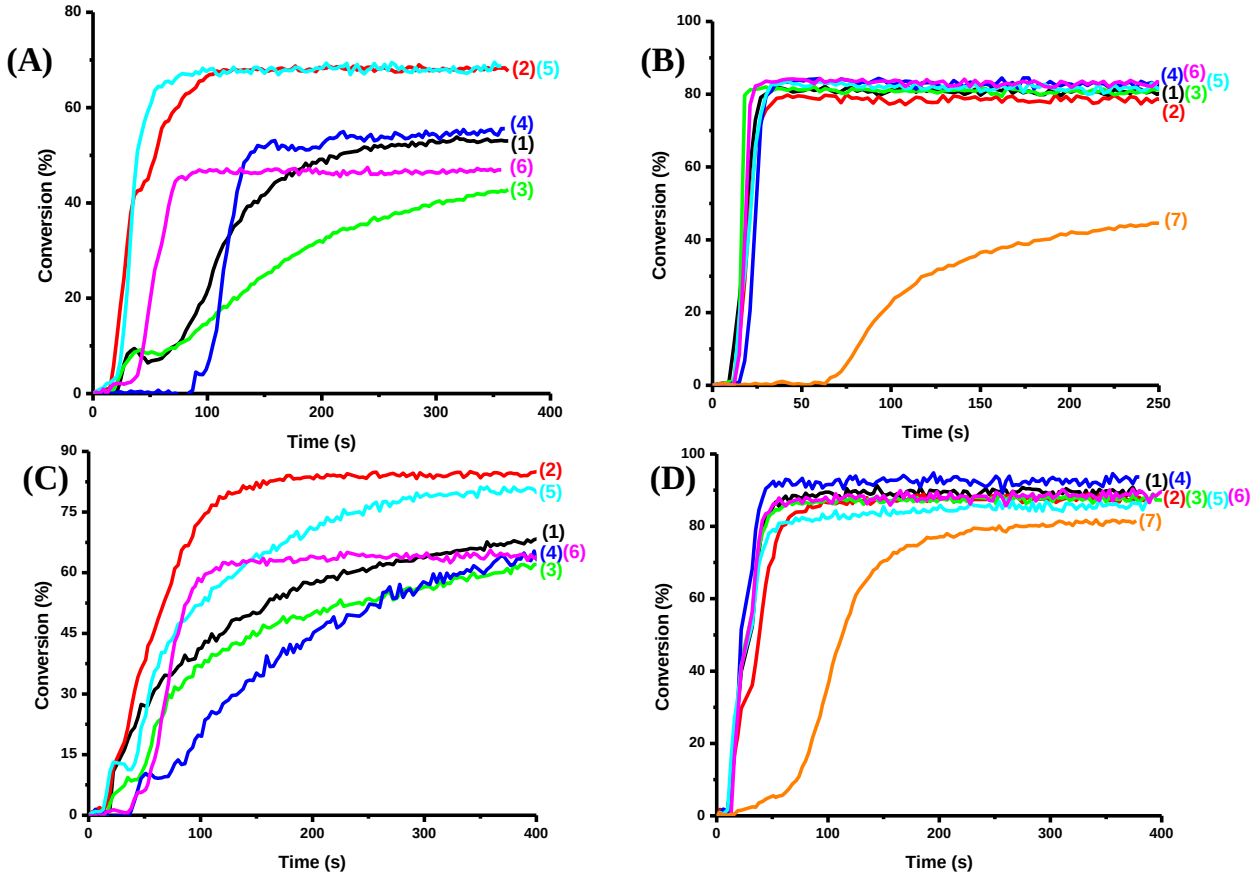

Figure 4. Polymerization profiles (acrylate function conversion vs. irradiation time): **(A)** and **(C)** for TMPTA and TA respectively (thick samples (1.4 mm)) in the presence of the two-component photoinitiating systems Napht/Iod (0.1%/1% w/w): **(1)** Napht-1, **(2)** Napht-2, **(3)** Napht-3, **(4)** Napht-4, **(5)** Napht-5, **(6)** Napht-6, **(B)** and **(D)** for TMPTA and TA respectively (thick samples (1.4 mm)) in the presence of the three-component photoinitiating systems Napht/Iod/NPG (0.1%/1%/1% w/w/w): **(1)** Napht-1, **(2)** Napht-2, **(3)** Napht-3, **(4)** Napht-4, **(5)** Napht-5, **(6)** Napht-6 and (7) Iod/NPG (1%/1% w/w) upon exposure to the LED @405 nm Irradiation starts at t = 10 s.

Table 2. Final reactive functions conversion (FC%) for different monomers and different PISs upon visible light irradiation using a LED @405nm (400 s of irradiation and thickness= 1.4 mm).

Thick samples						
	Two component PISs Napht/Iod (0.1%-0.2%/1% w/w)			**Three component PISs Napht/Iod/NPG (0.1%/1%/1% w/w/w)**		
	TA	**TMPTA**	**Mix-MA**	**TA**	**TMPTA**	**Mix-MA**
Napht-1	**68%**[a] **50%**[b]	**53%**[a] **61%**[b]	**66%**[a]	**90%**	**81%**	**78%**
Napht-2	**85%**[a] **67%**[b]	**70%**[a] **58%**[b]	**82%**[a]	**89%**	**79%**	**83%**
Napht-3	**62%**[a] **55%**[b]	**43%**[a] **44%**[b]	**73%**[a]	**88%**	**81%**	**71%**

Napht-4	**65%**[a] **74%**[b]	**56%**[a] **51%**[b]	**82%**[a]	**94%**	**84%**	**85%**
Napht-5	**81%**[a] **59%**[b]	**70%**[a] **60%**[b]	**79%**[a]	**87%**	**82%**	**85%**
Napht-6	**64%**[a] **74%**[b]	**47%**[a] **54%**[b]	**69%**[a]	**90%**	**83%**	**86%**

a: Napht/Iod (0.1%/ 1% w/w)
b: Napht/Iod (0.2% /1% w/w)

Table 3. Final reactive functions conversion (FC%) for different monomers and different PISs upon visible light irradiation using a LED @405nm (400 s of irradiation; and thickness= 25 µm in laminate).

Thin samples				
	Two component PISs Napht/Iod (0.1%-0.2%/1% w/w)		**Three component PISs Napht/Iod/NPG (0.1%/1%/1% w/w/w)**	
	TA	**TMPTA**	**TA**	**TMPTA**
Napht-1	**61%**[a] **71%**[b]	**33%**[a] **48%**[b]	**75%**	**54%**
Napht-2	**50%**[a] **61%**[b]	**32%**[a] **37%**[b]	**68%**	**52%**
Napht-3	**43%**[a] **63%**[b]	**23%**[a] **39%**[b]	**75%**	**53**
Napht-4	**55%**[a] **52%**[b]	**n.p%**[a] **40%**[b]	**77%**	**49%**
Napht-5	**57%**[a] **59%**[b]	**21%**[a] **49%**[b]	**76%**	**53%**
Napht-6	**29%**[a] **51%**[b]	**30%**[a] **n.p%**[b]	**72%**	**39%**

a: Napht/Iod (0.1%/ 1% w/w)
b: Napht/Iod (0.2% /1% w/w)

3.2.3. IPN synthesis

An interpenetrating polymer network (IPN) is a polymer based on two different monomers (more precisely, in our work, TA and EPOX) polymerizing in different conditions. Thus, two polymer networks are simultaneously formed, but they are not linked together (just tangled). The aim of such type of process is to improve the mechanical properties by widening the glass

transition regions of IPN materials relative to their components. The results obtained with different percentage of monomers are summarized in Table 4. The experiments showed that the 70% / 30% ratio in TA / EPOX monomers was the best composition in terms of the conversion rates of both functionalities (acrylates and epoxides). In fact, the cationic polymerization is not inhibited by O_2 improving the radical polymerization under air.

Table 4. Final monomer conversions (FC%) of acrylate and epoxide functions using the PISs based on Napht/Iod/NPG (0.1%/1%/1% w/w/w) upon visible light irradiation using a LED @405nm (1000 s of irradiation; thickness= 1.4 mm).

	TA/ EPOX (w/w)		
	50%/50%	**70%/30%**	**100%/0%**
Napht-1	93% / 29%	91% / 43%	68%
Napht-2	95% / 0%	80% / 15%	85%
Napht-3	93% / 40%	81% / 32%	62%
Napht-4	78% / 0%	87% / 0%	65%
Napht-5	94% / 37%	93% / 45%	80%
Napht-6	87% / 29%	87% / 21%	64%

3.3. 3D-printing experiments using Napht/Iod/Amine systems

The new Naphthalimide derivatives have been tested in direct laser write experiments, using a laser diode at 405 nm. Some examples of the polymers obtained under air using different PISs such as Napht/Iod/NPG (0.04%/0.4%/0.4% w/w/w) or Napht/Iod/NPG (0.04%/0.4%/0.4% w/w/w) in TA are presented in the Figure 5. Some of them have been obtained with a great thickness (going up to 1900 μm), a great spatial resolution (50 μm) and in a very short irradiation time (~2 minutes). Interestingly, these colored 3D patterns showed a very strong green fluorescence when characterized by digital light microscopy. An example of IPN 3D printed pattern is also given in Figure 5E.

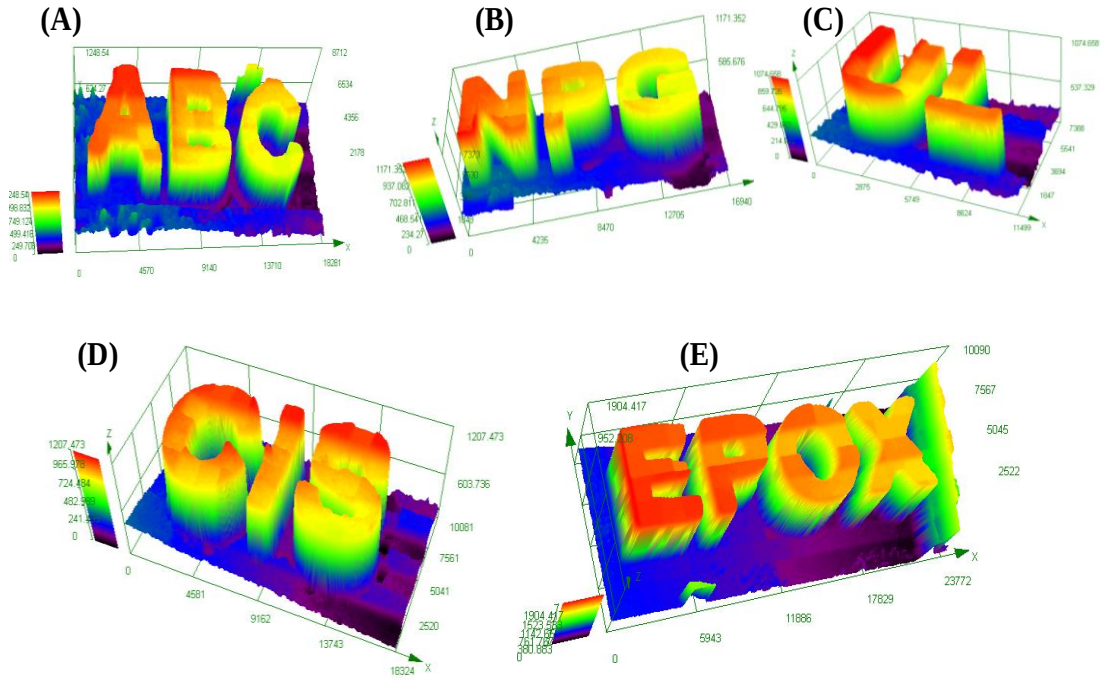

Figure 5. Free Radical photopolymerization (FRP) (using TA as benchmark monomer) for direct laser write experiments @405nm: Characterization of 3D patterns by numerical optical microscopy: **(A)** Napht-1/Iod/4NNTMA (0.04%/0.4%/0.042%) in TA, **(B)** Napht-2/Iod/NPG (0.04%/0.4%/0.4% w/w/w) in TA, **(C)** Napht-6/Iod/NPG (0.08%/0.4%/0.4% w/w/w) in TA, **(D)** Napht-3/Iod/NPG (0.05%/0.5%/0.5% w/w/w) in TA and **(E)** Napht-3/Iod/NPG (0.05%/ 0.5%/0.5% w/w/w) in TA/EPOX (50% / 50%)

3.4. Photocomposites synthesis using a LED conveyor

During the last decades and until today, the production of composites materials represents a very dynamic market, since it is estimated at 90.6 billion dollars in 2019, the world market should reach more than 131.6 billion in 2024 (with an average annual growth rate of 7.7%) [30]. This very important production is based on the very interesting mechanical properties of these new materials (lighter, chemically inert, with improved thermal and mechanical resistance …).

In this work, naphthalimide-based photoinitiators have shown high efficiency in FRP using the three-component PISs. Therefore, these PISs were used for the manufacture of photocomposites based on glass fibres. The interest of using these materials as a matrix is that they have very important properties (e.g. impact resistance ...) as well as they are widely used in different fields, such as transport, buildings, infrastructure and industrial equipment. First of all, the photocomposites materials were prepared by impregnation of glass fibres (in 1 or 3 layers) with an acrylic resin (50% glass fibres / 50% acrylic resin) and irradiated upon a

LED@395nm. Remarkably, a very fast curing was observed where the surface and the bottom are tack-free (thickness =2mm) after one pass only using different PISs in TA, but this is not the case for a greater thickness (three layers of glass fibres ~ 6 mm) where the bottom was tack-free after 13 passes using Napht-3/Iod/NPG (0.1%/1%/1% w/w/w), and it's not the case for a blend of monomers (TA and EPOX) where the surface and the bottom are tack-free after one and 40 passes, respectively. The curing results obtained are gathered in Figure 6.

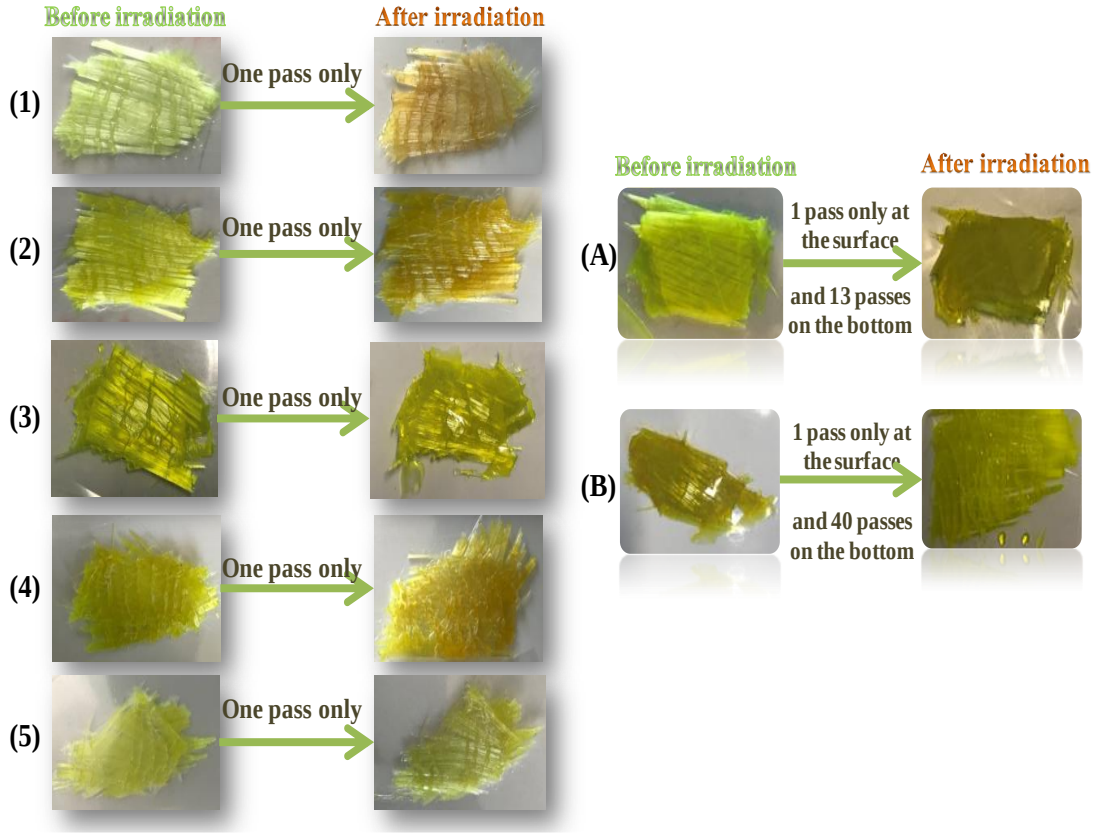

Figure 6. Photocomposites synthesis using FRP in the presence of glass fibres/ resin 50%/50% w/w (Thickness = 2 mm for one layer), using LED@395 nm and the Belt Speed was fixed at 2m/min: **(1)** Napht-1/Iod/NPG (0.1%/1%/1% w/w/w), **(2)** Napht-2/Iod/NPG (0.1%/1%/1% w/w/w), **(3)**Napht-3/Iod/NPG (0.1%/1%/1% w/w/w) , **(4)** Napht-4/Iod/NPG (0.1%/1%/1% w/w/w) and **(5)** Napht-5/Iod/NPG (0.1%/1%/1% w/w/w) in TA. **(A)** and **(B)** are photocomposites produced upon the near-UV irradiation @395nm in the presence of glass fibres/resin 50%/50% w/w (thickness ~ 6mm for 3 layers) for Napht-3/Iod/NPG (0.1%/1%1% w/w/w) in TA and Napht3/Iod/NPG (0.1%/1%/1% w/w/w) in Ebec40/EPOX (50%/50%).

3.5. Traction results

The traction results of the materials obtained are shown in the Figure 7. In fact, these data confirmed the advantage of developing IPN materials in order to improve of the mechanical

properties of the materials compared to those determined for polymers composed of only one type of monomer.

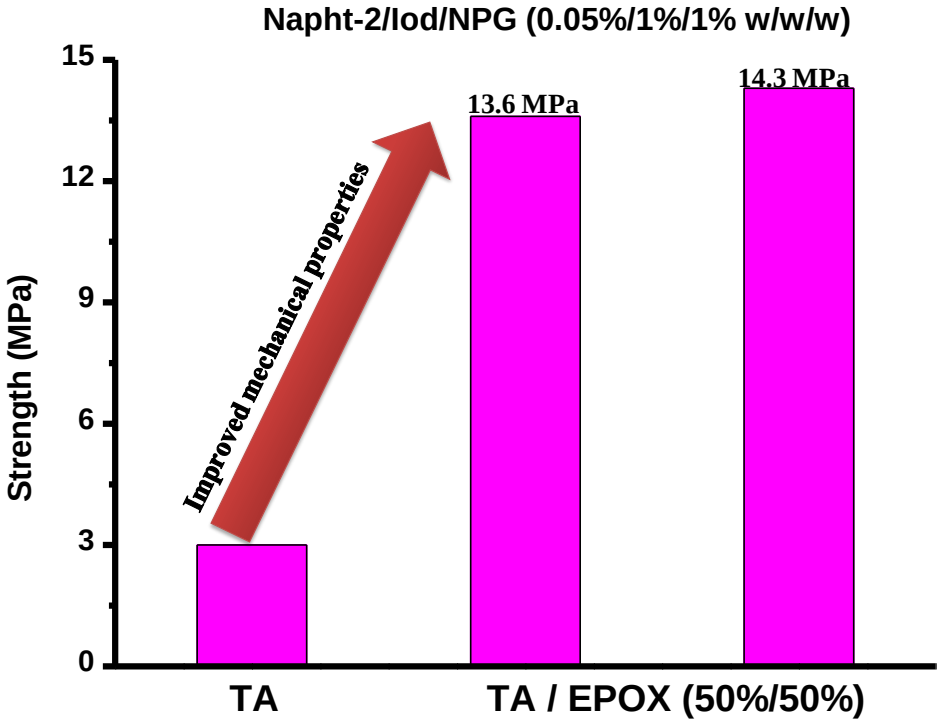

Figure 7. Traction results with the initiating system Napht-2/Iod/NPG (0.05%/1%/1% w/w/w) for polymerized TA vs. TA/EPOX (50%/50%).

3.6. Hydrogel synthesis using Napht-4/ Triethanolamine (0.1%/1% w/w), Photopolymerization in water.

Interestingly, Napht-4 was also water soluble and this compound could be advantageously used for photopolymerization in water and the preparation of hydrogels. Markedly, using the Napht-4/Triethanolamine system (0.1%/1% w/w) in polyethylene glycol diacrylate/water blend (SR610 from Sartomer Europe), hydrogels could be easily obtained by irradiation of the formulation using a LED @405nm (Figure 8).

It is important to note that the UV-visible spectrum of Napht-4 in water showed a hyperchromic effect (ε~7000 $M^{-1}cm^{-1}$ in water vs. 2570 $M^{-1}cm^{-1}$ in ACN) compared to that obtained in ACN (Figure 9), and Napht-4 is well soluble in ACN but the best solvent to solubilize Napht-4 is water for which this PI was chosen for hydrogel formation experiments.

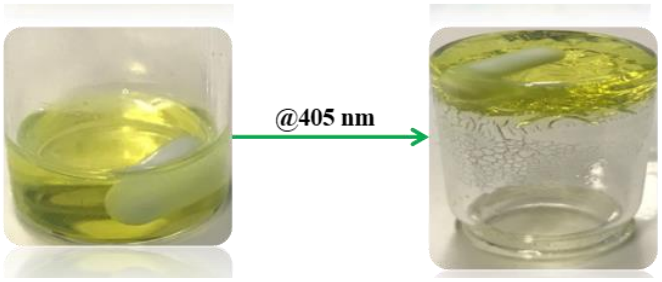

Figure 8. Hydrogels obtained before and after irradiation @ 405nm using Napht-4/Triethanolamine system (0.1%/1% w/w) in polyethylene glycol diacrylate/water blend.

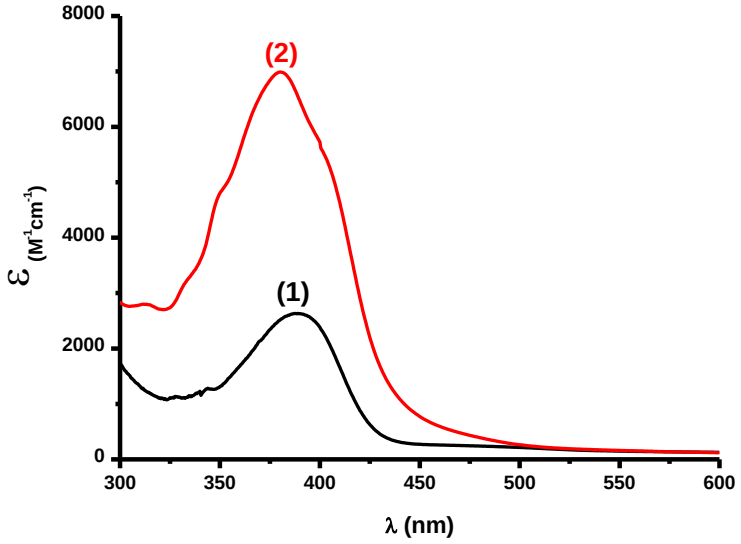

Figure 9. Absorption spectra of Napht-4 in: **(1)** ACN and **(2)** water.

4. Discussion

Photochemical and photophysical properties of the investigated Naphthalimides are now discussed in this part.

4.1. steady state photolysis

Steady state photolysis of the different Naphthalimides in acetonitrile and upon irradiation with LED@375nm have been carried out. Photolyses of Napht-2 alone, Napht-2/Iod and Napht-2/NPG are reported in Figure 10. Firstly, photolysis of the Napht-2/Iod couple is faster than that of Napth-2 alone which does not show any obvious photolysis upon irradiation @375nm. Therefore, Napht-2 alone is photostable (Figure 10A). The appearance of a new peak during the irradiation of the Napht-2/Iod couple, as well as the decrease of the Napht-2 absorption evidences a strong interaction between the PI and Iod by an electron transfer

process which results in the photolysis of the PI and the generation of a photoproduct observed between 475-550 nm. Actually, the photolysis of Napht-2 in the presence of the Iod/NPG couple (10^{-2} M) is very slow (Figure 10C) i.e. much less important than that observed with Iod alone (Figure 10D curve 2 and 3), clearly showing that Napht-2 is regenerated in the three-component system.

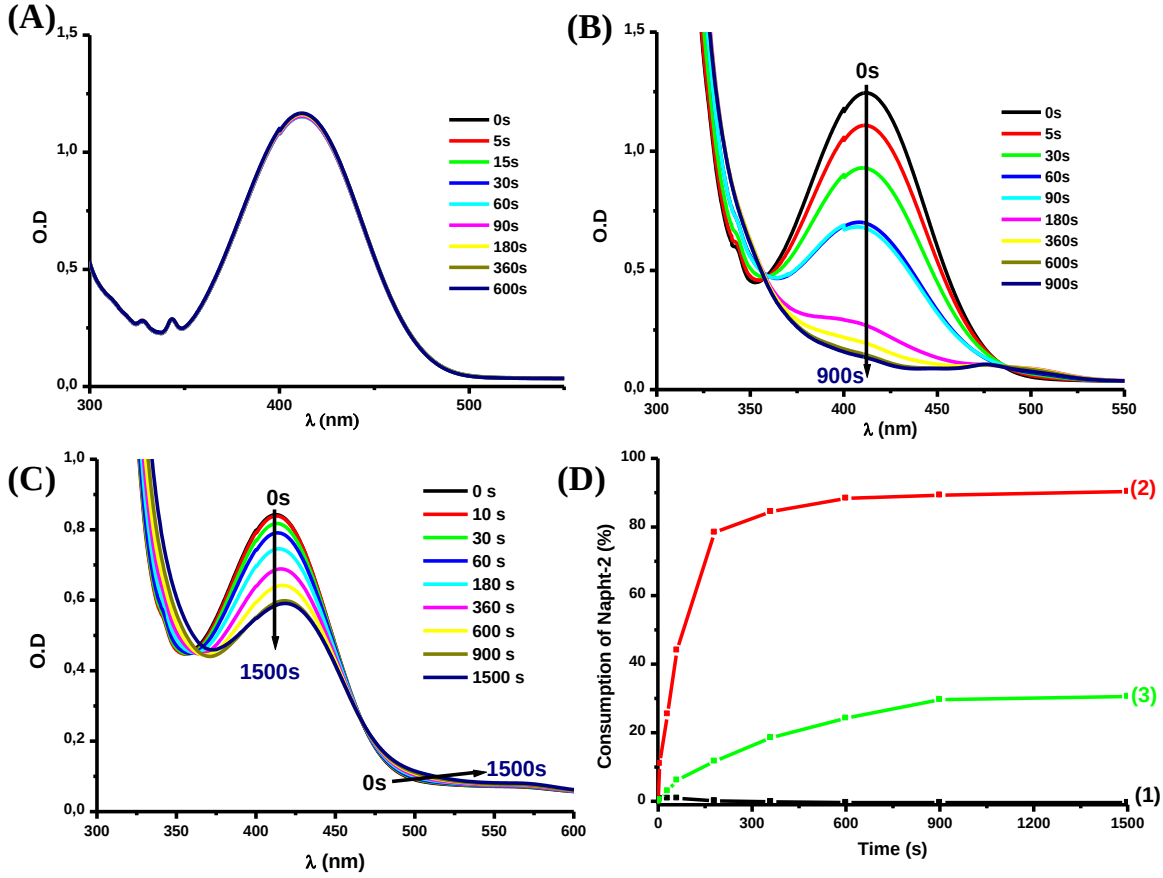

Figure 10. (A) Photolysis of Napht-2 alone in ACN, **(B)** Photolysis of Napht-2 with Iod (10^{-2} M) in ACN, **(C)** Photolysis of Napht-2 with Iod/NPG (10^{-2}M**)** couple **(D)** Percentage of consumption of Napht-2 **(1)** without and with **(2)** With Iod and **(3)** With Iod/NPG vs. irradiation time – upon exposure to the LED@375 nm in ACN.

4.2. Fluorescence quenching and cyclic voltammetry experiments

Emission and fluorescence quenching spectra of Naphthalimides have been obtained in ACN (e.g Napht-2) and the different curves are reported in Figure 11. First of all, the addition of Iod clearly showed a decrease in the emission intensity of Napht-2. This result confirms those obtained during the photolysis experiments and during the free radical polymerization, suggesting a strong interaction between the excited state of the PI and Iod. From these

fluorescence quenching data, Stern-Volmer coefficients could be extracted (e.g. Ksv= 43 M^{-1} for Napht-2 and 119 M^{-1} for Napht-3) and rather high electron transfer quantum yields were obtained (Table 5)) according to the equation 2:

$$\phi_{S1} = K_{SV}[Iod] / (1+K_{SV}[Iod]) \qquad \text{eq. 2}$$

The excited state energy (E_{S1}) of the Naphthalimide derivatives (determined by the crossing point of the emission and absorption spectra Figure 11D) and the electrochemical properties (oxidation potential) calculated by cyclic voltammetry allowed to determine the free energy change ΔG (using eq.1) e.g. ΔG = -1.48 eV for Napht-2 and -1.44 eV for Napht-3 (Table 5).

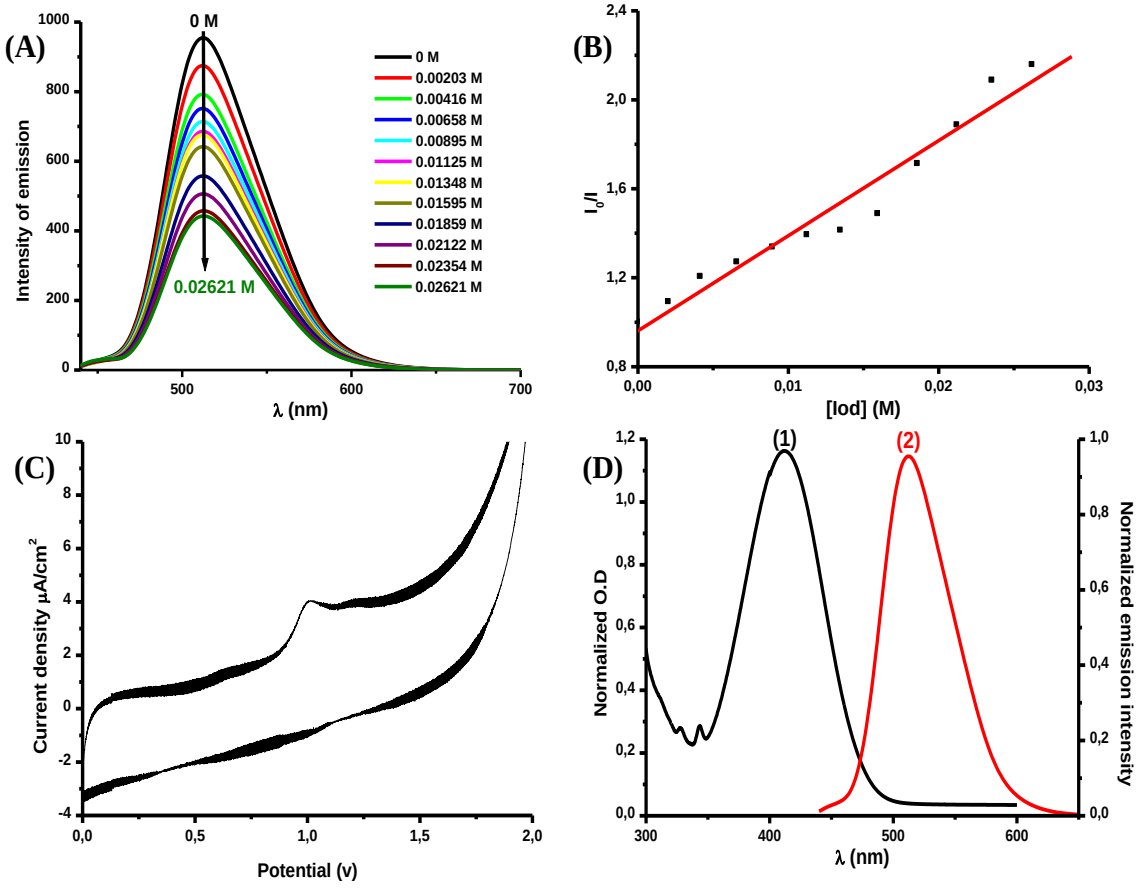

Figure 11. (A) Fluorescence quenching of Napht-2 by Iod, **(B)** Determiantion of K_{SV} (Stern-Volmer coefficient), **(C)** Oxidation potential (Eox) determination of Napht-2 and **(D)** E_{S1} determination.

Table 5. Parameters characterizing the chemical mechanisms associated with ^{1}Napht/Iod interaction in acetonitrile. For Iod, a reduction potential of -0.2 eV was used for the ΔGet calculations.

	E_{ox} (v)	E_{S1} (eV)	ΔG_{S1} (eV)	K_{SV} (M^{-1})	Φ_{et} (Naphtaimide/Iod)
Napht-1	1.02	2.63	-1.41	59.9	0.54
Napht-2	0.92	2.61	-1.48	42.8	0.46
Napht-3	0.95	2.59	-1.44	119.3	0.70
Napht-4	0.72	2.91	-1.99	3.25	0.06
Napht-5	0.97	2.57	-1.4	24.8	0.33
Napht-6	1.00	2.57	-1.37	93.4	0.65

Based on the different characterization techniques (Photolysis, fluorescence quenching, cyclic voltammetry), the free radical polymerization (FRP) results can be explained by a global chemical mechanism (See Scheme 3). Firstly, the photoinitiator goes to its excited state once it is irradiated by the LED@405nm, so that radicals ($Ar^{\bullet}$ and $Napht^{+\bullet}$) are generated by the interaction between PI and Iod (r2). Interaction between the Iod salt and the amine (NPG) lead to the formation of a Charge transfer complex (CTC), which is very sensitive to light, this complex will be, therefore, the source of the formation of radicals ($Ar^{\bullet}$) (r3-r4). In addition, a hydrogen transfer process from the amine to PI can occur which generates two types of radicals (Napht-$H^{\bullet}$ and $NPG_{(-H)}{}^{\bullet}$) (r5). Then, a decarboxylation of $NPG_{(-H)}{}^{\bullet}$ [31] leads to the formation of an intermediate radical ($NPG_{(-H,\ -CO2)}{}^{\bullet}$) which is capable of producing reactive species ($Ar^{\bullet}$ and $NPG_{(-H,\ CO2)}{}^{+}$) by interaction with Iod (r6-r7). Therefore, $Ar^{\bullet}$ and $NPG_{(-H,\ -CO2)}{}^{\bullet}$) (r1-r9) radicals can be considered to be the reactive species in charge of the FRP of the acrylate and methacrylate functions of TMPTA, TA and Mix-MA in two or three-component PISs. For the three-component system, the naphthalimide consumption is reduced (Figure 10C) in agreement with its regeneration in r8-r9 and a partial photoredox catalyst behavior.

$$\text{Naphthalimide } (h\nu) \rightarrow {}^{1,3}\text{Naphthalimide} \qquad \text{r1}$$

$$^{1,3}\text{Naphthalimide} + ArI^{+} \rightarrow \text{Naphthalimide}^{\bullet+} + Ar_2I^{\bullet} \rightarrow\rightarrow Ar^{\bullet} + ArI \qquad \text{r2}$$

$$NPG + Iod \rightarrow [NPG\text{-}Iod]_{CTC} \qquad \text{r3}$$

$$[NPG\text{-}Iod]_{CTC} \rightarrow Ar^{\bullet} \qquad \text{r4}$$

$$^{1,3}\text{Naphthalimide} + NPG \rightarrow \text{Naphthalimide-}H^{\bullet} + NPG_{(-H)}{}^{\bullet} \qquad \text{r5}$$

$NPG_{(-H)}^{\bullet} \rightarrow NPG_{(-H;-CO2)}^{\bullet} + CO_2$ r6

$NPG_{(-H;-CO2)}{}^{\bullet}{}_{+} Ar_2I^{+} \rightarrow NPG_{(-H;-CO2)}^{+} + Ar^{\bullet} + ArI$ r7

$Naphthalimide^{\bullet+} + NPG \rightarrow Naphthalimide + NPG^{\bullet+}$ r8

$Naphthalimide\text{-}H^{\bullet} + Ar_2I^{+} \rightarrow Naphthalimide + Ar^{\bullet} + ArI + H^{+}$ r9

Scheme 3. Expected chemical mechanisms

5. Conclusion

In this work, a series of six compounds based on Naphthalimide derivatives have been proposed for the first time as efficient photoinitiators for the free radical polymerization (FRP) of (meth)acrylates functions upon visible light irradiation using LED@405 nm. Interestingly, these naphthalimides have been tested for 3D printing experiments and for the synthesis of photocomposites with significant curing of the surface and the bottom using a LED conveyor @395 nm. A new water soluble photoinitiator (Napht-4) has also been proposed in this work. In light of the high efficiency of naphtalimides in FRP under visible light irradiation, future developments will consist in designing Naphthalimides absorbing in the near infrared range, where the light penetration is more important than in the near UV/visible range.

References

[1] Fouassier, J.P. Photoinitiation; photopolymerization; photocuring: Fundamental and Applications, Munich: Hanser, **1995**.

[2] Fouassier, J.P. Photochemistry and UV Curing, Research Signpost, Trivandrum, India, **2006**.

[3] Fouassier, J.P. Photoinitiator, Photopolymerization and Photocuring: Fundamentals and Applications, Gardner Publications: New York, **1995**.

[4] Fouassier, J.P.; Lalevée, J. Photoinitiators for Polymer Synthesis, Scope, Reactivity, Efficiency; Wiley-VCH Verlag GmbH & Co.KGaA: Weinheim, Germany, **2012**.

[5] Dietliker, K.A. Compilation of Photoinitiators Commercially Available for UV Today, Sita Technology Ltd., London, **2002**.

[6] Davidson, S. Exploring the Science, Technology and Application of UV and EB Curing, Sita Technology Ltd., London, **1999**.

[7] Crivello, J.V.; Dietliker, K.; Bradley, G. Photoinitiators for Free Radical Cationic & Anionic Photopolymerisation, John Wiley & Sons: Chichester, U. K., **1999**.

[8] Fouassier, J.P.; Lalevee, J. Recent advances in photoinduced polymerization reactions under 400-700 nm light. Photochemistry, **2015**, 42, 215.

[9] Dumur, F.; Gigmes, D.; Fouassier, J.P.; Lalevee, J. Organic Electronics: An El Dorado in the Quest of New Photocatalysts for Polymerization Reactions. J.Acc.Chem.Res. **2016**, 49, 1980.

[10] Dietlin, C.; Schweizer, S.; Xiao, P.; Zhang, J.; Morlet-Savary, F.; Graff, B.; Fouassier, J.P.; Lalevee, J. Photopolymerization upon LEDs : new photoinitiating systems and strategies. Polym.Chem. **2015**, 6, 3895.

[11] Zivic, N.; Bouzrati-Zerelli, M.; Kermagoret, A.; Dumur, F.; Fouassier, J.P.; Gigmes, D.; Lalevee, J. Photocatalysts in Polymerization Reactions. ChemCatChem. **2016**, 8, 1617.

[12] Middleton, R.W.; Parrick, J.; Clarke, E.D.; Wardman, P.; Synthesis and fluorescence of N-substituted-1,8-naphthalimides. J. Heterocycl. Chem. **1986**, 23, 849.

[13] Jacquemin, D.; Perpète, E.A.; Scalmani, G.; Frisch, M.J.; Ciofini, I.; Adamo, C. Fluorescence of 1,8-naphthalimide : A PCM-TD-DFT investigation. Chem.Phys.Lett., **2007**, 448, 3.

[14] Banerjee, S.; Veale, E.B.; Phelan, C.M.; Murphy, S.A.; Tocci, G.M.; Gillespie, L.J.; Frimannsson, D.O.; Kelly, J.M.; Gunnlaugsson, T. Recent advances in the development of 1,8-naphthalimide based DNA targeting binders, anticancer and fluorescent cellular imaging agents. Chem.Soc.Rev. **2013**, 42, 1601.

[15] Lee, M.H.; Kim, J.Y.; Han, J.H.; Bhuniya, S.; Sessler, J.L.; Kang, C.; Kim, J.S. Direct Fluorescence Monitoring of the Delivery and Cellular Uptake of a Cancer-Targeted RGD Peptide-Appended Naphthalimide Theragnostic Prodrug. J.Am.Chem.Soc. **2012**, 134, 30, 12668.

[16] Bonardi, A.H.; Zahouily, S.; Dietlin, C.; Graff, B.; Morlet-Savary, F.; Ibrahim-Ouali, M.; Gigmes, D.; Hoffmann, N.; Dumur, F.; Lalevee. J. New 1,8-Naphthalimide Derivatives as Photoinitiators for Free-Radical Polymerization Upon Visible Light. Catalysts, **2019**, 9, 637.

[17] Zhang, J.; Zivic, N.; Dumur, F.; Xiao, P.; Graff, B.; Fouassier, J.P.; Gigmes, D.; Lalevee, J. Naphthalimide-Tertiary Amine Derivatives as Blue-Light-Sensitive Photoinitiators. ChemPhotoChem. **2018**, 2, 481.

[18] Xiao, P.; Dumur, F.; Frigoli, M.; Tehfe, M.A.; Gigmes, D.; Fouassier, J.P.; Lalevée, J. Naphthalimide based methacrylated photoinitiators in radical and cationic photopolymerization under visible light. Polym. Chem., **2013**, 4, 5440.

[19] Xiao, P.; Dumur, F.; Graff, B.; Gigmes, D.; Fouassier, J.P.; Lalevée, J. Blue Light Sensitive Dyes for Various Photopolymerization Reactions: Naphthalimide and Naphthalic Anhydride Derivatives. Macromolecules. **2014**, 47, 601.

[20] Zhang, J.; Zivic, N.; Dumur, F.; Xiao, P.; Graff, B.; Gigmes, D.;. Fouassier, J.P.; Lalevée, J. A benzophenone-naphthalimide derivative as versatile photoinitiator of polymerization under near UV and visible lights. J.Polym.Sci. A Polym. Chem. **2015**, 53, 445.

[21] Xiao, P.; Dumur, F.; Zhang, J.; Graff, B.; Gigmes, D.; Fouassier, J.P.; Lalevée, J. Naphthalimide-phthalimide derivative based photoinitiating systems for polymerization reactions under blue lights. J.Polym.Sci. A Polym. Chem. **2015**, 53, 665.

[22] Zhang, J.; Dumur, F.; Xiao, P.; Graff, B.; Bardelang, D.; Gigmes, D.; Fouassier, J.P.; Lalevée, J. Structure Design of Naphthalimide Derivatives: Toward Versatile Photoinitiators for Near-UV/Visible LEDs, 3D Printing, and Water-Soluble Photoinitiating Systems. Macromolecules. **2015**, 48, 2054.

[23] Xiao, P.; Dumur, F.; Zhang, J.; Graff, B.; Gigmes, D.; Fouassier, J.P.; Lalevée, J. Naphthalimide Derivatives : Substituent Effects on the Photoinitiating Ability in Polymerizations under Near UV, Purple, White and Blue LEDs (385, 395, 405, 455, or 470 nm). Macromol.Chem.Phys. **2015**, 216, 1782.

[24] Xiao, P.; Dumur, F.; Graff, B.; Morlet-Savary, F.; Fouassier, J.P.; Gigmes, D.; Lalevée, J. Naphthalic anhydride derivatives: Structural effects on their initiating abilities in radical and/or cationic photopolymerizations under visible light. J.Polym.Sci. A Polym. Chem. **2015**, 53, 2860.

[25] Zivic, N.; Zhang, J.; Bardelang, D.; Dumur, F.; Xiao, P.; Jet, T.; Versace, D.L.; Dietlin, C.; Morlet-Savary, F.; Graff, B.; Fouassier, J.P.; Gigmes, D.; Lalevée, J. Novel naphthalimide–amine based photoinitiators operating under violet and blue LEDs and usable for various polymerization reactions and synthesis of hydrogels. Polym.Chem. **2016**, 7, 418.

[26] Xiao, P.; Dumur, F.; Zhang, J.; Graff, B.; Gigmes, D.; Fouassier, J.P.; Lalevée, J. New role of aminothiazonaphthalimide derivatives: outstanding photoinitiators for cationic and radical photopolymerizations under visible LEDs. RSC Advances, **2016**, 6, 48684.

[27] Rehm, D.; and Weller, A. Kinetics of Fluorescence Quenching by Electron and H-Atom Transfer. Isr.J.Chem., **1970**, 8, 259.

[28] Foresman, J.B.; Frisch, A. Exploring Chemistry with Electronic Structure Methods, second ed., Gaussian Inc., Pittsburgh, PA, **1996**.

[29] Frisch, M.J.; Trucks, G.W.; Schlegel, H.B.; Scuseria, G.E.; Robb, M.A.; Cheeseman, J.R.; Zakrzewski, V.G.; Montgomery, J.A.; Stratmann, J.R.E.; Burant, J.C.; Dapprich, S.; Millam, J.M.; Daniels, A.D.; Kudin, K.N.; Strain, M.C.; Farkas, O.; Tomasi, J.; Barone, V.; Cossi, M.; Cammi, R.; Mennucci, B.; Pomelli, C.; Adamo, C.; Clifford, S.; Ochterski, J.;

Petersson, G.A.; Ayala, P.Y.; Cui, Q.; Morokuma, K.; Salvador, P.; Dannenberg, J.J.; Malick, D.K.; Rabuck, A.D.; Raghavachari, K.; Foresman, J.B.; Cioslowski, J.; Ortiz, J.V.; Baboul, A.G.; Stefanov, B.B.; Liu, G.; Liashenko, A.; Piskorz, P.; Komaromi, I.; Gomperts, R.; Martin, R.L.; Fox, D.J.; Keith, T.; Al-Laham, M.A.; Peng, C.Y.; Nanayakkara, A.; Challacombe, M.; Gill, P.M.W.; Johnson, B.; Chen, W.; Wong, M.; Andres, J.L.; Gonzalez, C.; Head-Gordon, M.; Replogle, E.S.; Pople, J.A. Gaussian 03, Revision B-2, Gaussian Inc., Pittsburgh, PA, **2003**.

[30] Composites Market Global Forecast to 2024, MarketsandMarkets, **2019**.

[31] Schmitt, M.; Becker, D.; Lalevée. J. Performance analysis of the solidification of acrylic esters photo-initiated by systematically modified ZnO nanoparticles. Polymer, **2018**, 158, 83.

Partie IV : Photoamorceur (PA) organométallique à base de complexes de cuivre

Partie IV : Photoamorceur (PA) organométallique à base de complexes de cuivre.

Partie IV : Photoamorceur (PA) organométallique à base de complexes de cuivre.

Les photoamorceurs à base de métaux sont connus depuis longtemps pour leurs applications, et certains d'entre eux ont été largement étudiés comme les sels organométalliques de ferrocénium. De nombreuses structures organométalliques, telles que les complexes de ruthénium et d'iridium [1-4], ont été largement et avec succès utilisées comme photoamorceurs pour la synthèse de polymères au niveau académique. Ces complexes métalliques possèdent d'excellentes propriétés photochimiques : une forte absorption de la lumière visible, des états excités de durée de vie relativement longue et des potentiels redox appropriés. Ils peuvent aussi réagir comme catalyseurs photoredox par oxydation ou réduction pour produire des espèces réactives (radicaux ou cations). Cependant, ce sont souvent des métaux de transition (Ru, Ir) rares, il est donc très intéressant de développer des composés sans métal (parties précédentes) ou des complexes à base de métaux à faible coût (par exemple, Cu ou Fe). Dans ce contexte, cette partie du manuscrit proposera des photoamorceurs à base de complexes de cuivre.

Dans cette partie, deux nouveaux dérivés de complexes de cuivre ont été synthétisés et testés comme photoamorceurs de polymérisation radicalaire et cationique ainsi que la synthèse de réseaux polymères interpénétrés (IPN) (par polymérisation d'un mélange acrylate/époxyde). Ces composés ont montré une forte capacité d'amorçage des fonctions acrylates dans des systèmes à deux et trois composants en utilisant le TA comme monomère acrylique de référence. La formation de réseaux polyéthers par polymérisation des époxydes a été aussi montrée dans ce travail en combinant le colorant organométallique avec Iod ou Iod/NVK.

Afin d'expliquer la capacité d'amorçage de ces composés, des expériences de photolyse ont été réalisées dans l'ACN en présence d'Iod ou Iod/NPG. En fait, une forte diminution de l'absorbance a été observée sous irradiation en utilisant la LED à 405nm (ou 375nm) pour la combinaison Cu/Iod, ce comportement montre bien une interaction par photo-oxydation entre le PA et le sel d'iodonium confirmée aussi par le calcul de la variation d'enthalpie libre **ΔG** où une valeur négative a été obtenue montrant l'efficacité de la réaction Cu-Iod. D'autre part,

un caractère photoredox a pu aussi être détecté dans ce travail, où le PA a été régénéré à la fin de la polymérisation suivant un cycle photocatalytique.

La grande photoréactivité de ces complexes de cuivre a été montrée par des expériences d'écriture laser ainsi que la synthèse des photocomposites épais. Les résultats obtenus ont montré qu'avec l'augmentation de l'épaisseur du renfort la polymérisation en profondeur est de plus en plus difficile à cause de la diffusion de la lumière incidente par les fibres de verre. Les capacités d'amorçage des complexes de cuivre et leurs applications sont présentées dans le **Schéma 1.** La synthèse de ce couple de complexes de cuivre a été réalisé par nos collaborateurs de l'université d'Aix Marseille (Dr. Frédéric Dumur). Ce travail fait l'objet d'un article en cours de préparation.

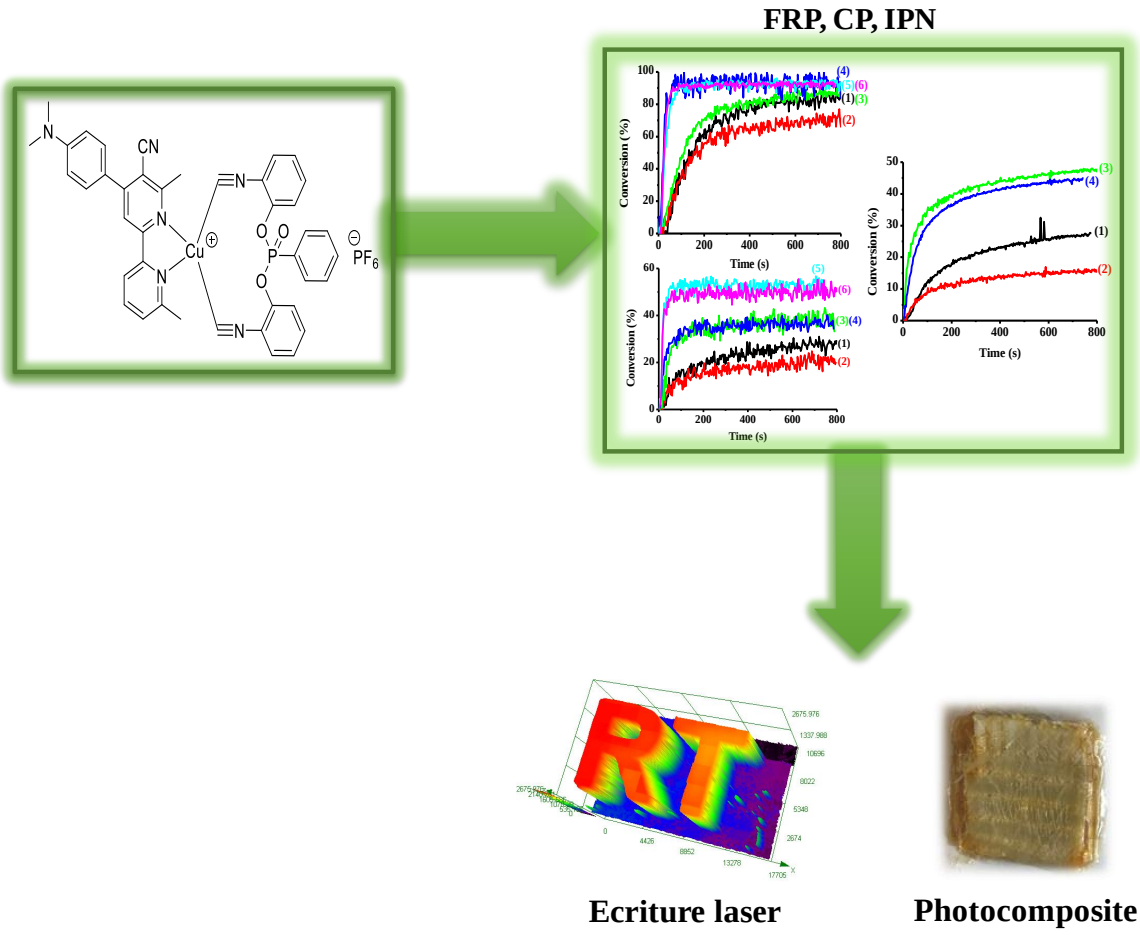

Schéma 1. Capacité de photoamorçage et applications des complexes de cuivre.

Références

[1] Lalevée, J.; Tehfe, M.A.; Dumur, F.; Gigmes, D.; Blanchard, N.; Morlet-Savary, F.; Fouassier, J.P. Iridium Photocatalysts in Free Radical Photopolymerization under Visible Lights. Acs Macro Letters. **2012**, 1(2), 286.

[2] Lalevée, J.; Blanchard, N.; Tehfe, M.A.; Morlet-Savary, F.; Fouassier, J.P. Green Bulb Light Source Induced Epoxy Cationic Polymerization under Air Using Tris (2, 2′-Bipyridine) Ruthenium (II) and Silyl Radicals. Macromolecules. **2010**, 43(24), 10191.

[3] Lalevée, J.; Blanchard, N.; Tehfe, M.A.; Peter, M.; Morlet-Savary, F.; Fouassier, J.P. A Novel Photopolymerization Initiating System Based on an Iridium Complex Photocatalyst. Macromolecular rapid communications. **2011**, 32(12), 917.

[4] Lalevée, J.; Blanchard, N.; Tehfe, M.A.; Peter, M.; Morlet-Savary, F.; Gigmes, D.; Fouassier, J.P. Efficient Dual Radical/Cationic Photoinitiator under Visible Light: A New Concept. Polymer Chemistry. **2011**, 2(9), 1986.

Partie IV : Photoamorceur (PA) organométallique à base de complexes de cuivre.

Novel Copper complexes as visible light photoinitiators for the synthesis of interpenetrating polymer networks (IPNs).

Abstract

This work is devoted to the study of two copper complexes (Cu) bearing pyridine ligands which are synthesized, evaluated and tested as a new high performance visible light photoinitators for the Free Radical photopolymerization (FRP) of acrylates functions in thick and thin sample upon Light Emitting Diode (LED) at 405 and 455nm irradiation. These latter wavelengths are considered to be safe to produce polymer materials. The photoinitiation abilities of these organometallic compounds have been evaluated in combination with Iod salt and/or amine (ex. *N*-phenylglycine – NPG). Interestingly, high final conversions and high polymerization rates were obtained for both compounds using two and three-component photoinitiating systems [Cu1 (or Cu2)/Iodonium salt Iod (0.1%/1% w/w) and Cu1 (or Cu2)/Iod/Amine(0.1%/1%/1% w/w/w)]. The new proposed copper complexes were also used for direct laser write experiments involving a laser diode at 405nm, and for the photocomposite synthesis with glass fibers using a UV-conveyor at 395nm. To explain the obtained poymerization results, different methods and characterization techniques were used : steady state photolysis, real-time Fourier transform infrared spectroscopy (RT-FTIR), emission spectroscopy and cyclic voltammetry.

Keywords : Copper complexe, Photocomposite, LED, Laser Write, Free Radical Photopolymerization.

1. Introduction

The elaboration of polymers by photochemical means such as Free Radical Photopolymerization (FRP) and Cationic Photopolymerization (CP) have been based mainly on the use of metal-free organic dyes and photoinitiators at the industrial and academic level [1-6], these synthetic processes (FRP and CP) are widely used in different fields, e.g, dentistry [7], adhesives [8], coatings [9], composites [10], medicine [11], direct laser write, 3D printing [12] etc. On the other hand, organometallic compounds are not really used in industry, in

other words, manufacturers avoid incorporating metallic compounds in their synthetic formulations due to their potential toxicity and price. With their photochemical properties, like high absorption properties in the near-UV and visible range, long-lived excited states, suitable redox potentials [13-14], copper complexes can be used as photoinitiators (PIs)/photoredox catalysts able to produce active species according to a catalytic cycle. Therefore, it is very important to develop new metal-free photoinitiators or low-cost organometallic based complexes [15,16].

In fact, copper complexes have attracted much attention and intense efforts have been devoted in recent years to the development of new efficient copper complexes photosensitive due to their comparative cost advantage. Copper complexes bearing a pyridine-based chelate ligand showed excellent photochemical properties for photocatalysis process, such as high oxidation potential in the excited state [17-20], long excited-state lifetime, high emission quantum yields and high absorption properties in the UV-visible region. Furthermore, copper complexes derivatives have already been tested as PI for the FRP, CP as well as the IPN synthesis [21-25].

In this paper, two new copper complexes (Cu1 – Cu2) **(Sheme 1)** were synthesized and investigated as visible light photoinitiators upon exposure to LEDs at 405 and 455nm for the FRP, CP and the synthesis of interpenetrating polymer networks (IPNs) of acrylate/epoxy monomer blends. These compounds will be incorporated in two [Cu1 (or Cu2)/Iod (0.1%/1% w/w)] and three-component [Cu1 (or Cu2)/Iod/NPG (0.1%/1%/1% w/w/w)] photoinitiating systems (PISs) to produce polymer materials by Free Radical Photopolymerization and the polymerization of acrylate/epoxy blend (IPNs). The photoinitiation ability of copper complexes will also be explained based on the interaction Cu1 (or Cu2)/Iod and Cu1 (or Cu2)/Iod/NPG which can be studied using different techniques and characterization processes e.g., steady state photolysis, cyclic voltammetry, fluorescence quenching and electron spin resonance spin trapping. Finally, to demonstrate the effectiveness of these new copper complexes-based photoinitiators, experiments by direct laser writing (DLW), 3D printing and photocomposites synthesis were carried out in this work using different irradiation source.

Partie IV : Photoamorceur (PA) organométallique à base de complexes de cuivre.

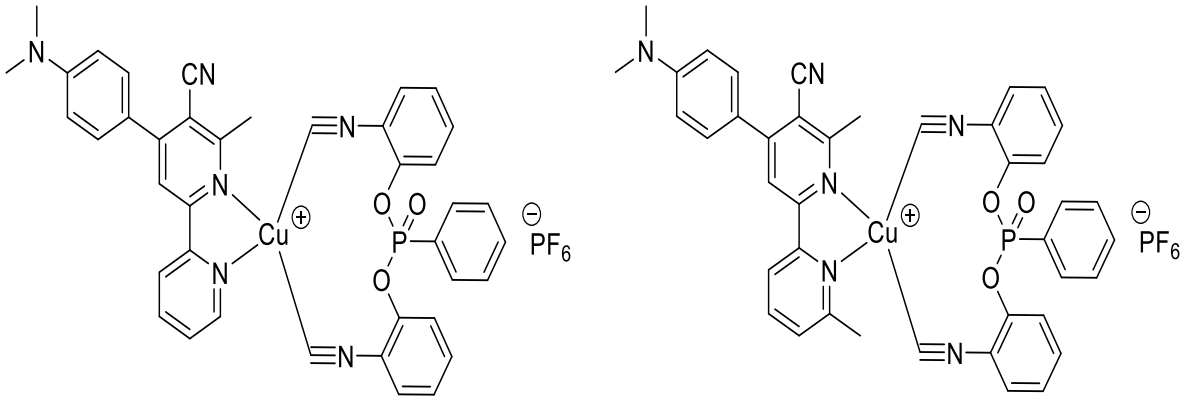

Cu1 **Cu2**

Scheme 1. Copper complexes structure used in this work as PI.

2. Experimental part

2.1. Synthesis of copper complexes

La synthèse de ce couple de complexes de cuivre a été réalisée par nos collaborateurs de l'université d'Aix Marseille (Dr. Frédéric Dumur).

2.2. Other chemicals

All other chemicals used in this work **(Scheme 2)** were selected with the highest purity available and the storage inhibitors of the monomers were not removed before experimentation. Di-tert-butyl-diphenyl iodonium hexafluorophosphate **(Iod)** and ethyl-4-(dimethylamino) benzoate **(EDB)** were obtained from Lambson Ltd (UK) and used as co-initiator and electron donor, respectively. Di(trimethylolpropane) tetraacrylate **(TA)**, Trimethylolpropane triacrylate **(TMPTA)**, (3,4 Epoxycyclohexane)methyl 3,4-epoxycyclohexylcarboxylate (EPOX; Uvacure 1500), N-phenylglycine **(NPG)** (used as electron donor), *N*-Vinylcarbazole (NVK) and N,N-dimethyl-p-toluidine **(TMA)** were obtained from Allnex or Sigma Aldrich. **TA**, **TMPTA**, and **EPOX** were selected as benchmark acrylic and cationic monomers for the radical and cationic polymerizations.

Partie IV : Photoamorceur (PA) organométallique à base de complexes de cuivre.

Additives

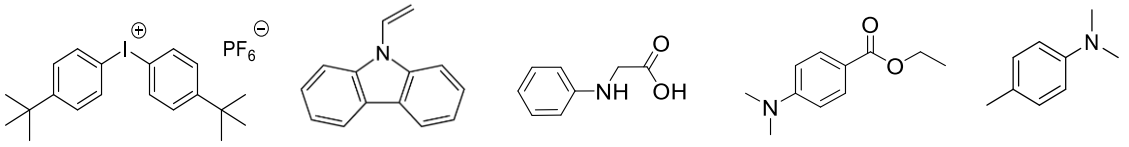

Iod **NVK** **NPG** **EDB** **4-N,N,TMA**

Monomers

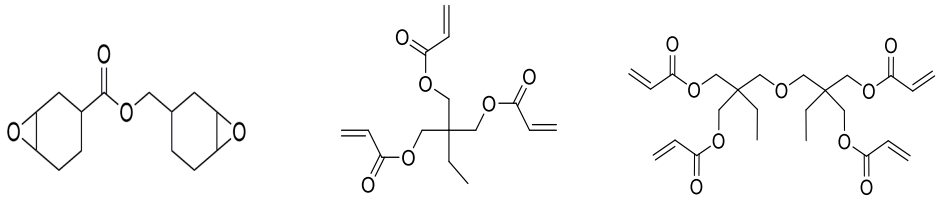

EPOX **TMPTA** **TA**

Scheme 2. Other organic compounds used.

2.3. Irradiation sources : Light Emitting Diodes

All the irradiation sources used in these experiments are based on Light Emitting Diodes (LEDs) as safe sources: **(1)** LED at 375 nm (I_0 = 75 mW.cm^{-2}) for the photolysis experiments, **(2)** LED at 405 nm (I_0 = 110 mW.cm^{-2}) and 455 nm (I_0 = 75 mW.cm^{-2}) for the photopolymerization experiments, **(3)** LED conveyor at 395 nm (I_0 = 4 W.cm^{-2}) for the photocomposite synthesis.

2.4. Photopolymerization kinetics determination by Real-Time Fourier Transform Infrared Spectroscopy (RT-FTIR)

In the present work, copper derivatives are used in two and three-component PISs for both FRP and CP under irradiation with LEDs at 405 and 455 nm. The PISs are mainly based on Cu1 (or Cu2)/Iod (0.1% - 0.2% - 0.5%/1% w/w) and Cu1 (or Cu2)/Iod/amine (NPG, NVK) (0.1%/1%/1% w/w/w). The weight percent of the photoinitiating (PI, co-initiator and amine) system is calculated from the global monomer content. Firstly, two different samples will be studied for each photosensitive formulation in i) thick (thickness = 1.4 mm) and ii) thin sample (thickness = 25 μm). The epoxy and acrylate conversions will be continuously followed by RT-FTIR using a **JASCO FTIR 6600**, so it will be possible to determine the final conversion of reactive functions and to calculate the polymerization rate of each kinetic.

Partie IV : Photoamorceur (PA) organométallique à base de complexes de cuivre.

The acrylate functions in thick and thin samples show peaks towards 6160 cm^{-1} and 1630 cm^{-1} respectively and the epoxide functions show peaks around 3600 cm^{-1} and 790 cm^{-1} for the thick and thin samples respectively.

2.5. Redox Potentials : Electrochemical properties

Redox potentials of copper derivatives were measured in acetonitrile (ACN) by cyclic voltammetry using tetrabutylammonium hexafluorophosphate as supporting electrolyte (potentials vs. Saturated Calomel Electrode-SCE). The free energy change (ΔG_{et}) for an electron transfer reaction was calculated from Equation (1) [26], where E_{ox}, E_{red}, E*, and C represent the oxidation potential of the electron donor, the reduction potential of the electron acceptor, the excited state energy level (determined from fluorescence experiments) and the coulombic term for the initially formed ion pair, respectively. Here, C is neglected asusually done for polar solvents.

$$\Delta G_{et} = E_{ox} - E_{red} - E^* + C \qquad (1)$$

2.6. UV- visible absorption, steady state photolysis and luminescence experiments

UV-visible absorption spectra, molar extinction coefficients and steady state photolysis (irradiation by LED at 375nm or 405nm) of the investigated copper complexes were studied by UV-vis spectroscopy using a JASCO V730 spectrometer. The luminescence properties (fluorescence properties) were studied using a JASCO FP-6200 spectrofluorimeter. These studies were performed in ACN at room temperature using a quartz cell.

2.7. Computational Procedure

Molecular orbital calculations were achieved with the Gaussian 09 suite of programs [27,28]. The electronic absorption spectra of copper compounds were calculated with the time-dependent density functional theory at the MPW1PW91/6-31G* level of theory on the relaxed geometries calculated at the UB3LYP/6-31G* level of theory.

2.8. Photocomposite access using a Near-UV conveyor

Photocomposite materials were obtained using a Dymax-UV conveyor at 395nm. Firstly, the photosensitive resins were deposited on the glass fibers (reinforcement), then, this mixture

is cured using an LED conveyor @395nm (I = 4 W.cm^{-2}). Distance between the belt and the LED was fixed to 15 mm, and the belt speed was fixed at 2 m/min.

2.9. Direct Laser Write (DLW) experiment

The photosensitive formulation is deposited on glass slide and 3D patterns were obtained using a computer-controlled diode laser at 405 nm (spot size = 50µm) which were achieved under air and analyzed by a numerical optical microscope (DSX-HRSU from OLYMPUS Corporation) [29].

3. Results

Light absorption properties, initiation ability and applications (Photocomposite synthesis and direct laser write) of the investigated copper complexes will be studied in this part of the chapter.

3.1. UV-visible absorption spectra of Cu1 and Cu2

The ground state absorption spectra of the new studied copper derivatives have been determined in ACN and the results are presented in **Figure 1.** Extinction coefficients at different emission wavelengths used in photopolymerization experiments are reported in **Table 1.** These new complexes are characterized by a broad absorption band which extends between 380 nm and 550 nm, and high extinction coefficients in the blue region e.g., ε = 10700 M^{-1}cm^{-1}, 6400 M^{-1}cm^{-1} @400 nm for Cu1 and Cu2 respectively. These compounds have also high extinction coefficients at the emission wavelengths of LEDs (at 405nm and 455 nm) used in different experiments achieved in this work, for example $\varepsilon_{@405nm}$ = 10400 and 6800 M^{-1}cm^{-1} for Cu1 and Cu2**,** respectively. Remarkably, a bathochromic shift in the absorption spectra of Cu2 is observed compared to Cu1. This effect can be related to the presence of a methyl group, which is considered an electron donating group (inductive effect), on the pyridine ligands of Cu2 (λ_{max} = 388 nm for Cu1 and 422 nm for Cu2). This difference could also be explained by the optimized geometries as well as the frontier orbitals (Highest Occupied Molecular Orbital - HOMO - and Lowest Unoccupied Molecular Orbital - LUMO) which are shown in **Figure 2.**

Partie IV : Photoamorceur (PA) organométallique à base de complexes de cuivre.

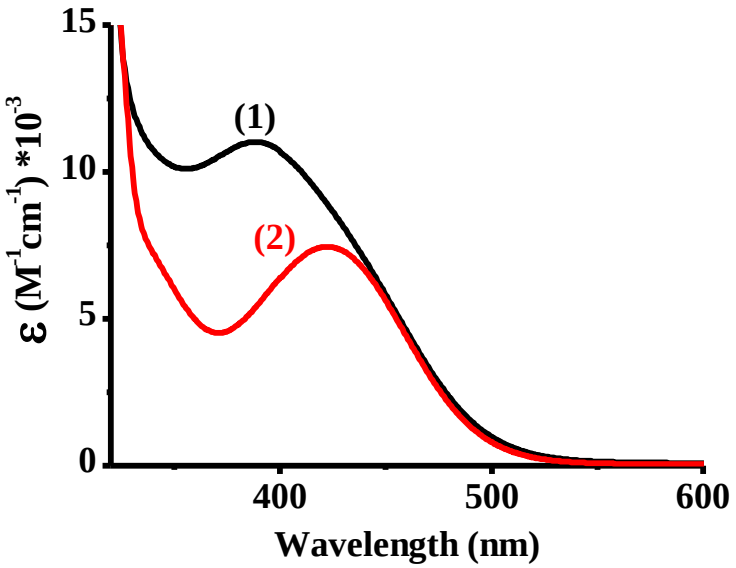

Figure 1. UV-visible absorption spectra of **(1)** Cu1 and **(2)** Cu2 in ACN.

Table 1. Maximum absorption wavelengths (λ_{max}), extinction coefficients at λ_{max}, and molar extinction coefficients for the investigated copper complexes at different emission wavelengths for different LEDs used.

	λ_{max} (nm)	ε_{max} ($M^{-1}cm^{-1}$)	ε_{375nm} ($M^{-1}cm^{-1}$)	ε_{405nm} ($M^{-1}cm^{-1}$)	ε_{455nm} ($M^{-1}cm^{-1}$)
Cu1	388	11000	10700	10400	5200
Cu2	422	7450	4600	6800	5000

Partie IV : Photoamorceur (PA) organométallique à base de complexes de cuivre.

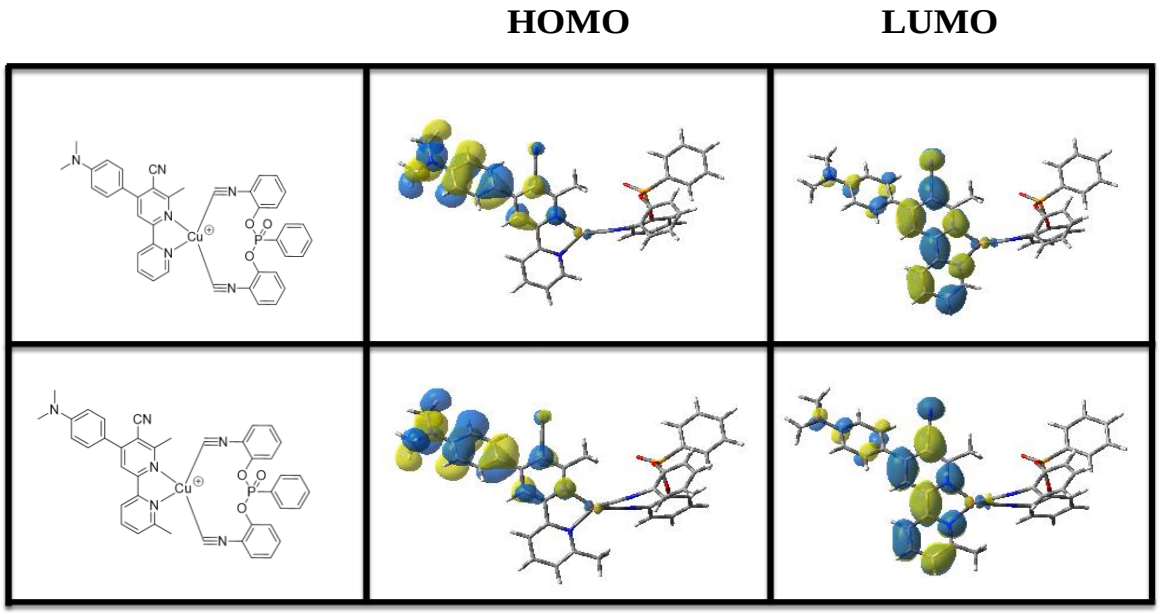

Figure 2. HOMO and LUMO for Cu1 and Cu2 at the UB3LYP/6–31G* level

3.2. Photopolymerization experiments

3.2.1. Free Radical Photopolymerization using TA as benchmarck monomer

Due to their good light absorption properties in the visible range, copper complexes were tested as photoinitiators for the FRP of acrylate-based monomer upon exposure to LEDs at 405nm (I = 110 mW.cm^{-2}) and 455nm (I = 75 mW.cm^{-2}).

In fact, photoinitiators (0.1% or 0.2%) were dissolved and mixed into the TA acrylate monomer in combination with Iod salt (1%) to make a two-component photoinitiating system on the one hand, and in combination with Iod/amine (1%/1% w/w) to form a three-component photoinitiating system on the other hand. Interestingly, these dyes exhibit excellent free radical photopolymerization performance in thick and thin samples. The related results are gathered in **Figure 3** and the data are summarized in the **Table 2.** Remarkably, copper complexe alone, Iod and amine alone cannot polymerize the sample. Iod salt and amine are used as co-initiators in this work because they do not absorb visible light. It is important to introduce the dyes (copper complexes) into the photosensitive formulation to obtain a good light absorption at 405nm and 455nm. The obtained results using copper derivatives in two-component PISs show that Cu2 is more efficient than Cu1 for the FRP of TA using different PI percentage e.g., FC ~ 64% for Cu1/Iod (0.1%/1% w/w) vs. 70% for Cu2/Iod (0.1%/1%

w/w) (**Figure 3A** curve **1** vs.**2**), and FC ~ 62% for Cu1/Iod (0.2%/1% w/w) vs. 85% for Cu2/Iod (0.2%/1% w/w) (**Figure 3A** curve **3** vs. **4**).

Furthermore, Iod/NPG couple shows a weak polymerization initiation ability upon exposure to LEDs at 405nm and 455 nm after 60 s (e,g., FC ~ 10% @405nm). Whereas, a greater efficienct was observed when NPG is incorporated into the formulation, the obtained three-component PISs show a better final conversion of reactive functions and a higher polymerization rate upon irradiation with LEDs at 405nm or 455nm (for example a FC up to 86% is obtained with Cu1/Iod/NPG (0.1%/1%/1% w/w/w), and 88% using Cu2/Iod/NPG (0.1%/1%/1% w/w/w) with a LED @455nm).

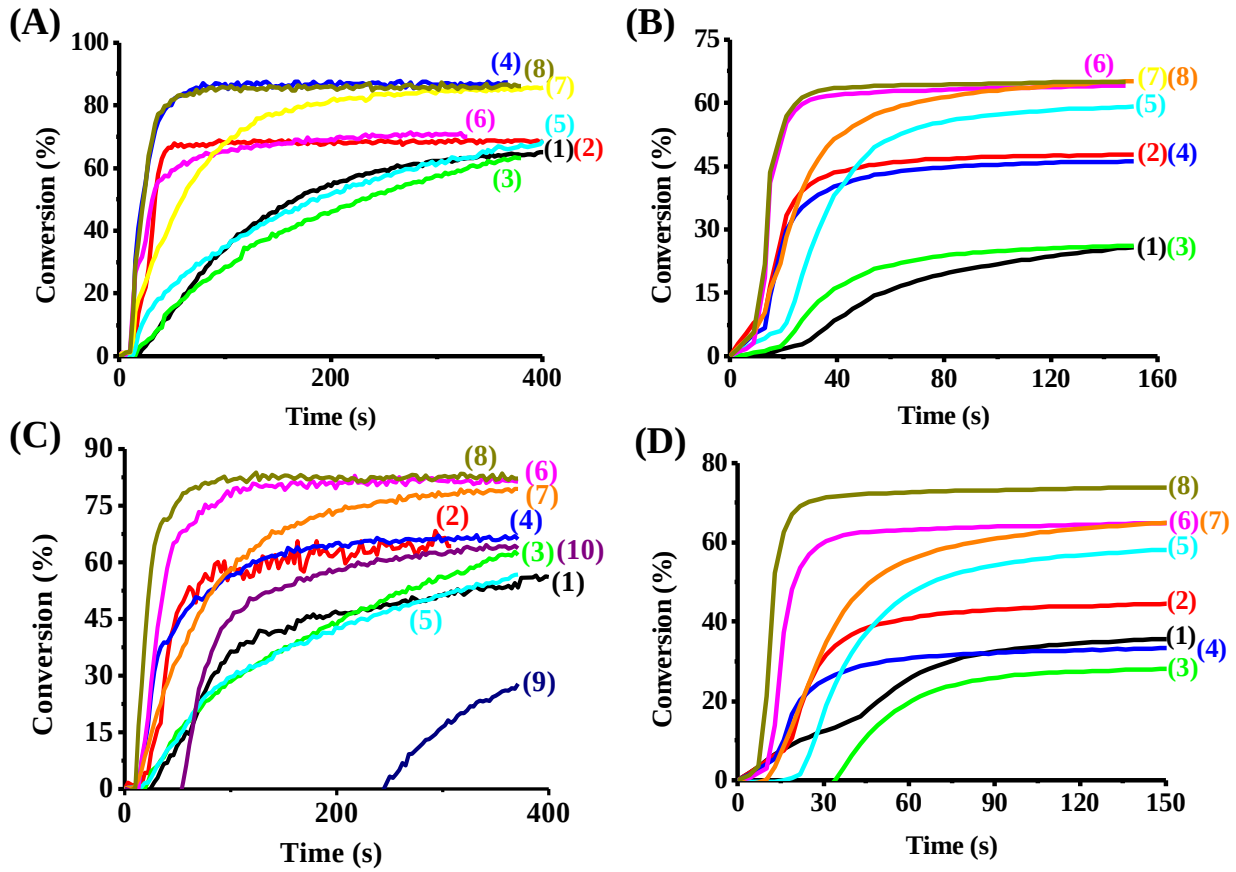

Figure 3. Free Radical Photopolymerization profiles of acrylate functions vs. irradiation time in : **(A)** Thick samples @455nm, **(B)** Thin sample @455nm, **(C)** Thick sample @405nm and **(D)** Thin sample @405nm : **(1)** Cu1/Iod (0.1%/1% w/w), **(2)** Cu2/Iod (0.1%/1% w/w), **(3)** Cu1/Iod (0.2%/1% w/w), **(4)** Cu2/Iod (0.2%/1% w/w), **(5)** Cu1/Iod/EDB (0.1%/1%/1% w/w/w), **(6)** Cu2/Iod/EDB (0.1%/1%/1% w/w/w), **(7)** Cu1/Iod/NPG (0.1%/1%/1% w/w/w), **(8)** Cu2/Iod/NPG (0.1%/1%/1% w/w/w), **(9)** Iod/EDB (1%/1% w/w) and **(10)** Iod/NPG (1%/1% w/w). Irradiation starts at t = 10s.

Table 2. Final reactive functions conversion (FC) for TA monomer using two or three-component PISs upon exposure at different wavelengths (LED at 405 and 455nm).

	At 405nm				At 455 nm			
	Thick sample		Thin sample		Thick sample		Thin sample	
Cu1/Iod	56%[a]	62%[b]	36%[a]	28%[b]	64%[a]	64%[b]	26%[a]	26%[b]
/Cu2/Iod	64%[a]	67%[b]	45%[a]	33%[b]	70%[a]	87%[b]	48%[a]	46%[b]
Cu1/Iod/amine	57%[c]	80%[d]	58%[c]	65%[d]	69%[c]	85%[d]	59%[c]	65%[d]
Cu2/Iod/amine	82%[c]	83%[d]	65%[c]	74%[d]	71%[c]	87%[d]	64%[c]	65%[d]

a : Cu/Iod (0.1%/1% w/w)

b : Cu/Iod (0.2%/1% w/w)

c : Cu/Iod/EDB (0.1%/1%/1% w/w/w)

d : Cu/Iod/NPG (0.1%/1%/1% w/w/w)

3.2.2 Cationic polymerization and IPN synthesis

Typical epoxides function conversion-time profiles for Cu1 and Cu2 based photoinitiating systems are given in **Figure 4** and the data are gathered in **Table 3**. In fact, the cationic polymerization of the epoxide functions was carried out under air and upon irradiation at 405 nm. As expected, copper complexes alone and the additives alone are not able to initiate the CP in these irradiation conditions. The addition of Iod salt or Iod/NVK into the formulation containing the PI induces good photopolymerization profiles i.e. the combination Cu/Iod/NVK (0.1%/2%/3% w/w/w) is very efficient to produce a polymer materials in terms of Rp and final epoxy function conversion compared to Cu/Iod (0.1%/1% w/w), e.g., [FC ~ 50% for Cu1/Iod/NVK (0.1%/2%/3% w/w/w) vs. 27% for Cu1/Iod (0.1%/1% w/w)]. The consumption of epoxide functions is accompanied by the formation of a polyether network (appearence of peak at ~1080 cm^{-1}) characterizing the obtained polymer.

Partie IV : Photoamorceur (PA) organométallique à base de complexes de cuivre.

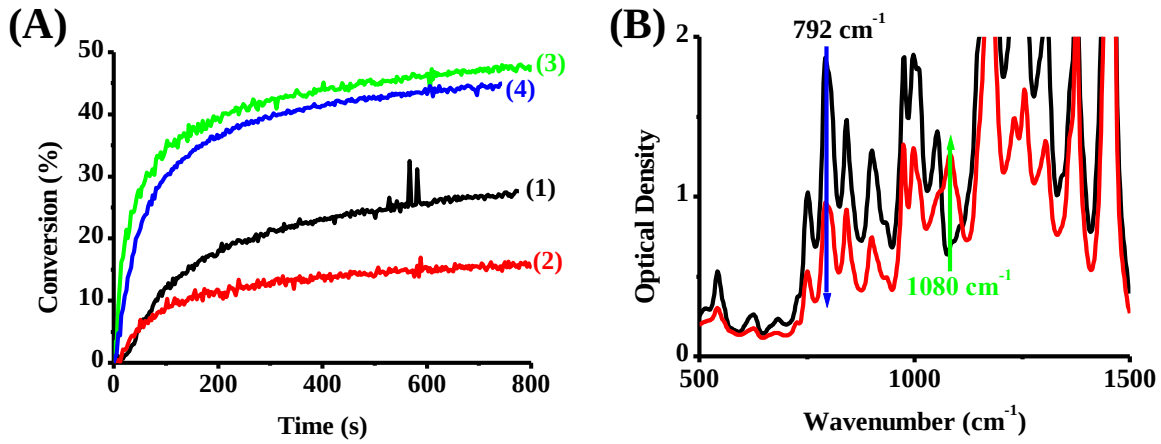

Figure 4. (A) Cationic polymerization (CP) profiles of epoxy functions (Thin sample) vs. irradiation time upon exposure to LED at 405nm : **(1)** Cu1/Iod (0.1%/1% w/w), **(2)** Cu2/Iod (0.1%/1% w/w), **(3)** Cu1/Iod/NVK (0.1%/2%/3% w/w/w) and **(4)** Cu2/Iod/NVK (0.1%/2%/3% w/w/w). **(B):** IR spectra recorded before and after polymerization. Irradiation starts at t = 10 s.

Table 3. Final reactive function conversions for EPOX monomer using two and three-component PISs upon irradiation at 405nm

	Thin sample using a LED at 405nm	
	Cu/Iod (0.1%/1% w/w)	**Cu/Iod/NVK (0.1%/2%/3% w/w/w)**
Cu1	27%	49%
Cu2	16%	45%

On the other hand, the IPNs synthesis was also carried out in this work and the polymerization was performed in thick and thin samples using LED emitting diodes at 405nm and 455nm. The photopolymerization profiles for the IPN formation are presented in **Figure 5.** For example, the acrylic network formation is very fast with a high final conversion (98%) for Cu2/Iod/NPG (0.1%/1%/1% w/w/w) in TA/EPOX (50%/50%) upon irradiation at 455nm, and the formation of epoxy network is also efficient (high final conversion and Rp) using this system (FC ~ 55%).

Partie IV : Photoamorceur (PA) organométallique à base de complexes de cuivre.

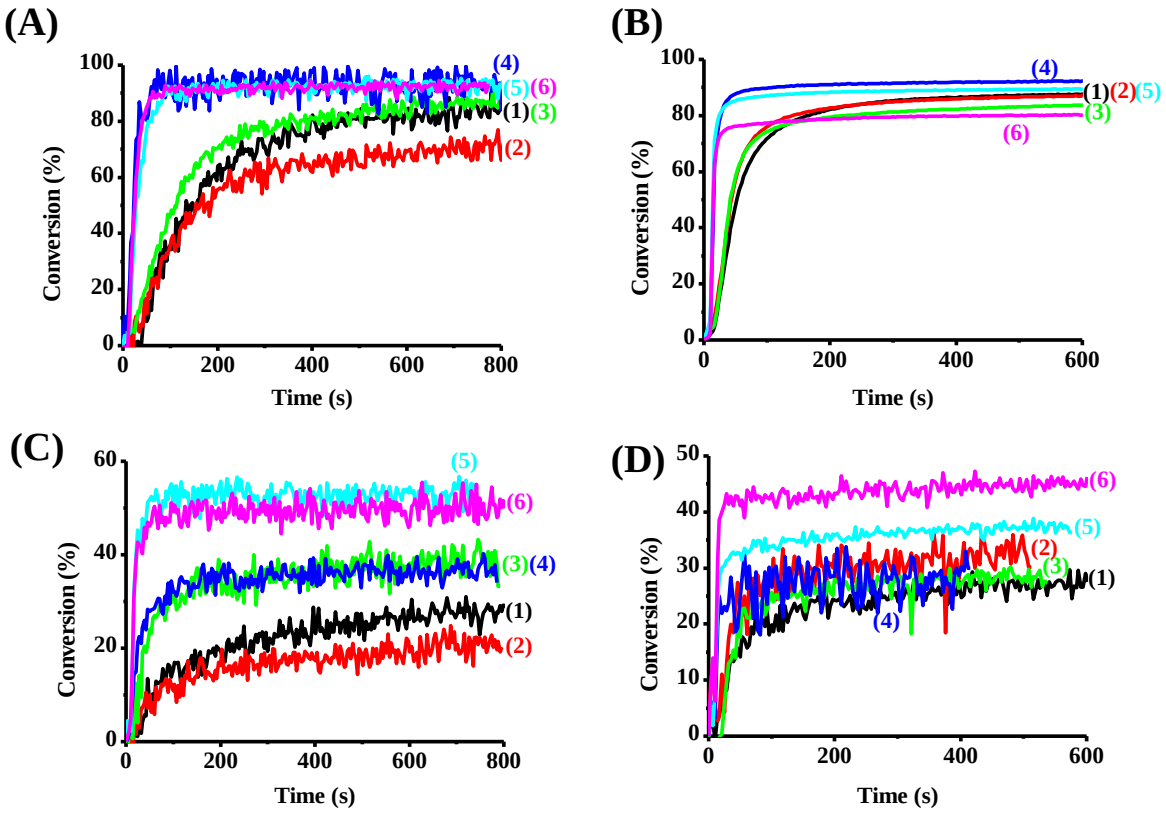

Figure 5. Photopolymerization profiles of acrylate functions **[A (Thick sample), B (Thin sample)]** upon irradiation @455nm, and epoxide function **[C (Thick sample), D (Thin sample)]** upon exposure to LED at 405nm of TA/EPOX using Cu1/Iod/NPG (0.1%/1%/1% w/w/w) : **(1)** 30%/70%, **(2)** 50%/50%, **(3)** 70%/30%, and Cu2/Iod/NPG (0.1%/1%/1% w/w/w) : **(4)** 30%/70%, **(5)** 50%/50%, **(6)** 70%/30%. The irradiation starts at t = 10s.

Table 4. Final conversions of acrylate and epoxides functions for the IPN synthesis of TA/EPOX blend using Cu1 (or Cu2)/Iod/NPG (0.1%/1%/1%/ w/w/w) as PIS upon exposure to visible light at 405 nm.

	IPN synthesis of TA/EPOX blend performed in Thick sample @405nm			**IPN synthesis of TA/EPOX blend performed in Thin sample @405nm**		
	30%/70%	**50%/50%**	**70%/30%**	**30%/70%**	**50%/50%**	**70%/30%**
Cu1	90%/25%	90%/15%	93%/27%	88%/25%	87%/31%	84%/47%
Cu2	99%/30%	98%/20%	96%/38%	92%/22%	90%/35%	80%/32%

Table 5. Final conversions of acrylate and epoxides functions for the IPN synthesis of TA/EPOX blend using Cu1 (or Cu2)/Iod/NPG (0.1%/1%/1%/ w/w/w) as PIS upon exposure to visible light at 455 nm.

	IPN synthesis of TA/EPOX blend performed in Thick sample @455nm			**IPN synthesis of TA/EPOX blend performed in Thin sample @455nm**		
	30%/70%	**50%/50%**	**30%/70%**	**30%/70%**	**50%/50%**	**70%/30%**
Cu1	90%/30%	90%/23%	90%/41%	90%/15%	90%/25%	90%/15%
Cu2	100%/38%	98%/55%	99%/51%	98%/22%	99%/30%	98%/22%

3.3. Photocomposites synthesis

Nowadays, many of our modern technologies require materials with enhanced properties. This is particularly true for materials used in aerospace, underwater and transportation applications. For example, for aeronautical applications engineers research materials with low density, rigid, solid, impact resistant, temperature and pressure resistant and obviously materials that does not easily corroded. For this purpose, composite materials have been used for high performance applications. As definition, a composite material is composed of a least two components that results in better properties than those of the individual components used alone: matrix (monomer blends) and reinforcement. The main advantages of composite materials are their high stiffness, strength and low density. The introduction of light for the synthesis of photocomposites will make the manufacture of these materials more ecological.

In this study, the matrix is based on acrylic monomers such as TMPTA or TA, and the second component (reinforcement) is based on glass fibers. Firstly, the acrylic resins were deposed on the reinforcement (50%/50% w/w) and the mixture were irradiated using a LED conveyor at 395nm. Interstingly, a very fast polymerisation on the surface and the bottom was observed with tack-free surfaces after one pass only using one layer of glass fibers (1 mm). Increasing the reinforcement thickness by adding several layers, the polymerization on the surface is always fast and take place after one pass, but the curing on the bottom is more

complicated and will be done after several passes using Cu1 or Cu2/Iod/NPG (0.1%/1%/1% w/w/w) as PISs. The curing photocomposites results are depicted in **Figure 6** and **Table 6**.

Partie IV : Photoamorceur (PA) organométallique à base de complexes de cuivre.

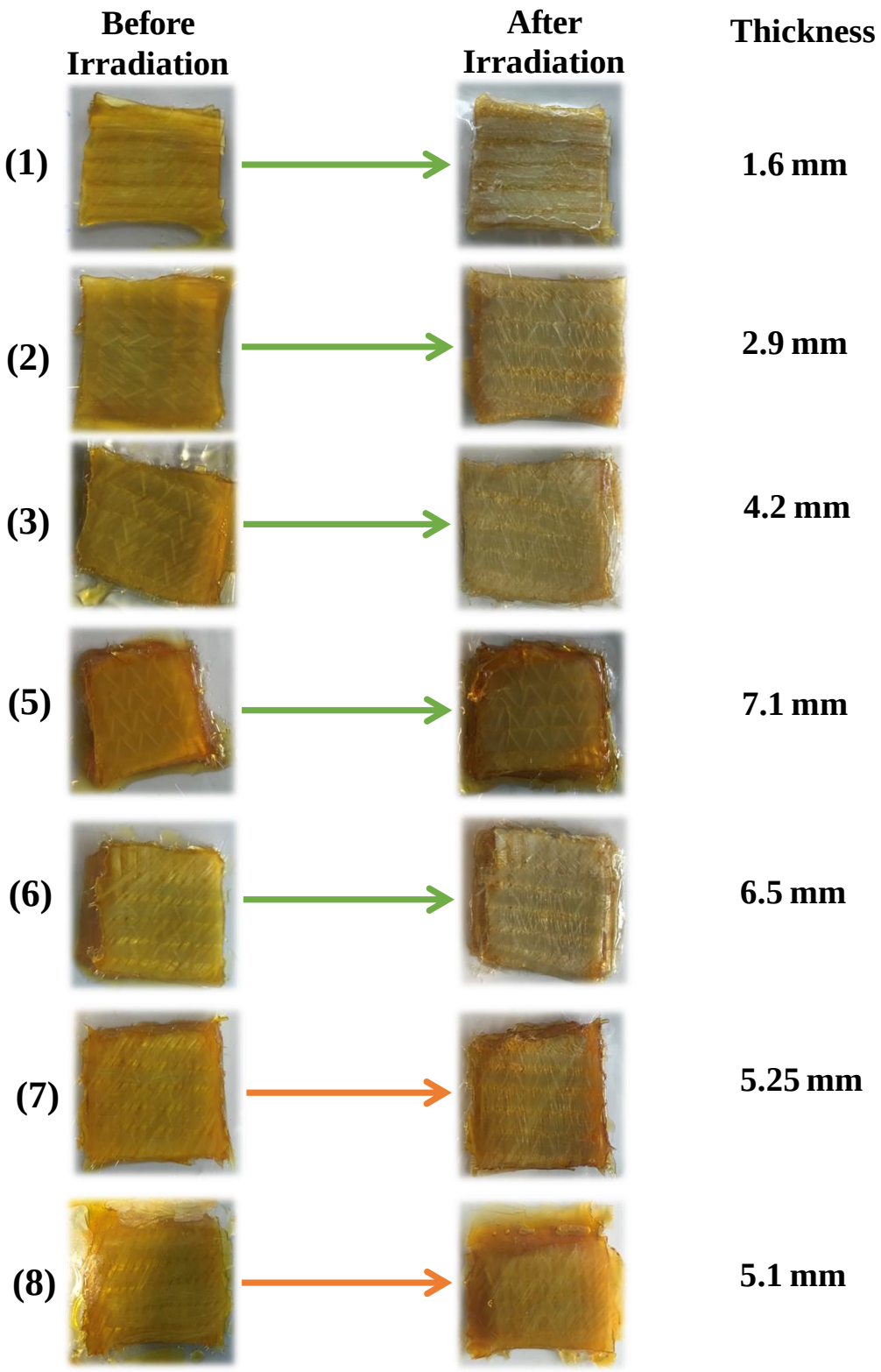

Figure 6. Free Radical photopolymerization for the photocomposites synthesis upon near-UV irradiation at 395nm (4 $W.cm^{-2}$) using Cu2/Iod/NPG (0.1%/1%/1% w/w/w) in TA [(1) – (4)], (5))

Cu2/Iod/NPG (0.1%/1%/1% w/w/w) in TMPTA, (6) Cu1/Iod/NPG (0.1%/1%/1% w/w/w) in TMPTA and (7) Cu1/Iod/NPG (0.1%/1%/1% w/w/w) in TA.

Table 6. Photocomposites synthesis results using TA as acrylic monomer (or TMPTA) and number of passes to reach the Tack-Free character on the surfaces.

	Thickness	**Number of passes to reach Tack-free Character on the Surface**	**Number of passes to reach Tack-free Character on the Bottom**
Cu2/Iod/NPG	1.6 mm	1	1
Cu2/Iod/NPG	2.9 mm	1	2
Cu2/Iod/NPG	4.2 mm	1	6
Cu2/Iod/NPG	7.1 mm	1	25
Cu2/Iod/NPG **(TMPTA)**	6.5 mm	1	30
Cu1/Iod/NPG	5.25 mm	1	40
Cu1/Iod/NPG **(TMPTA)**	5.1 mm	1	45

3.4 Direct Laser Write (DLW)

The new copper complexes were tested in some direct laser write experiments by FRP of TMPTA or TA using a laser diode at 405nm (spot size: 50 μm). The obtained 3D patterns were carried out under air and using different PISs based on Cu1/Iod/TMA, Cu2/Iod/TMA in TA or TMPTA **(Figure 7).** Due to thier high ability to initiate the FRP of acrylates, these systems were able to generate high spatial resolution 3D patterns with a great thickness of curing (~ 2500μm) in the irradiated area. 3D patterns have been generated with a very short irradiation times (2-3 minutes) and they are characterized by numerical microscopy.

Partie IV : Photoamorceur (PA) organométallique à base de complexes de cuivre.

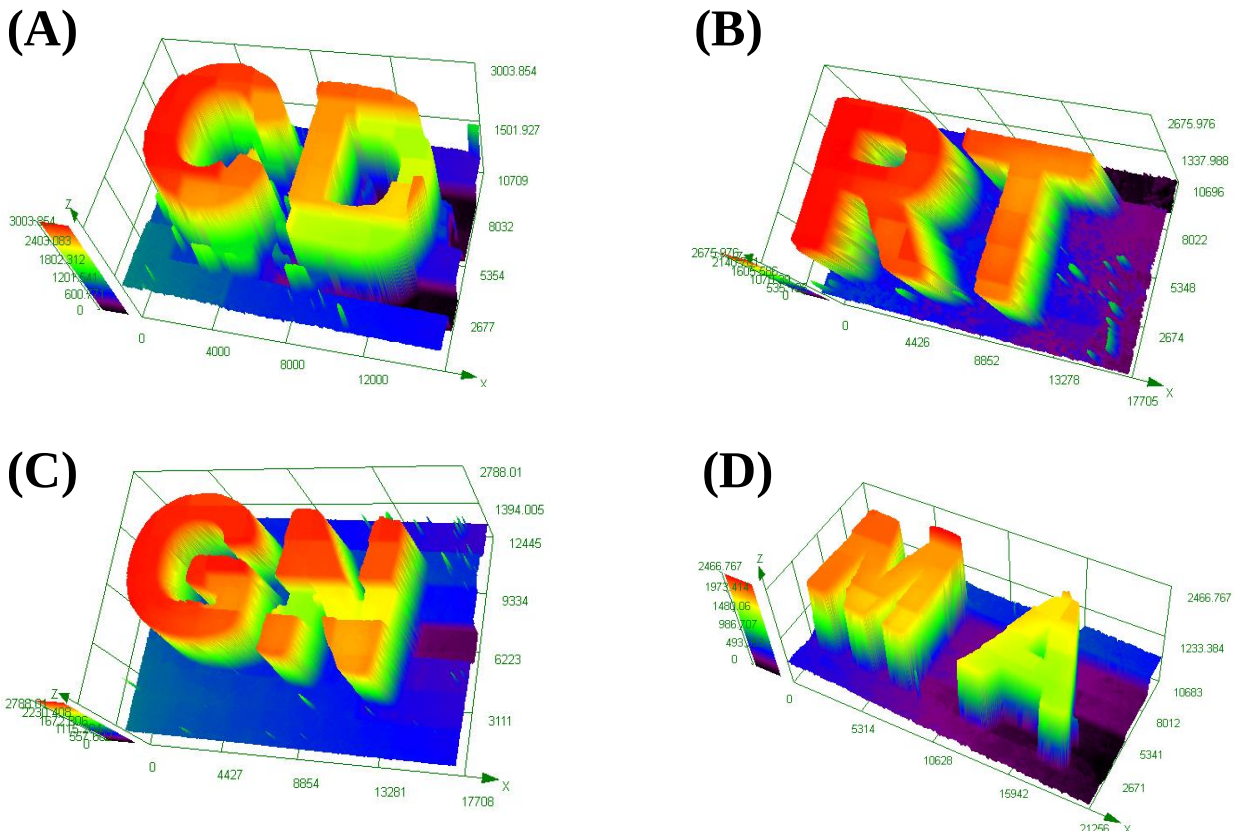

Figure 7 : 3D patterns produced by Free Radical photopolymerization of acrylate functions (TA or TMPTA) using a laser diode at 405nm and their characterization by numerical optical microscopy : **(A)** Cu2/Iod/TMA (0.057%/1%/0.46% w/w/w) in TA, **(B)** Cu1/Iod/TMA (0.058%/0.506%/0.44% w/w/w) in TMPTA; **(C)** Cu2/Iod/TMA (0.048%/0.65%/0.259% w/w/w) in TA and **(D)** Cu1/Iod/TMA (0.05%/0.5%/0.305% w/w/w).

4. Discussion

In order to explain the initiating ability of the organometallic complexes, their photochemical and photophysical properties have been studied using different characterization techniques allowing the characterization of the associated chemical mechanisms.

4.1. Steady state photolysis of the investigated compounds

The photolysis of Cu1 and Cu2 dyes in ACN were investigated upon irradiation at 375nm and 405nm, and the related results are shown in the **Figure 8**. First of all, no photolysis occurs for Cu1 and Cu2 alone (0% consumption) under irradiation at 375 nm and 405nm, but the incorporation of the iodonium salt into the photosensitive solution promotes the degradation

of the dyes, so a strong decrease of the absorbance band intensity was observed by increasing the irradiation time, e.g., consumption ~ 73% @375nm and 80% for Cu2/Iod at 375 nm and 405nm respectively **(Figure 9B)**. It is important to note that the photolysis of Cu1 in the presence of Iod salt involves the formation of a photoproduct after 60 s of irradiation of the solution, which has an absorption band more shifted in the visible (bathochromic effect), then this photoproduct degrades under the effect of the irradiation **(Figure 8A).**

This difference between these two consumption percentages may be due to the high light absorption ability of Cu2 at 405nm as well as the highest intensity of the LED at 405nm (110 mW/cm^{-2}) compared to that @375nm (75 $mW.cm^{-2}$). Furthermore, in case of three-components PISs, the consumption of Cu2 is lower compared to Cu2/Iod, this may be due to the regeneration of Cu2 or the formation of new photoproduct (%consumption ~ 12%).

Partie IV : Photoamorceur (PA) organométallique à base de complexes de cuivre.

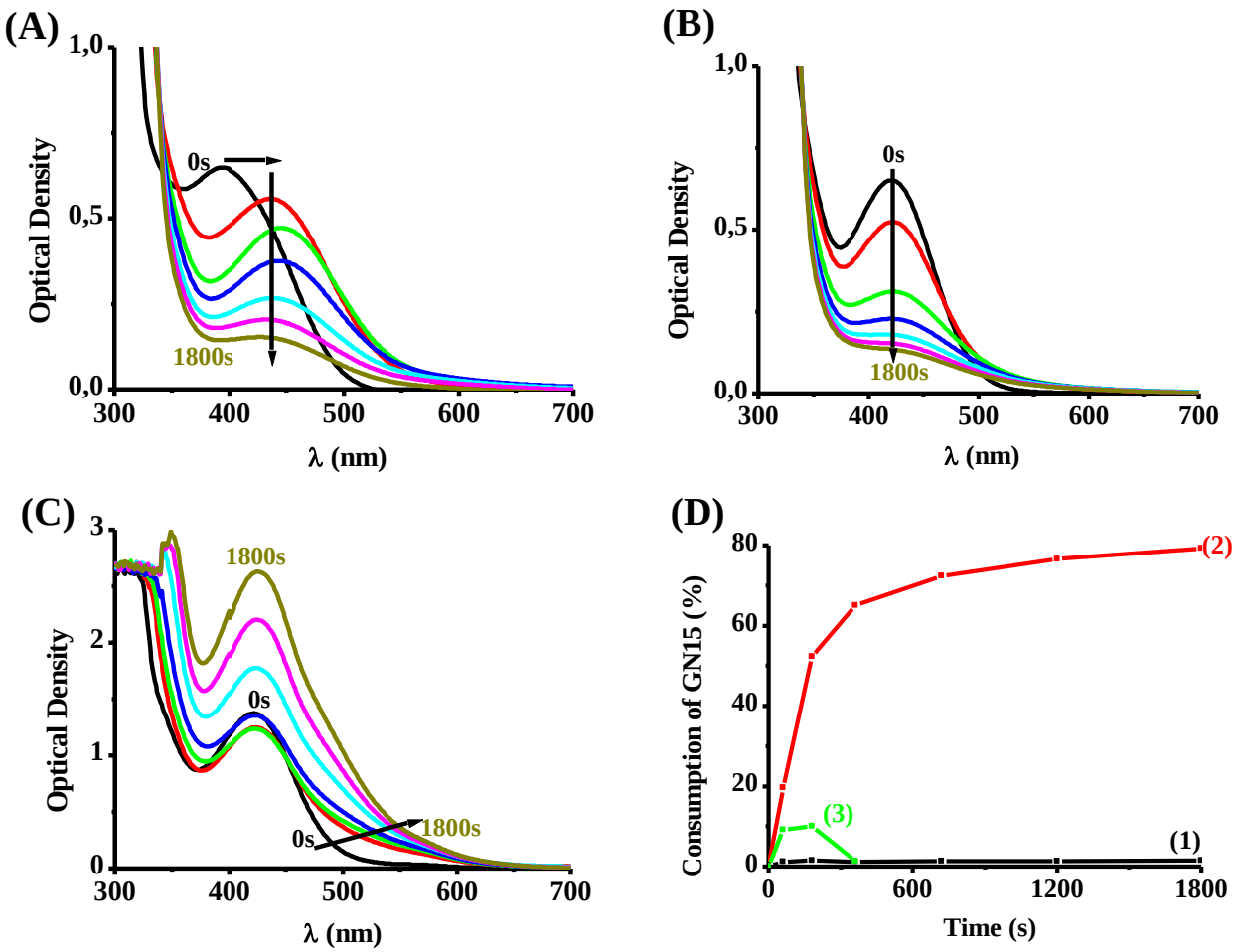

Figure 8. Photolysis experiments of **(A)** Cu1 with Iod salt (10^{-2} M), **(B)** Cu2 with Iod salt (10^{-2} M) and **(C)** Cu2/Iod/NPG (10^{-2} M) upon exposure to LED at 405nm. **(D)** Consumption percentage of Cu2 : **(1)** alone, **(2)** with Iod, **(3)** with Iod/NPG.

Partie IV : Photoamorceur (PA) organométallique à base de complexes de cuivre.

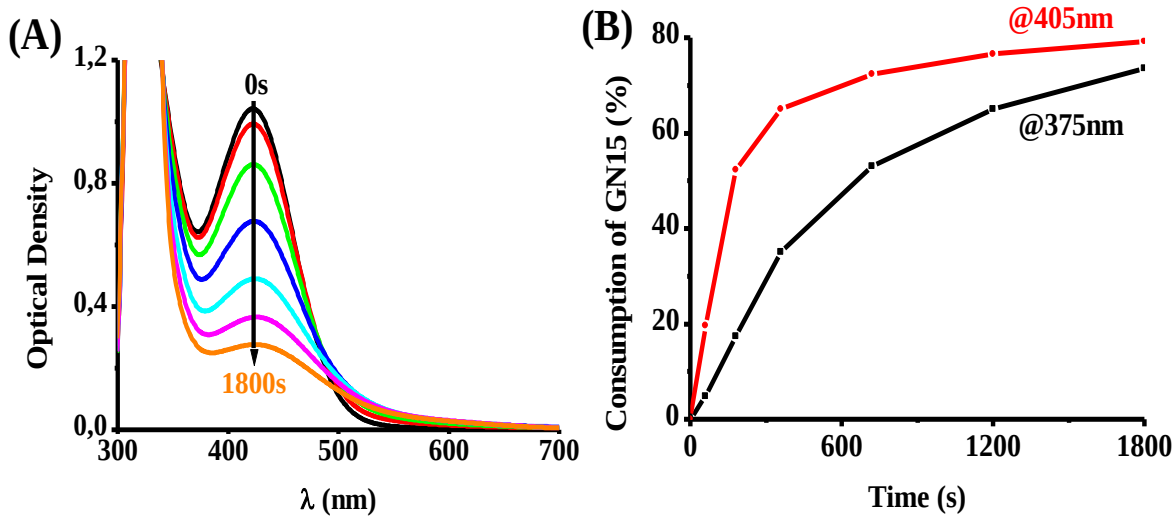

Figure 9. (A) Photolysis of Cu2 With Iod (10^{-2} M) upon irradiation @375nm. **(B)** Consumption of Cu2 with irradiation @375nm and 405nm.

4.2 Photoluminescence and electrochemical properties

Fluorescence emission spectra (measured using a JASCO FP-6200 spectrofluorimeter) and the oxidation potential (measured in ACN by cyclic voltammetry) results of the Cu derivatives are gathered in **Figuer 10** and **Table 7.** The excited state energy was calculated from the crossing point of the emission and absorption spectra. So, the free energy change **(ΔG)** was calculated, this parameter reflects the reactivity between Cu and Iod. In fact, the ΔG value is negative for both complexes, so the photo-oxidation interaction Cu1 (or Cu2)/Iod is favorable in both cases, with a superiority observed for Cu2 (ΔG = -0.74 and 0.62 eV for Cu2 and Cu1 respectively), this explains the high photoinitiation ability of Cu2 compared to Cu1

Partie IV : Photoamorceur (PA) organométallique à base de complexes de cuivre.

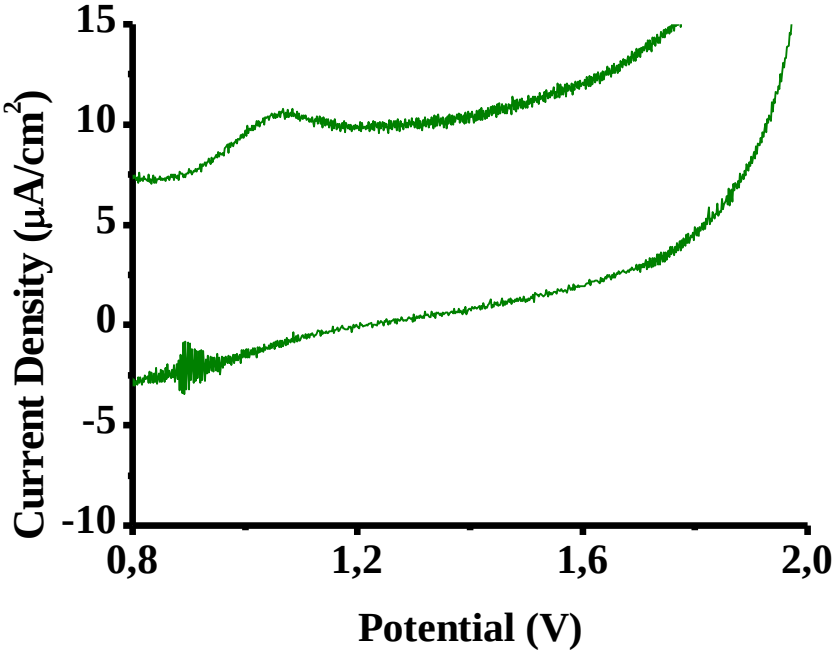

Figure 10. Oxidation potential determination of Cu2.

Table 7. Parameters characterizing the chemical mechanisms between Cu1 (or Cu2) and Iod. For Iod, a reduction potential of -0.7 eV was used for the ΔGet calculations.

	E_{ox} (V)	E_{S1} (eV)	$\Delta G_{(Cu/Iod)}$ (eV)
Cu1	1.07	2.39	-0.62
Cu2	0.97	2.41	-0.74

Finally, the initiation ability of the new copper complexes has been explained by different characterization techniques which allows us to propose a chemical photoinitiation mechanism. Firstly, Cu are excited upon irradiation at 405 or 455nm and interact with Iod to generate aryl radical ($Ar^{\bullet}$) and radical $Cu^{\bullet+}$ [r1-r2]. A charge transfer complexe **CTC** is formed after adding the NPG into the photosensitive formulation, this complex is able to produce aryl radical as active species for the radical photpolymerization [r3-r4]. Then, $^{1,3}Cu$ could react with NPG and generate two radicals ($NPG_{-H}^{\bullet}$, $Cu\text{-}H^{\bullet}$) [r5], the first radical undergoes a decarboxylation and produce active radical ($NPG_{(-H,-CO2)}^{\bullet}$) [r6], this radical leads to the formation of two active species after interaction with Iod salt ($NPG_{(-H,-CO2)}^{+}$, $Ar^{\bullet}$) [r7]. Lastly, copper complexes derivatives are regenerated [r8-r9].

$Cu\ (h\nu) \rightarrow {}^{1,3}Cu$ r1

${}^{1,3}Cu + Ar_2I^+ \rightarrow Ar^\bullet + ArI + Cu^{\bullet+}$ r2

$NPG + Iod \rightarrow [NPG\text{-}Iod]_{CTC}$ r3

$[NPG\text{-}Iod]_{CTC} \rightarrow Ar^\bullet$ r4

${}^{1,3}Cu + NPG \rightarrow Cu\text{-}H^\bullet + NPG_{(-H)}{}^\bullet$ r5

$NPG_{(-H)}{}^\bullet \rightarrow NPG_{(-H;-CO2)}{}^\bullet + CO_2$ r6

$NPG_{(-H;-CO2)}{}^\bullet + Ar_2I^+ \rightarrow NPG_{(-H;-CO2)}{}^+ + Ar^\bullet + ArI$ r7

$Cu^{\bullet+} + NPG \rightarrow Cu + NPG^+$ r8

$Cu\text{-}H^\bullet + Ar_2I^+ \rightarrow Ar^\bullet + ArI + Cu + H^+$ r9

Scheme 3. Proposed chemical mechanisms

5. Conclusion

In the present paper, new copper complexes have been synthesized and tested as photoinitiators. These compounds have strong visible light absorption and are able to initiate both the free radical photopolymerization and cationic polymerization. The IPN synthesis by simultaneous polymerization of acrylate/epoxy monomer blends was performed under air upon irradiation at 405nm and 455nm using a very low quantity of copper complex in two or three component PIS. Cu2 showed a very interesting photoinitiation capacity compared to Cu1 in terms of final conversion of reactive functions and polymerization rates. The high reactivity of these compounds have been demonstrated by some direct laser write experiments where high spatial resolution 3D patterns are obtained. In addition, the synthesis of thick glass fiber photocomposites was possible. This work paves the way for the development of new organometallic photoinitiators.

Partie IV : Photoamorceur (PA) organométallique à base de complexes de cuivre.

References

[1] Fouassier, J.P.; Lalevée, J. Photoinitiators for Polymer Synthesis, Scope, Reactivity, and Efficiency; Wiley-VCH Verlag, Weinheim, **2012**.

[2] Fouassier, J.P. Photoinitiator, Photopolymerization and Photocuring : Fundamentals and Applications, Hanser Publishers, Munich, **1995**.

[3] Dietliker, K.A. Compilation of Photoinitiators Commercially Available for UV Today, Sita Technology Ltd., London, **2002**.

[4] Davidson, S. Exploring the Science, Technology and Application of UV and EB Curing, Sita Technology Ltd., London, **1999**.

[5] Crivello, J.V.; Dietliker, K.; Bradley, G. Photoinitiators for Free Radical Cationic & Anionic Photopolymerisation; John Wiley &Sons: Chichester, U.K., **1999**.

[6] Cunningham, A.F.; Desobry. V. In Radiation Curing in Polymer Science and Technology, Fouassier, J.P.; Rabek, J.F. Eds.; Elsevier: Barking, UK, **1993**, 2, 323.

[7] Bouzrati-Zerelli, M.; Maier, M.; Dietlin, C.; Morlet-Savary, F.; Fouassier, J.P.; Klee, J.E.; Lalevée, J. A novel photoinitiating system producing germyl radicals for the polymerization of representative methacrylate resins: Camphorquinone/R3GeH/iodoniumsalt. Dent. Mater. **2016**, 32, 1226.

[8] Maruno, T.; Murata, N. Properties of a UV-Curable,Durable Precision Adhesive. J.Adhes. Sci.Technol., 1995, 9, 1343.

[9] Wu, L.; Baghdachi, J. Functional Polymer Coatings: Principles, Methods, and Applications. Wiley Series on Polymer Engineering and Technology: New York, NY, USA, **2015**.

[10] Mokbel, H.; Anderson, D.; Plenderleith, R.; Dietlin, C.; Morlet-Savary, F.; Dumur, F.; Gigmes, D.; Fouassier, J.P.; Lalevee, J. Copper Photoredox Catalyst “G1” : A New High Performance Photoinitiator for near-UV and Visible LEDs. Polym. Chem., **2017**, 8, 5580.

[11] Pereira, R.F.; Bártolo, P.J. Photopolymerizable Hydrogels in Regenerative Medicine and Drug Delivery, in Hot Topics in Biomaterials. Future Science Book Series, Future Science Ltd. **2014**, 6.

Partie IV : Photoamorceur (PA) organométallique à base de complexes de cuivre.

[12] Lee, J.Y.; An, J.; Chua, C.K. Fundamentals and Applications of 3D Printing for Novel Materials. Appl. Mater. Today. **2017**, 7, 120.

[13] Fors, B.P.; Hawker, C.J. Control of a Living Radical Polymerization of Methacrylates by light. Angew. Chem., Int. Ed., **2012**, 51, 8850.

[14] Ohtsuki, A.; Goto, A.; Kaji, H. Visible-Light-Induced Reversible Complexation Mediated Living Radical Polymerization of Methacrylates with Organic Catalysts. Macromolecules. **2013**, 46, 96.

[15] Zivic, N.; Bouzrati-Zerelli, M.; Kermagoret, A.; Dumur, F.; Fouassier, J.P.; Gigmes, D.; Lalevée, J. Photocatalysts in Polymerization Reactions. ChemCatChem, **2016**, 8, 1617.

[16] Baralle, A.; Fensterbank, L.; Goddard. J.P.; Ollivier, C. Aryl Radical Formation by Copper (I) Photocatalyzed Reduction of Diaryliodonium Salts. NMR Evidences for a Cu (II)/Cu (I) Mechanism. Chem.Eur.J. **2013**, 19, 10809.

[17] Paria, S.; Reiser, O. Copper in Photocatalysis. ChemCatChem, **2014**, 6, 2477.

[18] Reiser, O. Shining Light on Copper: Unique Opportunities for Visible-Light-Catalyzed Atom Transfer Radical Addition Reactions and Related Processes. Acc.Chem.Res., **2016**, 49, 1990.

[19] Hernandez-Perez, A.C.; Collins, S.K. Heteroleptic Cu-Based Sensitizers in Photoredox Catalysis.Acc.Chem. Res., **2016**, 49, 1557.

[20] Hernandez-Perez, A.C.; Collins, S.K. A visible-light-mediated synthesis of carbazoles. Angew.Chem., Int.Ed., **2013**, 52, 12696.

[21] Mau, A.; Dietlin, C.; Dumur, F.; Lalevee, J. Concomitant initiation of radical and cationic polymerisations using new copper complexes as photoinitiators: Synthesis and characterisation of acrylate/epoxy interpenetrated polymer networks. Eur.Polym.J. **2021**, 152, 110457.

[22] Mau, A.; Noirbent, G.; Dietlin, C.; Graff, B.; Gigmes, D.; Dumur, F.; Lalevee, J. Panchromatic Copper Complexes for Visible Light Photopolymerization Photochem, **2021**, 1, 167.

Partie IV : Photoamorceur (PA) organométallique à base de complexes de cuivre.

[23] Mokbel, H.; Anderson, D.; Plenderleith, R.; Dietlin, C.; Morlet-Savary, F.; Dumur, F.; Gigmes, D.; Fouassier, J.P.; Lalevee, J. Simultaneous initiation of radical and cationic polymerization reactions using the "G1" copper complex as photoredox catalyst : Applications of free radical/cationic hybrid photopolymerization in the composites and 3D printing fields Prog.Org.Coat., **2019**, 132, 50.

[24] AL Mousawi, A.; Kermagoret, A.; Versace, D.L.; Toufaily, J.; Hamieh, T.; Graff, B.; Dumur, F.; Gigmes, D.; Fouassier, J.P.; Lalevee, J. Copper photoredox catalysts for polymerization upon near UV or visible light: structure/reactivity/efficiency relationships and use in LED projector 3D printing resins. Polym.Chem. 2017, **8**, 568.

[25] Mokbel, H.; Anderson, D.; Plenderleith, R.; Dietlin, C.; Morlet-Savary, F.; Dumur, F.; Gigmes, D.; Fouassier, J.P.; Lalevee, J. Copper photoredox catalyst " G1" : a new high performance photoinitiator for near-UV and visible LEDs Polym.Chem. 2017, **8**, 5580.

[26] Wang, X.; Bai, X.; Su, D.; Zhang, Y.; Li, P.; Lu, S.; Gong, Y.; Zhang, W.; Tang, B. Simultaneous Fluorescence Imaging Reveals N-Methyl-d-aspartic Acid Receptor Dependent Zn2+/H+ Flux in the Brains of Mice with Depression. Anal. Chem. **2020**, 92, 4101.

[27] Foresman, J.B.; Frisch, A. Exploring Chemistry with Electronic Structure Methods, second ed., Gaussian Inc., Pittsburgh, PA, **1996**.

[28] Frisch, M.J.; Trucks, G.W.; Schlegel, H.B.; Scuseria, G.E.; Robb, M.A.; Cheeseman, J.R.; Zakrzewski, V.G.; Montgomery, J.A.; Stratmann, J.R.E.; Burant, J.C.; Dapprich, S.; Millam, J.M.; Daniels, A.D.; Kudin, K.N.; Strain, M.C.; Farkas, O.; Tomasi, J.; Barone, V.; Cossi, M.; Cammi, R.; Mennucci, B.; Pomelli, C.; Adamo, C.; Clifford, S.; Ochterski, J.; Petersson, G.A.; Ayala, P.Y.; Cui, Q.; Morokuma, K.; Salvador, P.; Dannenberg, J.J.; Malick, D.K.; Rabuck, A.D.; Raghavachari, K.; Foresman, J.B.; Cioslowski, J.; Ortiz, J.V.; Baboul, A.G.; Stefanov, B.B.; Liu, G.; Liashenko, A.; Piskorz, P.; Komaromi, I.; Gomperts, R.; Martin, R.L.; Fox, D.J.; Keith, T.; Al-Laham, M.A.; Peng, C.Y.; Nanayakkara, A.; Challacombe, M.; Gill, P.M.W.; Johnson, B.; Chen, W.; Wong, M.; Andres, J.L.; Gonzalez, C.; Head-Gordon, M.; Replogle, E.S.; Pople, J.A. Gaussian 03, Revision B-2, Gaussian Inc., Pittsburgh, PA, **2003**.

[29] Al Mousawi, A.; Dumur, F.; Garra, P.; Toufaily, J.; Hamieh, T.; Goubard, F.; Bui, T.T.; Graff, B.; Gigmes, D.; Fouassier, J.P.; Lalevee, J. Azahelicenes as visible light photoinitiators

for cationic and radical polymerization: Preparation of photoluminescent polymers and use in high performance LED projector 3D printing resins. J. Polym. Sci. A Polym. Chem. **2017**, 55, 1189.

Partie Expérimentale

1. Spectroscopie infrarouge a transformée de Fourier

1.1. Généralités

La Spectroscopie Infrarouge à Transformée de Fourier est une technique spectroscopique qui permet de caractériser les groupements fonctionnels présents dans les molécules organiques (OH, NH_2, acrylate…), elle sert donc pour l'identification d'un composé ou même déterminer la composition d'un échantillon. Elle traite la région Infrarouge du spectre électromagnétique qui correspond à la différence d'énergie entre deux états vibrationnels. Dans notre travail, cette technique est adaptée à l'étude des réactions de photopolymérisation par un suivi cinétique du processus de polymérisation en suivant la variation de l'intensité de la bande caractérisant les doubles liaisons des (méth)acrylates, les fonctions époxydes des monomères cationiques... le spectre de vibration de la formulation photosensible se voit donc modifié avec le temps d'irradiation **(Figure 1).**

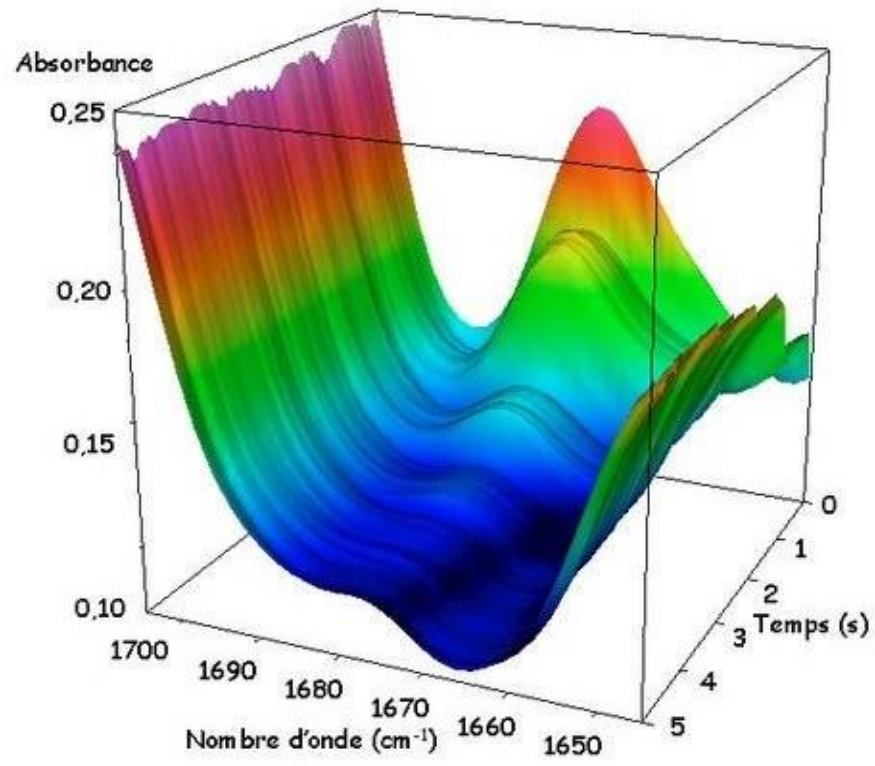

Figure 1 : Suivi de la disparition de la bande 1650-1700 cm^{-1} par spectroscopie infrarouge en temps réel (notée Real-Time FTIR (RT-FTIR) en anglais)

La Spectroscopie à Transformée de Fourier (FTIR) repose sur l'utilisation d'un interféromètre de Michelson qui module le rayonnement IR d'analyse. Par démodulation du signal reçu, un spectre IR de l'échantillon en un temps très court est obtenu. Elle permet de suivre une réaction avec une bonne résolution temporelle (< sec) particulièrement bien adaptée à la réaction de photopolymérisation.

1.2. Principe

Le principe de la FTIR en temps réel consiste à irradier la formulation photosensible par un rayonnement UV-visible capable d'induire le processus de polymérisation et l'exposer simultanément à un faisceau d'analyse IR **(Figure 2).** L'avancement de la polymérisation relative à la décroissance de l'intensité des bandes caractéristiques des fonctions acrylates ou époxydes peut ainsi être suivie en continu. La vitesse à laquelle les bandes disparaissent ou diminuent est lié à la capacité d'amorçage du photoamorceur mis en jeu.

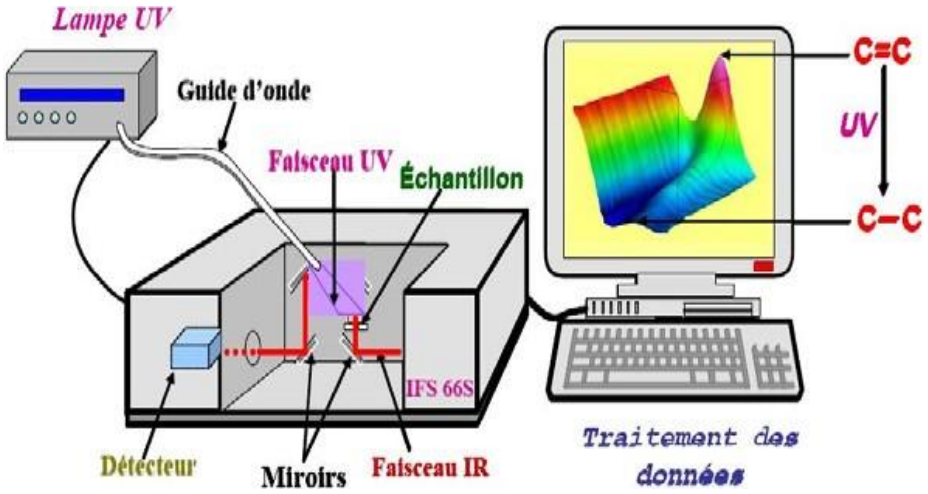

Figure 2 : Montage expérimental.

L'analyse quantitative par spectroscopie IR est basée sur la loi de Beer-Lambert relative à l'absorption lumineuse. Le dispositif expérimental utilisé est un spectromètre JASCO FTIR 6600 couplé avec des sources énergétiques telles que des diodes électroluminescentes (LEDs) en utilisant une fibre optique assurant le trajet de la lumière d'irradiation. Les spectres d'émission des LED sont présentés dans la **Figure 3.**

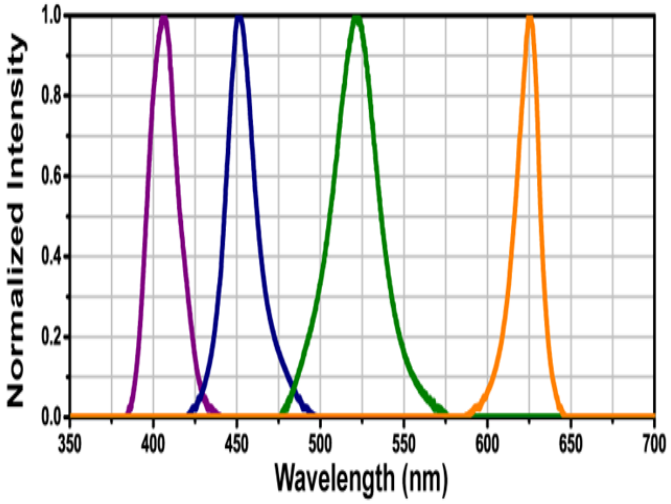

Figure 3 : Spectres d'emission des diodes electroluminescentes

1.3. Préparation de formulation

1.3.1. Polymérisation en laminé

Ce type de mise en œuvre est utilisé pour réduire l'effet de l'inhibition par l'oxygène et par la suite comparer l'effet de l'O_2 sur le processus de polymérisation. En effet, la résine est appliquée entre deux films de polypropylène **(Figure 4)**, le contrôle de l'épaisseur dépend de la viscosité de la résine choisie et est réalisé soit par la mesure de l'absorbance de la bande IR étudiée (pour les résines relativement ou peu visqueuses comme le **TMPTA, TA Ebecryl 605**…), soit par l'utilisation d'un anneau de téflon de 25 µm d'épaisseur (cas de monomères fluides tels que **HDDA, MMA**…).

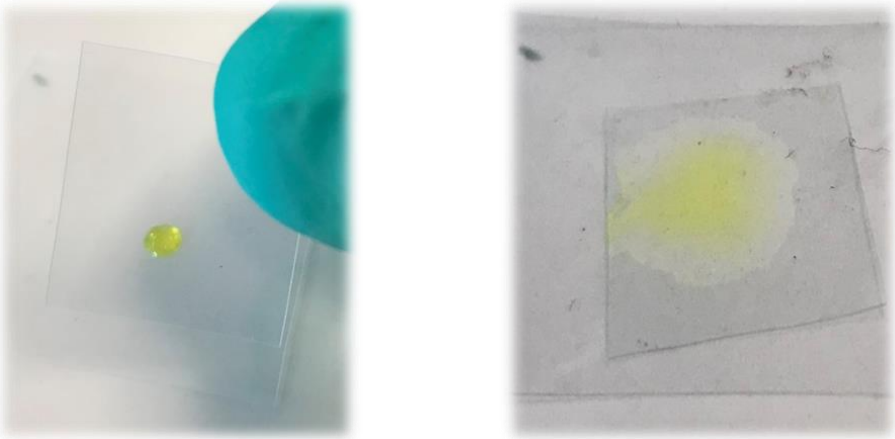

Figure 4 : Mise en œuvre de la polymérisation en laminé

Le dioxygène initialement présent sera rapidement consommé par le système photoamorceur en donnant une petite période d'inhibition et n'entrera plus en compte par la suite lors de la cinétique de polymérisation.

1.3.2. Polymérisation sous air

Ce montage permet d'étudier l'effet de l'O_2 sur le mécanisme réactionnel lors de la photopolymérisation. En effet, la résine photosensible est appliquée dans une moule de 1.4 mm d'épaisseur **(Figure 5)** et les résultats obtenus seront comparés avec ceux obtenus en laminé ce qui permet de voir si on a un effet significatif de l'oxygène.

Figure 5 : Mise en œuvre sous air.

1.3.3. Grandeurs caractéristiques

Les résultats de photopolymérisations obtenus par RT-FTIR sont des surfaces 3D **(Figure 1)** représentant l'absorbance en fonction de deux paramètres : **le nombre d'ondes** et **le temps.** On peut donc extraire, soit un spectre à un temps donné, soit l'évolution temporelle de l'absorbance pour un nombre d'onde donné.

Le nombre d'onde observé varie en fonction des monomères choisis ainsi du procédé de polymérisation (en laminé ou sous air). Par exemple, les systèmes à base de monomères acryliques tels que **l'Ebecryl 605** ou **le TA** présentent des bandes d'absorption caractéristiques dans l'IR vers **1635 cm^{-1}** pour une polymérisation en laminé, d'autre monomères tel que le **TMPTA et l'EPT** présentent des pics plutôt vers **1650 cm^{-1}.**

Il est donc possible d'obtenir un profil de polymérisation de monomères acryliques en suivant l'évolution du taux de conversion au cours du temps **(Figure 6).** En effet, le taux de conversion est lié directement à l'évolution des pics caractéristiques des monomères étudiés après avoir lancé l'irradiation :

$$\varphi(t) = \frac{A^0_{1635} - A^t_{1635}}{A^0_{1635}}$$

A^0 et A^t représentent respectivement l'aire de la bande d'absorption IR à 1635 cm^{-1} avant et après irradiation au temps (t).

À partir de cette courbe de conversion, il est possible de déterminer les paramètres suivants :

- La période d'induction de la polymérisation due à la présence d'inhibiteurs (oxygène, stabilisants...).
- La vitesse de polymérisation maximale **(Rp)** que l'on égale à la tangente à la courbe donnant le taux de conversion en fonction du temps dans les premiers instants de la réaction **(Figure 6).**
- La conversion finale (FC).

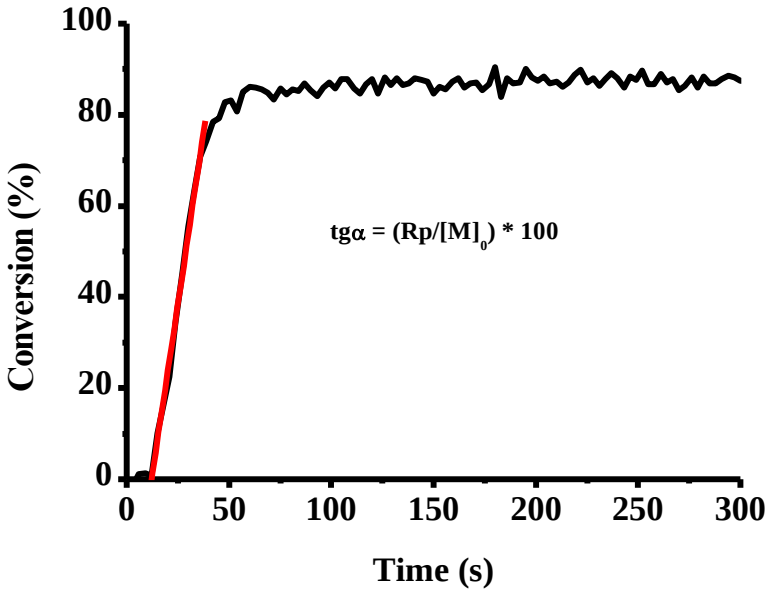

Figure 6 : Méthode de détermination de la vitesse de polymérisation.

2. Spectroscopie d'absorption UV-visible

Cette technique spectroscopique de caractérisation porte sur l'absorption de la lumière **UV et/ou visible** (200-800 nm) par une solution connue (e.g. colorants organiques…). En effet, le principe consiste à provoquer la transition d'électrons entre différentes orbitales moléculaires (niveaux énergétiques) de la molécule.

Cette méthode suit la loi de Beer-Lambert : soit une lumière monochromatique traversant une solution absorbante de concentration C contenue dans une cuve d'épaisseur l. Une partie de ce rayonnement sera absorbée par l'échantillon et une autre partie sera transmise. De ce fait, l'intensité de la lumière traversant le milieu où elle est absorbée décroit exponentiellement :

$$I = I_0 \times e^{-klC}$$

Avec :

- I : L'intensité après passage à travers la cuve contenant la solution / ou intensité transmise.
- I_0 : L'intensité de la lumière incidente.
- l : trajet optique (distance traversée par la lumière) (en cm).
- C : La concentration des espèces absorbantes.
- k : Constante caractéristique de l'échantillon.

Cette relation peut s'écrire aussi :

$$\log\left(\frac{I_0}{I}\right) = \varepsilon l C$$

- **log (I_0/I)** représente l'absorbance de la solution.
- **I/I_0** correspond au rapport de l'intensité transmise à celle incidente ou appelé aussi **Transmittance** (T).
- **ε** est le coefficient d'extinction molaire qui représente la capacité de la molécule a absorbé la lumière incidente.

La détermination du coefficient d'extinction ou la concentration molaire des espèces présentes demeurent possible en utilisant cette méthode. Les interactions intermoléculaires additif/colorant peuvent également être étudiées par la spectroscopie UV-visible en suivant l'évolution de la bande d'absorption caractéristique du photoamorceur (PA) étudié par photolyse **(Figure 7)**, ainsi nous sommes capables de calculer le pourcentage de consommation en PA :

$$\%Consommation = \frac{A_0 - A_t}{A_0} \times 100$$

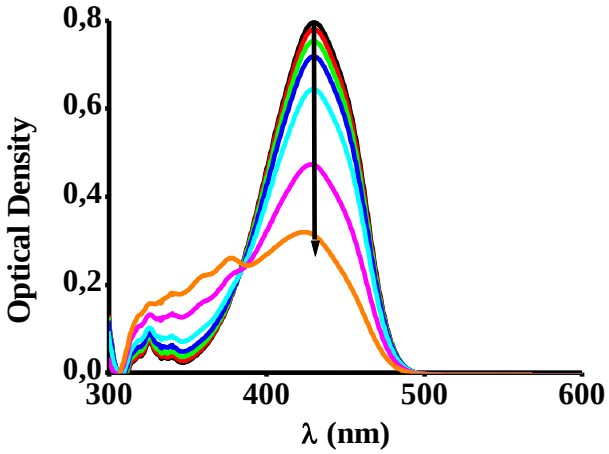

Figure 7 : Photolyse suivie par spectroscopie UV-visible.

3. Résonance paramagnétique électronique (RPE)

3.1. Principe

Le principe de la RPE est analogue à celui de la résonance magnétique nucléaire (RMN), à la différence près qu'en RPE, ce sont les spins des électrons qui sont excités plutôt que les spins des noyaux atomiques. La résonance de spin électronique (RSE) est une méthode de spectroscopie sous champ magnétique. Grâce à sa spécificité et sa grande sensibilité, elle permet une détection directe des espèces magnétiques (radicaux, éléments de transition, défauts de structure...) caractérisées par la présence d'un électron non apparié (appelé aussi électron célibataire) sur la couche de valence. Son principe repose sur l'effet Zeeman : soumis à l'action d'un champ magnétique extérieur intense H, les niveaux d'énergie d'un spin S se séparent en (2S + 1) états, chacun affecté d'un nombre quantique m_S (m_S = -S, -S+1, -S+2, ..., S). Ainsi, pour le cas d'un composé magnétique ne présentant qu'un seul électron célibataire (donc pour lequel S = 1/2), la présence du champ magnétique extérieur donne lieu à (2S + 1) = 2 états, correspondant à m_S = -1/2 et m_S = +1/2. L'énergie magnétique associée à chacun de ces états est donnée par $m_S g \mu B H$, où g est le facteur de Landé lorsqu'il s'agit d'un électron libre mais qui est désigné, dans le cas général, par le facteur g, et μB (qui est parfois noté β) est le magnéton de Bohr. Puis, sous l'action d'un rayonnement micro-onde perpendiculaire au

premier et d'amplitude beaucoup plus faible, ayant une fréquence ν, un photon d'énergie hν peut être absorbé (ou émis) si la séparation énergétique entre les 2 niveaux concernés, c'est-à-dire gμBH, se trouve égale à hν. C'est à cette valeur particulière de H que le phénomène de résonance se produit. Ainsi, la condition de résonance se résume par :

$$h\nu = E_f - E_i = g\mu_B H$$

Avec :

- E_f = Energie de l'état final.
- E_i = Energie de l'état initial.
- g = Facteur de Landé (dans le cas d'un électron libre) ou facteur g en général.
- μ_B (ou β) = Magnéton de Bohr (μ_B= 9,2741 x 10^{-24} $J.T^{-1}$).
- H = Valeur du champ magnétique à la condition de résonance.
- h = Constante de Planck (h = 6.6261 x 10^{-34} J.s).
- ν = Fréquence du champ micro-onde.

3.2. Méthode de détection des radicaux : Spin-traps

Cette technique est basée sur l'obtention d'un adduit radicalaire dont la durée de vie était bien plus importante que le radical d'origine. Le principe réside dans la réaction entre le radical étudié et une nitrone (ou un nitrosoalcane) formant un adduit paramagnétique pouvant être caractérisé par RPE stationnaire **(Figure 8)**.

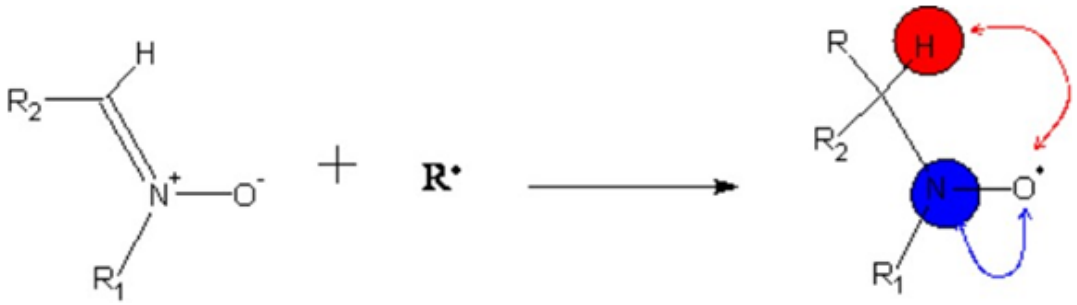

Figure 8 : Addition d'un radical sur une nitrone et représentation des couplages hyperfins sur l'adduit (aN en bleu et aH en rouge), R• est en général un radical centré sur un atome de C, N ou O.

Ces adduits (nitroxydes) sont particulièrement stables grâce à la délocalisation de l'électron célibataire sur l'atome d'azote et d'oxygène de la fonction nitroxyde **(Figure 9)**.

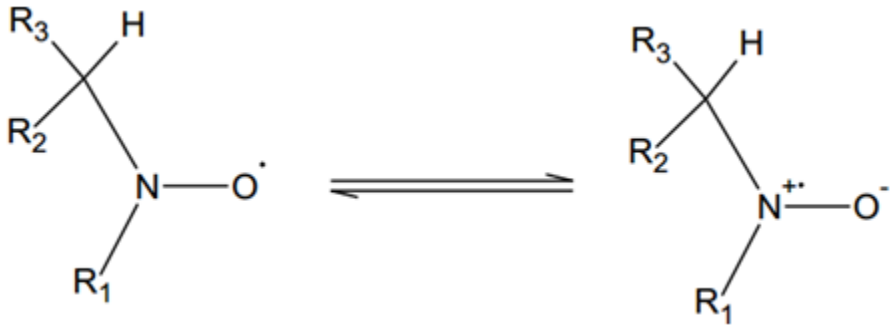

Figure 9 : Résonance de l'adduit nitroxyde.

Le spectre RPE de l'adduit permet de déterminer la nature du radical additionné en mesurant les couplages hyperfins de l'électron célibataire avec l'azote et l'hydrogène en α de la fonction nitroxyde (voir ci-dessus). Les nitrones sont les « Spin-Traps » (ST) les plus utilisés de par leur capacité à réagir avec des radicaux d'intérêt biologiques ($O2^{\bullet -}$, $HO^{\bullet}$...) et d'être solubles dans des milieux aqueux. Deux nitrones sont particulièrement efficaces, fiables et ont été largement utilisés en spin-trapping (PBN, DMPO ; Figure 10) :

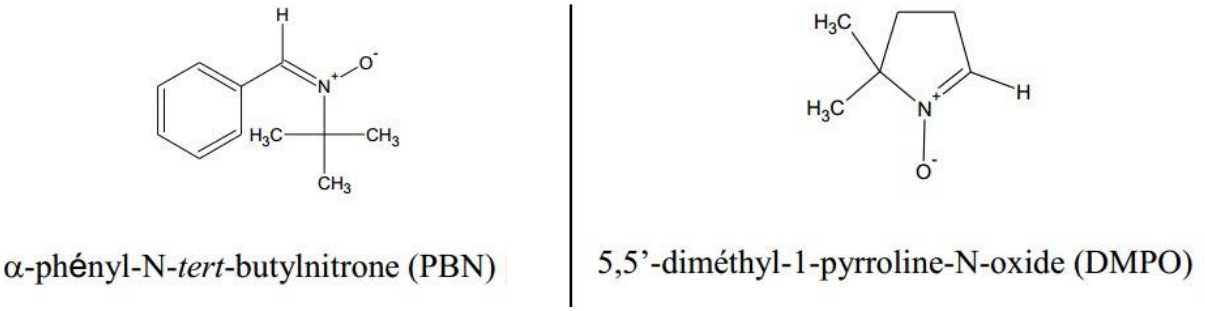

α-phényl-N-*tert*-butylnitrone (PBN) | 5,5'-diméthyl-1-pyrroline-N-oxide (DMPO)

Figure 10 : Structures chimiques de PBN et DMPO

Ces deux molécules présentent l'avantage d'être peu sensibles à la lumière et permettent la capture des radicaux issus de photolyse. Les adduits avec PBN [2] ont été les plus étudiés ; par conséquent, la base de données des couplages hyperfins de radicaux captés est plus importante. La DMPO [3] présente l'avantage d'avoir un couplage hyperfin avec l'hydrogène en α exalté, dû à la contrainte du cycle, et permet de déterminer avec plus de précision la nature du radical capté.

4. Spectroscopie de Fluorescence

Les spectres de fluorescence stationnaire ont été réalisés grâce à un spectrofluorimètre Fluoro max-2 de Jobin-Yvon équipé d'un photomultiplicateur. En général, la solution étudiée

est placée dans une cuve de quartz. Toutes les expériences ont été menées à la température de la salle 22°C (±3). Les résultats sont aussi obtenus avec un fluorimètre JASCO FP-750.

5. Fluorescence Résolue en Temps

Cette technique hautement sensible permet de détermine la durée de vie de fluorescence, autrement dit, elle permet de déterminer la durée de vie de l'état excité de la molécule étudiée grâce à un système de comptage de photons uniques corrélé dans le temps (HORIBA®Delta Flex avec un HORIBA®PPD-850 comme détecteur ; la source d'excitation est un HORIBA® nano LED - 370 avec une longueur d'onde d'excitation de 367 nm et une durée d'impulsion inférieure à 1,4 ns). La décroissance de l'intensité de fluorescence a été mesurée dans une cellule de quartz en utilisant le solvant convenable. Une solution de silice colloïdale LUDOX® a été utilisée pour évaluer la fonction de réponse impulsionnelle (IRF) de l'appareil

6. Mesure des potentiels Redox

Un montage classique à trois électrodes a été utilisé pour mesurer les potentiels d'oxydoréduction (électrode auxiliaire en platine et électrode au calomel saturé (ECS) comme référence). Les produits sont dissous dans une solution d'acétonitrile saturée en azote et contenant 0,1 M de hexafluorophosphate de tétra-butylammonium comme sel de fond. Les potentiels redox donnés sont les potentiels de demi-vague. Les données ont été obtenues avec le montage Voltalab 6 Radiometer.

7. Modélisation Moléculaire (Gaussian G03)

La modélisation moléculaire permet dans le cadre de notre étude :

- De donner des informations et des pistes de réflexion sur les propriétés des molécules.
- D'anticiper les caractéristiques recherchées pour une molécule (absorption lumineuse, donneur d'hydrogène...).

Les logiciels utilisés sont les suivants :

- Hyperchem pour la conception et les premières optimisations des molécules ; modélisation en dynamique moléculaire puis en PM3.
- Gaussian 03 pour la modélisation finale.
- Interface graphique pour visualiser les molécules sur GaussView

8. Ecriture Laser et impression 3D

L'imprimante laser utilise une diode laser à 405 nm dont la taille d'un point est de 50 µm. L'avantage de cette technique est la capacité de pouvoir dessiner la forme de l'objet voulu sur la surface du support contenant le mélange réactionnel. Suite à l'exposition à la diode laser, uniquement les parties irradiées polymérisent. Les zones liquides, non irradiées, sont nettoyées avec un solvant compatible avec le polymère formé.

Des motifs polymères en 3D ont été obtenus par stéréolithographie en utilisant une imprimante 3D du type **Anycubic Photon S.** La résine photosensible est placée dans un bac situé en dessous de la plateforme de construction. Une lumière visible vers 405nm est fournie en utilisant un écran LCD pour la génération du matériau polymère 3D.

Conclusion générale et perspectives

Conclusion générale et perspectives

Le travail mené au cours de cette thèse a été principalement axé sur la recherche de nouveaux systèmes photoamorceurs pour une déclinaison dans les deux grands modes de photopolymérisation (radicalaire et cationique) ainsi que la polymérisation de systèmes hybrides qui combinent les propriétés des deux polymères en un seul matériau. Les résultats obtenus durant ces trois années de doctorat ont répondu avec succès aux objectifs visés au début de la thèse et ont mené finalement à des progrès scientifiques importants. Particulièrement, nous nous sommes intéressés au développement de systèmes absorbant fortement dans le proche-UV et le visible permettant l'utilisation de dispositifs d'irradiation douce comme les diodes électroluminescentes (LED). Des systèmes à deux et/ou trois composants sensibles à la lumière bleue ont pu être développés et ont été testés pour l'amorçage des processus de polymérisation radicalaire et cationique sous de faibles intensités lumineuses. La réactivité de ces nouveaux composés nous a poussé vers l'étude de la relation entre la structure, les propriétés photochimiques/photophysiques et la capacité d'amorçage de ces colorants examinés.

Dans **la première partie** de ce manuscrit, une introduction générale a été reportée suivie d'une partie bibliographique traitant des différents modes de polymérisation (radicalaire, cationique et polymérisation hybride), la problématique, les défis et finalement l'originalité et le but de notre travail. Chaque mode de polymérisation est détaillé et décrit dans un chapitre.

En fait, le choix de ces molécules n'était pas fortuit, mais il se basait sur les propriétés d'absorption de ces molécules issues de calculs de modélisation moléculaire. Dans **la deuxième partie de la thèse,** une étude approfondie sur le développement de nouveaux photoamorceurs non métalliques à base de colorants organiques basés sur des structures coumarines et céto-coumarines pour la polymérisation de monomères acryliques a fait l'objet d'une étude spécifique. Cette partie est divisée principalement en deux chapitres. Dans le premier chapitre, deux nouvelles familles de coumarines ont été synthétisées et développées en tant que photoamorceurs capables d'amorcer les processus de polymérisation radicalaire sous irradiation bleue (LED à 405nm) soit par un processus de photo-oxydation soit par un processus de photo-réduction. Dans tous les cas, d'excellentes performances ont été obtenues en accord avec leurs bonnes propriétés d'absorption dans la zone proche-UV et visible, la

réactivité de leurs états excités et finalement les variations d'énergie libre de transfert d'électron très favorables. D'autre part, 9 composés dérivés de céto-coumarines ayant leur spectre d'absorption localisé dans la région proche-UV et visible ont pu être examinées dans **le chapitre II.** Ces derniers ont la particularité d'être très réactifs une fois combinés avec un additif et/ou un co-amorceur menant à des systèmes bi et tricomposants très efficaces vis-à-vis des acrylates. La forte réactivité de ces systèmes permet leurs utilisations dans des applications spécifiques telles que : l'écriture laser, la préparation des photocomposites et l'impression 3D avec de faibles intensités d'irradiation pour préparer des motifs polymères en 3D (cube) avec une bonne résolution spatiale.

Dans **la troisième partie de la thèse,** la recherche de nouveaux colorants organiques en tant que photoamorceurs de processus de polymérisation est toujours au cœur de notre travail. De nouveaux chromophores organiques fluorescents ayant une grande capacité à absorber dans le visible ont alors été développés. Précisément, deux nouvelles familles de colorants ont pu être synthétisées, étudiées et caractérisées comme amorceurs photoredox sensibles à la lumière bleue. En fait, cette partie est divisée en deux chapitres, et chacun d'eux traite une série des composés : le **chapitre I** étudie un ensemble de quatre dérivés de phénothiazine (deux d'entre eux n'ayant jamais été synthétisés avant) avec leur spectre d'absorption fortement centré dans le visible assurant un bon chevauchement avec la LED d'émission. Ces colorants avaient la capacité d'amorcer efficacement les processus de polymérisation radicalaire et cationique lorsqu'ils sont combinés au sel d'iodonium. Les systèmes à trois composants ont aussi été étudiés, l'incorporation d'une amine (NPG) dans la formulation photosensible favorise la formation d'un CTC ainsi que la régénération du photoamorceur suivant un cycle catalytique ; ce comportement aboutit finalement à des excellents profils de polymérisation radicalaire. La synthèse de photocomposites par imprégnation des fibres de verre par une résine acrylique et la génération des motifs polymères en 3D par écriture laser reflètent l'efficacité et l'intérêt d'utiliser ces chromophores dans le domaine de photopolymérisation. Dans **le deuxième chapitre** de cette partie, des composés dérivés de Naphthalimide ont été synthétisés dans le but d'amorcer les processus de polymérisation radicalaire et la polymérisation hybride (acrylate/époxyde). Ces composés hétérocycliques absorbent fortement à 405nm et possèdent un caractère fluorescent dans le visible. Cet aspect de fluorescence est fortement inhibé par l'ajout d'un additif (sel d'iodonium), expliquant ainsi la forte réactivité de ces dérivés vis-à-vis des monomères (méth)acryliques. Les systèmes à trois composants (Napht/Iod/amine) ont également été étudiés, et montrent bien une

performance supérieure à celle observée dans les systèmes à deux composants Napht/Iod. Un de ces colorants porte une fonction carboxylate qui lui assure une bonne solubilité dans l'eau, ainsi il avait la capacité de former des hydrogels une fois irradié avec une LED à 405 nm. Des composites épais par polymérisation radicalaire et hybride, et des polymères en 3D par écriture laser des formulations acryliques et hybrides ayant une grande résolution spatiale ont été obtenus. Remarquablement, un faible retrait, une épaisseur et résolution plus importante sont observés pour un système acrylate/époxyde.

La troisième partie a été dévolue à l'étude d'un ensemble de deux dérivés de complexe de cuivre. En effet, des complexes organométalliques à base de cuivre ont été proposés comme photoamorceurs en les combinant avec le sel d'iodonium (Iod) dans des systèmes à deux composants. De très bonnes performances ont été observées pour les systèmes GN/Iod. De plus, le caractère 'catalyseur photoredox' de ces composés a été mis en évidence par l'ajout d'un troisième composant (amine) à la formulation photosensible, ce comportement a pour effet d'augmenter le taux de conversion finale et la vitesse de polymérisation. Grâce à leurs propriétés d'absorption dans le visible, les complexes de cuivre ont montré une grande capacité à amorcer des réactions de polymérisation radicalaire (FRP) et cationique (CP) lors d'une irradiation avec une LED à 405 nm. Des bons profils de polymérisation ont été également observés pour la polymérisation des systèmes hybrides pour la synthèse des **Réseaux Polymères Interpénétrés (IPN).** Finalement, des échantillons de polymère en 3D ont été préparés par impression 3D à faible intensité d'irradiation, la synthèse de photocomposites épais montre bien l'efficacité de ces systèmes dans les applications à haute valeur ajoutée.

Un travail en perspective pourrait consister à développer de nouveaux systèmes photoamorceurs cationiques capables d'initier efficacement la CP d'époxy pour générer des motifs polymères en 3D. Obtenir des polymères épais par voie photochimique reste toujours un défi, pour cela, il pourrait être avantageux de développer de nouveaux amorceurs dont le spectre d'absorption serait décalé vers le proche IR où une meilleure pénétration de la lumière est généralement observée. Il est également important que les propriétés mécaniques des polymères obtenues soient évaluées par différentes techniques de caractérisation telle que (DSC, DMA, ATG …). Ces techniques peuvent nous servir à évaluer la rigidité, la souplesse, la dureté ainsi que la viscoélasticité (Tg…) des polymères produits. Il est aussi intéressant de développer d'autres systèmes amorceurs hydrosolubles capables d'initier efficacement la

polymérisation dans l'eau et d'aboutir donc à la formation d'hydrogels utilisés, par exemple, dans des applications biomédicales. Dans le but de limiter la toxicité provenant des composés organiques utilisés en tant que photoamorceurs, il est nécessaire de développer des composés naturels à haute performance.